Animal model of cirrhosis with hepatocellular carcinoma : a reliable tool for testing new therapies.

Keerthi Kurma

Communauté
UNIVERSITÉ Grenoble Alpes

THÈSE

Pour obtenir le grade de

DOCTEUR DE LA COMMUNAUTE UNIVERSITÉ GRENOBLE ALPES

Spécialité : Biologie du développement - Oncogenèse

Arrêté ministériel : 25 mai 2016

Présentée par

Keerthi KURMA

Thèse dirigée par **Thomas DECAENS**

préparée au sein du **Laboratoire IAB : Epigenetics, Environment, Cell Plasticity, Cancer (UGA / Inserm U1209 / CNRS UMR 5309)**
dans **l'École Doctorale Chimie et Sciences du Vivant**

Modèle animal de carcinome hépatocellulaire sur foie cirrhotique: description et utilisation pour essais thérapeutiques pré-cliniques

Animal model of cirrhosis with hepatocellular carcinoma: a reliable tool for testing new therapies.

Thèse soutenue publiquement le **18 octobre 2019**,
devant le jury composé de :

Monsieur THOMAS DECAENS
PROFESSEUR DES UNIV - PRATICIEN HOSP., CHU GRENOBLE ALPES, Directeur de thèse
Monsieur ROMAIN PARENT
CHARGE DE RECHERCHE, INSERM DELEGATION RHONE-ALPES, AUVERGNE, Rapporteur
Monsieur ARMAND ABERGEL
PROFESSEUR DES UNIV - PRATICIEN HOSP., CHU ESTAING - CLERMONT-FERRAND, Rapporteur
Madame SABINE BAILLY
DIRECTRICE DE RECHERCHE, INSERM DELEGATION ALPES, Présidente
Madame CLAUDE CARON DE FROMENTEL
CHARGE DE RECHERCHE, INSERM DELEGATION RHONE-ALPES, AUVERGNE, Examinatrice
Monsieur ARNAUD MILLET
CHARGE DE RECHERCHE, INSERM DELEGATION ALPES, Examinateur

Madame ZUZANA MACEK JILKOVA,
INGENIEUR DE RECHERCHE, CHU-GA
Invité

Acknowledgements

This journey would not have been possible and completed with the support of numerous people. Firstly, I would like to express my sincere gratitude to my supervisors Prof. Thomas Decaens and Dr. Zuzana Macek Jílková for the continuous support of my Ph.D. study and related research which is the first step of my academic career. I would also like to thank them for encouraging my research and allowing me to grow as a research scientist. Their advice on both research as well as on my career has been priceless. From the beginning of my academic life, their incomparable guidance, understanding, encouragement, confidence and everlasting support have maximized my motivation and have helped me to carry out this project by keeping warm the love of science in my heart. It is a big honor to work with such a wonderful person. I would like to express my gratitude to my team leader Dr. Patrice MARCH for his insightful comments and encouragement, but also for the hard question which incented me to widen my research from various perspectives. Besides, I am very much thankful to Fonds Agir pour les Maladies Chroniques for funding me to perform my thesis.

I am very thankful to every present and past members of Institute for Advanced Biosciences (IAB), Grenoble who have helped me in making wonderful memories. Especially, I would like to thank Team Marche members (Ayca Zeybek, Marion Ressejac, Zhang Jianhui, Khaldoun Gharzeddine, Arindam Dey, Carole Fournier, Lydie Carreres, Herve Lerat and Mylene Pezet), who were able to give me a real human dimension and share their experiences and culture. I would like to thank various platforms and facilities at IAB (Mylene Pezet: Microscopy platform), GIN (Animal facility), and PHTA (Animal facility), Grenoble for a great support.

I would like to express my appreciations to my Comité de Suivi Individuel (CSI) members: Jean-Jacques Feige and Bertrand Favier for their kindly help and advice. I would also like to thank my

thesis jury members: Prof. Armand Abergel (Rapporteur), Dr. Romain Parent (Rapporteur), Dr. Sabine Bailly (Examinatrice), Dr. Claude Caron de Fromentel (Examinatrice) and Dr. Arnaud Millet (Examinateur) for taking their time to evaluate my thesis.

I am grateful to my dear friends Arindam Dey, Marion Ressejac, Daria Dasha, Celine Coppard, Ayca Zebek, Nastaran, Fabienne Agasse, Maria Cristina Capizzi, Soumya Katamani, Lahari Yeramala and IAB members for their good friendship, encouragements, and constructive comments. My special thanks to my parents and brother a great debt of gratitude for their everlasting support, motivation, patience, and limitless love. Especially my friend Mohammed Ashfaq Ahmed who has been a constant source of support and encouragement during the challenges of graduate school and life.

The Institute for Advanced Biosciences (IAB) is an internationally renowned institute in basic biomedical and translational research in the areas of epigenetic, chronic diseases and cancer. The IAB is supported jointly by the National Institute of Health and Medical Research (INSERM), the University of Grenoble Alpes (UGA) and the National Centre for Scientific Research (CNRS).

My study was conducted in the Prevention and Therapy of chronic diseases Department in the IAB in collaboration with IRMaGE platform in the Grenoble Institute of Neuroscience (GIN, INSERM, and University of Grenoble-Alpes, France).

Abstract

Liver cancer is currently the second most common cause of cancer-related death worldwide, with hepatocellular carcinoma (HCC) accounting for the majority of these cases. 90% of HCC cases are associated with liver fibrosis or cirrhosis developed from chronic liver injuries. Although each underlying condition might involve different carcinogenic pathways, fibrosis/cirrhosis is regarded as a crucial factor in the carcinogenesis of liver tissue. Moreover, the immune system of the liver contributes to the severity of the necrotic-inflammatory tissue damages, the establishment of the fibrosis and cirrhosis and the disease progression towards HCC.

Small animal models represent the essential tools of cancer research. As fibrosis/cirrhosis modifies liver vascularization, extracellular matrix composition and drugs metabolism, it is essential to use a cirrhotic animal model to test HCC drugs for their efficiency against tumour initiation and/or progression. The current mouse model failed to reproduce all the fibrosis stages, especially cirrhosis. One of the rodent models that most faithfully reproduce human cirrhosis are the diethyl nitrosamine-injured rats (DEN rats). However, limited information exists about the inflammation status or immune system features of this model during progression from liver cirrhosis to carcinoma. Therefore, the aim of our project is to deeply characterize DEN-induced HCC rat models during cirrhosis progression and HCC development, with a special focus on liver inflammatory micro-environment.

In this study, we demonstrate that the DEN-induced HCC rat model displays tumour initiation, development and the several stages of liver fibrosis, including cirrhosis, and also helps understand the related modulation of the immune micro-environment. Furthermore, we demonstrate that intrahepatic immune cells, especially T lymphocytes and macrophages in this DEN induced

cirrhotic rat model, are modified during the development of HCC, mimicking human HCC. For instance, we show that during HCC development, Treg, CTLA-4 and macrophages (of which most are polarized towards the M2 phenotype in tumor areas), contribute to an immunosuppressive environment and probably promote the progression of HCC. Thus, these findings help to comprehensively understand the DEN-induced HCC rat model, which mimics the pathological process of human HCC quite accurately, including immune system features. In this context, the DEN-induced cirrhotic HCC rat model might be a relevant pre-clinical model tool to evaluate the new HCC treatment's efficacy and tolerance in a liver cirrhotic background. Therefore, we also tested for the safety and efficacy of a new allosteric inhibitor (ARQ 751) and a combination of an AKT inhibitor (ARQ 751) and sorafenib and compared it to the sorafenib and control. Here, our MRI results showed a lower tumor progression, reduced tumor numbers and size in groups of rats treated with the new therapeutic strategy. Thus, ARQ 751 as single agent, and its combination with sorafenib, exerted a strong suppression in tumor progression, improved liver fibrosis and demonstrated a good safety profile, making this experimental drug promising in the treatment of HCC in cirrhotic patients. Thus, the results provide a strong rationale for testing ARQ 751 in clinical settings, and confirm the importance of targeting AKT in HCC development and progression.

Resume

Le cancer du foie représente le deuxième cancer le plus meurtrier dans le monde, le carcinome hépatocellulaire (CHC) étant responsable de la majorité de ces cas. 90% des CHC sont associés à une fibrose hépatique ou à une cirrhose développée à la suite de lésions hépatiques chroniques. Bien que chaque affection sous-jacente puisse impliquer différentes voies cancérogènes, la fibrose / cirrhose est considérée comme un facteur crucial de la carcinogenèse du tissu hépatique. De plus, le système immunitaire du foie contribue à la sévérité des dommages tissulaires nécrotiques et inflammatoires, à l'établissement de la fibrose et de la cirrhose et à la progression de la maladie vers le CHC. Les modèles animaux de petite taille représentent des outils essentiels dans la recherche sur le cancer. Étant donné que la fibrose / cirrhose modifie la vascularisation du foie, la composition de la matrice extracellulaire et le métabolisme des médicaments, il est essentiel d'utiliser un modèle animal pertinent présentant un état cirrhotique pour tester les médicaments contre le CHC. Les modèles de souris actuels ne parviennent pas à reproduire tous les stades de la fibrose, en particulier la cirrhose. L'un des modèles de rongeurs qui reproduit le plus fidèlement la cirrhose humaine est celui du rat exposé à la d'éthyle nitrosamine (rats DEN). Cependant, le statut inflammatoire et les caractéristiques du système immunitaire dans ce modèle n'ont été que peu étudiés au cours de la progression de la cirrhose hépatique vers le carcinome. Le but de notre étude est alors de caractériser en profondeur le modèle de rat du CHC induit par DEN au cours de la progression de la cirrhose et du développement du CHC, en investiguant plus particulièrement le micro-environnement inflammatoire du foie.

Dans cette étude nous avons démontré que le CHC induit par DEN chez le rat présente les différentes étapes du développement tumoral et les différents stades de la fibrose hépatique jusqu'à la cirrhose. Ce modèle aide aussi à mieux comprendre les modulations du micro-environnement

immunitaire associées au CHC. En effet, nous avons montré que les cellules immunitaires intrahépatiques, particulièrement les lymphocytes T et les macrophages, sont modifiées au cours du développement du CHC induit par DEN, mimant ainsi le CHC humain. Nous avons montré qu'au cours du développement du CHC, les Tregs, CTLA-4+ lymphocytes et les macrophages (dont la majorité sont polarisés en M2 au niveau de la tumeur), contribuent à un microenvironnement immunosuppressif et favorisent probablement la progression du CHC. L'ensemble de ces résultats aide donc à comprendre le modèle de rat de CHC induit par DEN qui est un modèle mimant le processus pathophysiologique du CHC humain notamment les caractéristiques du système immunitaire intra-tumoral. Dans ce contexte, le modèle de CHC induit par DEN chez le rat pourrait être un outil pertinent comme modèle pré-clinique afin d'évaluer l'efficacité de nouveaux traitements contre le CHC et la tolérance dans un contexte de foie cirrhotique. Nous avons alors testé la sécurité et l'efficacité d'un nouvel inhibiteur allostérique d'AKT (ARQ 751) ainsi que sa combinaison avec le sorafenib à comparaison du sorafenib seul et du contrôle. Nos analyses par IRM montrent une progression tumorale moindre en raison de la diminution du nombre et de la taille des tumeurs dans les groupes d'animaux traités avec la nouvelle molécule thérapeutique. L'administration de ARQ 751 seul ou en combinaison avec le sorafenib ralentit drastiquement la progression tumorale, améliore la fibrose hépatique et montre un bon profil de sécurité. Tout ceci supporte l'utilisation de cette molécule expérimentale prometteuse dans le traitement de patients cirrhotiques atteints de CHC. L'ensemble de ces résultats fournit une base solide pour tester le ARQ 751 dans un contexte clinique et confirme également l'importance de cibler la voie AKT pour contrer le développement et la progression du CHC.

Table of Contents

List of Figures

List of Tables

Abbrevations

AFB1: Aflatoxin B1

ALP: Alkaline phosphatase

ALT: Alanine aminotransferase

Arg-1: Arginase-1

ASR: Age standardized incidence rate

AST: Aspartate aminotransferase

CCl4: Carbon tetra chloride

CTLA-4: Cytotoxic T-lymphocyte antigen 4

DAMP: Damage-associated molecular patterns

DEN: Diethyl nitrosamine

EGF: Epidermal growth factor

EGFR: Epidermal growth factor receptor

EPCAM: Epithelial cell adhesion molecule

ERK: Extracellular signal-regulated kinase

FDA: Food and Druf Administration

FGF: fibroblast growth factor

FGFR: Fibroblast growth factor receptor

GGT: Gamma-glutamyl transpeptidase

GMM: Genetically modified mouse models

GST-P: Placental Glutathione S -transferases

HBV: Hepatitis B virus

HCC: Hepatocellular carcinoma

HCV: Hepatitis C virus

HRP: Horseradish peroxidase

IGF: Insulin-like growth factor

IGFR: Insulin-like growth factor receptor

IL: Interlukine

INF-γ: Interferon gamma

iNOS: Inducible nitric oxide synthase

IVC: Individually ventilated cage

KC: Kupffer cells

LPS: lipopolysaccharide

LSEC: Liver sinusoidal endothelial cells

MAMP: Microbial associated molecular patterns

MEK: Mitogen-extracellular activated protein kinase kinase

MMPs: Matrix metalloproteases

mTOR: mammalian target of rapamycin

NAFLD: Non alcoholic fatty liver disease

NASH: Non-alcoholic steatohepatitis

NO: Nitric oxide

OS: Overall survival

PB: Phenobarbital

PD-1: Programmed cell death protein-1

PDGF: Platelet-derived growth factor

PDGFR: Platelet-derived growth factor receptor

PD-Ls: Programmed cell death protein ligands

PFS: Progression-free survival

PI3K: Phosphatidylinositol-3- kinase

PRR: Pattern recognition receptors

PTEN: Phosphatase and tensin homologue deleted on chromosome ten

qPCR: Real time polymerase chain reaction

RT: Room temperature

SEM: Standard error mean

STAT: Signal transducer and activator of transcription

TAA: Thioacetamide

TAMs: Tumor associated macrophages

TGF: Transforming growth factor

TGM2: Transglutaminase-2

Th: Helper T

TIMP1: Tissue inhibitor of metalloproteinases-1

TNF: Tumor necrosis factor

Treg: T-regulatory

TTP: Median time to progression

VEGF: Vascular endothelial growth factor

VEGFR: Vascular endothelial growth factor receptor

α-SMA: α-smooth muscle actin

1. INTRODUCTION

Liver cancer is the sixth most common cancer and second most lethal malignancy, afflicting more than one million people and causing 829,000 deaths worldwide. Globally, the incidence of liver cancer is seen more in males, with 1 in 38 men developing liver cancer, than in females—1 in 111 women [1] . Hepatocellular carcinoma (HCC) is predominantly constitutive of ~90% primary liver cancer [2] . Chronic hepatitis infection by the hepatitis B (HBV) or hepatitis C viruses (HCV), aflatoxin, alcoholic liver disease and nonalcoholic fatty liver disease are the major risk factors for HCC incidence (Figure 1) [3]. The distribution of these risk factors depend on geographic regions and race or ethnic group, and they are highly variable among patients with HCC (Figure 2) [4, 5]. The development of HCC is a complex multistep process that involves sustained inflammatory damage, including hepatocyte necrosis and regeneration, associated with fibrotic deposition [6]. 80–90% of HCC is associated with the formation and progression of fibrosis and cirrhosis. Moreover, the immune system of the liver also contributes to the severity of the necrotic-inflammatory tissue damage, the establishment of the fibrosis and cirrhosis and the disease progression towards HCC [7]. The details of each etiology developing HCC are presented further.

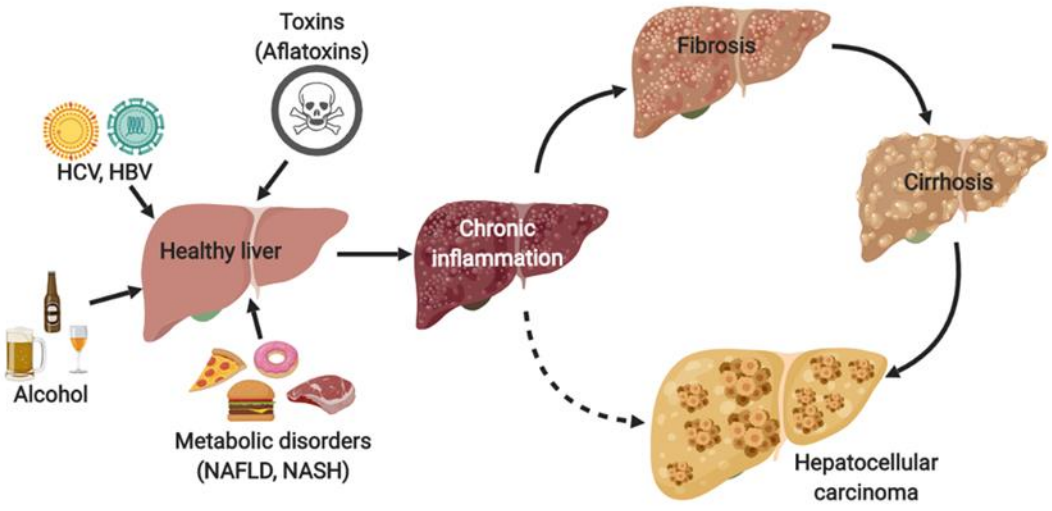

FIGURE 1: PROCESS OF DEVELOPMENT OF HCC BY RISK FACTORS SUCH AS HBV, HCV, AFLATOXIN, ALOCOHOLIC LIVER DISEASE AND NON-ALCOHOLIC FATTY LIVER DISEASE.

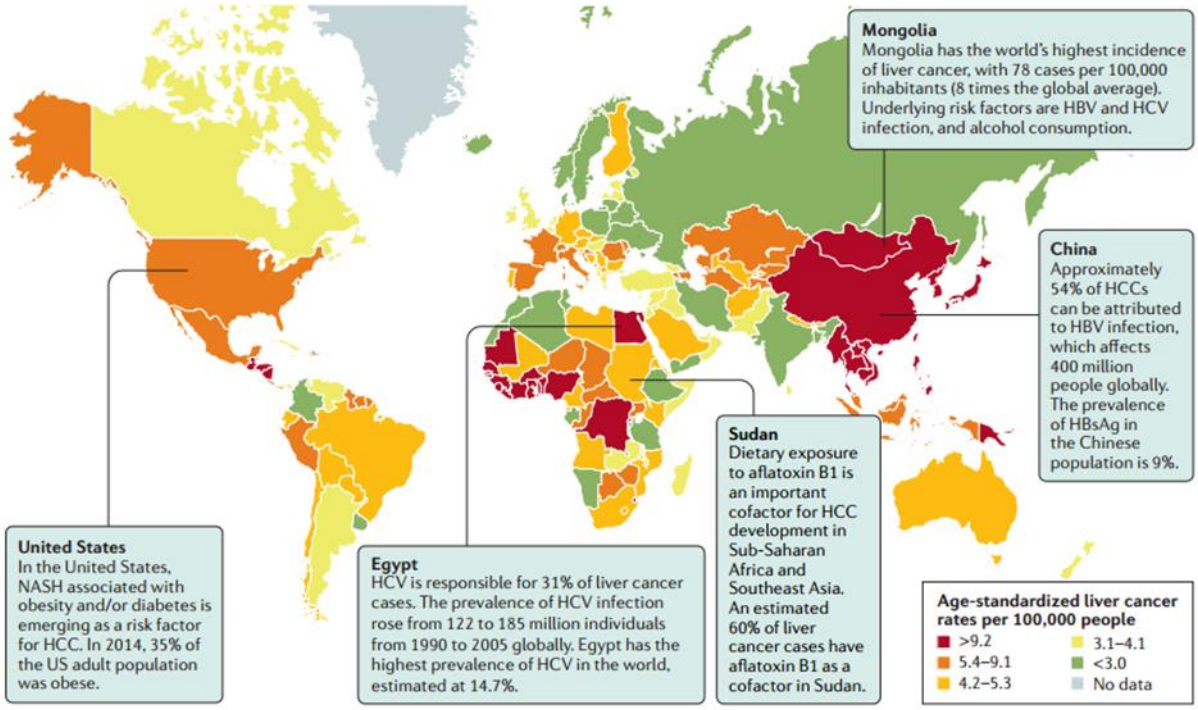

FIGURE 2: THE INCIDENCE OF HCC WITH DIFFERNET ETIOLOGIES DEPENDING ON GEOGRAPHIC AREAS. (IMAGE SOURCE: LLOVET, J. M et al., 2016, NATURE REVIEW [4])

1.1 ETIOLOGY OF HCC

1.1.1 HBV

HBV is considered one of the main etiological factors of HCC, as the virus infection generates various pathological alterations inside the liver structure, facilitating the development of HCC. Globally, approximately 43.3% of the total cases of liver cancer (436,500) were ascribed to hepatitis B [8]. The age standardized incidence rate (ASR) of liver cancer due to hepatitis B, was significantly heterogeneous across the world, with the highest ASR observed in East Asia. Moreover, in highly endemic regions, HBV is primarily transmitted from mother to child during birth, and through parental contact with infected blood in developed countries or sexual contact [9]. Multiple variables, such as the virus or host-related factors and the patient's lifestyle, have to be considered in order to correctly assess the risk of carcinogenesis triggered by chronic HBV infection [10]. Besides, 9% of the HIV-infected patients are co-infected with HBV, resulting in an increased risk of developing HCC, as compared to having a chronic HBV infection alone [11].

HBV is a partially double-stranded DNA virus (genome length: 3200 bp), a member of the *Hepadnaviridae* family [12]. Hepatitis B surface, e and the core antigens are the markers of an active infection (but the HBe negative antigen can be associated with an active infection as well). The hepatitis B e antigen-positivity and elevated HBV DNA levels are risk factors for the development of liver cirrhosis in patients with chronic hepatitis B [13, 14]. The development of HCC through chronic HBV infection is a multistep process that involves the rearrangement of intracellular DNA, leading to an inflammation of the hepatocytes and escorted by an increased rate of proliferation [15]. Once the viral DNA is integrated into the host's genome, the telomerase reverse transcriptase is altered, and the genes involved in the malignant process undergo various insertional mutation [16]. Further continuation in the inflammation process results in liver injury

through necrosis of the affected area, which is followed by compensatory regeneration and hepatic fibrosis. Hence, altogether the hepatic architecture is altered and it leads to a cirrhosis background [17]. Besides, the effect of HBV proteins on pathways, such as p38MAPK and PI3K/AKT, also increase the invasive potential of an HBV infection [18, 19]. Moreover, the association of an HBV infection with HCV, or with increased alcohol intake or aflatoxin consumption, increases the carcinogenic risk of HBV [20].

1.1.2 HCV

HCV infection is another major risk factor for developing HCC. In 2016, among the total number of liver cancer cases, hepatitis C triggered almost 18.7% (188,700). Even though antiviral therapies are effective in reducing the incidence of HCC, the risk has not been eradicated, since diabetes and obesity in individuals with HCV contribute to an increased risk of HCC [8]

HCV is associated with the *Hepacivirus genus* of *Flaviviridae* origin [21], and its carcinogenesis is mediated by viral-induced factors and host-induced immunologic responses. Investigation of HCV revealed that its core protein might impair oxidative stress metabolism and drive lipogenesis [22]. In the process of promoting HCC, HCV viral proteins act directly on cell signaling pathways through the activation of signaling pathways that up-regulate growth and division, or by inhibiting tumor suppressor genes and cell cycle points [23]. Moreover, the inhibition of specific tumor suppressor genes, such as the retinoblastoma protein and the p53 tumor suppressor of the HCV core proteins, also increases the rate of carcinogenesis [24, 25]. Additionally, nonstructural protein genes of HCV stimulate fibrosis and the progression of HCC, by inducing the transforming growth factor-beta and activating hepatic stellate cells [26]. Furthermore, the HCV virus and the host-mediated immune response induces oxidative stress on hepatocytes, which leads to regeneration and cell death, accompanied by hepatic mutations and the development of HCC

1.1.3 AFLATOXIN

Aflatoxins are naturally prevailing subsidiary metabolites of the fungi *Aspergillus flavus* and *Aspergillus parasiticus*. It is a mycotoxin that can be found in food items, which include peanuts, meat, milk, oilseeds, corns and dried fruits, primarily in regions of tropical and subtropical climates, wetlands and high temperatures, which can lead to food contamination and a well-known human hepatocarcinogen, which is the prime agent in the pathologic process of HCC [27]. It is estimated that 4.5 billion people worldwide are exposed to Aflatoxin B1 (AFB1) and may develop HCC, and about 5–28% of global HCC cases can be attributed to aflatoxin exposure [28]. Once consumed, AFB1 is metabolized to a functional transitional compound—AFB1-exo-8,9-epoxide—that can attach to the DNA, causing further mutations and leading to HCC [29, 30]. Evidently, the AFB1 interact with different factors, such as HBV, with which it has a synergistic interaction favoring hepatocarcinogenesis. Moreover, studies have shown that patients who had HCC and HBV with a "high" AFB1 consumption, 10-times higher mortality rates than those with "low" consumption. For instance, the odds ratio for developing HCC with exposure to aflatoxin alone was 6.37, with HBV infection alone it was 11.3, and with both risk factors was 73.0 [31, 32].

1.1.4 ALCOHOL

In 2016, 14.7% (147,700) of total liver cancer cases were attributed to alcohol consumption. The proportion of liver cancer due to alcohol consumption has increased up to 40% in Western European countries, such as France, Belgium, Germany, Denmark etc. [8]. Extreme alcohol consumption modifies/compromises functional capacity and the architecture liver, through liver injuries from steatosis, steatohepatitis and fibrosis, eventually leading to cirrhosis and HCC [33]. Moreover, extreme alcohol consumption drives HCC through a number of pathophysiological

factors such as the formation of acetaldehyde, which leads to proteins and DNA adducts, the impairment of antioxidant defense and DNA repair mechanisms by increasing the production of cytochrome P450 2E1-, and/or iron-induced reactive oxygen species, inducing chronic inflammation by altering the immune system and interference with methyl group transfer and alterations to gene expression [34-37]. A higher incidence of HCC has been found in patients with an HBV-infection and alcoholic cirrhosis, compared to viral infections and alcoholism alone [38, 39].

1.1.5 NONALCOHOLIC FATTY LIVER DISEASE (NAFLD)

Risk factors such as obesity (51%), type 2 diabetes mellitus (23%) and metabolic syndrome (43%) lead to the development of NAFLD, followed by non-alcoholic steatohepatitis (NASH) and its progression to HCC [40-42]. Compared to the other etiological development, HCC in NAFLD is associated in the absence of established cirrhosis, suggesting its specific mechanism of carcinogenesis that is less dependent on hepatic fibrosis. Moreover, in NAFLD, hepatic lipid accumulation leads to metabolic reprogramming, characterized by a combination of cellular metabolic alterations and an accumulation of potentially toxic metabolites that favor the development of liver tumorigenesis [43]. Furthermore, NASH underlies an extremely versatile and dynamic inflammatory microenvironment. This mixture of an inflammatory microenvironment, aberrant metabolism and ongoing liver regeneration contributes to DNA instability and cancer (HCC) [44].

1.2 TREATMENT OF HCC

Despite the high incidence of HCC with various etiologies, as seen previously, only 40–50% of HCC patients are led to early diagnosis through surveillance programs in developed countries [45]. Therapeutic options are available for HCC, including surgical resection, local ablative therapy or transarterial chemoembolization, radio embolization, radiation treatment and systemic treatment. In the very early and early stages, curative treatments such as liver resection, transplantation or radiofrequency ablation have survival benefits. Local treatment such as trans-arterial chemoembolization is the main treatment option for the intermediate stage [46] (Figure 3). However, for patients with advanced HCC, some systemic therapies have been approved for treatment, as few agents could demonstrate significant benefits over the placebo, which are discussed further.

1.2.1 SYSTEMIC THERAPIES OF HCC

Systemic therapies are recommended for patients who are in an advanced disease stage (Barcelona Clinic Liver Cancer [BCLC] stage C), or are at the intermediate stage (BCLC stage B), as well as progression with transarterial therapies (Figure 3). Following are the details of systemic therapies approved by the Food and Drug Administration (FDA).

1.2.1.1 First line therapies

Sorafenib (Nexavar) emerged as the first effective systemic treatment of unresectable HCC, after 30 years of research, and was approved by the FDA in December 2007, that extended the median overall survival (OS) over the placebo by nearly three months (10.7 vs. 7.9 months) [47, 48]. It acts by inhibiting multiple intracellular (c-RAF, BRAF, and mutant BRAF) and cell surface kinases, Fms-related tyrosine kinase, vascular endothelial growth factor receptor (VEGFR)-1,

VEGFR-2, VEGFR-3 and platelet-derived growth factor receptors (PDGFR)-β). These "kinases are involved in tumor cell signaling, angiogenesis, and apoptosis [49]. Certainly, sorafenib is now the standard therapeutic agent for advanced HCC. However, in spite of sorafenib's proven efficacy to significantly increase overall survival in patients with advanced HCC, it was unable to stop the disease progression because of development of resistance to anti proliferative therapies, and its systemic toxicity is relatively high [50]. Therefore, novel molecular targeted agents with more potency or similar effects, but less toxicity, have been the unmet need.

Lenvatinib another first line HCC treatment approved by the FDA in July 2018, is a multiple-receptor tyrosine kinase inhibitor that inhibits the kinase activities of VEGF receptors VEGFR1, VEGFR2, VEGFR3; it also inhibits other receptor tyrosine kinases including fibroblast growth factors (FGF) and receptors FGFR 1, 2, 3 and 4. Research conducted by Kudo et al, compared lenvatinib with sorafenib in the first-line setting for treatment of patients with unresectable HCC [51, 52]. Their data showed that the median overall OS, progression-free survival (PFS) and median time to progression (TTP) were 13.6 months (vs. 12.3 months), 7.4 months (vs. 3.7 months) and 8.9 months (vs. 3.7 months) in the lenvatinib group (vs. sorafenib), respectively. Therefore, the OS for lenvatinib was non-inferior to sorafenib, while the PFS and TTP were in favor of lenvatinib [53] .

Further several phase III clinical trials with other tyrosine kinase inhibitors in first-line settings, including brivanib [54], sunitinib (Sutent) [55], erlotinib (Tarceva) [56], and linifanib [57] alone or in combination with sorafenib were conducted. Unfortunately, none of the trails showed greater survival benefits than sorafenib.

1.2.1.2 Second line therapies

Regorafenib (Stivarga), an oral multi-kinase inhibitor, showed a survival benefit in HCC patients progressing on sorafenib treatment, and obtained approval by the FDA as a second-line treatment for HCC, following sorafenib in April 2017. HCC patients treated with regorafenib following with the sorafenib treatment showed an improvement in the median OS of 10.6 months, as compared to 7.8 months with placebo. It acts by binding and inhibiting VEGFRs 2 and 3, PDGFR and Raf kinases, which result in the inhibition of tumor angiogenesis and its cell proliferation [58-60]. The regorafenib molecular structure is similar to sorafenib, as it is synthesized by binding fluorine to sorafenib, but has stronger toxicity profile. Therefore, unlike other drugs, a placebo-controlled phase III study (RESORCE trial) was performed that included only patients who had progressed under the sorafenib treatment and those intolerant to sorafenib were excluded [59, 60]. At present, regorafenib is the standard second-line chemotherapy for patients who are refractory to sorafenib. However, only a few patients were eligible for regorafenib treatment due to their intolerance to sorafenib and deterioration of liver function.

Cabozantinib is an oral multi-kinase inhibitor that inhibits the activity of VEGF, c-MET etc., and was accepted by the FDA in May 2018 for the treatment of patients previously treated with advanced HCC. The application was based on findings from the phase III CELESTIAL trial, in which the survival-prolonging effects of cabozantinib as a second-line agent for patients with HCC refractory/intolerant to the sorafenib treatment, as compared with the placebo control, were 10.2 months vs. 8.0 months [61, 62]. Thus these finding concluded that cabozantinib improves OS and PFS in patients with advanced HCC who had received sorafenib as the prior systemic therapy regardless of the duration of prior sorafenib treatment [63]. However, the adverse effects of cabozantinib were fatigue (12.4%), diarrhea (17%) and palmarplantar erythrodysesthesia (8.7%).

Ramucirumab is a recombinant human immunoglobulin G1 monoclonal antibody, directed against VEGFR-2 that plays an important role in VEGF induced tumor angiogenesis. It is currently pointed to for unresectable advanced/recurrent gastric cancer, colorectal cancer and non-small-cell lung cancer and is used in routine clinical practice. A randomized phase III trial (REACH-2) investigated ramucirumab as a second-line treatment, following sorafenib therapy for advanced HCC patients with an alpha-fetoprotein level ≥ 400 ng/mL, and the results demonstrated the superiority of ramucirumab over the placebo with a median OS of 8.5 vs. 7.3 months, respectively [64-66].

Further, immunotherapy with ***nivolumab,*** a fully human immunoglobulin G4 programmed cell death protein-1 (PD-1) immune checkpoint inhibitor antibody. It acts through the disrupting of the interaction between PD-1 and its ligands [programmed cell death protein ligands (PD-Ls), PD-L1/PD-L2], leading to promising response rates and survival durations in a phase I–II study involving patients previously treated with sorafenib [67]. Based on the results of the phase I/II study described, the United States marked nivolumab for priority review as a second-line agent, following its response failure to first-line treatment with sorafenib; it was approved by the FDA in September 2017. The approval was granted for patients, regardless of their PD-L1 status. The median survival of patients treated with nivolumab as a first-line therapy was 28.6 months, whereas that of patients treated with nivolumab as second-line was 15 months. The confirmed overall response rate by the blinded independent central review for treatment with nivolumab was 14.3% [67]. Besides, recent results of CheckMate -459 Phase III clinical trial of nivolumab versus sorafenib in patients with unresectable HCC, failed to meet the primary endpoint of the OS (https://www.drugdevelopment-technology.com/news/bms-checkmate-459-trial/).

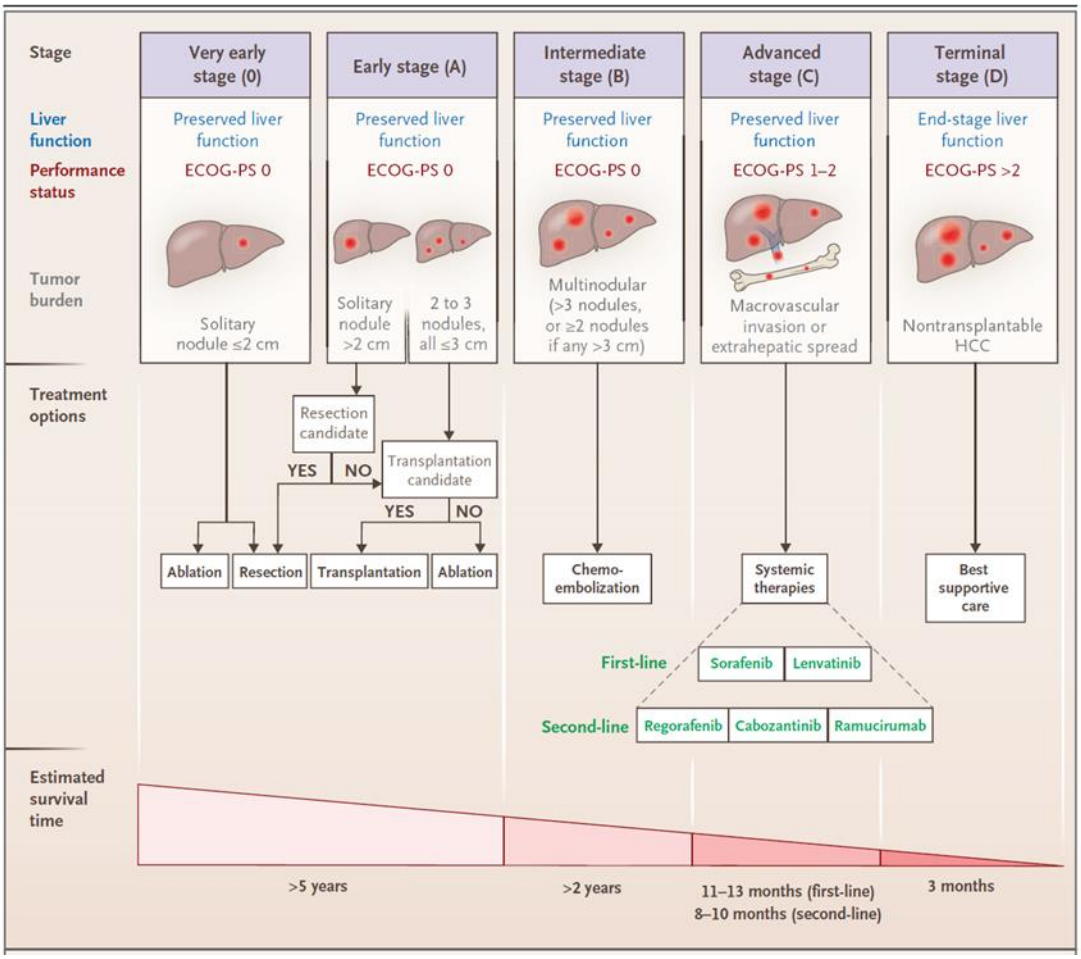

FIGURE 3: TREATEMENT OPTIONS DEPENDING ON STAGE OF HCC DEVELOPMENT (IMAGE SOURCE: AUGUSTO VILLANUEVA, 2019, THE NEW ENGLAND JOURNAL OF MEDICINE [4])

Therefore, according to the treatment history and their survival benefits, it's clear that there is an urgent need to develop new and more effective therapeutic strategies and agents to treat HCC.

1.3 IMMUNE SYSTEM OF LIVER AND HCC

Treatment of HCC illustrated the growing importance of immunotherapy. Hence better understanding the immune system of HCC is remarkably for the development of efficient therapy against HCC. Besides the contribution of immunity to hallmarks of cancer by Hannahan & Weinberg illustrated the importance of the immune system in the development of cancer (HCC) [68].

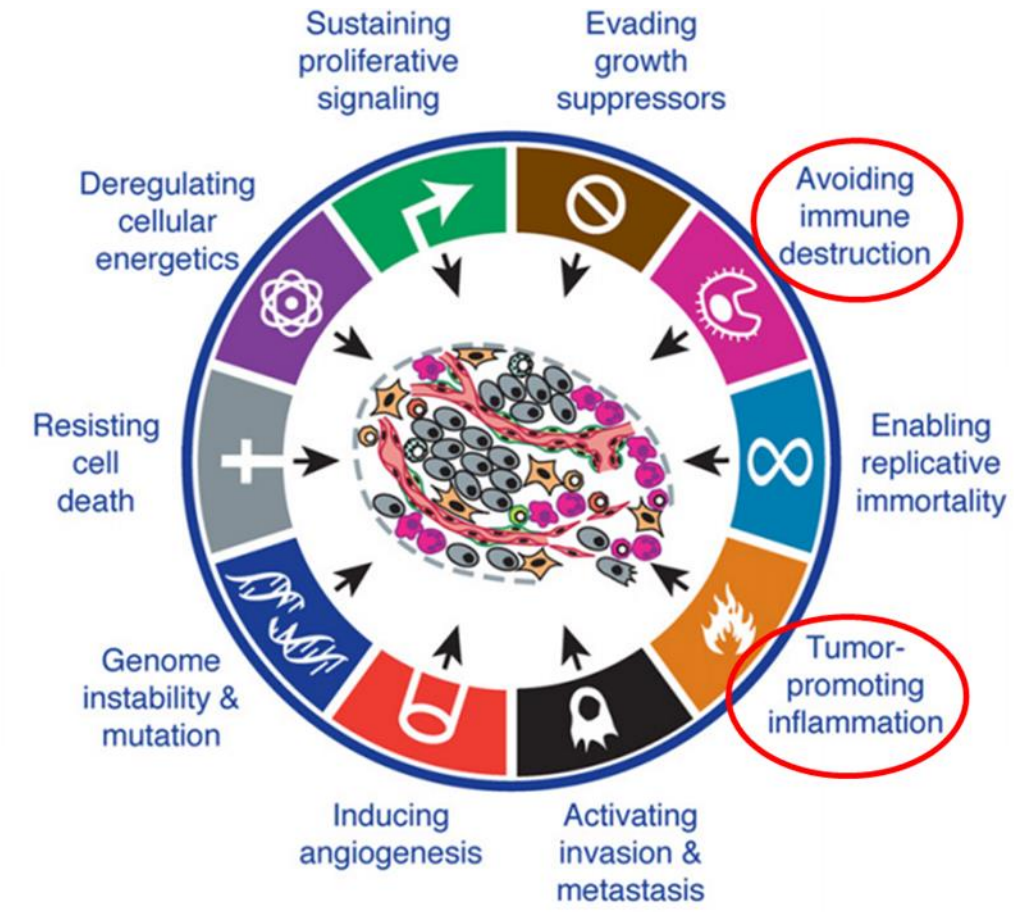

FIGURE 4: CONTRIBUTION OF IMMUNITY TO HALL MARKS OF CANCER (IMAGE SOURCE: HANAHAN & WEINBERG, 2011, CELL [68])

1.3.1 LIVER AND IMMUNE SYSTEM

Anatomically liver is an organ that allows two blood supplies i.e. arterial and venous blood. It functions as an important defense between gut contents and systemic circulation. 80% of the blood entering the liver is supplied by portal vein (blood flow derives from many of the gastrointestinal organs) which is rich with harmless dietary and environmental antigens as well as molecules from the microflora of the gut. Besides, arterial oxygen-rich blood enters the liver through hepatic, which is the minor source of the blood supplier [69-71]. Upon entering the liver venous blood from the gut mixes with oxygen-rich blood from the hepatic artery and drains through the hepatic sinusoids to the central veins through plates of hepatocytes. The sinusoids are lined by specialized liver sinusoidal endothelial cells (LSEC) which allowing blood to pass through the LSEC layer to the underlying hepatocytes (Figure 5) [72]. LSECs comprise around ~20% of liver cells and are located at the interface between hepatic microcirculation and hepatocytes. On the luminal side, LSECs continuously survey blood from the gastrointestinal tract, exerting a close relationship with resident liver macrophages (Kupffer cells) and all leukocytes that are in the circulation or those that constantly patrol liver vessels (including monocytes, natural killer, and natural killer T cells). On the other side (facing the Disse Space), LSECs interact with hepatic stellate cells and hepatocytes. This is crucial for liver metabolism since LSECs are a permeable barrier that mediates the exchange, active uptake, and degradation of circulating molecules [73-76].

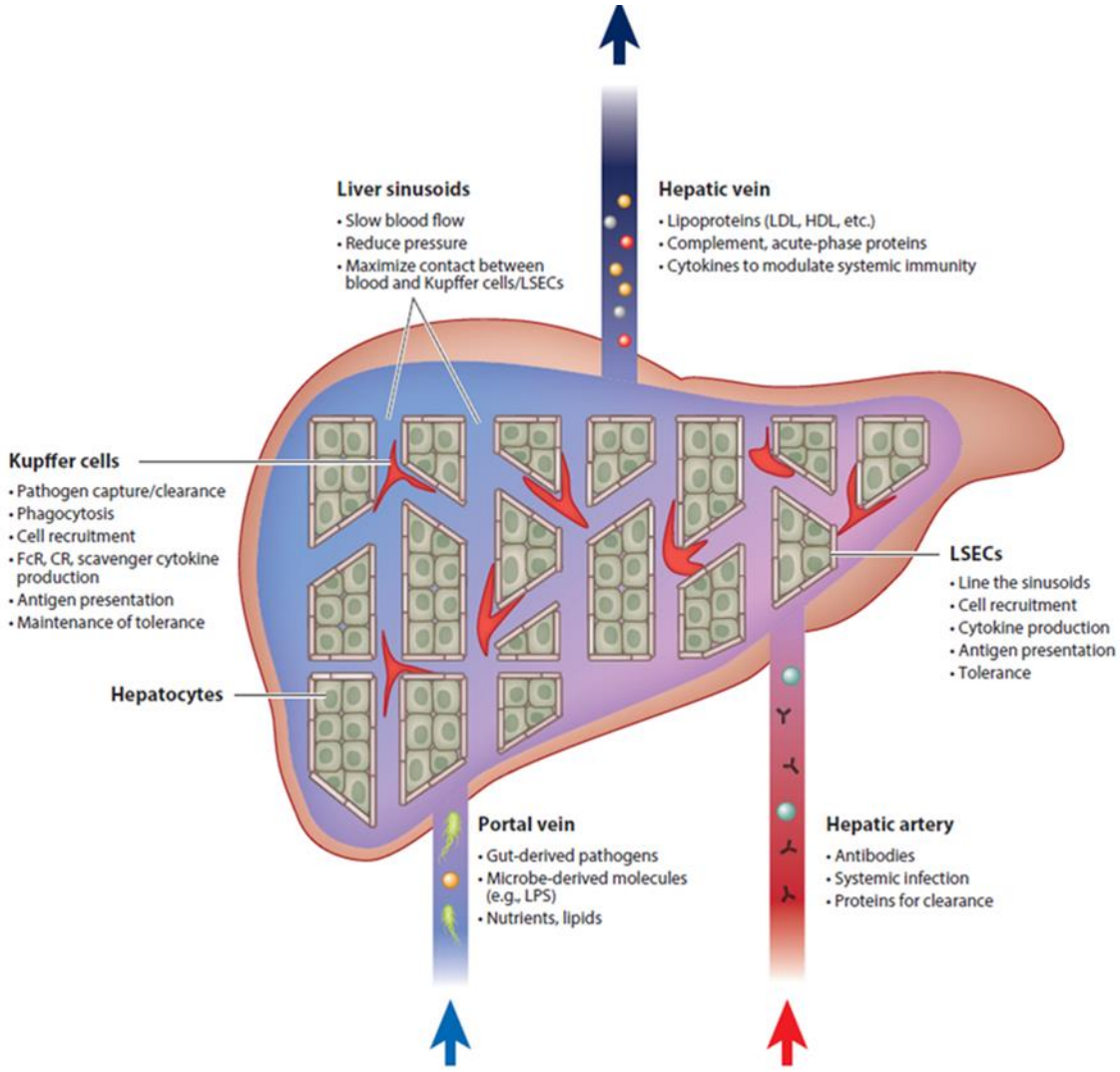

FIGURE 5: ANATOMICAL ORGANIZATION OF THE LIVER AS AN IMMUNE ORGAN (SOURCE IMGAE: KUBES ETAL., 2018, ANNUAL REVIEW OF IMMUNOLOGY [76])

Moreover, blood arriving from portal vein also contains a high quantity of microbial associated molecular patterns (MAMP) [77] and damage-associated molecular patterns (DAMP) [78] which binds to pattern recognition receptors (PRR) expressed by hepatocytes and liver-resident macrophages (Kupffer cells (KC)). Once binding to PRR, these MAMPs and DAMPs are phagocytosed and subsequently degraded by hepatocytes and KCs, without the production of inflammatory mediators that usually accompany PRR signaling. Hence clearing of blood from the

gut safeguards the rest of the body from, excessive immune activation and influences the unique immunological environment within the liver. Thus, the hepatic environment harbors one of the largest populations of immune cells in the body. In homeostatic conditions, leukocyte subsets and resident phagocytes can be found, which are well located within the different hepatic compartment such as intravascular and subcapsular (Figure 5). Conversely, the liver immune cell population can be rapidly and dramatically changed during inflammation, and this can be associated with the pathogenesis of several diseases such as HCC [76, 79].

Among various immune populations, our interest is to study the role of lymphocytes especially CD8, CD4 and T-regulatory cells (Adaptive immunity) and macrophages (innate immunity) during development and progression of HCC (Figure 6).

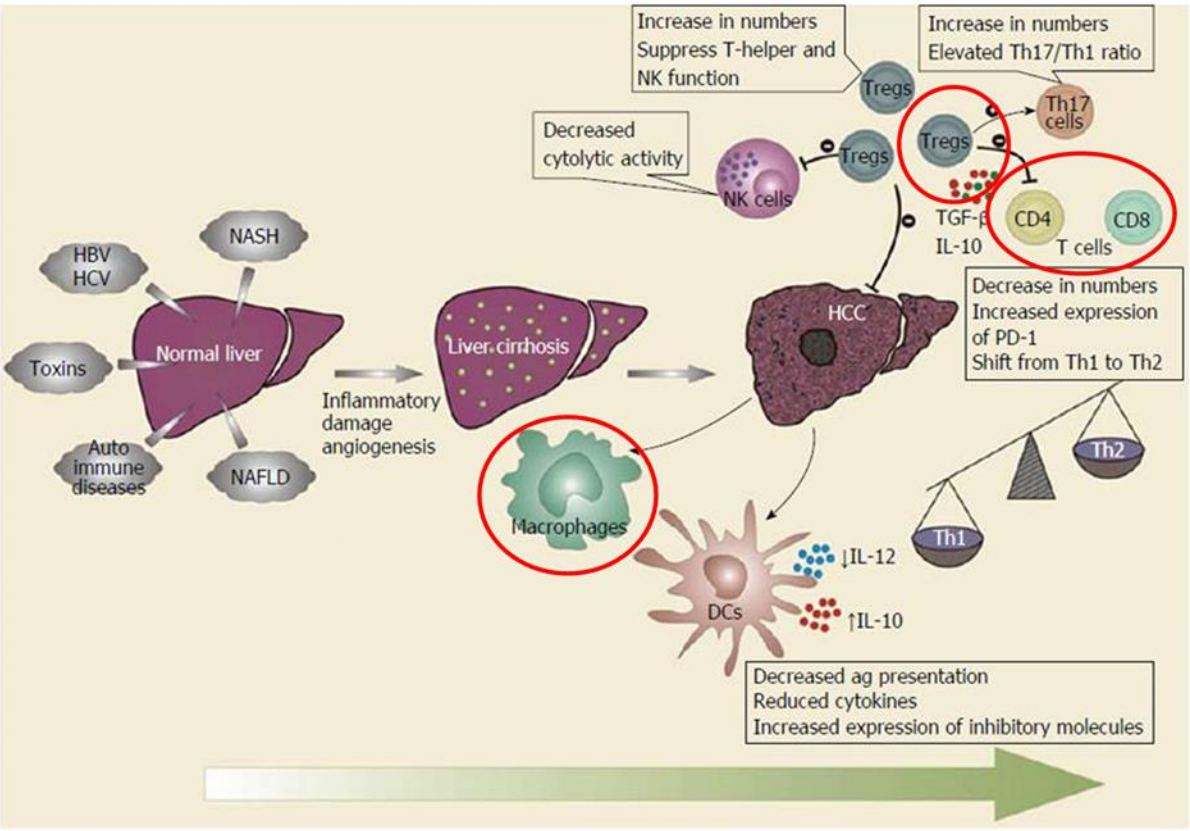

FIGURE 6: IMMUNE SYSTEM OF HCC (SOURCE IMAGE: SACHDEVA ET AL 2015 WORLD JOURNAL OF HEPATOLOGY [80])

1.3.1.1 Adaptive immunity (CD4, CD8 & T-regulatory cells)

In the liver, lymphocytes are among the commonest non-parenchymal cells, are present along the portal tracts as well as throughout the parenchyma. Normal liver contains resident large granular lymphocytes in the sinusoids. These cells enter the liver from the circulation via the sinusoidal endothelium and are retained in the sinusoids where they provide protection against viral infections and tumor cells. The Lymphocytes seen in the liver include conventional and unconventional lymphocyte subpopulation of innate (natural killer and natural killer T cells) and adaptive immune systems (T and B cells).

Conventional T lymphocytes involved in adaptive immunity include CD4 T cells, CD8 T cells, and γδ-T cells. CD4 T cells have at least five functional subsets, including helper T (Th)1, Th2, Th17, and follicular helper T cells, which tend to promote innate and adaptive immune responses, and the T-regulatory (Treg- CD4+CD25+Foxp3+ T cells) cells, which usually suppress the inflammation resulting from innate and adaptive immunity [81]. CD8 T cells which are composed of cytotoxic T cells are the main cell killer in adaptive immunity. γδ-T cells participate in both innate and adaptive immunity. Their function involves not only in immune effector pathways but also phagocytosis and tumor killing. Therefore, these T-cell subsets in adaptive immunity of the liver are highly orchestrated in terms of their roles and specific functions at each stage of various disorders [82]. In HCC CD4+ helper T cells and CD8+ cytotoxic T cells attribute a significant role in either inducing or inhibiting tumor cell progression.

1.3.1.1.1 CD4+Tcells & HCC

CD4+ T cells have opposing roles in chronic liver disease and HCC that range from effector cell function to regulate cell function. In terms of effector cell function, CD4 Th cells are essential for the CD8 T-cell response nevertheless, Th cells are reduced in HCC. Besides, tumor-associated antigen-specific CD4 Th cells are still detected in the circulation and hepatic tumors at lower frequencies in early stages of HCC although they are drained in advanced HCC [83, 84]. Among the CD4 T-cell subsets in HCC, Treg cells have the most important immunoregulatory role. It is well known that Tregs cells play a crucial role in the inhibition of the immune response [85] and their function is depending on the expression of transcription factor Forkhead box P3. Marked infiltration of Treg cells has been observed in the livers from patients with HCC, and the number of intra-tumors Treg cells is increased compared with the peritumor regions and periphery. They are also associated with tumor vascular invasion. However, the number of CD8 T cells in the liver decreases as the number of infiltrating Treg cells increases. Indeed, CD8 T cells proliferation and perforin production are also suppressed by the autologous Treg cells isolated from patients with HCC [86-88]. Furthermore, the secretion of inhibitory cytokines (Interleukin-10 (IL-10), Transforming growth factor-β (TGF-β) and so on) is one of the major immunosuppressive mechanisms of Treg cells [89]. Additionally, a study in an HCC mouse model showed that TGF-β promotes Treg differentiation in an HCC mouse model, which contributes to the progression of HCC [90]. This implies that Treg activation produces a positive, immunosuppressive feedback loop in HCC.

1.3.1.1.2 CD8+ Tcells & HCC

CD8+ T cells are the fundamental adaptive immunocytes that serve opposing roles in promoting a chronic pro-inflammatory microenvironment and in anti-tumor surveillance. CD8+ cytotoxic T

lymphocytes kill their target cells by direct contact and by lysing them via perforin, granzyme A and granzyme B in concert with signaling via the cell-surface receptor Fas and its ligand, FasL [91, 92], as well as via secretion of interferon-gamma (INF-γ) and tumor necrosis factor (TNF) [93]. Likewise, several HCC tumor-associated antigen-specific CD8 T cells such as alpha-fetoprotein [94], telomerase reverse transcriptase [95], the targeting protein for Xklp-2 [96], glypican-3, NY-ESO-1 [97], melanoma antigen gene-A and SSX-2 [98] have been identified. Among them the most common tumor-associated antigen is alpha-fetoprotein and its epitopes are recognized by specific CD8 T cells and are broadly distributed on the alpha-fetoprotein polypeptide, suggesting strong and broad immunogenicity [94]. However, tumor-associated antigen-specific CD8 T cells loses their ability to effectively suppress or kill malignant hepatic cells in individuals with HCC.

Besides, in established HCC impaired secretion of INF-γ, TNF, granzyme A and granzyme B by cytotoxic T lymphocytes has been reported; this correlates with an exhausted effector-cell phenotype, including upregulation of inhibitory receptors, such as PD-1, Cytotoxic T-lymphocyte antigen 4 (CTLA-4), etc. and leads to a poor prognosis [99].

1.3.1.1.3 CTLA-4 & HCC

CTLA-4, a transmembrane glycoprotein, is induced largely on activated T cells, including memory and regulatory T cells. It is constitutively expressed by regulatory T cells (Tregs) but is also expressed transiently by other types of T cells during the early phase of activation [100]. Moreover, CTLA-4 and CD28 are homologous receptors expressed by both CD4 and CD8 T cells, which mediate opposing functions in T-cell activation. Both receptors share a pair of ligands (B7 (CD80/CD86)) expressed on the surface of antigen-presenting cells. CD28 interacts with the CD80 dimer with relatively high affinity and the CD86 monomer with lower affinity, mediating T-cell costimulation in conjunction with T-cell receptor [41] signals. In contrast, interactions of the

ligands with CTLA-4 serve to inhibit T-cell responses, as the affinity of CTLA-4 to T cells activated via the B7/CD28 pathway (stimulatory signal 2) is greater that of CD28 (Figure 7). Thus, CTLA-4 binds to B7-1/B7-2 by competing with CD28 and transmits an inhibitory signal to the T cell [101]. Under normal physiological conditions, CTLA-4 terminates T cell activity, which is no longer needed to regulate excessive immune response mediated by T cells [102]. However, in cancer, CTLA-4 suppresses the proliferation (activation and production) of T cells that have undergone tumor-associated antigen recognition and differentiation which further functions as an immune checkpoint and down regulates an immune response.

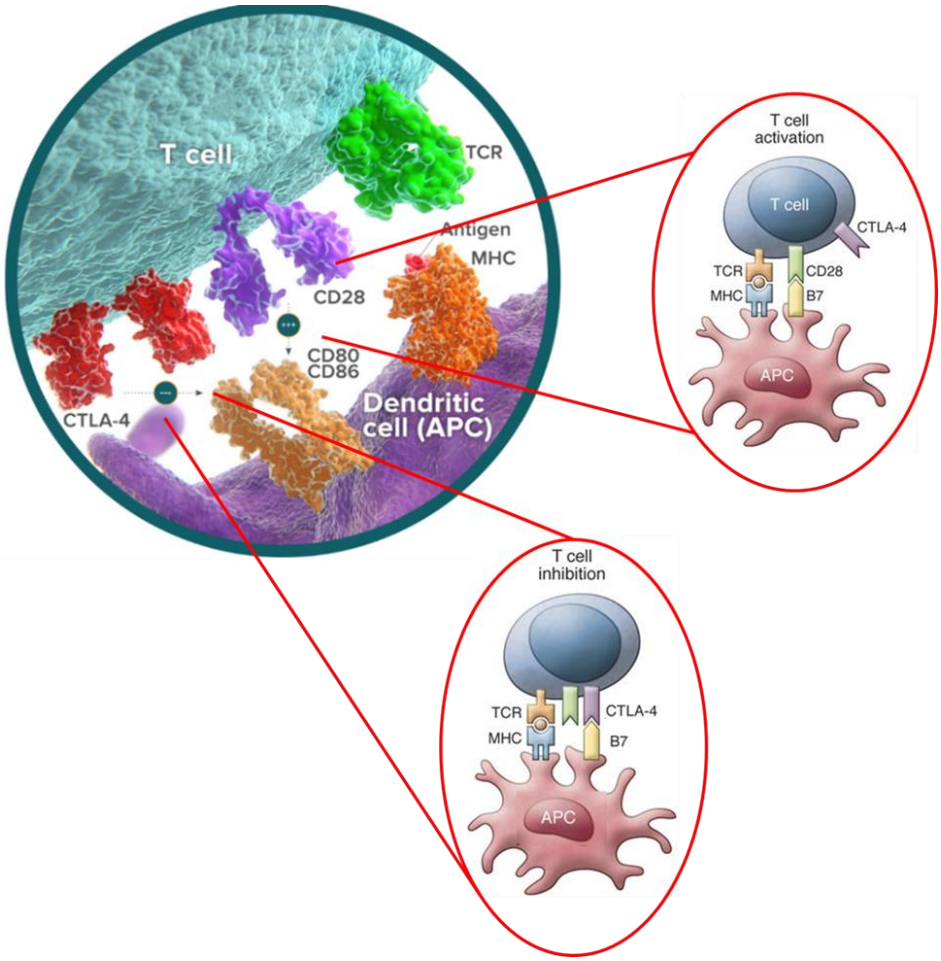

FIGURE 7: INHIBITION OF TCELL ACTIVITY BY CTLA-4

1.3.1.2 Hepatic macrophages (innate immunity)

Liver macrophages consist of ontogenically distinct populations, namely, the resident Kupffer cells (KCs) and monocyte-derived macrophages. KCs were first observed in 1876 by Karl Wilhelm von Kupffer, who described them as an integral part of the sinusoid endothelium and were initially called “Sternzellen” (star cells). Later, in 1898, after several years of research, Tadeusz Browicz correctly identified them as macrophages, and they received the name of Kupffer-Browicz cells, also known as Kupffer cells [103]. Further liver comprises the largest population of resident macrophages in the body representing ~80–90% of total fixed macrophages and 35% of the liver non-parenchymal cells [104, 105]. KCs are self-renewing and non-migratory phagocytes. They originate from yolk sac-derived specific progenitor cells that seed the liver during embryogenesis. In the tumoral microenvironment, chemokines secreted by malignant and stromal cells recruit bone marrow-derived monocytes. These infiltrating monocytes subsequently give rise to large numbers of monocyte-derived macrophages. Monocyte-derived macrophages further differentiate and can replace and acquire a phenotype that is almost indistinguishable from resident KCs under specific circumstances. After infiltration, monocyte-derived macrophages even seem to acquire the ability to proliferate [106, 107].

A key feature of macrophages is their ability to adjust and alter their responses according to environmental stimuli [108]. In general, macrophages possess a plastic phenotype [109, 110]. They exhibit two different polarized phenotypes: M1 macrophages or the “classically activated macrophages” and M2 macrophages also known as the “alternatively activated macrophages” [111, 112]. These different phenotypes are distinct in terms of morphology, surface markers and function.

M1 macrophages are polarized by IFN-γ, TNF and lipopolysaccharide (LPS). These macrophages are pro-inflammatory and anti-tumor macrophages and are linked to the activation of Th-1 immune response [113]. They secrete pro-inflammatory cytokines such as IL-1β, IL-6, IL-12 and TNF which aid in the liver inflammation. In addition, M1 macrophages express inducible nitric oxide synthase (iNOS) which is a key enzyme in generating nitric oxide (NO) from the amino acid L-arginine. NO has a potentially tumoricidal and cytotoxic effect on the tumor [114].

On the contrary, M2 macrophages which are polarized and activated by IL-4, IL-10, IL-13 and TGF-β [115], are anti-inflammatory pro-tumor and immunosuppressive macrophages and play a role in wound healing and tissue remodeling [111]. These macrophages activate the Th-2 immune response and secrete immunosuppressive cytokines such as IL-10 and TGF-β which recruit Tregs and exert an inhibitory effect on cytotoxic immune cells including CD8+ T cells and NK cells. Moreover, M2 macrophages promote angiogenesis and metastasis by secreting VEGF and matrix metalloproteases (MMPs), respectively.

While M1 macrophages express iNOS, M2 macrophages express Arginase-1 (Arg-1) which catalyzes the metabolism of L-arginine into urea and L-ornithine as a final step in the urea cycle. The resulting polyamines play a role in tumor proliferation [116]. By degrading arginine, Arg-1 deprives iNOS from its substrate and thus downregulates NO promoting the progression of tumors. M2 macrophages express specific markers such as transglutaminase-2 (TGM2) and Galectin-3.

1.3.1.2.1 TAMs and HCC

HCC, as any other type of cancers, utilizes its microenvironment as a factor for its development and progression. During HCC development tumor associated macrophages (TAMs) are recruited to the liver by several cytokines such as CCL2, TGF-β and Monocyte colony stimulating factor

[117]. These TAMs display a phenotype similar to that of M2 macrophages characterized by the expression of immunomodulatory cytokines and poor capability of antigen presentation capacity [118]. By interacting with liver stromal cells as well as other immune cells, TAMs exert an anti-inflammatory, pro-tumor and immunosuppressive role within the tumor environment [119]. This microenvironment favors the development and progression of HCC mediated by immunosuppression along with angiogenesis and metastasis.

As key players in fighting cancer, CD8+ T cells should infiltrate tumor areas and interact with cancerous cells. Interestingly, TAMs interact with CD8+ T cells impeding their infiltration to tumor islets and establishing a T cell-excluded tumor phenotype [120]. In fact, Tregs are recruited to the tumor microenvironment by TAMs where both secrete anti-inflammatory and immunosuppressive cytokines such as IL-10 and TGF-β which establish an immunosuppressive microenvironment that suppresses cytotoxic immune cells such as CD8+ T cells and NK cells rendering them dysfunctional [117]. This promotes the development of tumor and constitutes resistance to cancer immunotherapy.

Moreover, an imbalance in the Th1/Th2 cytokine milieu towards an increased Th2 profile is established by TAMs. Nevertheless, by secreting VEGF and MMPs, TAMs promote angiogenesis and metastasis[121]. These processes that are mediated by TAMs during HCC progression, prime many carcinogenic processes, but are not well known yet.

In addition, various molecular signaling pathways are involved in inflammation-mediated cancer and immune activation, and major signaling pathways of HCC are discussed further.

1.4 SIGNALING PATHWAYS OF HCC

HCC is a very complex molecular pathogenesis, with two major predominant mechanisms, such as fibrosis/cirrhosis associated with hepatic regeneration after tissue damage and alterations in three types of genes: proto-oncogenes, tumor-suppressor genes and stability genes [122-124]. Among the mutated genes in HCC, TP53 is at the top, and its mutation frequency varies by approximately 25.9% of HCCs [125]. Besides, promoter mutation of telomerase (encoded by the TERT gene) has been seen in 54% of human HCCs and 25% of cirrhotic preneoplastic nodules, which could be the earliest recurrent genetic event in hepatocarcinogenesis [126, 127].

In addition, HCC is also a highly vascularized tumor, and the central role of angiogenesis in its initiation, growth and subsequent dissemination to other tissues, is well recognized. Angiogenesis in HCC is dependent on endothelial cell activation, proliferation and migration, which occur in response to angiogenic cues (e.g., inflammation) and involve several molecular effectors—such as growth factors, extracellular matrix proteins, and proteases [128]. The binding of growth factors to their receptor proteins activates the protein-phosphorylating enzymes, thus activating a cascade of proliferative signaling pathways to transmit proliferative signals into the nucleus. Growth factors, such as the epidermal growth factor (EGF), transforming growth factor (TGF)-α/-β, insulin-like growth factor (IGF) and vascular endothelial growth factor (VEGF), also function in liver regeneration after injury, while the fibroblast growth factor (FGF) and the platelet-derived growth factor (PDGF) families are involved in liver fibrosis and HCC growth [129]. Many of the growth factor receptors and oncogenes have tyrosine kinase activity, which are classified into transmembrane receptor tyrosine kinases—such as the EGFR and VEGFR. On the other hand, Raf, MAP kinase/extracellular signal-regulated kinase (ERK) and mammalian target of rapamycin (mTOR) are serine/threonine kinases. In general,

the mitogen-activated protein kinase (MAPK), phosphoinositide 3-kinase (PI3K)/Akt/mTOR signaling pathways, and the VEGFR and PDGFR signaling cascades show altered activity in the HCC. Additionally, the key signal transduction pathways that have been implicated in the pathogenesis of HCC, mediated by receptor tyrosine kinase, are EGF/EGF receptor (EGFR), VEGF/VEGF receptor (VEGFR), PDGF)/PDGF receptor (PDGFR), IGF/IGF receptor (IGFR), and the Ras/Raf/MEK/ERK, Wnt/β-catenin, and PI3K/phosphatase and tensin homologue deleted on chromosome ten (PTEN)/Akt/mTOR signaling pathways, IL-6, signal transducer and activator of transcription (STAT) and hedgehog signaling pathways.

Among all the pathways, nearly 50% of patients with HCC have shown activation of the AKT/mTOR pathway, which may be partially attributable to activation signals from receptor tyrosine kinases such as IGFR and/or EGFR pathways [130]. Hence, here we mainly focus on RAF/ERK/MAPK and (PI3K)/Akt/mTOR signaling pathways, which are elaborated further.

1.4.1RAF/ERK/MAPK PATHWAY

The ubiquitous signal transduction pathway i.e., the RAF/ERK/MAPK pathway, regulates crucial cellular processes, including proliferation, differentiation, angiogenesis and survival [131]. Signals from membrane-bound tyrosine kinase receptors, such as EGFR, IGFR, vascular EGFR, c-Met and PDGFR, are transduced to the cell nucleus through the Ras/RAF/MAPK pathway, in order to regulate multiple cellular functions, including cell growth and survival, and differentiation. Essentially, the overexpression or activation of components of this pathway is believed to contribute to tumorigenesis, tumor progression and disease metastasis in a variety of solid tumors, including HCC [132].

In the mechanism of the RAF/ERK/MAPK pathway, the MAPK intracellular signaling pathway consists of serine/threonine kinases, which is mainly involved in cell growth and survival. It regulates cell differentiation and is upregulated in cancer cells. The MAPK pathway is a common downstream pathway for EGFR, PDGFR and VEGFR, and is universally used for the signal transduction downstream of cytokine receptors, integrin complexes and G-protein receptors to Ras. The downstream ERK is activated by two upstream protein kinases, which are coupled to growth factor receptors by Ras proteins. Ras, which is activated by ligand binding, activates Raf serine/threonine kinases and MEK (MAP kinase/ERK kinase), while MEK phosphorylates and activates ERK, which phosphorylates the proteins involved in cell growth, apoptosis resistance, extracellular matrix production and angiogenesis [133]. Hence, the MAPK pathway plays an important role in HCC, in that, its activation is reportedly involved in HCC growth and survival [130].

A large amount of preclinical and clinical evidence has shown that the abnormal activation of the Ras/RAF/MEK/ERK signaling pathway frequently results in HCC [131, 134-137]. All research results showed that the activation of the Ras/RAF/MEK/ERK pathway may lead to HCC development functionally. However, its effective blockade can be achieved using inhibitors such as sorafenib or regorafenib (presented in treatment of HCC part) [138]. Besides, the long term usage of these inhibitors lead to the resistance and activation of pathways, such as PI3K/Akt, and upregulate the phosphorylation of its downstream targets, such as mTOR, the activation of hypoxia-inducible pathways and epithelial-mesenchymal transition [139].

1.4.2PI3K/AKT/mTOR Pathway

The PI3K/Akt/mTOR pathway is a major intracellular signaling cascade that is involved in the regulation of cell growth, proliferation and survival. In the mechanism of activation of the PI3K/Akt/mTOR pathway, the membrane lipid phosphatidylinositol 4,5-bisphosphate (PIP_2) is phosphorylated by phosphatidylinositol 3-kinase into phosphatidylinositol 3,4,5-triphosphate (PIP_3), binds to and activates the serine/threonine kinase Akt [140]. Once activated, the Akt activates downstream signaling effectors to regulate cell survival, proliferation, cell cycle progression, migration and angiogenesis. Akt then induces the activation (phosphorylation) of mTORC1, a serine/threonine kinase. The mTOR protein, in turn, regulates its downstream effectors, p70S6 kinase and translational repressor protein 4E-BP1 by phosphorylation. It is known that both of the proteins regulate the translation of several important proliferative and angiogenic factors, such as c-myc, cyclinD1, HIF1α and VEGF [141, 142]. While the PI3K/Akt/ mTOR signaling is also known to be activated by various growth factors and cytokines, this pathway can also be negatively regulated by the PTEN homolog deleted on chromosome 10, a well-known tumor suppressor, which dephosphorylates PIP3. Other than PTEN, there are also several negative regulators, such as SH2- containing inositol phosphatase-1 and PITenins [143, 144]. Moreover, comprehensive cancer genomic analyses have recently revealed that components of the PI3K pathway, frequently alter HCCs and the mechanisms that are dysregulated by PI3K/Akt/mTOR pathway are the gain-of-function mutation or amplification of PIK3CA, the p110a catalytic subunit [145], amplification or increased activity/expression of PIK3CB, the p110b catalytic subunit [146], the loss-of-function of PTEN through gene deletion, mutation, or epigenetic silencing [147], amplification or mutation of the Akt isoforms (mainly Akt1 and Akt2; while Akt3 mutations are very rare) and ppstream activation through RTK signaling—for example the EGFR family or IGF1-R [148].

Nearly 50% of patients with HCC have shown the activation of the AKT/mTOR pathway [130] which may be partially attributable to activation signals from receptor tyrosine kinases, such as IGFR and/or EGFR pathways [130]. Interestingly, a study conducted by Zhou et al. demonstrated that the PI3K/Akt/mTOR pathway is more significantly activated in high-grade HCC tumors and is associated with the poor prognosis in HCC patients [149]. All these evidences indicate that the activation of the PI3K/Akt/mTOR pathway may functionally contribute to HCC progression.

Overall, growing evidence shows that AKT is an essential actor in liver cancer tumorigenesis and progression and a potential target in the management of HCC. Thus, we postulate that a therapy with an AKT inhibitor will be able to treat a fully developed HCC, by inhibiting the PI3K/Akt/mTOR pathway. Moreover, the AKT inhibitor may prevent/overcome the sorafenib resistance in HCCs. Therefore, the combination of sorafenib with AKT-inhibitors represent new therapeutic strategies, which can improve treatment effectiveness in HCCs.

1.4.2.1 Inhibitor of PI3K/AKT/mTOR pathway

As we have seen that activation of PI3K/AKT/mTOR pathways play a crucial role in HCC development and progression, therefore, it is an attractive target for the treatment of HCC (pharmacological intervention). The first PI3K pathway-target agents approved for the treatment of cancer were the rapamycin analogs—Everolimus and Temsirolimus, which allosterically inhibit mTORC1 [150]. The treatments targeting the PI3K/AKT/mTOR pathway are illustrated in Figure 8.

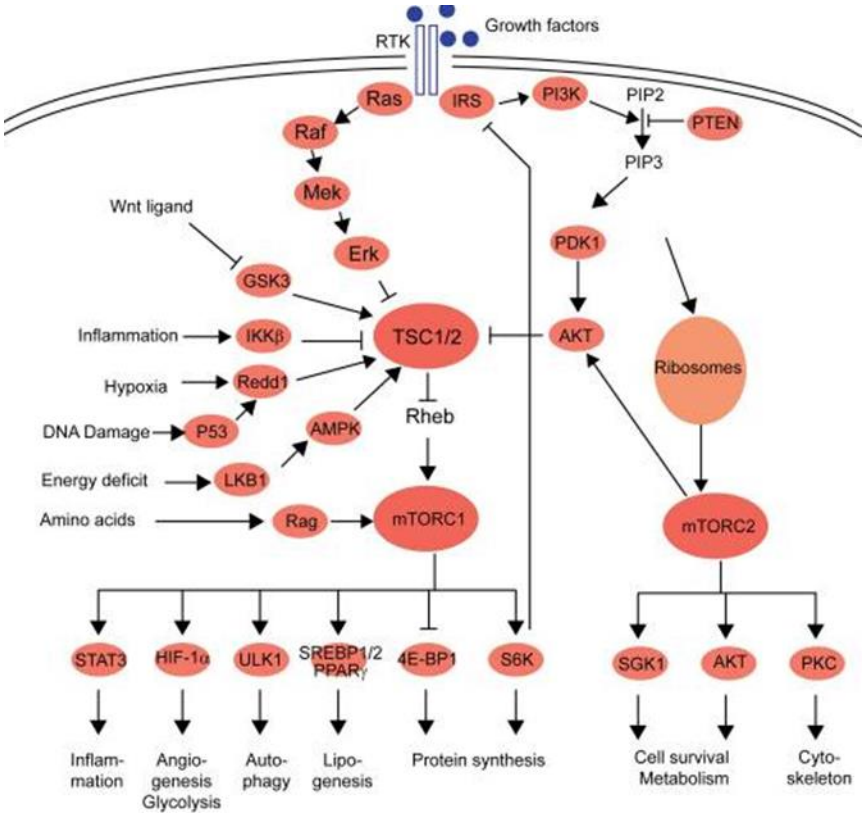

FIGURE 8: INHIBITORS OF PI3K/AKT/MTOR PATHWAY (SOURCE IMAGE: MATHAIAS.S.M ET AL, 2014, JOURNAL OF HEPATOLOGY (MATTER, 2014 #596))

Currently, allosteric and catalytic AKT inhibitors are being investigated as advances in drug design in clinical studies is reached [151]. Among them, the allosteric inhibitors ARQ 092 and its next generation ARQ 751, synthesized by ArQule, Inc., are interesting, as they bind to both the active and inactive forms of AKT [152].

1.4.2.1.1 AKT inhibitor – ARQ 751 (by ArQule)

ArQule is a biopharmaceutical company, engaged in the research and development of targeted therapeutics to treat cancers and certain rare diseases. This company develops and commercializes novel, small molecule drugs. To date, five drug candidates were synthesized, all of which are in targeted and biomarker-defined patient populations, making ArQule a leader in precision medicine. Among them, we are interested in studying ARQ 092 and its next generation ARQ 751 (synthesized

by ArQule, Inc.), which are highly potent and selective allosteric inhibitors of AKT. The general chemical structures of ARQ 092 and ARQ 751 are demonstrated in Figure 9 [152], and differ from their R1, R2 and R3 groups.

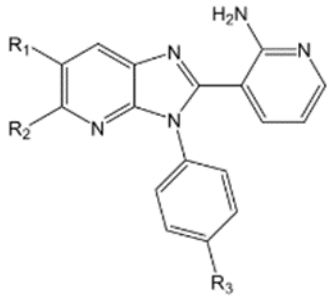

R1, R2 and R3 are substituted or unsubstituted alkyl or aryl groups

FIGURE 9: CHEMICAL STRUCTURE OF THE CORE MOIETY OF ARQ 092 AND ARQ 751 [152] (SOURCE IMAGE: SAVAGE ET AL, 2015, PLOS ONE [152])

Of course, we have previously reported that the preclinical characterization of ARQ 092 showed a strong affinity for unphosphorylated full-length AKT1, and it potently inhibited the phosphorylated form of full-length AKT isoforms. Moreover, we also demonstrated that the potent effect of ARQ 092 exhibited anti-proliferative activity and strong anti-tumor activity in an in-vivo model of carcinogen-induced HCC [153, 154]. Therefore, we are further interested in testing the curative effect of a new allosteric inhibitor of AKT, ARQ 751, as it displayed a six-fold better affinity for AKT than the ARQ 092 (0.6 nM and 0.8 nM for Akt1 and Akt2, respectively), which is the highest affinity described so far in the anti-AKT elements currently being tested in clinical trials [152, 155].

The proposed pathway inhibition by ARQ 751 is presented in Figure 10, where it binds to both the active and inactive forms of AKT and suppresses not only the AKT activation of the active form

(as do ATP-competitive inhibitors) but also of the inactive form, by disrupting its membrane translocation.

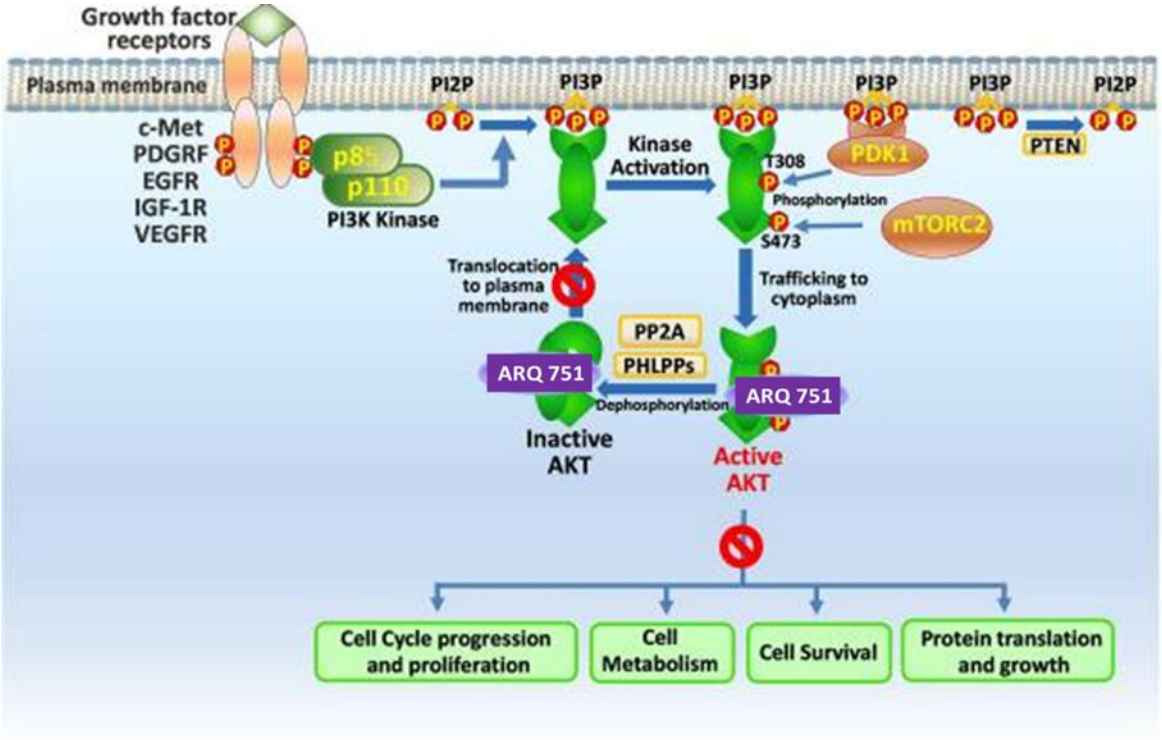

FIGURE 10: AKT PATHWAY INHIBITION BY ARQ INHIBITORS: ARQ 751 (SOURECE IMAGE: YU, SAVAGE ET AL, 2015, PLOS ONE [152])

However, in order to identify specific adverse effects that could be related to the background of cirrhosis, this newly developed therapeutic strategy should be pre-clinically tested in an appropriate animal model. As fibrosis/cirrhosis modifiy liver vascularization, extracellular matrix composition and drugs metabolism, it is essential to use a cirrhotic animal model to test HCC drugs, in order to test their efficacy on tumors but also tolerance to the treatment. Details of different animal models of HCC are illustrated further.

1.5 ANIMAL MODEL OF HCC

Animal experimentation has played a crucial role in cancer research, throughout history [156]. In HCC studies, animal models have become increasingly important, due to the physiological and genetic similarities between rodents and humans, the short lifespan and the breeding capacity of rodents [157]. Establishing potent animal models that are analogous to human disease settings, for both basic and translational research of HCCs, is challenging due to the complex etiology and tumor heterogeneity of human HCCs. Therefore, an "ideal" animal model must be able to reproduce human HCC genetically, anatomically and patho-physiologically [158] (Figure 11). Moreover, the ideal animal models must be fundamental tools to help evaluate potential novel therapeutic drugs in preclinical trials, and also contribute to the development of molecular target therapeutic strategies of HCCs [159].

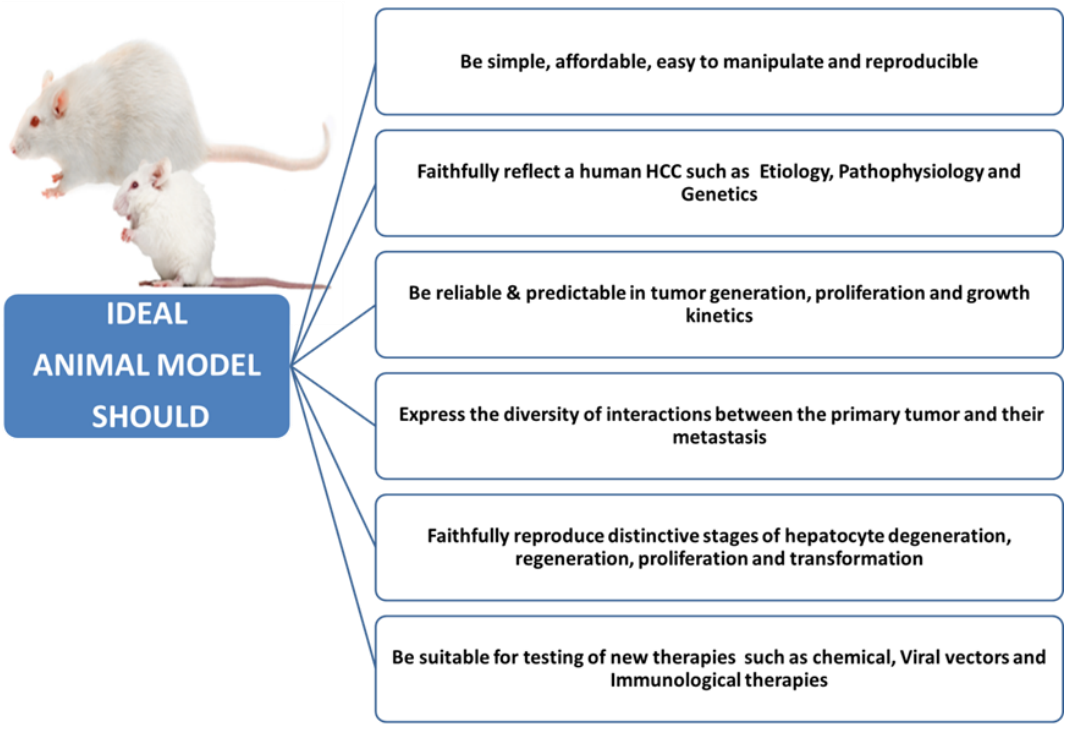

FIGURE 11: CRITERIA OF AN IDEAL ANIMAL MODEL

A relatively wide range of animal models to study HCC are currently available, which can be categorized as follows: 1) chemically induced models, 2) xenograft models and 3) genetically modified models (Figure 12).

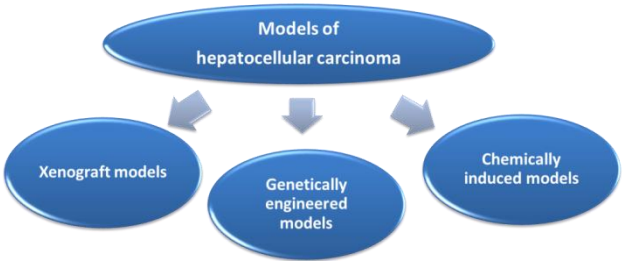

FIGURE 12: MODELS OF HCC

Among them, the chemically induced models are widely used to study HCCs. As several genetically modified mouse models (GMM) developing HCC often represent one, or a few specific mutation(s), while natural tumors are a dynamic environment, consisting of a heterogenic cell population with different genotypes, which can change over time as a response to variable external conditions [160]. Xenograft models are relevant for fast drug screening and proof-of-principle experiments [161], but face similar limitations as the GMMs, since only one cell phenotype is assessed, while tumors exist of a large variety of phenotypes. Results should always be interpreted with care, because introducing foreign cells in an animal system, as done in a xenograft mouse model, creates an altered physiological interaction between the tumor and the environment [162], leading to spectacular results that can seldom be confirmed in cancer patients [163].

Therefore, chemically induced models are favorable for research that require HCCs to develop in the natural background of liver damage; the details of chemically induced models are illustrated further.

CHEMICALLY INDUCED MODELS

Chemically induced animal models have been remarkably faithful in revealing underlying mechanisms of carcinogenesis such as both genetic and environmental factors that influence cancer susceptibility in the human population [164]. Moreover, the chemically induced models are favorable when HCC development on the natural genetic background is considered, especially when compared to other animal models of hepatocarcinogenesis such as xenograft models and genetically induced models. Therefore, these characteristics of chemically induced models favoring them to study the tumor microenvironment and the immune reaction against the tumor. Several chemical carcinogenic compounds are able to induce carcinogenesis after acute, short, or long-term exposure, depending on, the chemical structure, chemical concentration, animal species and animal susceptibility.

Therefore, depending on their activity and specific pathogenic mechanism, chemical carcinogenic compounds are categorized as either genotoxic carcinogens or non-genotoxic carcinogens [165] [166].

1.5.1 GENOTOXIC CARCINOGEN INDUCED MODELS

Cancer is induced by genotoxic or direct-acting carcinogens such as diethylnitrosamine, aflatoxins, etc. that interact directly with DNA through the formation of covalent bonds, resulting in the DNA-carcinogen complexes (DNA adducts).

1.5.1.1 Diethyl nitrosamine induced model (DEN)

DEN is widely reported to be found in the environment, in tobacco smoke and is also synthesized endogenously. The presence of DEN in wide varieties of foods, such as cheese, soybean, smoked,

salted and dried fish, cured meat, alcoholic beverages, and groundwater having high level of nitrates makes the human population vulnerable to its exposure [167]. DEN is an N-nitroso compound which is well known for the mutagenic, teratogenic and carcinogenic activity and it belongs to the category of genotoxic chemical carcinogens, as it damages DNA. Moreover, DEN is frequently used to induce liver fibrosis and HCC in rodents. Once DEN is administrated to rodents, a series of chemical reactions undergo. Firstly DEN is hydroxylated to alpha-hydroxyl nitrosamine which is mediated by cytochrome P450 an enzyme that is activated in centrilobular hepatocytes. After further modification as seen in Figure 13 diazonium hydroxide and carbonium ion are formed, which causes DNA damage by reacting with nucleophiles such as DNA-bases (Figure 13) [168]. Besides, DNA damage can also occur by oxidative stress, which is generated by the P450-dependent enzymatic system inducing oxidative stress by the formation of hydrogen peroxide and superoxide anions (Figure 13) [169]. Thus, these principle metabolizing pathways induced by DEN in rodent models are similar to human carcinogenesis when compared [170]. Therefore, due to these carcinogenic properties of nitrosamines, the application of DEN has become highly attractive for inducing liver tumorigenesis in rodents as an experimental model of human HCC and also become a well-established model for studies aimed at understanding the pathogenetic alterations underlying the formation of liver cancer.

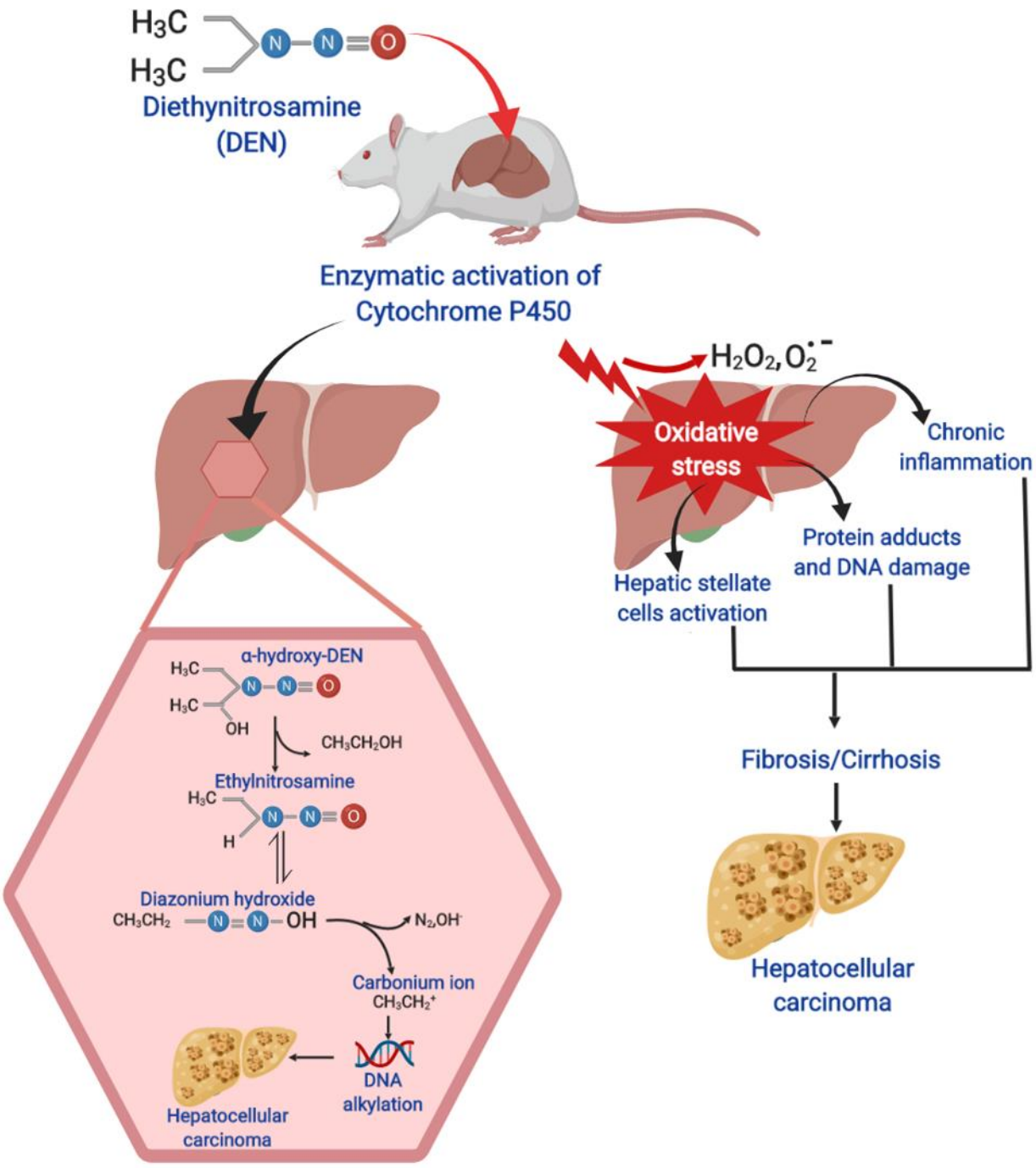

FIGURE 13: MECHANISM OF DEN INDUCING HEPATOCELLULAR CARCINOMA

HCC developed by DEN depends on specific characteristics such as species, the dosage of administration, age and sex of the rodents.

Species dependent: Regardless of the etiology, the liver tumors usually originate on the background of fibrosis, cirrhosis and finally culminate in HCC [171]. Besides, liver fibrosis and cirrhosis are not only critical risk factors in the development of HCC, but also the most significant risk factors for HCC recurrence and postoperative complications [172]. Therefore, the development of fibrosis and cirrhosis followed by HCC in animal models are crucial, but most DEN-induced hepatocarcinogenesis mice models do not feature liver fibrosis, calling into question whether these models can reliably recapitulate key events observed during human hepatocarcinogenesis and HCC progression. Besides, DEN-induced hepatocarcinogenesis in rats recapitulates the human scenario of developing HCC followed with fibrosis and cirrhosis [153] [173].

Dose dependency – HCC development by DEN: Indeed, prolonged oral feeding or parenteral application of DEN in rodents at high doses is extremely effective in inducing hepatic tumors [174]. Besides, detailed studies performed with DEN in F344 rats have confirmed that DEN carcinogen is highly reproducible and will dose-dependently induce liver damage within defined thresholds [153, 175]. A dose-dependent formation of carcinomas after a single injection (5–90 mg/kg) of DEN in 15-day-old mice is observed after 45–104 weeks [176, 177].

Age and sex dependency – HCC development by DEN: Several studies on HCC development by DEN demonstrated the importance of age and sex of the rodents. For instance, single low doses of DEN have shown that the livers of infant mice are the most susceptible to the inception of carcinogenesis [178]. The time and percentage of tumor development differ between strains [179-181]. Moreover, the incidence of HCC development is gender-dependent rodents, with a high prevalence in males, similarly as in humans. Several studies have also demonstrated that female mice and rats are largely resistant to DEN-driven hepatocarcinogenesis [182, 183]. Therefore, in

order to avoid unnecessary complications and to reduce the number of experimental rodents, it is recommended that male rodents are used exclusively.

DEN combination with other carcinogens: HCC induced by DEN is often combined with another non-genotoxic carcinogen (tumor promoters) which is known as two-stage model. In this two-stage model, DEN is used as an initiator and non-genotoxic carcinogen such as phenobarbital [184], and carbon-tetrachloride etc. are used as promoting agents [185]. However, the effects of phenobarbital promotion on DEN-initiated mice also vary considerably depending upon strain, sex and age of the mice [186]. Besides, combination of DEN and carbon-tetrachloride was employed in a landmark study in which the contribution of the toll-like receptor 4 signaling the development of hepatic inflammation, fibrosis and a setting of HCC [187, 188].

DEN induced models and immune response: DEN induced models are being a promising tool to study the role of immune response and the tumor microenvironment in the process of hepatocarcinogenesis development. For instance, Carlo Schneider et al, with the help of well-established DEN induced HCC model in mice, showed that liver tumor development provokes local and systemic inflammatory responses, characterized by intrahepatic induction of distinct pro-inflammatory (macrophage and T-cell attracting) chemokines, intrahepatic accumulation of macrophages and CD8 cytotoxic T cells and extrahepatic expansion of myeloid-derives suppressor cells [189]. Likewise, Tao Wei et al., hypothesized that G protein-coupled estrogen receptor activation may be a potential strategy for the prevention and treatment of HCC by demonstrating the role of G protein-coupled estrogen receptor against HCC tumorigenesis through regulating inflammatory responses in DEN induced HCC model [190]. More immune system studies using DEN induced models are presented in Table 1.

Chemically induce model	Strain /Sex	Dose, Age & administration route	Fibrosis	HCC development	Immune system study or tumor micro environment
DEN, Mice	C57BL/6j - mice, male, i.p	25-35mg/kg, 14-15 days old, i.p	No information	8 months after DEN administration	Pro-inflammatory myeloid cell surface receptor TREM-1 expressed by Kupffer cells is a crucial factor in the development and progression of liver cancer. [191]
				8 months after DEN administration	Therapeutic effect of hyper IL-15 in promoting tumor specific CD8+Tcells responses to suppress metastasis of liver cancer. [192]
				8 months after DEN administration	Role of nicotinamide adenine dinucleotide phosphate oxidase 1 (NOX1), in HCC progression. Ablation of NOX1 in macrophages dramatically abolishes NOX1's HCC promoting activity by diminishing inflammatory cytokine production from macrophages.[193]
				22 weeks after DEN administration	Roles of CXCR6-dependent immune mechanisms in hepatocarcinogenesis. [194]
				24 weeks after DEN administration	Over expression of nitro domain containing protein 1 (NOR1) in tumor associated macrophages accelerate HCC carcinogenesis through promoting M2 polarization and TAMs mediated inflammation. [195]
			++	30 weeks after DEN administration	Role of hepatic neutrophil and their tumor promoting activity for the development of carcinogen-induced HCC. [196]
			++	8 months after DEN administration	Inhibition of IL18 production of TLR2 which further suppressed tumor induced immunosuppressive network in HCC. [197]
			No information	42 weeks after DEN administration	Role of adaptive immune cells in controlling the early tumor formation and the growth of established tumors. [189]
	Male mice	35mg/kg - 5 weeks old, i.p	No information	20 weeks after DEN administration	Role of TGF-β in HCC tumorigenesis and development by inducing polarization of Treg. [90]
	C57BL6/ J-mice, Male	DEN-25mg/kg - 14 days old +CCL4-0.6ml/kg in corn oil -8weeks old, i.p	++	24 weeks	Characterizing the role of $CCR2^{+}$ monocyte-derived TAMs in the tumor-prone environment of fibrotic livers. [198]
	Lysm-Cre (Stk4 fl/fl), male	DEN (100mg/kg) - 8 weeks old, CCl4 (0.5ml/kg)-12 weeks for 12 weeks , i.p	++	28 weeks	STK4 as a promising strategy for interrupting the pro-inflammatory microenvironment and blocking of HCC. [199]
DEN, Rats	Male (120±20g)	8mg/kg/day -for 6 weeks, intra gastical	+++	16 weeks	Influence of tumor associated immune cells in HCC progression plus the role of DCs, Treg and Breg in enhancing tumor specific immune response in different stages of HCC development.[200]

	Sprague–Dawley, Female, 5-6 weeks	**100mg/kg for initiation, i.p**	**++**	**20 weeks after DEN administration**	**Potential role of estrogen in inhibiting lung metastasis from rat HCC in vivo through modulation of inflammatory tumor microenvironment via suppression of HGF and IL-6 production. [201]**
	Sprague–Dawley, Male (160-180 g)	**70mg/kg for 6 weeks, i.p**	**+++**	**10 weeks**	**Mechanism associated with p53 activation and hepatic inflammation during HCC. [202]**
	Sprague–Dawley, Male, 6 week	**0.4%(w/vol), oral**	**+++**	**24weeks**	**Sympathetic nervous system role in activation of alpha1-adrenergic receptor of Kupffer cells to promote hepatocarcinogenesis. [203]**
	Male SD, 10-12 weeks	**100 p.p.m (95µg/ml) for 13 weeks, oral**	**+++**	**10-13 weeks**	**Role of TNF-α in liver injury and tumorigenesis. [204]**

TABLE 1: TUMOR MICROENVIRONMENT STUDY OF HCC IN DEN INDUCED HCC ANIMAL MODELS.

1.5.1.2 Aflatoxins

Aflatoxins are a mycotoxin that is primarily produced by the food-borne fungi *Aspergillus flavus* and *Aspergillus parasiticus*, which colonize a variety of food commodities, including maize, oilseeds, spices, groundnuts, and tree nuts in tropical and subtropical regions of the world. There are four major aflatoxins known as B_1, B_2, G_1, and G_2 [205]. Among them, AFB1 is well-known as the most potent naturally occurring biological carcinogens with activities such as acute toxicity, teratogenicity, mutagenicity and carcinogenicity [206]. AFB1 is also a genotoxic hepatocarcinogen

that presumptively causes cancer by inducing DNA adducts, leading to genetic changes in the target cells, which then cause DNA strand breakage, DNA base damage and oxidative damage that may ultimately lead to cancer [207].

Liver is the targeted organ for the metabolism of AFB1, where its mechanism of action initiates. Firstly, AFB1 is biotransformed by the cytochrome-P450 enzyme, which results in the production of a reactive intermediate chemical compound, aflatoxin B1-8, 9-oxide. This highly reactive genotoxic compound binds to liver cell DNA as a result, DNA adducts are formed, namely 8, 9-dihydro-8 (N7guanyl)-9-hydroxy-AFB1 (AFB1 N7-Gua). Therefore, this DNA adducts further interact with the guanine base of the DNA and cause mutational effects resulting in hepatocarcinogenesis [208, 209]. Thus, AFB1 exposure in food is a significant risk factor for HCC [210].

AFB1 carcinogenic potency is not only known in humans but also well established in rodents. Its carcinogenicity also depends on certain parameters such as route of administration, level and frequency of dose, and the sex, age, and strain of the test animal. Studies by Wogan et al, demonstrated that when aflatoxin was chronically administrated to rats at levels of 1, 5, 15, 50, and 100 parts per billion, the incidence of the liver tumor were increasing respectively (as such 9, 4.5, 19, 80, and 100%) [211]. Thus, from this study it's clear that even a small dosage of aflatoxin per day could induce liver cancer. Hence, this finding provided a context for human cancer investigations exploring the linkage between aflatoxin and HCC. Although administration to newborn mice produces liver tumors, adult mice are resistant to aflatoxin hepatocarcinogenesis due to the glutathione S-transferase enzyme which detoxify AFB1 metabolite [212].

As AFB1 induced hepatocarcinogenesis is more or less similar in human and rodents. AFB1 induced rodents' models help us to better understand the immunomodulation's in hepatocarcinogenesis. For instance, immunosuppression by AFB1 can result from various mechanisms such as decreased protein and/or DNA synthesis, changes or loss in enzymatic activity, and changes in metabolism or cell cycles, which may result in apoptosis or necrosis. Immune mechanisms affected by AFB1, in addition to T-cell dependent immunity, include reduced production of complement by the liver and decreased phagocytosis by neutrophils and macrophages [213, 214]. Toxic effects of AFB1 on T-lymphocytes and/or other lymphoid cells such as the cytotoxic T-cells and natural killer cells, which impair the function of direct or indirect killing of tumor cells, can have pronounced effects on tumorigenesis [215].

1.5.2 NON-GENOTOXIC CARCINOGEN INDUCED MODELS

Non-genotoxic carcinogen-induced models are induced by the chemicals such as carbon tetrachloride, phenobarbital [184], and thioacetamide etc., which have no direct interaction with DNA. They cause tumors by disrupting cellular structures and by altering the kinetics of either cell proliferation or of a process that increases the risk of genetic error. Details of non-genotoxic induced models by carbon tetrachloride, phenobarbital and thioacetamide are illustrated below.

1.5.2.1 Carbon tetra chloride (CCl4)

CCl4 as a non-genotoxic carcinogen has been widely used to experimentally induce liver injury in rodents [216]. Liver cell injury induced by CCl4 involves initially the metabolism of CCl4 by cytochrome P450 superfamily of monooxygenases (CYP family) to form trichloromethyl (CCl3) free radical [217]. Subsequently, this radical reacts with nucleic acids, proteins, and lipids, thereby impairing key cellular processes resulting in altered lipid metabolism (fatty degeneration and

steatosis) and lowered protein quantities. Besides, the formation of trichloromethyl peroxy radicals resulting from oxygenation of CCl3 further initiates lipid peroxidation and the destruction of polyunsaturated fatty acids. Consequently, the membrane permeability in all cellular compartments (mitochondria, endoplasmic reticulum, and plasma membrane) is lowered and generalized hepatic damage occurs that is characterized by inflammation, fibrosis, cirrhosis and HCC. In the most routinely followed strategy, CCl_4 is injected intraperitoneally 2 to 3 times per week during 4 to 6 weeks at a dose range of 300 to 1000 µl/kg resulting in robust and highly reproducible liver fibrosis [218]. Alternatively, CCl_4 can be administered orally, subcutaneously or through inhalation.

Secondly, CCl4 also causes the induction of an inflammatory response by Kupffer cells through the production of cytokines, chemokines and other proinflammatory factors, causing severe centrilobular necrosis [219]. Hence, CCl4 induced HCC models can help to determine role of inflammatory responses in chronically injured liver towards the development of HCC. For instance, Delire et al evaluated the potential roles of macrophages infiltrated within the tumor in mice chronically treated with CCl_4 for 7 weeks (CCl_4 7w group) [220]. Besides, several studies have shown that CCl4 is used as a tumor promoter in combination with DEN in two-stage HCC mice model, to develop HCC in the context of fibrosis [187, 188].

1.5.2.2 Phenobarbital (PB)

Phenobarbital [184], is a non-genotoxic barbiturate widely used as a hepatic tumor promoter in rodents initiated by a variety of liver carcinogens, which acts on the processes that influence cell proliferation and survival. PB is known as a modifier of xenobiotic metabolism, the mechanism by which it induces P450-dependent reactions is still unclear. It exerts its action not only on phase I enzymes (CYP 1, 2 and 3) but it also has a pleiotropic effect on the liver, including an increase in

liver mass, proliferation of the smooth endoplasmic reticulum, promotion of liver tumors, increased activities of phase II enzymes (uridine-diphospho (UDP)-glucuronosyl transferase, glutathione S-transferase, epoxide hydrolase, and aldehyde dehydrogenase) and enzymes involved in heme synthesis, lipid metabolism, and so on. About 50 different genes in total are activated by PB in the liver [221, 222]. PB was the first tumor promoter used for rodents in combination with DEN in two-stage HCC models. In mice given a genotoxic agent, the administration of phenobarbital can produce a 5-fold increase in HCC development when using post-weaning DEN administration. In several cases phenobarbital appeared to be tumor protective, however, mice given DEN pre-weaning followed by chronic phenobarbital administration post-weaning showed at 90% multiplicity of HCC tumor burden relative to DEN controls [186].

1.5.2.3 Thioacetamide

Thioacetamide (TAA) represents a second widely used model for the induction of experimental liver fibrosis. Similar to CCl4, TAA requires metabolic activation to become toxic and it is a potent inducer of liver injury; however, the molecular mechanism underlying the induction is not fully understood. TAA is used in conjunction with another hepatocarcinogen such as DEN in a two-stage model to induce hepatocellular carcinoma (HCC) [223]. TAA intoxication was established as a reliable and reproducible experimental model of fibrosis and cirrhosis in rodents by the oral or intraperitoneal routes [224, 225]. Acute exposure to TAA at higher doses is a well-characterized model of acute liver failure. Intraperitoneal administration leads to hepatic centrilobular necrosis, elevated transaminase activity and robust liver fibrosis in about 6 weeks in mice. TAA on its own can induce primary HCC in rats after a year of treatment [226, 227].

1.5.3 CONCLUSION

Among various chemically induced models of HCC, one of the models that most faithfully reproduce human cirrhosis is diethyl nitrosamine-injured rats (DEN). Indeed, most HCC models have the background of normal surrounding liver or moderately fibrotic liver. Indeed fibrosis/cirrhosis modifies liver vascularization, extracellular matrix composition, and drug metabolism, it is essential to use a cirrhotic animal model to test HCC drugs for their efficiency against tumor initiation and/or progression. Current mouse model failed to reproduce all fibrosis stages, especially cirrhosis. Hence in my thesis, we choose to develop characterise the DEN induced HCC rat model during cirrhosis progression and HCC development. Also to test the safety and efficacy of AKT inhibitor ARQ 751 as described before in our developed HCC rat cirrhotic model.

2. OBJECTIVE

2.1 PROJECT 1 – CHARACTERIZATION OF DEN INDUCED HCC RAT MODEL

The objective of the first part is to deeply characterize DEN-induced HCC rat model during cirrhosis progression and HCC development with a special focus on liver inflammatory micro-environment.

2.2 PROJECT 2 - AKT INHIBITOR (ARQ 751) PROJECT

The objective of the second part is to test the safety and efficacy of AKT inhibitor ARQ 751 alone and in combination with sorafenib (ARQ 751+sorafenib), compared to control (non-treated) and sorafenib alone in cirrhotic HCC rat DEN model.

3. MATERIAL AND METHODS

3.1 ANIMALS

Fischer 344 male rats (Charles River Laboratories, France) were housed in the animal facility of Plateforme de Haute Technologie Animale (Jean Roget, University of Grenoble-Alpes, France). Rats were kept in individually ventilated cage (IVC) systems at constant temperature and humidity with 3 animals per cage.

3.1.1 RAT MODEL – CHARACTERIZATION OF DEN-INDUCED HCC

To characterize the process of fibrosis, cirrhosis and HCC development, 4 different time points named 0, 8, 14 & 20 weeks have been chosen (n=13 rats /group). In 0 week, rats were euthanized without any DEN-injection which is considered as baseline group. In 8 and 14 weeks, rats were treated during 8 or 14 weeks once in a week with intraperitoneal injection of 50mg/kg of DEN (Sigma-Aldrich, Germany), diluted in pure olive oil and then euthanized. Lastly, in 20 weeks group, rats were treated with 14 weeks of DEN injection followed with 6 weeks of no DEN injection and the euthanized, Figure 14.

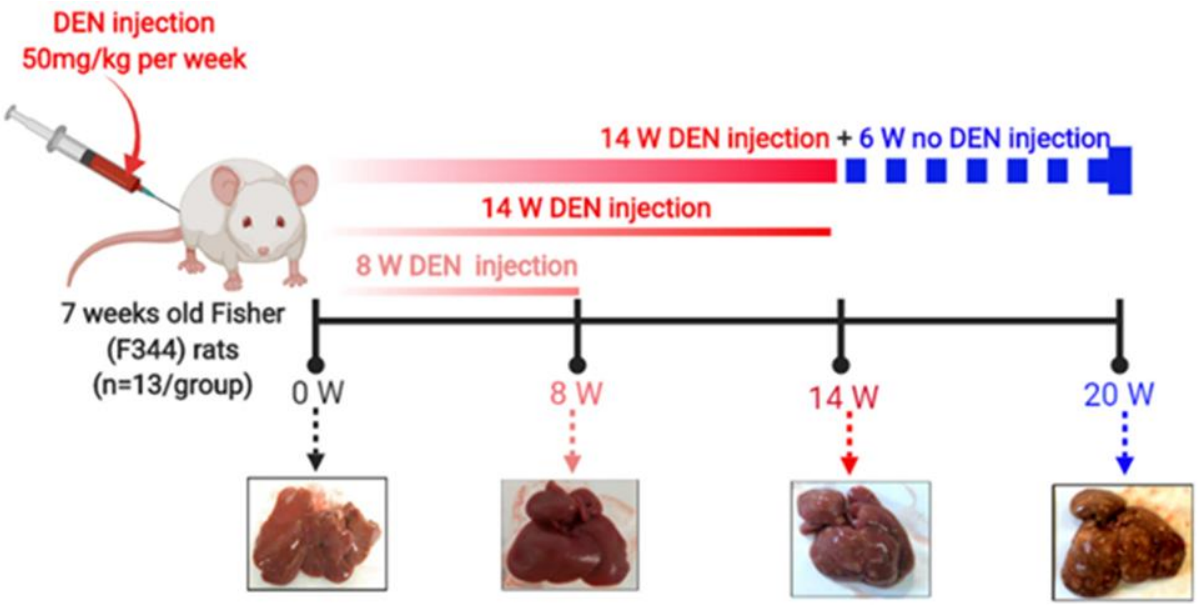

FIGURE 14: TIME LINE PROTOCOL OF DEN INJECTION (50MG/KG PER WEEK) TO CHARACTERIZE DEN INDUCED CIRRHOTIC RAT MODEL OF HCC. 0 W-INDICATES NO DEN INJECTION, 8W-8WEEKS OF DEN INJECTION, 14W -14WEEKS OF DEN INJECTION AND 20W -14WEEKS OF DEN INJECTION PLUS 6 WEEKS NO DEN INJECTION. W=WEEK.

3.1.2 RAT MODEL AND TREATMENT PROTOCOL - AKT INHIBITOR (ARQ 751) PROJECT

7-week-old Fischer 344 male rats (Charles River Laboratories, France) were housed in the animal facility of Plateforme de Haute Technologie Animale (Jean Roget, University of Grenoble-Alpes, France). They were treated weekly with intra-peritoneal injections of 50mg/kg DEN (Sigma-Aldrich, Germany), diluted in pure olive oil in order to obtain a fully developed HCC on a cirrhotic liver after 14 weeks. Figure 15A represents normal rat liver and Figure 15 B shows rat liver with DEN induced HCC. To perform oral gavages and MRI analyses, rats were transported to the Grenoble Institute of Neuroscience (GIN, INSERM, U1216, University of Grenoble-Alpes, France) equipped by Grenoble MRI facility IRMaGE.

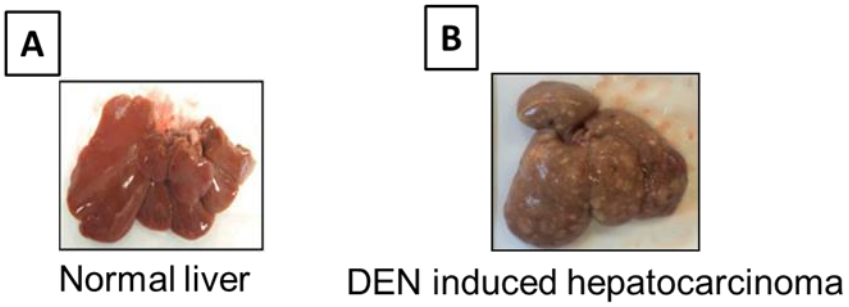

FIGURE 15: REPRESENTATIVE PICTURES OF RAT LIVER A) NORMAL RAT LIVER AND B) RAT LIVER WITH DEN INDUCED HCC.

3.1.2.1 Preparation of sorafenib and ARQ751 treatment

For sorafenib treatment, 200 mg Sorafenib tosylate tablets (Nexavar®, Bayer HealthCare, Germany) were used. First the sugar coating on the tablet was dissolved in DMSO and then to emulsify and solubilize, sorafenib was mixed with 1 mL of poly-oxyl castor oil (Cremophor® EL, Sigma- Aldrich) and 1 mL of 95% ethanol per tablet. To finish, the emulsion was diluted in purified water to obtain a 10 mg/mL solution of sorafenib suitable for oral gavages. The dose strategy for ARQ 751 was based on a previous toxicity study. ARQ 751 was dissolved in a 0.01M phosphoric acid solution to obtain a 10 mg/mL ARQ solution suitable for oral gavages with a final pH of 2.25 ± 0.15. For each drug, fresh solution was prepared every week and stored at room temperature, protected from light. Combination was prepared by mixing the same volume of each drug just before oral gavages.

3.1.2.2 Treatment protocol

After 14 weeks, rats were randomized in four different groups (n=7 rats /group) as follows: ARQ 751 group, Sorafenib group, combination group (ARQ 751 plus sorafenib) and control (untreated) group which is illustrated in Figure 16. Treatments were administrated by daily oral gavage for a period of six weeks. ARQ 751 treatment was administered for 5 days on 9 days off (for a total of

15 days of treatment) at a dose 10 mg/kg/day as recommended by ArQule Inc. In fact, during the first week, the dose of ARQ 751 was used 15 mg/kg/days but after one week of treatment, it was reduced to the dose of 10 mg/kg/days due to its toxic effects. From the second week, the dose of 10 mg/kg/days of ARQ 751 was administered and no adverse effects were observed. Sorafenib was administered continuously at a dose of 10 mg/kg/day every day. The control group was treated by vehicle. During treatment, all rats were daily weighed to monitor the nutritional state and to adapt treatment doses. Protein-rich nutrition was added to the standard food in cages when a loss of weight was observed. All animals received humane care in accordance with Guidelines on the Humane Treatment of Laboratory Animals, and experiments were approved by the GIN animal Ethic committee.

3.1.2.3 MRI analyses

All rats from ARQ 751 project were subjected to three MRI scans. MRI1 was performed before randomization. MRI2 and MRI3 were done after three weeks and six weeks of treatment, which is illustrated in Figure 16.

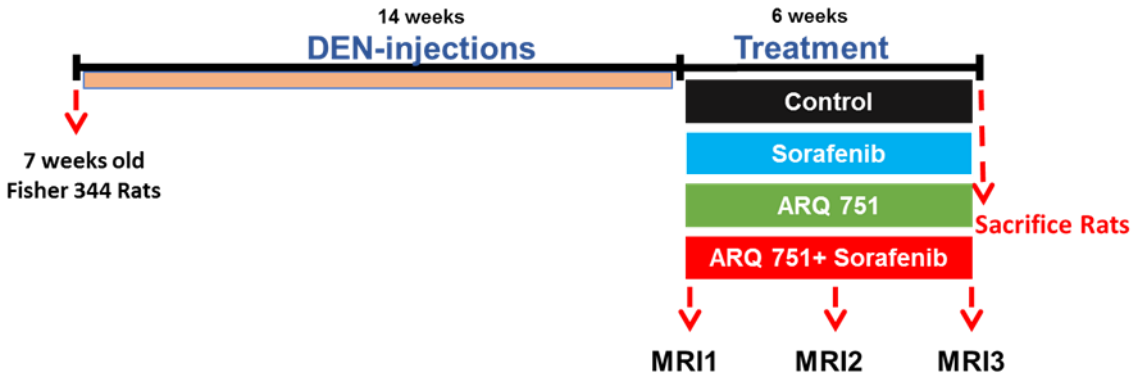

FIGURE 16: TREATMENT PROTOCOL. AFTER 14 WEEKS, DEN INJECTED RATS WERE RANDOMIZED INTO 4 GROUPS. SINGLE TREATED-GROUP SORAFENIB (N=7), ARQ751 (N=7), ARQ751+SORAFENIB (COMBINATION; N=7) AND CONTROL GROUP (N=7). THREE MRI SCANS WERE PERFORMED DURING 6 WEEKS OF TREATMENT.

In the three MRI scans imaging study was performed with a 4.7 Tesla MR Imaging system (BioSpec 47/40 USR, Bruker Corporation, Germany) and Transmit/Receive Volume Array. Coil for rat body 8x2 (Bruker Corporation, Germany) in the Grenoble MRI facility IRMaGE. Rats were fitted in ventral decubitus position and anesthetized with isoflurane inhalation (Forane®, Abbott, USA), breathing was continuously monitored to maintain a respiratory rate between 35 and 45 breaths per minute and body temperature was maintained around 37°C. We used Turbo rapid acquisition with relaxation enhancement T2-weighted (Turbo-RARE T2) sequence (repetition time (TR): 1532.9 msec, echo time (TE): 27.4 msec, flip angle (FA): 180°). MRI parameters adjustment and image acquisition were realized by using Paravision 5.1 software.

A morphological analyzes was realized based on the TurboRARE T2 sequences and according to the Response Evaluation Criteria in Solid Tumors (RECIST) criteria. Five liver tumors were selected and measured on MRI1, 2 and 3. Estimated tumor size corresponded to the sum of the largest diameter of these 5 lesions. For each rat, MRI1 was considered as the baseline (i.e.: 0%) and tumor progression corresponded to the comparison between MRI2 or 3 and the baseline, (i.e: "(tumor size MRI2/3 - tumor size MRI1) / tumor size MRI1). Histopathological and Morphological Analyses

After the third MRI scan, all rats euthanized with intra-cardiac blood sampling for hematologic and biochemical analyses. Serum and plasma were taken to test biological safety and efficacy parameters. Each liver was weighted, the number of tumors larger than 1 mm at the surface of livers was counted and the largest diameter of the five largest tumors was measured. The sum of these 5 diameters was calculated to obtain a histopathological estimation of the tumor size.

3.1.3 HISTOPATHOLOGICAL AND MORPHOLOGICAL ANALYSES

All rats at selected time points were euthanized by isoflurane overdose followed by blood collection from abdominal aorta for hematologic and biochemical analyses. Serum and plasma were taken to test biological safety and efficacy parameters. Each liver was weighted, the number of tumors larger than 1 mm at the surface of livers was counted and the diameter of the five largest tumors was measured. The mean of these 5 diameters was calculated to obtain a histopathological estimation of the tumor size. Liver tissues (tumoral and non-tumoral tissue) were collected. Tissue samples were snap-frozen in liquid nitrogen and stored at -80°C and further used for western blot and ELISA analysis. For histological analysis, tissue samples were fixed in formalin and embedded into formalin-fixed paraffin-embedded blocks of tissue. For qPCR analysis, tumoral and non-tumoral samples are preserved in RNA stabilization solution (Thermofisher scientific, USA).

3.1.4 IMMUNOHISTOCHEMICAL AND IMMUNOFLUORESCENCE ANALYSES

Liver tissues were fixed in formalin solution, neutral buffered, 10% (Sigma-Aldrich, USA), paraffin-embedded and four-micrometer sections of tissue were prepared. The hematoxylin-eosin (HE) staining was used for histopathological examination. Grading of inflammatory activity and staging of fibrosis were performed according to the METAVIR scoring system, a histological scale used to quantify the degree of fibrosis (F). “F” refers to the extent of fibrosis and may vary from F0 to F4 (F0 = no fibrosis, F1 = portal fibrosis without septa, F2 = portal fibrosis with rare septa, F3 = numerous septa without cirrhosis, and F4 = cirrhosis). The development of fibrosis and HCC was studied by an experienced pathologist who was blind to the study.

In order to detect HCC development and cancer stem cells in liver tissue, paraffin-embedded sections were incubated overnight at 4°C with the primary anti-GST-P or anti-CD133 (Table 2), followed by incubation with the anti-rabbit EnVision system HRP Labelled Polymer (Dako

Agilent, USA). DAB was used as the chromogen for immune detection. The positive area was quantified using ImageJ software (NIH, USA) on 10-15 randomly selected fields/section (20x magnification) captured by an Olympus BX41 microscope. All analyzes were performed in a double-blinded manner. Data are presented as percentage of positive surface area (HPF: high-power fields; 20x magnification).

To detect proliferating cells, paraffin-embedded sections were incubated overnight at 4 °C with the primary anti-Ki67 antibody or with anti-Cyclin D1 antibody (Table 2) followed by incubation with the anti-rabbit EnVision system HRP Labelled Polymer (Dako Agilent, USA) (Table 2). DAB was used as the chromogen for immune detection. Positively stained cells were quantified using ImageJ software (NIH, USA) on 10-15 randomly selected fields/sections (20x magnification) captured by an Olympus BX41 microscope. Data are presented as percentage of cells with positive nuclei per total cells (HPF: high-power fields; 20x magnification).

To detect vascularization, paraffin-embedded sections were incubated overnight at 4 °C with an anti-rat CD34 antibody followed by incubation with Alexa 647-conjugated donkey anti-goat IgG (Life Technologies, Carlsbad, CA, USA) (Table 2). Images were captured using the ApoTome microscope (Carl Zeiss, Germany) equipped with a camera AxioCam MRm and collected by AxioVision software. The positive area threshold was quantified using ImageJ software (NIH, USA) on 10 randomly selected fields/sections (10x magnification). All analyzes were performed in a double-blinded manner.

Collagen was detected on paraffin-embedded sections with picro-sirius red stain solution (Sigma-Aldrich). The positively stained area was quantified using ImageJ software (NIH, USA) on 10-15 randomly selected fields/sections (10x magnification) captured by an Olympus BX41 microscope. All analyzes were performed in a double-blinded manner. Data are presented as a positive area.

For detection of immune checkpoint Cytotoxic T-lymphocyte-associate protein-4 (CTLA-4) paraffin-embedded sections were incubated overnight with primary anti-CTLA-4 (Table 2), followed by incubation with Alexa 647-conjugated donkey anti-mouse IgG (Life Technologies, Carlsbad, CA, USA) (Table 2). Images were captured using the ApoTome microscope (Carl Zeiss, Germany) equipped with a camera AxioCam MRm and collected by AxioVision software. Data presented as the number of positively stained cells per area (high-power fields; 20x magnification). All analyzes were performed in a double-blinded manner.

To analyze macrophages and their phenotype, tissue slides were incubated overnight at 4 °C with primary anti-mouse CD68/SR-D1, galectin 3 and TGM2 antibodies respectively (Table 2), followed by incubation with anti-rabbit EnVision system HRP Labelled Polymer (Dako Agilent, USA). DAB was used as the chromogen for CD68, and TGM2 immunodetection. Alexa 647-conjugated donkey anti-goat IgG (Life Technologies, Carlsbad, CA, USA) was used for immune fluorescence detection of galectin3. Quantification of $CD68^{+}$ and $galectin3^{+}$ cells is presented as the number of positively stained cells per area (high-power fields; 40 & 20x magnifications). For $TGM2^{+}$, 20x magnification images were captured and stained areas were quantified by using thresholds (ImageJ software) and data were presented as positively stained area.

Primary antibody	Clone	Host species	Dilution	Application	Buffer	Time for antigen retrieval	Secondary antibody
GST-P - MBL International	Polyclonal	Rabbit	1:2000	IHC	NA	NA	Anti-rabbit polymer - Agilent
CD133 (PROMININ) - Gene Tex	Polyclonal	Rabbit	1:2000	IHC	Citrate buffer	20 minutes	Anti-rabbit polymer - Agilent
Ki67 – Thermofisher scientific	SP6	Rabbit	1:150	IHC	Citrate buffer	10 minutes	Anti-rabbit polymer - Agilent
Cyclin D1 – ABCAM	EPR2241	Rabbit	1:200	IHC	Citrate buffer	10 minutes	Anti-rabbit polymer - Agilent
CD34 - R&D systems	Polyclonal	Goat	1:100	IF	Citrate buffer	10 minutes	Alexa 647-anti-goat IgG - Life Technologies
CTLA-4 - My BioSource	WK H203	Mouse	1:100	IF	EDTA buffer	10 minutes	Alexa 647-anti-mouse IgG - Life Technologies
CD68/SR-D1 - Novusbio-NB600-985	ED1	Mouse	1:100	IHC	Citrate buffer	10 minutes	anti-mouse polymer – Agilent
Galectin3 - Santa Cruz biotech	B2C10	Mouse	1:100	IF	EDTA buffer	20 minutes	Alexa 647-anti-mouse IgG - Life Technologies
TGM2 - Thermo Fisher Scientific	CUB7402	Mouse	1:100	IHC	Citrate buffer	10 minutes	anti-mouse polymer – Agilent

TABLE 2: LIST OF ANTIBODIES USED FOR IMMUNOHISTOCHEMISTRY (IHC) AND IMMUNOFLUORESCENCE (IF) ANALYSIS; NOT APPLIED (NA), ETHYLENEDIAMINETETRAACETIC ACID (EDTA).

3.1.5 REAL TIME POLYMERASE CHAIN REACTION (QPCR)

Total RNA was extracted from rat liver tissue samples preserved with an RNA stabilization solution (Thermo scientific, USA). RNA purification was performed with RNeasy Mini Kit® (Qiagen, USA). Reverse transcription was realized with iScript™ Reverse transcription supermix Kit (BioRad, USA), and amplification reactions were performed in a total volume of 20µL by using a Thermocycler sequence detector (BioRad CFX96, USA) with qPCR kit iTaq™ Universal SYBR®Green Super mix (BioRad, USA).

GADPH was used as a housekeeping gene. Primers listed in Table 3 were designed with Primer 3 software (version 4.0.0) and verified on BLAST. Oligonucleotide sequences were synthesized by Eurofins Genomics ® in 0.01µmol scale, with a Salt-Free level of purification. Every analysis was done in duplicates.

Gene	**Reverse Sequence (5'-3')**	**Forward Sequence (5'-3')**
EPCAM	TCGTCACACTCGGGATCATA	GACGTCACGGTGCTATGAGA
CYCLIN D1	GGCTCCAGAGACAAGAAACG	GCGTACCCTGACACCAATCT
COL1	CTTCTGGGCAGAAAGGACAG	GCCAAGAAGACATCCCTGAA
α-SMA	CATCTCCAGAGTCCAGCACA	ACTGGGACGACATGGAAAAG
TGF-β1	TGGGACTGATCCCATTGATT	ATACGCCTGAGTAGCTGTCT
TIMP1	TGGCTGAACAGGGAAACACT	CAGCAAAAGGCCTTCGTAAA
MMP2	GGGTTTCTTCTGGCTCAGG	TCTGGCTATCCACAAGACTGG
MMP9	GGAAAAGGAAGGAGGGTACG	CCACTCAGGGCCTTCAGAC

CD4	AGAATAGGATGCAGAGCCCC	AAGGCTCCTTCTTCCCAGTC
CD8	CCAATCCCATTCCCTCCACT	TTCTGTCGCTGAACCTGCTA
GAPDH	TTCAGCTCTGGGATGACCTT	CTCATGACCACAGTCCATGC

TABLE 3: LIST OF PRIMERS SEQUENCES FOR QPCR ANALYSIS

3.1.6 FLOW CYTOMETRY ANALYSIS

To characterise the immune system of rats, flow cytometry analyses were performed on collected fresh liver tissue and fresh blood. Liver tissue samples collected in RPMI media is resolved into a single cell suspension by mechanical disruption. Later, cells were washed with PBS (1X) and stained for multi-parametric flow cytometry analyses. Similarly, whole fresh peripheral blood, collected in heparin tubes, was washed with PBS (1X) was stained for multi-parametric flow cytometry analyses. In the process of staining, cells were primarily incubated for 10 minutes in dark at room temperature (RT) with Zombie UV™ Fixable Viability Kit (BioLegend) to detect the nonviable cells. Later, followed with washing step with PBS (1X) by centrifugation, cells were immunostained with following extracellular anti-rat antibodies: CD45, CD3, CD8, CD4, CD25 and CTLA-4 without any stimulation and incubated for 20 min in dark at 4°C and after washed with PBS (1X) by centrifugation. Further, for internal staining - cells were permeabilized and fixed with Foxp3/Transcritn kit (Thermo Fisher scientific, USA) for 45 minutes. Following washing steps with PBS (1X) by centrifugation, cells were immunostained with intracellular anti-rat Foxp3antibody and incubated for 45 minutes. Lastly, cells are washed with PBS (1X) by centrifugation and measured by the BD-LSRII flow cytometer (BD-LSRII flow cytometer (BD Biosciences, Le Pont-De-Claix, France). Isotype-matched antibodies were used as control. Data

acquired on BD-LSRII flow cytometer were collected with BD FACSDiva 6.3.1 software and analyzed using FCS Express 6 PLUS software.

Antibody	**Clone**	**Fluorophore**	**Company**
CD45	OX-1	APC/Cy7	BioLegend
CD3	1F4	Alexa Fluro	Bio-Rad
CD8a	G28	APC	BioLegend
CD4	W3/25	PE/Cy7	BioLegend
CD25	OX-39	BV421	BD Bioscience
FoxP3	FJK-16s	PE-Cyanine5	eBioscience
CD152(CTLA-4)	WKH203	PE	BioLegend

TABLE 4: LIST OF ANTIBODIES USED FOR FLOW CYTOMETRY ANALYSIS

3.1.7 IMMUNOBLOT ANALYSIS

Liver homogenates were prepared in EZ buffer (20 mM Tris; 100 mM NaCl; EDTA 1mM; 0.5% NP40; 10% glycerol; 1X anti phosphatase and 1X protease) containing proteins were then denatured in Laemmli Sample Buffer (Bio-Rad) containing 5% β-mercaptoethanol and separated by gel electrophoresis (Mini Protean Gels ®, Bio-Rad) and transferred to nitrocellulose (Bio-Rad) membranes using a wet blot method. Membranes were blocked in TBS-Tween solution with 5% BSA for 1 h at 4 °C. Primary antibodies anti-iNOS rabbit polyclonal (ab3523, Abcam) and anti-

Arg-1 rabbit polyclonal (PA5-29645, Invitrogen) were added and membranes were incubated at 4 °C overnight under shaking conditions. Incubation with the secondary antibody (HRP-anti-rabbit IgG, 1:2000; Cell Signaling, 1:1000; Cell Signaling) was performed under shaking conditions for 1 h. Detection was achieved with Clarity™ Western ECL Blotting Substrate (Bio-Rad) using a ChemiDoc™ MP Imaging System (FUSION FX7 with the DarQ-9 and eVo-6 cameras). Densitometric quantification of the bands was performed using the EvolutionCapt. Fusion FX Software.

3.1.8 ENZYME-LINKED IMMUNOSORBENT ASSAY (ELISA) ANALYSIS

ELISA experiment was performed to detect the expression of pro-inflammatory cytokines TNF-α and INF-γ by using rat TNF-alpha DuoSet ELISA Kit (R&D Systems) and mouse IFN-gamma Uncoated ELISA (Thermo Fisher Scientific). In addition, anti-inflammatory cytokines IL-4 and IL-10 were measured using Mouse Interleukin IL-4 Ready-Set-Go Elisa kit (E030212, eBiosciences) and Rat Il-10 BD OptEIA Set (8029217EU). For TNF-α, ELISA plate (Maxisorp, Thermo Scientific) was coated at 4 μg/mL with Mouse Anti-rat TNF-α capture antibody (AYX1215081) and incubated overnight at room temperature (RT). Further, blocking was performed with 1% BSA in PBS for 1 hour at RT. After washing with PBS + 0.05% Tween 20 (PBST), equivalent concentration of serum or protein extracts from tumor and non-tumor liver tissue were added to wells and incubated for 2 hours at RT. After washing, the detection antibody was added and incubated for 2 hours at RT. Following washing steps, Streptavidin-horseradish peroxidase (HRP) was added and plates were incubated in dark for 20 minutes at RT. Finally, the plates were washed and incubated with a 1:1 ratio of 3,3V,5,5V-tetramethylbenzidine and hydrogen peroxidase in dark for 20 minutes at room temperature and later 2 mol/l sulfuric acid was added to stop the reaction. The optical density (OD) was measured at 450 nm. The same

experimental steps were followed for IFN-γ, IL-10, and IL-4 but plates were coated with capture antibody overnight at 4°C. For IL-10, blocking was done with 10% FBS in PBS and plates were incubated with the detection antibody directly coupled with Streptavidin- horseradish peroxidase (HRP) during 1h at RT.

3.1.9 PROTEIN ARRAY

Serum samples collected from rats of each time point were analyzed by Rat XL Cytokine Array Kit (Catalog ARY030, R&D System, USA) according to the protocol provided by the manufacturer. Detection was achieved using a ChemiDoc™ MP Imaging System (Bio-Rad). Dot densities were quantified using The Protein Array Analyzer programmed in ImageJ software (NIH). Values are expressed as the mean intensity relative to the mean intensity of control dots of the respective membrane.

3.1.10 ASSOCIATION OF GALECTIN-3 GENE EXPRESSION WITH SURVIVAL OF PATIENTS WITH HCC

To explore the galectin3 gene expression and patient's survival curve with HCC, Gene Expression Profiling Interactive Analysis tool (GEPIA, http://gepia.cancer-pku.cn/) and UALCAN (http://ualcan.path.uab.edu/) tools were used. GEPIA is a tool that delivers functionalities based on TCGA and GTEx data [228] including differential expression analysis, profiling plotting, correlation analysis, patient survival analysis, similar gene detection and dimensionality reduction analysis. UALCAN tool is a user-friendly, interactive web resource for analyzing transcriptome data of cancers from The Cancer Genome Atlas (TCGA) [229].

3.1.11 STATISTICAL ANALYSIS

All data were tested for normality and the appropriate statistic test was chosen. Comparisons of means were calculated by using ANOVA tests with Tukey HSD correction for multiple means comparisons, and independent T-tests only when two means were compared. Data are presented as mean values ± standard error mean (SEM). Statistical analyses were performed using Prism 6 (GraphPad Software Inc., CA, USA).

4. RESULTS

4.1 RESULTS - CHARACTERIZATION OF DEN INDUCED HCC RAT MODEL

4.1.1 CHRONIC DEN TREATMENT INDUCES TUMOR DEVELOPMENT

To examine the effect of chronic DEN treatment on tumor development and progression, the number of surface liver tumor nodules was measured right after euthanizing of rats at 0, 8, 14 and 20 weeks respectively. Tumor number and size were determined by macroscopic examination of the liver. The quantification of tumor number and size clearly demonstrates that the tumors are induced after 8 weeks of chronic DEN injection and the significant increase in tumor number and size is observed at 14 and 20 weeks (ANOVA, $p < 0.0001$ & $p < 0.0001$), (Figure 17). Besides, the examination also revealed significant increase in tumor size in 20 weeks compared to 14 weeks ($p<0.0001$), Figure 17B. Hence, these results depicted that 14 weeks of chronic DEN treatment-induced 100% tumor (HCC) development.

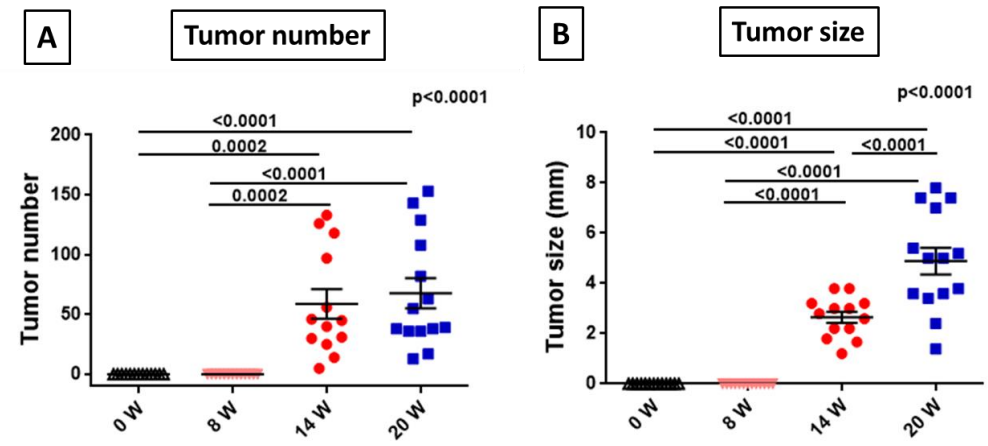

FIGURE 17: A) MACROSCOPIC EXAMINATION OF LIVERS WITH ASSESSMENT OF TUMOR NUMBER AT THE SURFACE OF LIVERS AND B) TUMOR SIZE (AVERAGE OF DIAMETER OF THE FIVE LARGEST TUMORS). QUANTIFICATION GRAPH IS REPRESNTED IN SCATTER PLOT AND VALUES ARE MEANS ± SE, N=13/GROUP.COMPARISON OF MEAN WAS DONE BY ANOVA TEST WITH TUKEY CORRECTION.

4.1.2 *CHRONIC DEN TREATMENT INDUCES HEPATOCARCINOGENESIS*

To examine the hepatocarcinogenesis induced by chronic DEN treatment, immunohistochemistry staining of placental Glutathione S -transferases (GST-P) and CD133 (marker of stem cells) were performed (Figure 18 & Figure 19).

GST is a family of detoxification enzymes catalyzing the conjugation of glutathione with a large number of carcinogens. GST-P is specifically expressed during rat hepatocarcinogenesis and has been used as a reliable tumor marker for preneoplasia in experimental hepatocarcinogenesis in rats [230]. Results from GST-P immunohistochemistry staining exemplified that chronic DEN treatment increased the expression of GST-P in 8, 14 and 20 weeks respectively compared to 0 week, Figure 18A.

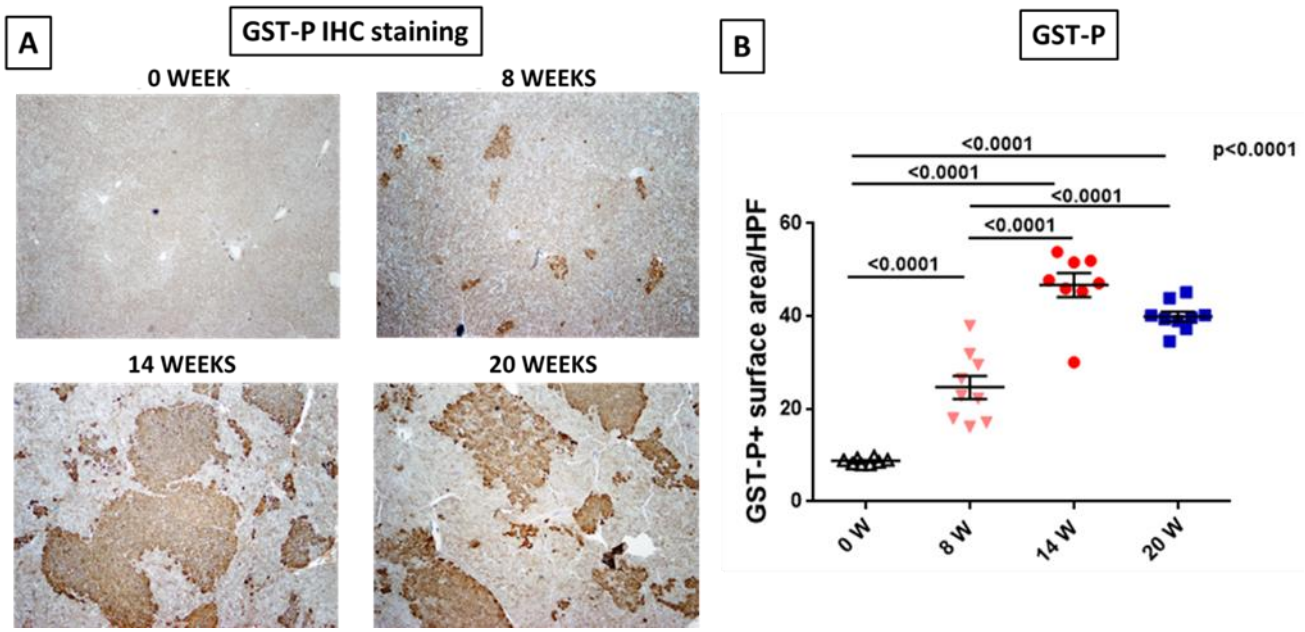

FIGURE 18: A) REPRESENTATIVE IMAGES OF GST-P STAINING, 4X MAGNIFICATION. B) QUANTIFICATION OF GST-P+ SURFACE AREA PER HIGH POWER FIELD (HPF) REPRESENTED IN SCATTER PLOT GRAPH. VALUES ARE MEANS ± SE, N=9/GROUP.COMPARISON OF MEAN WAS DONE BY ANOVA TEST WITH TUKEY CORRECTION. W=WEEKS

The quantification of the GST-P expression, determined as positively stained GSTP surface area, showed significantly increase with chronic DEN treatment (ANOVA, $p<0.0001$). In 0 week, GST-P was hardly expressed, as shown in Figure 18B. At 8 weeks, the expression of GST-P was increased compared to 0 week ($p<0.0001$). At 14 weeks, GST-P expression reached the highest positive surface area and was significantly higher compared to 0 and 8 weeks ($p<0.0001$, $p<0.0001$). Similarly, the expression of GST-P in samples of a group of 20 weeks showed a significant increase compared to 0 and 8 weeks ($p<0.0001$, $p<0.0001$). Hence, an increased marker of preneoplasia (GST-P staining) at 8, 14 and 20 weeks indicated that chronic DEN treatment-induced hepatocarcinogenic changes already before 8 weeks of treatment.

CD133 is a marker of stem cells and is abundantly expressed in both the cytoplasm and nucleus of HCC tumor tissues compared with adjacent normal liver tissues. Results from CD133 staining (Figure 19A) showed that chronic DEN treatment increased the expression of CD133 in 14 and 20 weeks compared to 0 and 8 weeks respectively.

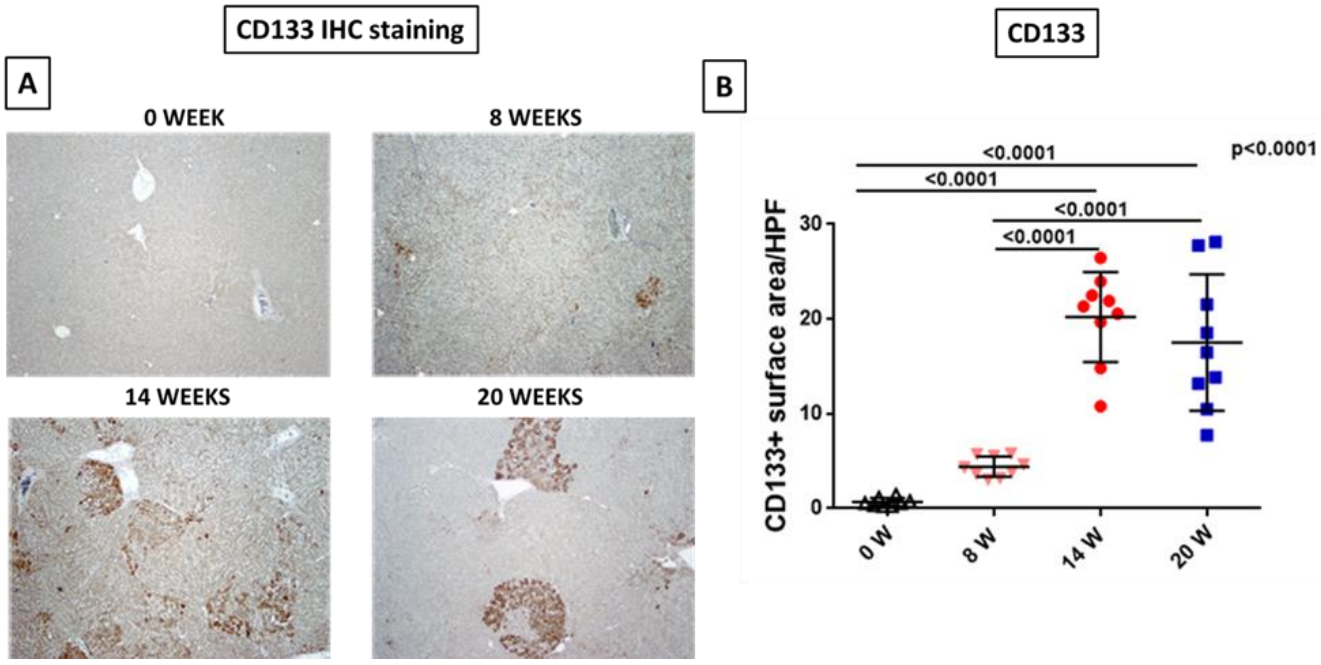

FIGURE 19: A) REPRESENTATIVE IMAGES CD133 STAINING, 4X MAGNIFICATION. B) QUANTIFICATION OF CD133⁺ SURFACE AREA PER HIGH POWER FIELD (HPF) REPRESENTED IN SCATTER PLOT GRAPH. VALUES ARE MEANS ± SE, N=9/GROUP.COMPARISON OF MEAN WAS DONE BY ANOVA TEST WITH TUKEY CORRECTION. W=WEEKS

Quantification of CD133 expression was determined as a positive surface area stained with CD133. We observed significantly higher expression of CD133 at 14 (20.2±1.58) and 20 weeks (17.5±2.39) when compared to 0 and 8 weeks (0.68±0.15 & 4.41±0.35, $p<0.0001$). Hence, the marker of stem cells (CD133) is enhanced in the liver by chronic DEN treatment.

Moreover, hepatocarcinogenesis induced by DEN in this rat model was also confirmed by qPCR analysis of epithelial cell adhesion molecule (EPCAM) (Figure 20). EPCAM is expressed in hepatic progenitor cells and HCC, and is considered as a marker of liver cancer stem cells [231]. Quantification of gene expression of the EPCAM was projected as mRNA fold change normalized to 0 weeks (0 week=1). The expression of EPCAM gene was upregulated in non-tumoral (NT)

liver sample at 8, 14 and 20 weeks compared to 0 weeks (p=0.0321, p<0.0001, p=0.0214) with chronic DEN treatment, Figure 20. Furthermore, we also observed that EPCAM gene expression in tumoral liver tissue of 14 & 20 weeks upregulated significantly compared to non-tumoral tissue of 14 & 20 weeks (2.501±0.24, p=0.0003 & 1.70±1.17, p=0.0003).

Therefore, analyses of GST-P, CD133, and EPCAM depicted the time sequence of events associated with chronic DEN treatment-induced hepatocarcinogenesis in this rat model.

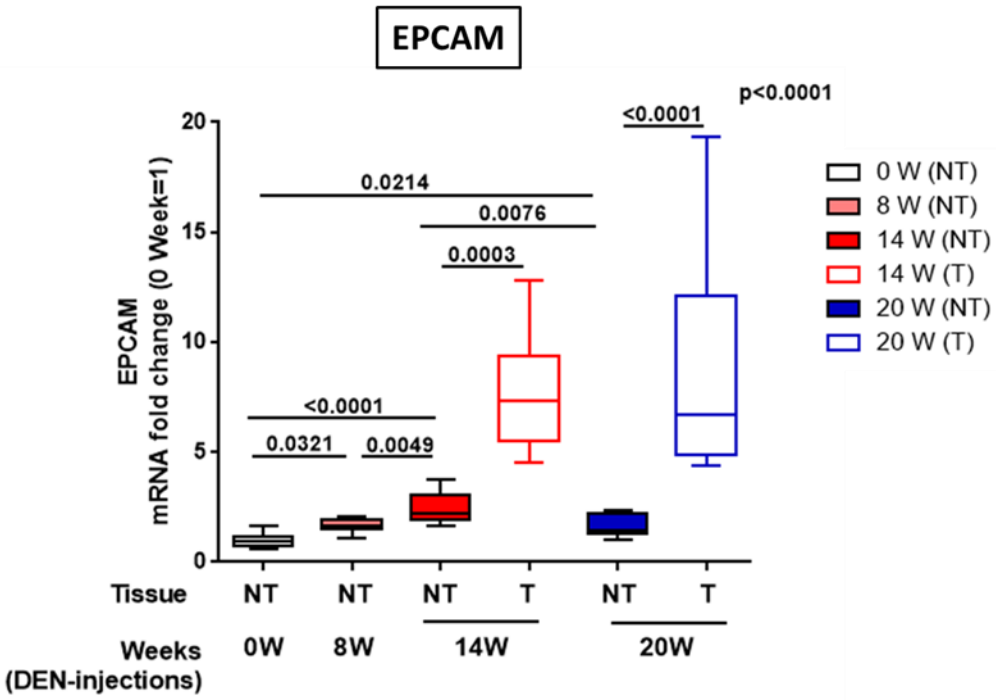

FIGURE 20: QPCR ANALYSIS EPCAM GENE EXPRESSION IN NON-TUMORAL (NT) & TUMORAL (T) LIVER SAMPLE REPRESNTED IN BOX&WISKER GRAPH. 0 WEEK WAS SET AS 1, VALUES ARE MEDIAN ± SE, N=9/GROUP.COMPARISON OF MEAN WAS DONE BY ANOVA TEST WITH TUKEY CORRECTION.

4.1.3 CHRONIC DEN TREATMENT INDUCES HEPATOCYTE PROLIFERATION

To examine the effect of chronic DEN treatment on hepatocyte proliferation, Ki67 and CyclinD1 immuno-staining were performed.

Figure 21A shows that chronic DEN treatment is increasing the frequency of $Ki67^+$ hepatocytes in 8, 14 and 20 weeks compared to 0 week.

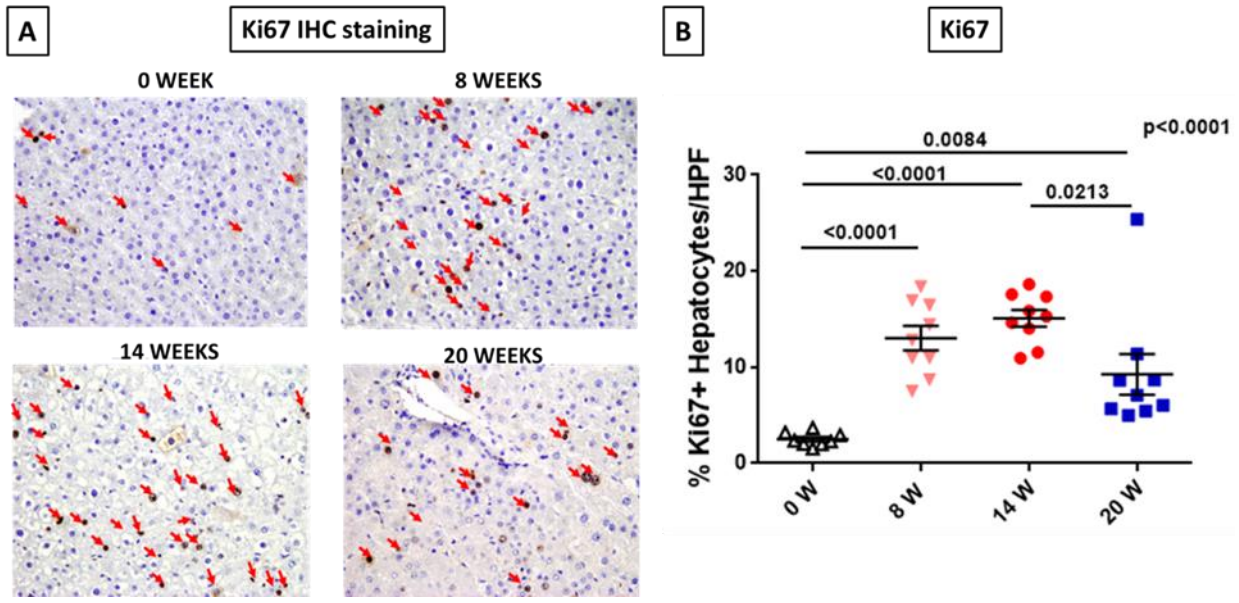

FIGURE 21: A) REPRESENTATIVE IMAGES OF NUCLEAR KI67 STAINING (RED ARROW), 20X MAGNIFICATION. B) QUANTIFICATION OF NUCLEAR $KI67^+$ STAINED HEPATOCYTES PER HIGH POWER FIELD (HPF) REPRESENTED IN SCATTER PLOT GRAPH. VALUES ARE MEANS ± SE, N=9/GROUP.COMPARISON OF MEAN WAS DONE BY ANOVA TEST WITH TUKEY CORRECTION.W=WEEKS

The quantification of Ki67 expression showed that the percentage of $Ki67^+$ hepatocytes increased with chronic DEN treatment (ANOVA, $p<0.0001$) (Figure 21B). Compared to the limited frequency of $Ki67^+$ cells in 0 week (2.51±0.25 %), Ki67 expression increased after 8 weeks (13.0±1.26 %, $p<0.0001$) and 14 weeks (15.1±0.88 %, $p<0.0001$) of DEN injection (Figure 21B). At 20 weeks, the expression of Ki67 was still higher compared to 0 weeks with mean labeling index 9.24±2.13 ($p=0.0084$).

Cyclin D1 is a known oncogene and a key regulator of cell cycle progression. Amplification of the Cyclin D1 gene and its overexpression has been associated with aggressive forms of human

HCC [232]. Hence, to examine the expression of Cyclin D1, we have performed immunohistochemistry staining and qPCR analysis of Cyclin D1. From immunohistochemical staining of hepatocytes with anti-Cyclin D1 antibody, we observed that chronic DEN treatment increased the expression of Cyclin D1 at 8, 14 and 20 weeks compared to 0 week, Figure 22.

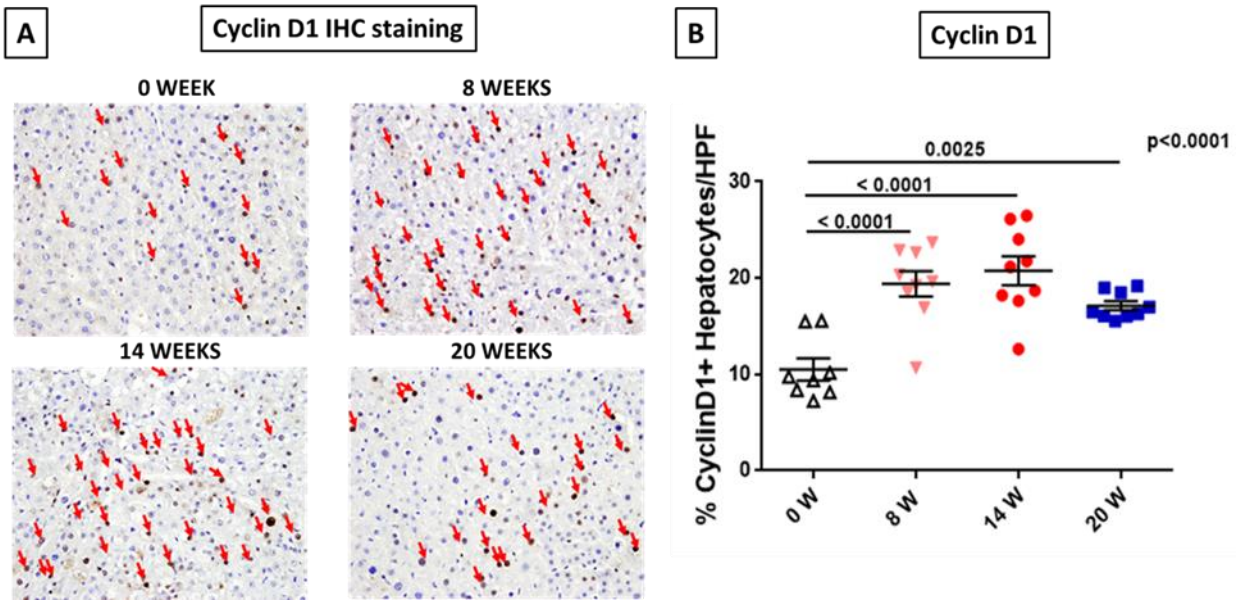

FIGURE 22: A) REPRESENTATIVE IMAGES OF NUCLEAR CYCLIND1+ STAINING (RED ARROW), 20X MAGNIFICATION. B) QUANTIFICATION OF NUCLEAR CYCLIND1+ STAINING HEPATOCYTES PER HIGH POWER FIELD (HPF) IS REPRESENTED IN SACTTER PLOT. VALUES ARE MEANS ± SE, N=9/GROUP.COMPARISON OF MEAN WAS DONE BY ANOVA TEST WITH TUKEY CORRECTION.

Quantification of the Cyclin D1 expression was estimated as the percentage of positively nuclear-stained hepatocytes. Results demonstrated that compared to 0 week, the number of Cyclin D1-positively stained nucleus of hepatocytes was significantly increased at 8 (19.40 ± 1.32 %, $p<0.0001$), 14 (20.75 ± 1.49 %, $p<0.0001$) and 20 weeks (17.12 ± 0.46 %, $p=0.0025$) of chronic DEN treatment (ANOVA, $p<0.0001$), Figure 22B.

Besides, the Cyclin D1 gene expression was analyzed by qPCR (Figure 23). Compared to 0 week, the expression of the Cyclin D1 gene was upregulated in the liver sample at 8 weeks (p=0.0297), in non-tumoral tissue of 14 weeks (p<0.0001) and in tumoral tissue of 14 weeks (p<0.0001). Furthermore, we also observed that Cyclin D1 gene expression in tumoral liver tissue of 20 weeks upregulated significantly compared to 0 week (p<0.0001) but no change was observed in non-tumoral tissue compared to 0 weeks.

Therefore, the increased expression of Ki67 and Cyclin D1 confirmed the induction of hepatocyte proliferation and hepatocarcinogenesis during chronic DEN treatment in DEN induced HCC rat model.

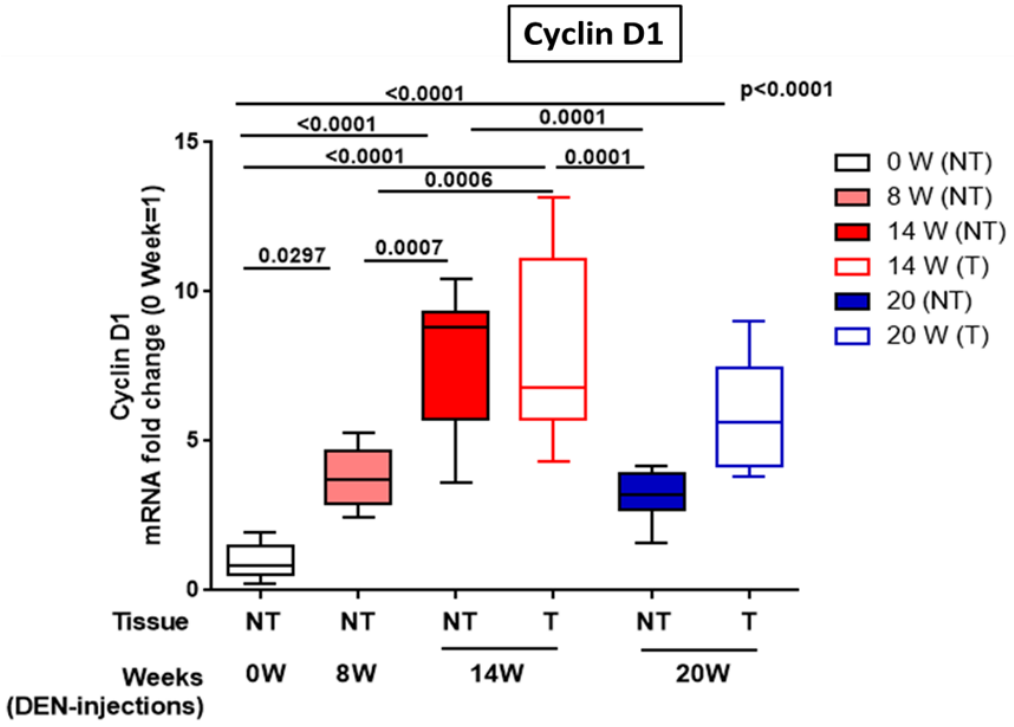

FIGURE 23: QPCR ANALYSIS EPCAM GENE EXPRESSION IN NON-TUMORAL (NT) & TUMORAL (T) SAMPLES REPRESNTED IN BOX&WISKER. 0 WEEK WAS SET AS 1, VALUES ARE MEDIAN ± SE, N=9/GROUP.COMPARISON OF MEAN WAS DONE BY ANOVA TEST WITH TUKEY CORRECTION.

4.1.4 CHRONIC DEN TREATMENT EFFECT ON ANGIOGENESIS

In order to investigate the anti-angiogenic effect, tumor vascularization was studied by using a rat specific anti-CD34 antibody to perform immunofluorescence staining of liver tissues. From the staining of CD34 (Figure 24), we observed that with chronic DEN treatment structural abnormalities of the tissue vascularization were increased mainly at 14 weeks.

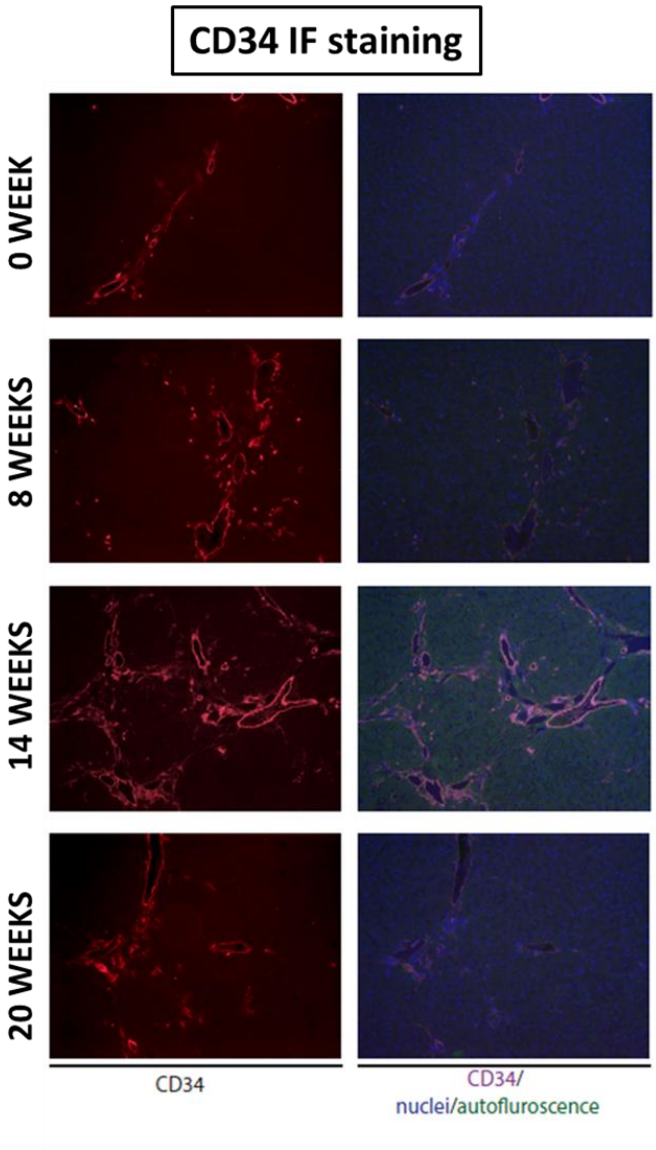

FIGURE 24: REPRESENTATIVE IMAGES OF CD34 IMMUNOFLUORESCENCE STAINING IN LIVER TISSUE, 10X MAGNIFICATION.

Quantification of the vascular density ($CD34^+$ staining) was estimated as the percentage of positively stained surface area normalized to 0 weeks (0week = 100%). The quantification of vascular density revealed a significant increase at 14 (272.5±24.73 %, $p<0.0001$) and 20 weeks (187.4±18.18 %, $p=0.0280$) compared to 0 week (ANOVA, $p<0.0001$), Figure 25. The results indicate that chronic DEN treatment enhanced expression of CD34 which reflects the phenotypic changes of tissue vascularization in this DEN induced HCC rat model.

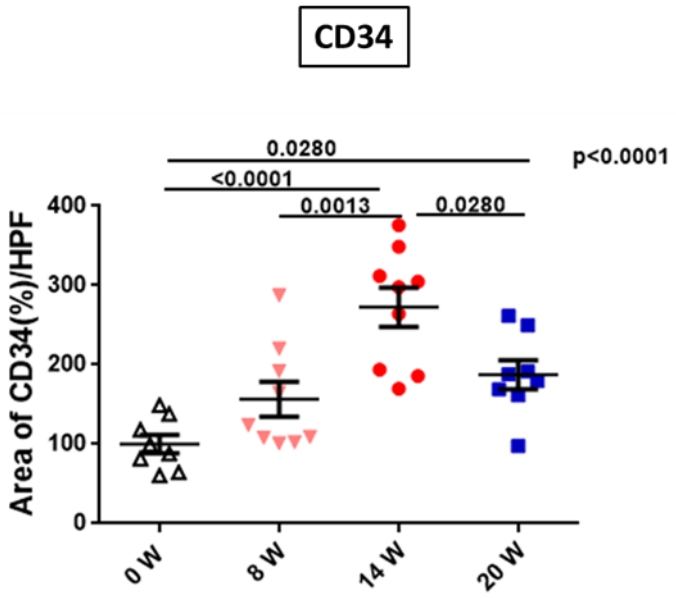

FIGURE 25: QUANTIFICATION OF %OF $CD34^+$ STAINED SURFACE AREA PER HIGH POWER FIELD (HPF) IS REPRESENTED IN SACTTER PLOT. 0 WEEKS WAS SET AS 100%. VALUES ARE MEANS ± SE, N=8-9/GROUP. COMPARISON OF MEAN WAS DONE BY ANOVA TEST WITH TUKEY CORRECTION.

4.1.5 CHRONIC DEN TREATMENT EFFECT ON FIBROSIS/CIRRHOSIS

HCC development is majorly associated with fibrosis/cirrhosis deposition. To observe the fibrosis/cirrhosis deposition by chronic DEN treatment, Sirius red staining was performed (Figure 26A).

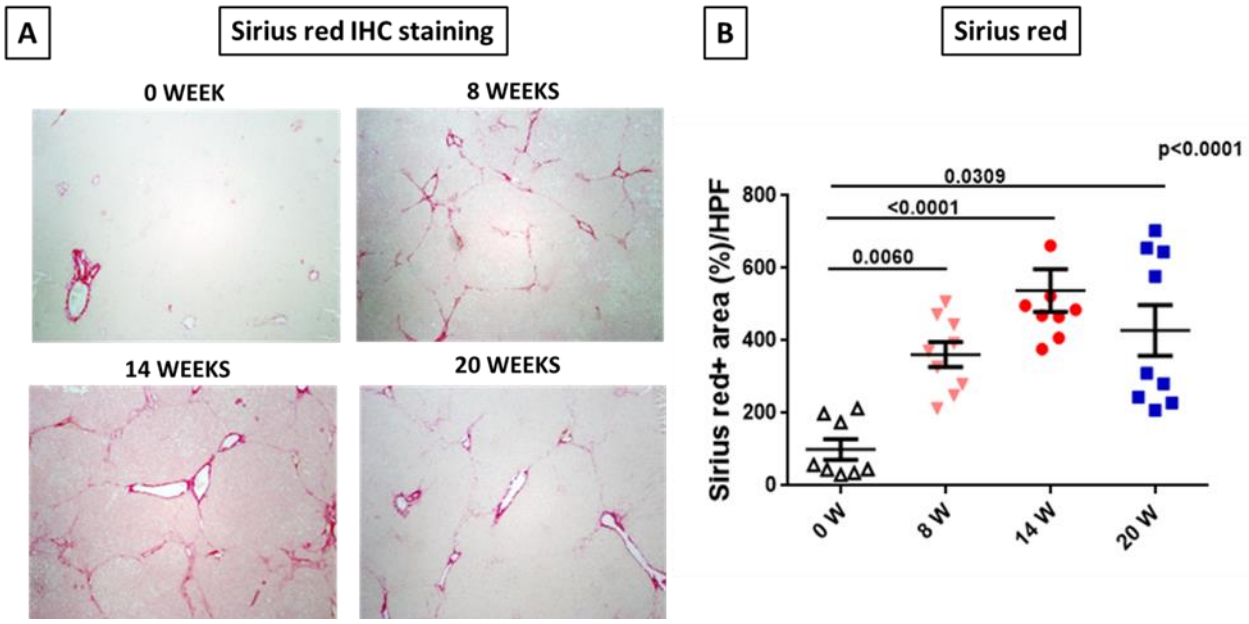

FIGURE 26: A) REPRESENTATIVE IMAGES OF LIVER TISSUE STAINED WITH SIRIUS RED, 4X MAGNIFICATION. B) QUANTIFICATION OF % OF SIRIUS RED⁺ STAINING AREA PER HIGH POWER FIELD (HPF) REPRESENTED IN SACTTER PLOT; 0 WEEK WAS SET AS 100%. VALUES ARE MEANS ± SE, N=9/GROUP.COMPARISON OF MEAN WAS DONE BY ANOVA TEST WITH TUKEY CORRECTION

Quantification of the stained fibrotic area was estimated as the percentage of positively stained surface area normalized to 0 weeks (0 week = 100 %). As shown in Figure 26B, the quantification of positive area of fibrosis revealed a significant increase in fibrosis at 8 (361.9±34.19%, $p=0.0060$), 14 (538.2±58.63%, $p<0.001$) and 20 (428.2±70.10%, $p=0.0309$) weeks respectively, compared to 0 week (ANOVA, $p<0.0001$), Figure 25.

Moreover, the METAVIR score, a tool to evaluate the severity of the fibrosis, was determined by an experienced pathologist and the analysis showed that the fibrosis scores at 8 weeks is F1 while at 14 weeks is increased to F2 - F4. Fibrosis score of liver from group of 20 weeks is between F1-F3, (Figure 27). Thus, results of Sirius red staining and METAVIR score confirm that chronic DEN treatment effectively augmented collagen and led to liver fibrosis at 8 ,14 and 20 weeks.

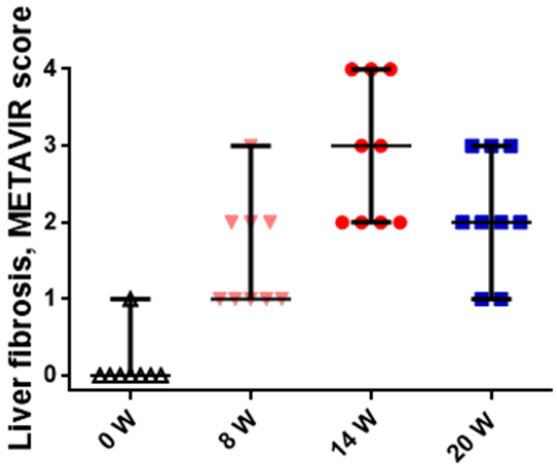

METAVIR score fibrosis (F0-F4)	
No fibrosis	F0
Portal fibrosis without septa	F1
Portal fibrosis with few septa	F2
Numerous septa without cirrhosis	F3
Cirrhosis	F4

FIGURE 27:METAVIR SCORE FOR FIBROSIS STAGING AT 0, 8, 14 AND 20 WEEKS RESPECTIVELY. SCORING IS REPRESENTED IN SACTTER PLOT.

Enhancement of liver fibrosis by chronic DEN treatment was later confirmed by qPCR analysis, Figure 28. The expression of collagen1 was upregulated in NT liver samples of 14 weeks compared to 0 week and 8 weeks ($p=0.0088$ & $p=0.0100$). In addition, compared to 0 week, α smooth muscle actin (α-SMA) expression was increased at 14 and 20 weeks ($p=0.0424$ & $p<0.0001$). Similarly, transforming growth factor (TGFβ1) expression was higher in liver tissue of 20 weeks group compared to 0 week ($p=0.0361$).

Tissue inhibitor of metalloproteinases-1 (TIMP1) expression was also upregulated in NT liver samples of 14 weeks and 20weeks compared to 0 week ($p=0.0132$ & $p=0.0118$). Accordingly,

matrix metalloproteinases (MMP) MMP2 and MMP9 were down-regulated with chronic DEN treatment in 14 and 20 weeks (ANOVA, p=0.0484 & p=0.0101) compared to 0 week, Figure 29. Overall, chronic DEN treatment significantly increased hepatic fibrosis and detail analyses of markers of fibrosis helped to describe the time sequences of events associated with the fibrotic process in this model.

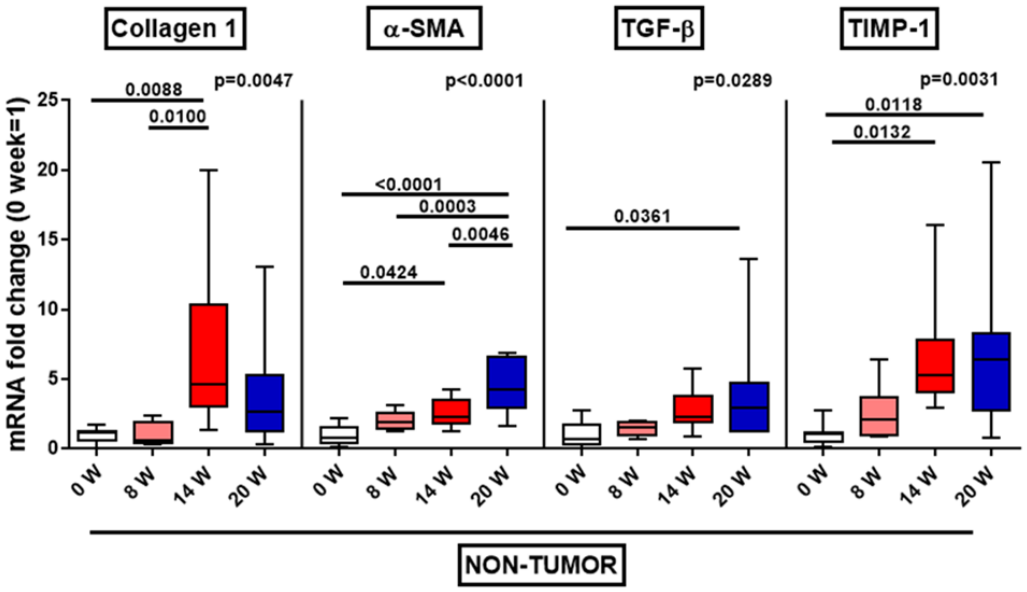

FIGURE 28: QPCR ANALYSIS OF COLLAGEN1, α-SMA, TGF-β and TIMP1 GENE EXPRESSION IN NON-TUMOR LIVER SAMPLES REPRESNTED IN BOX&WISKER. 0 WEEK WAS SET AS 1, VALUES ARE MEDIAN ± SE, N=9/GROUP.COMPARISON OF MEAN WAS DONE BY ANOVA TEST WITH TUKEY CORRECTION.

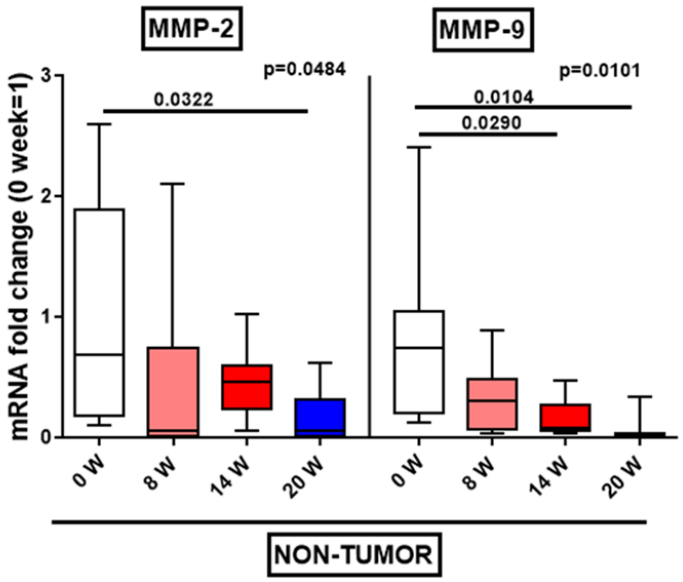

FIGURE 29: QPCR ANALYSIS OF MATRIX METALLOPROTEINASES 2 & 9 (MMP-2 & MMP-9) GENE EXPRESSION IN NON-TUMOR LIVER SAMPLES REPRESNTED IN BOX&WISKER GRAPH. 0 WEEK WAS SET AS 1, VALUES ARE MEDIAN ± SE, N=9/GROUP.COMPARISON OF MEAN WAS DONE BY ANOVA TEST WITH TUKEY CORRECTION.

4.1.6 MODULATION OF ADAPTIVE IMMUNE SYSTEM (T CELLS AND ITS SUBPOPULATION) IN CIRCULATING AND INTRA HEPATIC LEVEL BY CHRONIC DEN TREATMENT

To characterize the effect of DEN treatment on the circulating and intrahepatic immune system, the whole fresh blood and liver tumoral and non-tumoral tissue were analyzed by flow cytometry. Immune cells were identified accordingly to their respective rat-specific markers: Lymphocytes (CD45), Natural killer cells (NK –$CD161^{+}CD3^{-}$), T cells ($CD3^{+}$), T cells subpopulation CD4 ($CD3^{+}CD4^{+}$), CD8 ($CD3^{+}CD8^{+}$) and regulatory T cells (Treg-$CD3^{+}CD4^{+}CD25^{+}Foxp3^{+}$), (Figure 30).

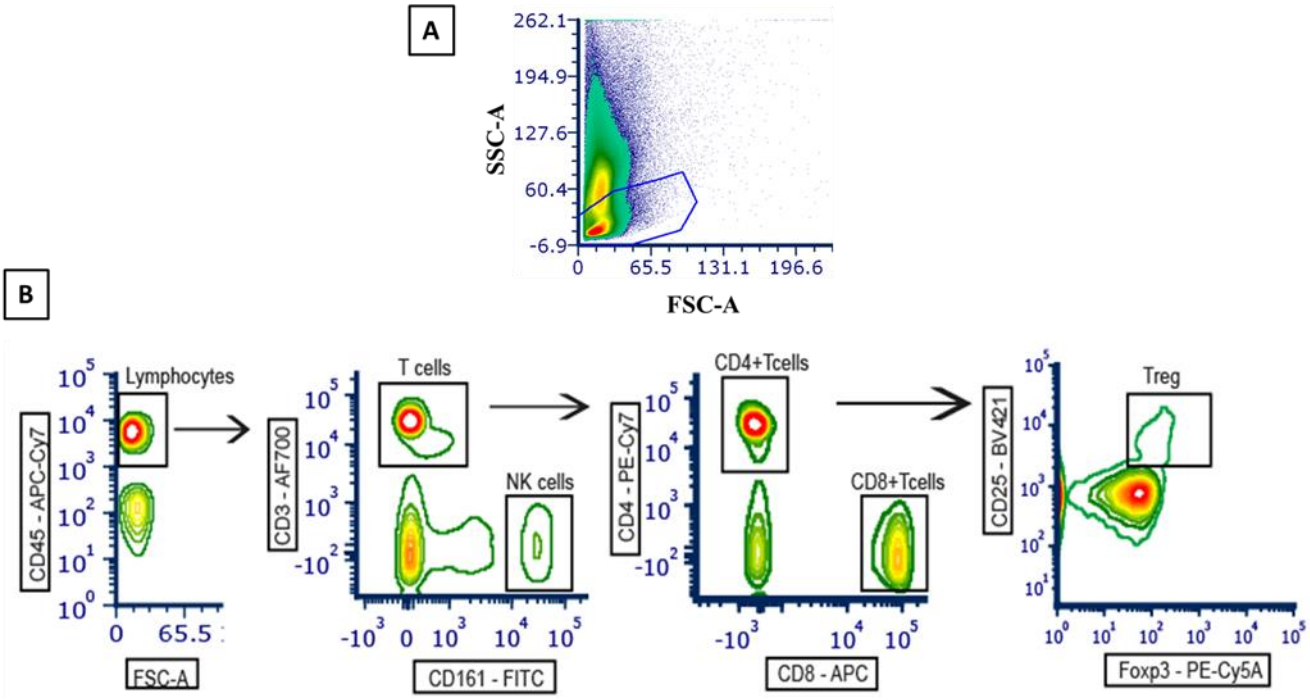

FIGURE 30: FLOW CYTOMETRY STRATEGY TO INVESTIGATECIRCULATORY AND INTRAHEPATIC IMMUNECELLS OF RAT INJECTED BY DEN. IMMUNE CELLS ARE FIRST IDENTIFIED ACCORDING THEIR FORWARD SCATTER CELLS (FSC) AND SIDE SCATTER CELLS PARAMETERS AND FURTHER GATED BASED ON THEIR CD45^{+} EXPRESSION. B) AMONG CD45^{+}POPULATION, NK (CD161^{+}CD3^{-}) AND T (CD161^{-}CD3^{+}), T CELL SUBPOPULATIONS (CD3^{+}CD8^{+}), (CD3^{+}CD4^{+}) AND (CD3^{+}CD4^{+}CD25^{+}FOXP3^{+}) CELLS WERE SELECTED.

4.1.6.1 Modulation of T cell-subpopulation at circulating level during the development of hepatocarcinogenesis by chronic DEN treatment.

From flow cytometry analysis of blood, we have observed modulation in the subpopulation of T cells such as frequency of CD4^{+} T cells, which was significantly decreased at 8 weeks compared to 0 week (p=0.0001) and increased compared to 14 weeks (p=0.0185) and 20 weeks (p=0.0041) respectively (Figure 31A). In accordance with the decrease of CD4^{+} T cells frequency, we also observed a significant increase in CD8^{+} T cells % in 8 weeks compared to 0 week (p=0.0014) and decreased compared to 14 weeks (p=0.0088) and 20 weeks (p=0.0088) respectively (Figure 31B).

More interestingly, the frequency of circulating Treg cells ($CD25^{+}FoxP3^{+}$ cells/$CD4^{+}$ T cells) increased significantly in 8 ($p=0.0038$), 14 ($p=0.0020$) and 20 ($p<0.0001$) weeks compared to 0 weeks (ANOVA, $p<0.0001$) (Figure 31B). Since Treg acts like suppressor cells that control the immune system, a significant increase in Treg (Figure 31C) indicates the induction of immune tolerant status contributing to pro-tumor activity.

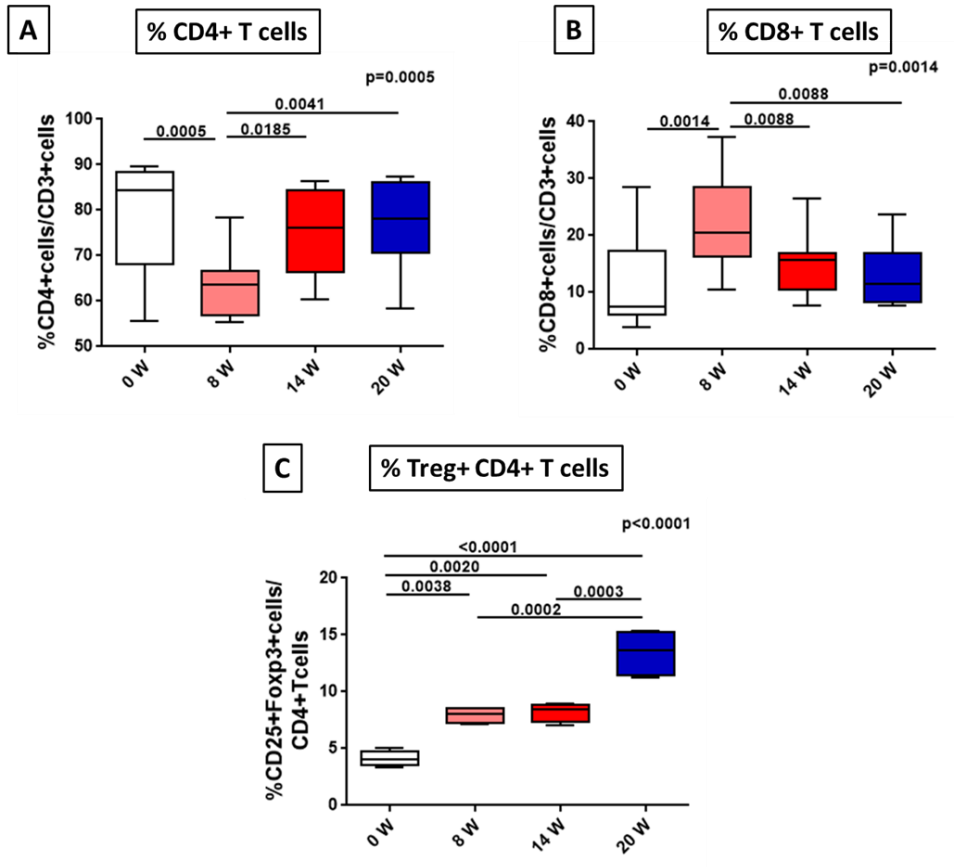

FIGURE 31: FLOW CYTOMETRY ANALYSIS OF SUBPOPULATION OF T CELLS IN BLOOD. A, B AND C REPRESENTS, %$CD4^{+}$T-CELLS, %$CD8^{+}$T-CELLS AND %$CD25^{+}FOXP3^{+}$/ $CD4^{+}$T-CELLS (TREG CELLS) OF 0, 8, 14 &20 WEEKS IN BLOOD RESPECTIVELY BY BOX&WISKER GRAPH. VALUES ARE MEDIAN ± SE, N=9/GROUP.COMPARISON OF MEAN WAS DONE BY ANOVA TEST WITH TUKEY CORRECTION.DEN

4.1.6.2 Modulation of Tcell-subpopulation at intrahepatic immune level during the development of hepatocarcinogenesis by chronic DEN treatment.

In liver tissue, flow cytometry analyses showed no significant changes in the frequency of $CD4^+$ and $CD8^+$ T cells in non-tumor tissue at 8, 14 and 20 weeks compared to 0 week, (Figure 32A & B). Interestingly, we found the frequency of $CD4^+$ T cells significantly increased in tumor compared to non-tumor at 20 weeks ($p=0.0008$) (Figure 32A). In contrast, the frequency of $CD8^+$ T cells significantly decreased in tumor compared to non-tumor at 14 ($p=00014$) and 20 ($p<0.0001$) weeks respectively (Figure 32B). Accordingly, % of Treg cells ($CD25^+FoxP3^+/CD4^+$T cells) increased significantly in tumor compared to non-tumor at 14 ($p=00001$) and 20 ($p=0.0334$) weeks with no significant changes in non-tumor tissue at 8, 14 and 20 weeks compared to 0 week (Figure 32C).

Significantly decreased frequency of $CD8^+$ T cells and an increase in Treg cells % in tumor at 14 and 20 weeks confirms the shift in tumor microenvironment, contributing to pro-tumor activity and hepatocarcinogenesis by chronic DEN treatment.

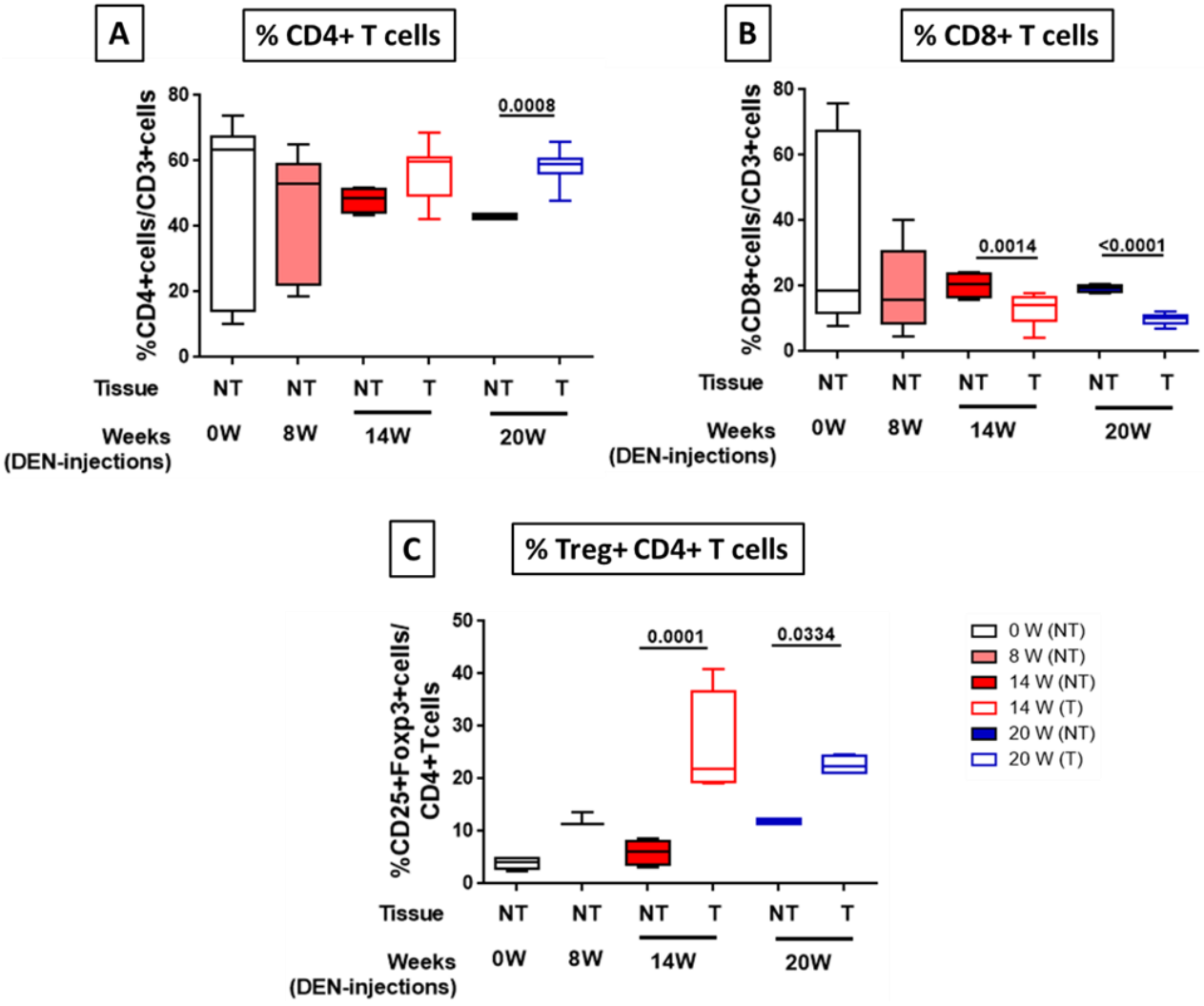

FIGURE 32: FLOW CYTOMETRY ANALYSIS OF SUBPOPULATION OF T CELLS IN LIVER TISSUE. A, B AND C REPRESENTS %CD4⁺T-CELLS AND %CD8⁺T-CELLS AND %CD25⁺FOXP3⁺/ CD4⁺T-CELLS (TREG CELLS) IN TUMORAL AND NON-TUMORAL LIVER TISSUE OF 0, 8, 14 & 20 WEEKS IN BOX&WISKER GRAPH. VALUES ARE MEDIAN ± SE, N=9/GROUP. COMPARISON OF MEAN WAS DONE BY ANOVA TEST WITH TUKEY CORRECTION.

Furthermore, we performed qPCR analysis to examine the gene expression levels of CD4 and CD8 in tumor and non-tumor liver tissue to confirm the previous analysis. Quantification of gene expression is projected as mRNA fold change normalized to 0 weeks (0 week=1). Results of qPCR analysis clearly demonstrated a significant increase in CD4 (ANOVA, $p= 0.0003$) and CD8 (ANOVA, $p< 0.0001$) gene expression at 8, 14 and 20 weeks compared to 0 week, Figure 33 A&B.

Moreover, the comparisson of CD8 and CD4 gene expression between tumor and non-tumor (Figure 33 A&B) revealed no significant differences in CD4 gene expression. However, a significant decrease in CD8 gene expression in tumor compared with non-tumor was observed at 14 weeks (p=0.0405) and 20 weeks (p= 0.0064). Thus, a decrease in the CD8 gene expression in tumor compared to non-tumor at 14 & 20 weeks re-confirmed the pro-tumor activity of the immune system in this model.

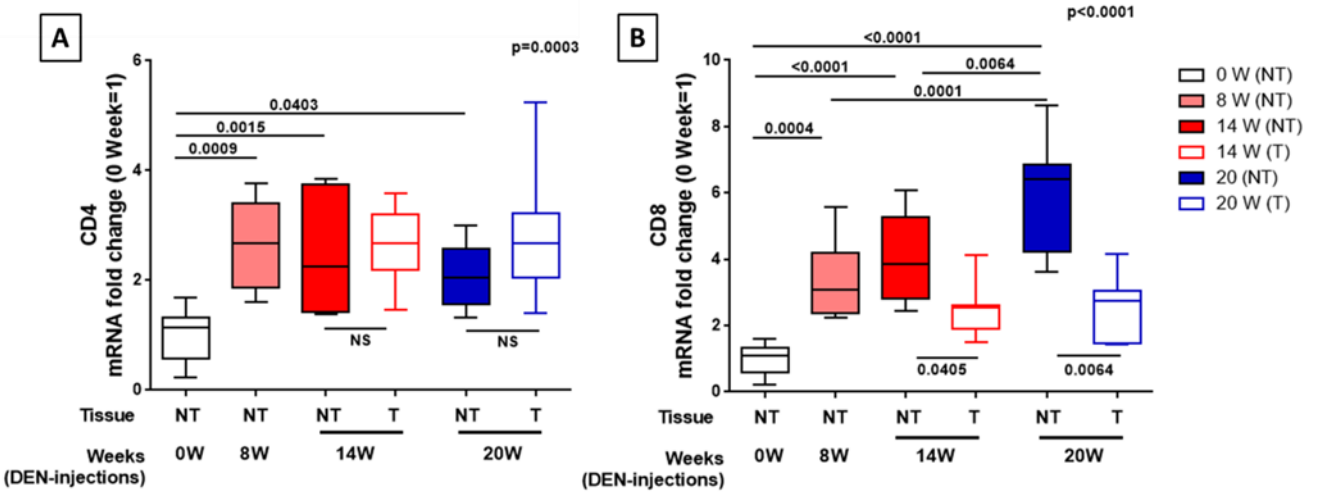

FIGURE 33: QPCR ANALYSIS OF CD4 AND CD8 GENE EXPRESSION IN NON-TUMORAL AND TUMORAL LIVER SAMPLE. A & B, REPRESENTS THE GENE EXPRESSION ANALYSIS OF CD4 AND CD8 IN NON-TUMORAL LIVER TISSUE REPRESNTED IN BOX&WISKER GRAPH. 0 WEEK WAS SET AS 1, VALUES ARE MEDIAN ± SE, N=9/GROUP.COMPARISON OF MEAN WAS DONE BY ANOVA TEST WITH TUKEY CORRECTION.

4.1.7 IMMUNE CHECKPOINT - CYTOTOXIC T LYMPHOCYTE ASSOCIATED PROTEIN 4 (CTLA-4) MODULATION DURING HEPATOCARCINOGENESIS INDUCED BY CHRONIC DEN TREATMENT.

CTLA-4 is a protein receptor that functions as an immune checkpoint and down-regulates the immune response. Interestingly the relation between CTLA-4 and Treg is gaining importance in HCC, for instance, CTLA-4 pathway also involved in the regulation of T-cell mediated immune

response [233] [100].Moreover, increased expression of Treg cells in the tumor at 14 and 20 weeks from flow cytometry analysis (Figure 32) triggered us to check the CTLA-4 (CD152) expression in liver tissue.

We performed flow cytometry staining and checked the expression of CTLA-4 in T cells and its subpopulation such as $CD4^+$ T cells and Treg cells. From results of flow cytometry analysis (Figure 34A & B), we have clearly observed that the frequency of CTLA-4^+ T (ANOVA, $p<0.0001$) and frequency of CTLA-4^+CD4^+ T (ANOVA, $p<0.0001$) cells significantly increased in non-tumor tissue at 8 ($p=0.0001$ & $p=0.0023$) and 14 ($p<0.0001$ & $p<0.0001$) weeks compared to 0 week. Besides, a significant decrease of CTLA-4^+T cells and CTLA-4^+CD4^+T cells in tumoral compared to non-tumoral tissue of 14 weeks ($p=0.0344$ & $p=0.0038$) was also observed. In contrast, we didn't observe any significant changes of CTLA-4^+ T and CTLA-4^+CD4^+T cells at 20 weeks compared to 0 weeks and also in tumoral tissue compared to non-tumoral tissue at 20 weeks.

The frequency of CTLA-4^+ Treg cells significantly increased in non-tumor tissue at 8 ($p<0.0001$) and 14 ($p<0.0001$) weeks compared to 0 week. More interestingly, a significant increase in the frequency of CTLA-4^+ $Treg^+$ cells in tumoral ($p=0.0030$) compared to non-tumoral tissue at 14 weeks was also observed (Figure 34C).

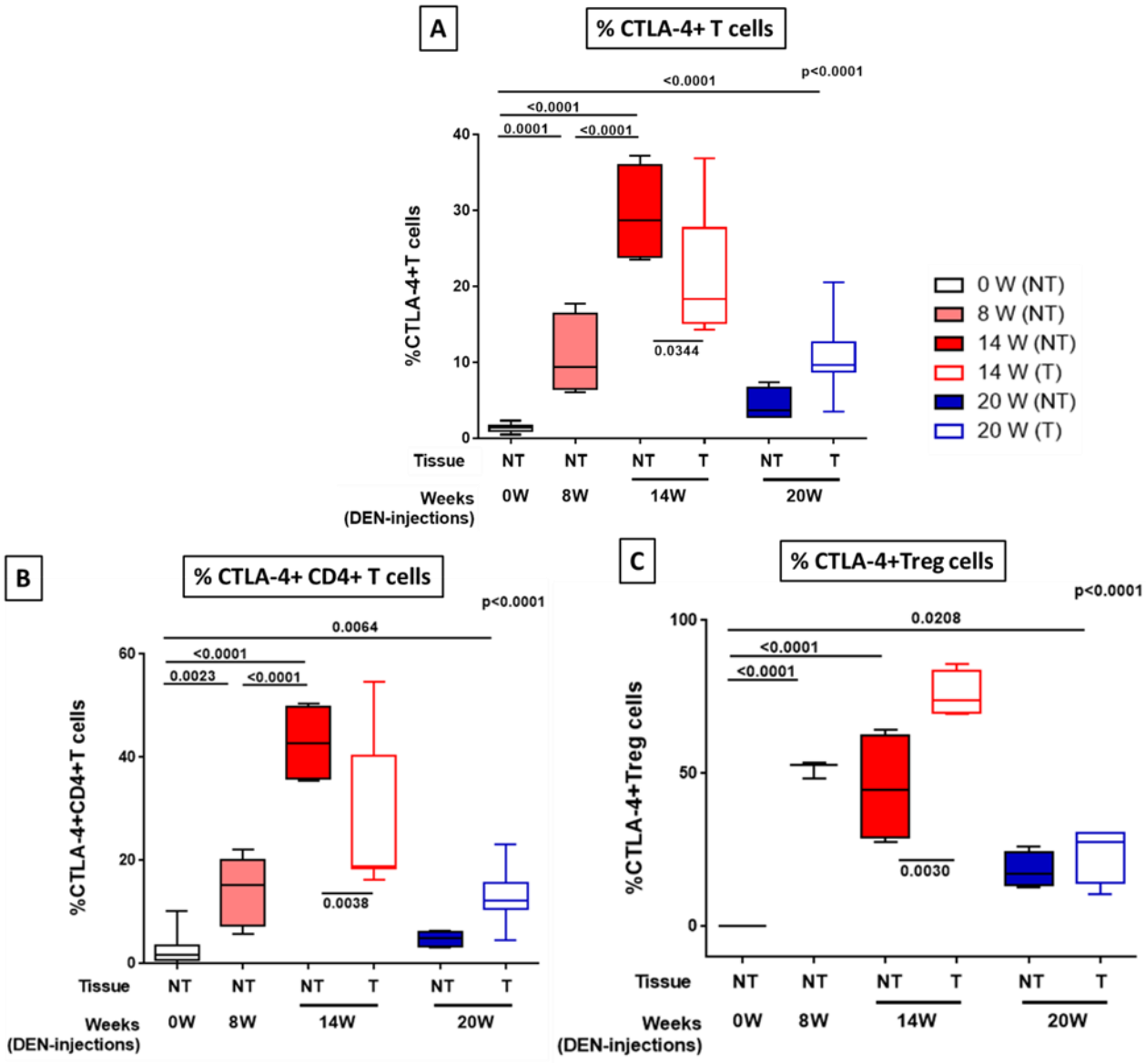

FIGURE 34: FLOW CYTOMETRY ANALYSIS OF SUBPOPULATION OF CTLA-4⁺ CELLS IN LIVER TISSUE. A, B AND C REPRESENTS, %CTLA-4⁺T-CELLS AND % CTLA-4⁺CD4⁺T-CELLS AND % CTLA-4⁺TREG⁺CELLS IN TUMORAL AND NON-TUMORAL LIVER TISSUE OF 0, 8, 14 & 20 WEEKS IN BOX&WISKER GRAPH. VALUES ARE MEDIAN ± SE, N=9/GROUP.COMPARISON OF MEAN WAS DONE BY ANOVA TEST WITH TUKEY CORRECTION.

Secondly, we have performed immunofluorescence staining of the anti-CTLA-4 antibody on liver tissue. Quantification of CTLA-4^{+} staining cells clearly demonstrated that chronic DEN treatment

significantly increased expression of CTLA-4 at 8 ($p<0.0001$), 14 ($p<0.0001$) and 20 weeks ($p<0.0001$) compared to 0 week, Figure 35.

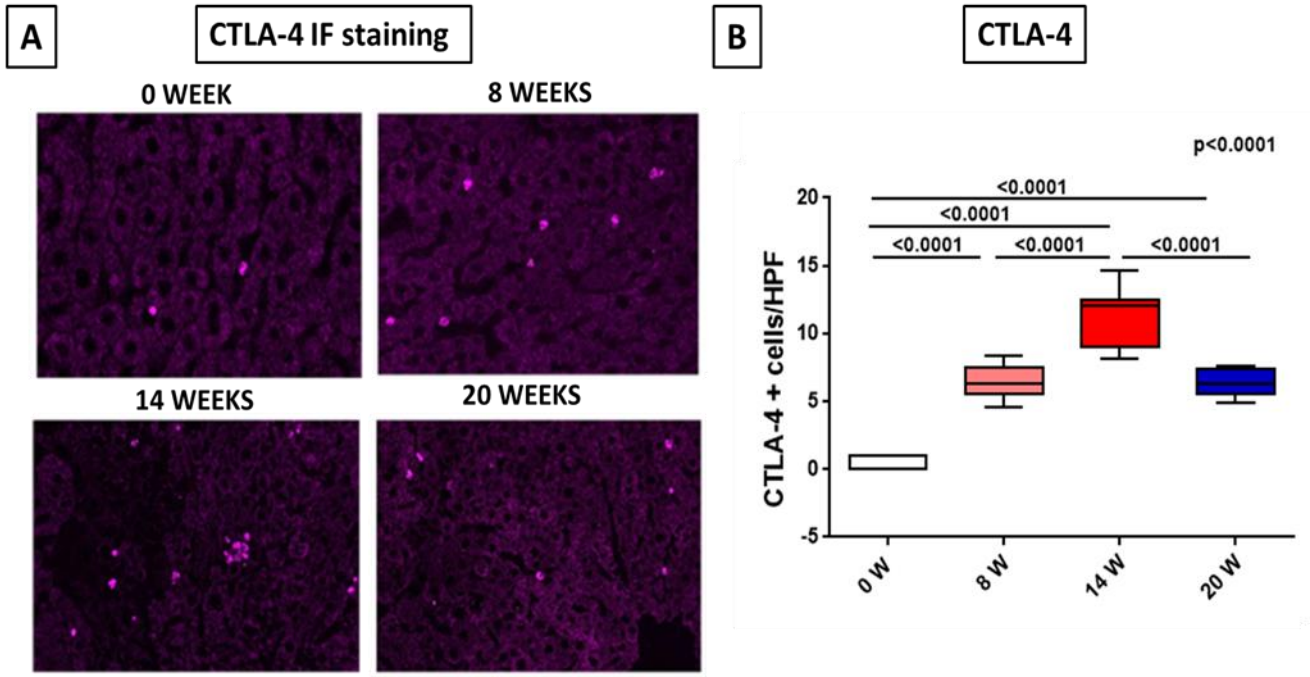

FIGURE 35: A) REPRESENTATIVE IMAGES OF CD34 IMMUNOFLUORESCENCE STAINING IN LIVER TISSUE, 20X MAGNIFICATION. B) QUANTIFICATION OF CTLA-4+ STAINED CELLS PER HIGH POWER FIELD (HPF) REPRESENTED IN SACTTER PLOT. VALUES ARE MEANS ± SE, N=9/GROUP.COMPARISON OF MEAN WAS DONE BY ANOVA TEST WITH TUKEY CORRECTION.

Overall, the increased expression of CTLA4+ Treg cells ((Figure 34C) and CTLA-4+ cells (Figure 35B) by chronic DEN treatment demonstrated the modifications of the immune system further favoring the hepatocarcinogenesis by chronic DEN treatment

4.1.8 Modulation of macrophage (innate immune system) and its phenotype at intra hepatic level during hepatocarcinogenesis induced by chronic DEN treatment

Macrophages belong to a heterogeneous innate immune population. They act as important mediators during liver inflammation and play a crucial role in the tumor microenvironment. Therefore, to check the effect chronic DEN treatment on global expression of macrophages, immunohistochemistry staining of CD68 was performed on liver tissue of 0, 8, 14 and 20 weeks (Figure 36A). The quantification results of CD68 staining from Figure 37A revealed a significant upregulation of the number of $CD68^+$ cells in 14 weeks (23.92 ± 1.074) compared to 8 and 0 week (13.28 ± 1.644 & 16.13 ± 1.341, ANOVA, p=0.0287). Besides, no difference was observed in 20 weeks compared to 0, 8 and 14 weeks.

Furthermore, to examine the effect of chronic DEN treatment on the activation state of macrophages, immunohistochemistry and immunofluorescence analyses of M2 macrophages i.e., transglutaminase 2 (TGM2) and galectin-3 staining, were performed (Figure 36 B&C). The TGM^+ area was significantly higher in 14 weeks (4.617 ± 0.558) compared to 0 week (1.970 ± 0.163; $p<0.0001$) and 8 weeks (2.725 ± 0.241; p=0.0013). Similarly, galectin-3+ cells significantly increased in 8 ($p<0.0001$), 14 ($p<0.0001$) and 20 ($p<0.0001$) weeks compared to 0 week (ANOVA, $p<0.0001$), (Figure 37 C).

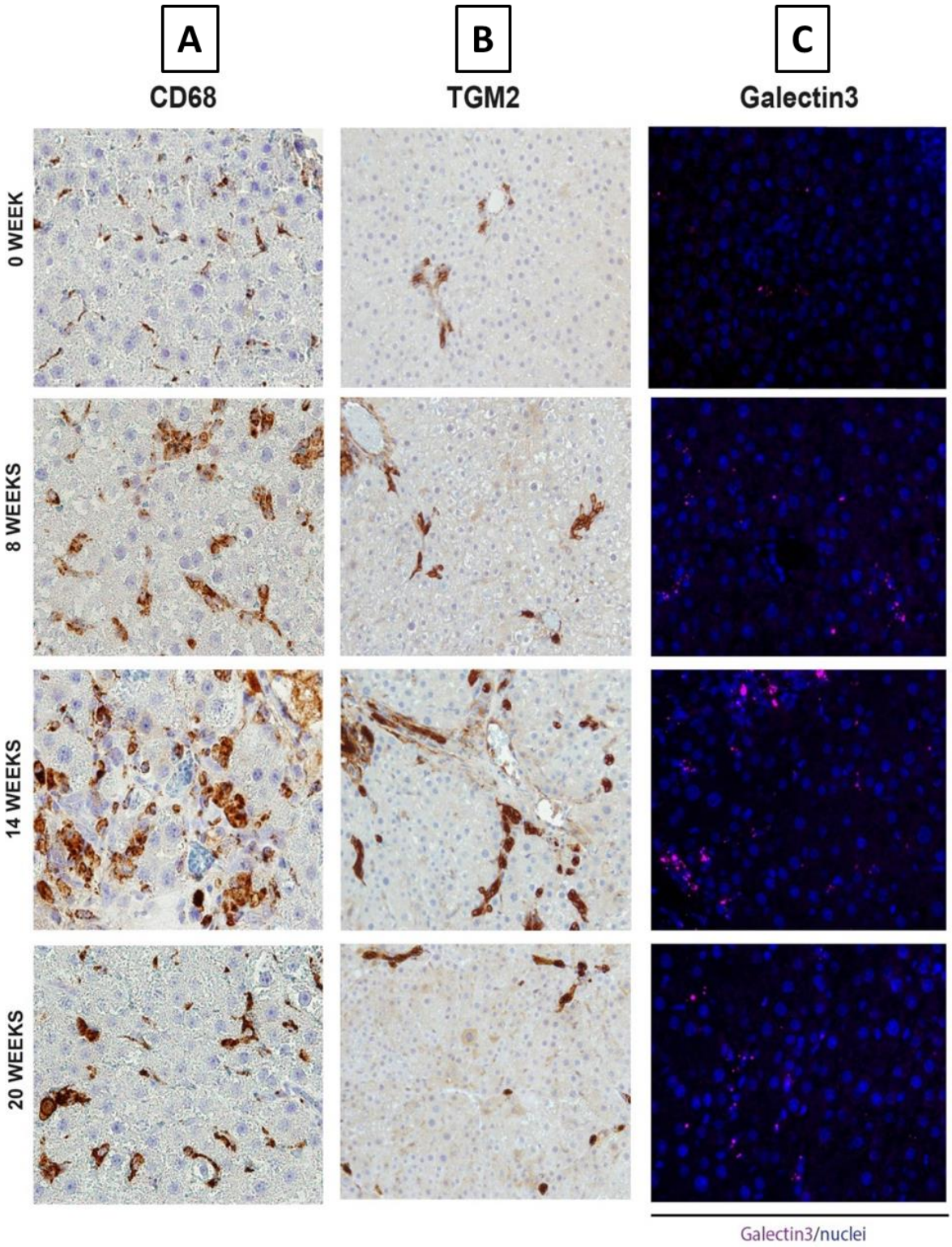

FIGURE 36: REPRESENTATIVE IMAGES OF A) CD68, B) TGM2 IMMUNOHISTOCHEMISTRY AND 3) GALECTIN-3 IMMUNOFLUORESCENCE STAINING IN LIVER TISSUE, 20X & 10X MAGNIFICATION.

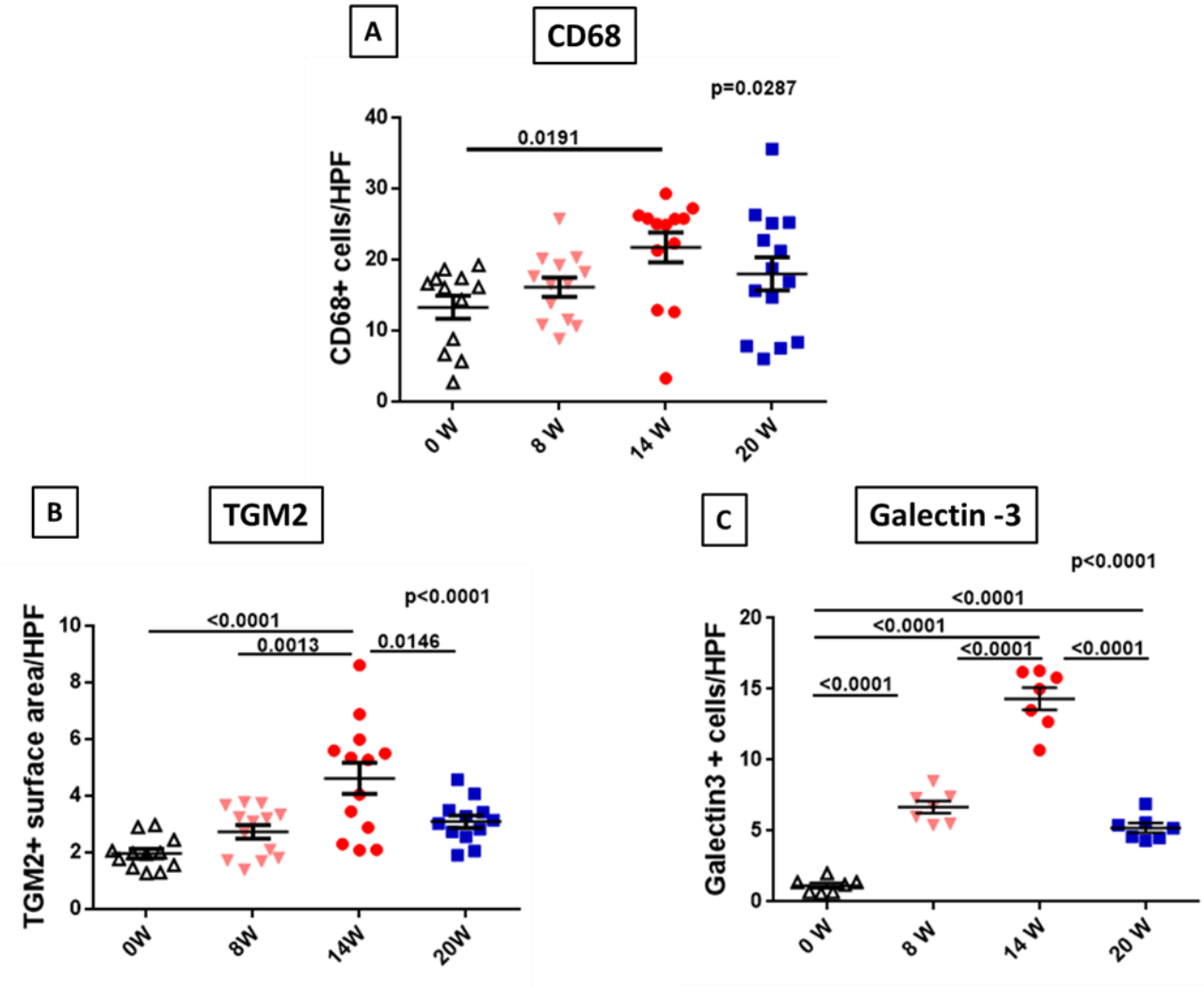

FIGURE 37: A) QUANTIFICATION OF CD68⁺ STAINED CELLS PER HIGH POWER FIELD (HPF) REPRESENTED IN SACTTER PLOT. VALUES ARE MEANS ± SE, N=13/GROUP. B) QUANTIFICATION OF TGM2⁺ STAINED SURFACE AREA PER HIGH POWER FIELD (HPF) REPRESENTED IN SACTTER PLOT. VALUES ARE MEANS ± SE, N=13/GROUP. C) QUANTIFICATION OF GALECTIN3⁺ STAINED CELLS PER HIGH POWER FIELD (HPF) REPRESENTED IN SACTTER PLOT. VALUES ARE MEANS ± SE, N=7/GROUP. COMPARISON OF MEAN WAS DONE BY ANOVA TEST WITH TUKEY CORRECTION.

4.1.8.1 Role of galectin-3 over-expression in HCC progression and development

The increased expression of galectin-3 by chronic DEN treatment observed form immunofluorescence analysis triggered us to check its expression at the circulating level. Hence, we performed a protein array assay on serum samples of 0, 8, 14 and 20 weeks. The results showed that galectin-3 expression is amplified by chronic DEN treatment at circulation level, Figure 38. Thus, this observation re-confirms the possible role of galectin-3 (a marker of M2 macrophage) in hepatocarcinogenesis induced by chronic DEN treatment.

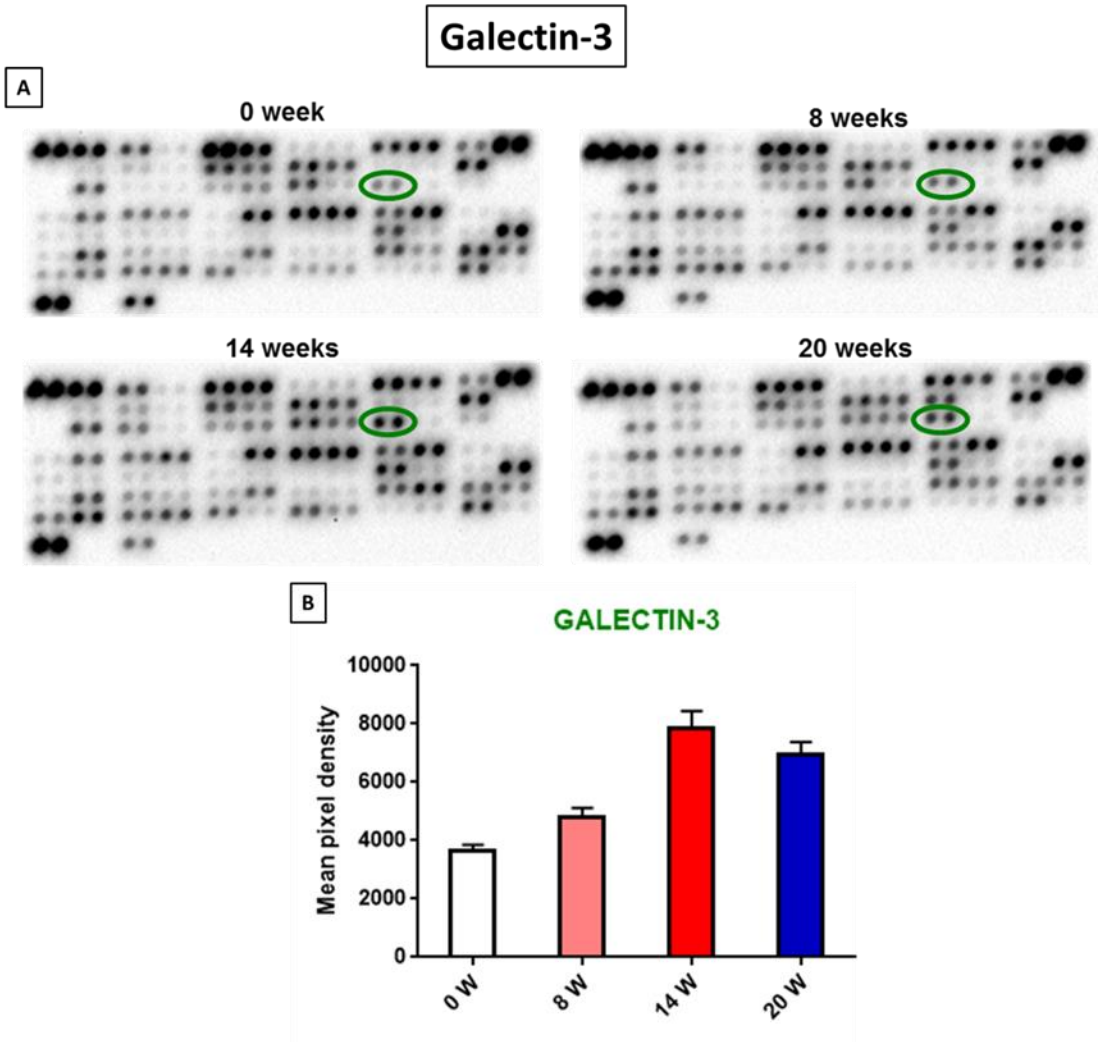

FIGURE 38: EXPRESSION OF GALECTIN-3 IN RAT SERUM. A) PROTEIN ASSAY MEMBRANE FROM A 100-SECOND EXPOSURE TO CHEMIDOC MP, IMAGING SYSTME. B) QUNATIFICATION OF GALECTIN-3 PROTEIN. VALUES ARE EXPRESSED AS THE MEAN INTENSITY RELATIVE TO MEAN INTENSITY OF CONTROL DOTS OF RESPECTIVE MEMEBRANE.

Additionally, knowing the importance of galectin-3 in inducing hepatocarcinogenesis by chronic DEN treatment at intrahepatic and circulating levels, we decided to check the possible link between patient survival and galectin3 level using GEPIA and UALCAN web portals. Data revealed a significantly shorter overall survival in patients with galectin3 high expression levels compared to a group of patients characterized by lower expression levels of galectin3. Thus, galectin-3 is associated with the worst prognosis in HCC, Figure 39.

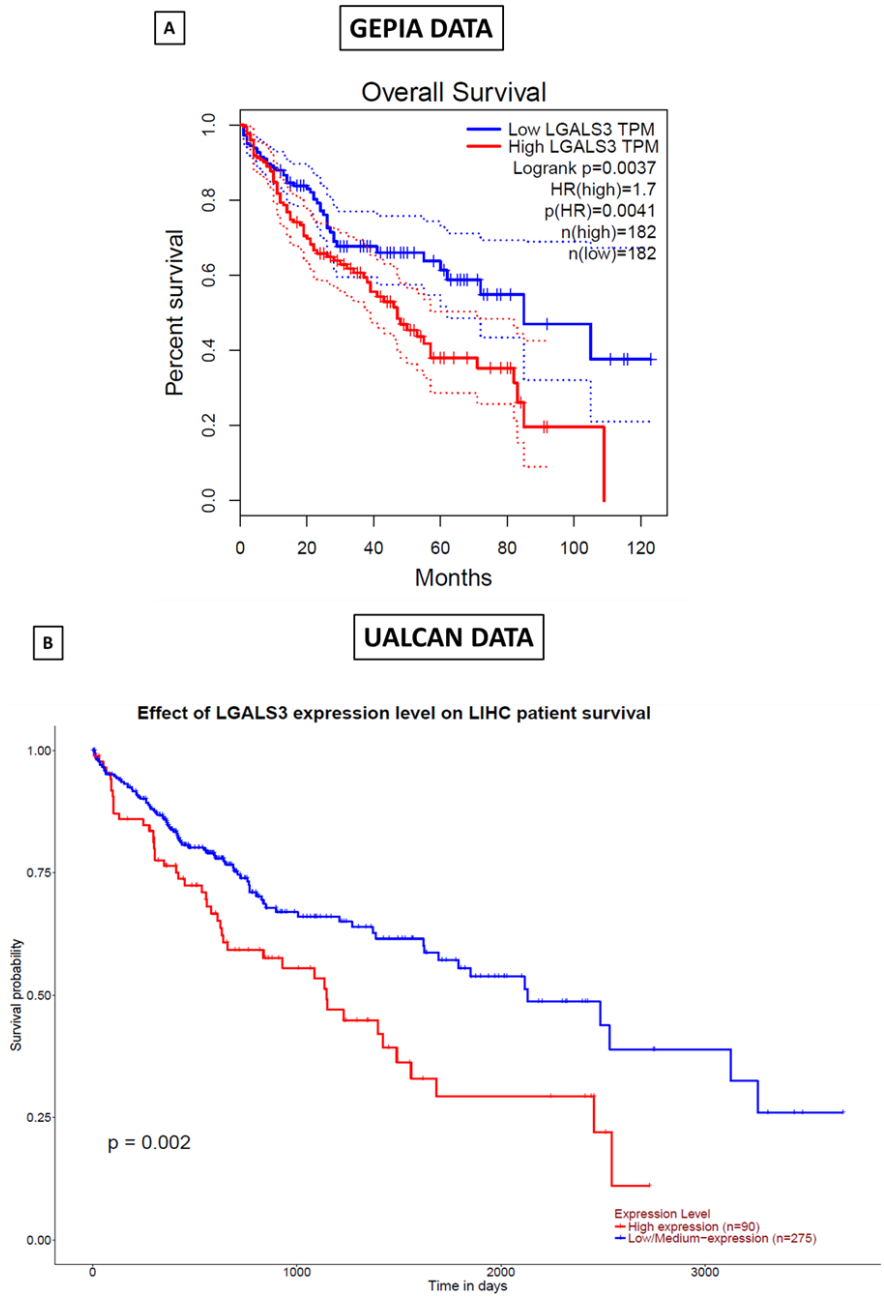

FIGURE 39: PATIENT SURVIVAL CURVES IN COMPARISON WITH GALECTIN3 EXPRESSION. A) GEPIA, & B) UALCAN, SURVIAL CURVES SHOWED THAT GALECTIN3 EXPRESSION WAS NEGATIVELY CORRELATING WITH PROGNOSIS PRIDICTION OF HCC.

Overall, our analysis suggests the importance of galectin 3 (a marker of M2 macrophages) and its involvement during hepatocarcinogenesis.

4.1.8.2 Effect of chronic DEN treatment on expression levels of macrophages phenotypes (M1 & M2) intrahepatically

Furthermore, knowing that macrophages are highly recruited during HCC progression, the relative protein expression of iNOS (M1 marker) and Arg-1 (M2 marker) was assessed by Western Blot using equivalent concentrations of proteins extracted from tissue homogenate samples. Interestingly, the relative protein expression of iNOS (M1 marker) was significantly lower in tumor areas of 14 weeks and 20 weeks compared to non-tumor areas of 14 ($p=0.0286$) and 20 weeks ($p<0.0001$), Figure 40A. On the contrary, the relative protein expression of Arg-1 (M2 marker) was significantly upregulated in tumor areas of 14 weeks and 20 weeks compared to non-tumor areas of 14 ($p<0.001$) and 20 ($p=0.0101$) weeks, Figure 40B. This illustrates the fact that the ratio of M2/M1 macrophage in tumor areas of 14 and 20 weeks is greater than that in non-tumor areas of 14 (1.82 versus 0.88) and 20 weeks (1.78 versus 0.67), respectively, Figure 40C.

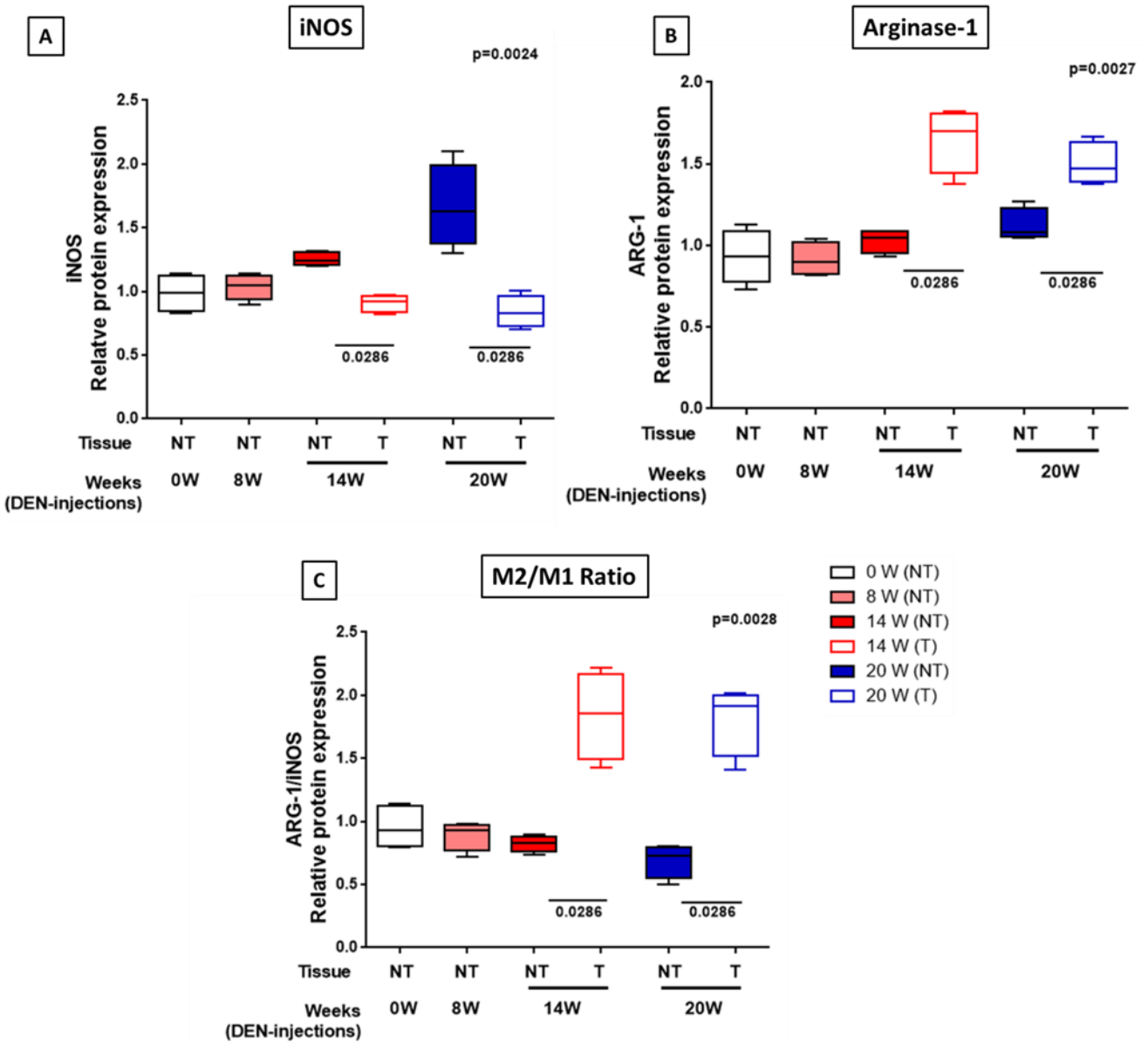

FIGURE 40: REPRESENTATION OF WESTERNBLOT ANALYSIS OF INOS, ARGINASE-1 AND ITS RATION IN BOX&WISKER GRAPH. VALUES ARE MEDIAN ± SE, N=4/GROUP.COMPARISON OF MEAN WAS DONE BY ANOVA TEST WITH TUKEY CORRECTION.

Together, these all results show that the population of macrophages increased at 8, 14 and 20 weeks by chronic DEN treatment, is mostly possessing M2 (anti-inflammation) like phenotype. Thus, M2 macrophages are highly recruited to the liver during the development and progression of HCC by

chronic DEN treatment. Moreover, we identified galectin-3 as a possible key molecule in the development of HCC. In addition, our results also demonstrate that in tumor areas, there is an increase in the ratio of M2/M1 macrophages which further elucidates the immune-suppressive performance of M2 macrophages, leading to pro-tumor microenvironment induced by chronic DEN treatment.

4.1.9 Modulation of inflammatory cytokine expression during hepatocarcinogenesis induced by chronic DEN treatment

4.1.9.1 Intra-hepatic level

Next, we investigated the levels of pro-inflammatory cytokines TNF-α and IFN-γ and anti-inflammatory cytokines IL-4 and IL-10 during the development of hepatocarcinogenesis by chronic DEN treatment in liver tissue homogenates by ELISA. The results depicted in Figure 41A show significant decrease of the IFN-γ expression in tumor areas of 14 weeks (269.6 ± 21.15) and 20 weeks (339.5 ± 18.74) compared to non-tumor areas from 14 weeks (486.2 ± 28.33; $p<0.0001$) and 20 weeks (509.6 ± 32.28; $p<0.001$). Similarly, the concentration of the pro-inflammatory cytokine TNF-α was significantly lower in tumor areas from 14 (103.0 ± 10.01) and 20 weeks (90.49 ± 10.78) groups compared to non-tumor areas of 14 (1250.0 ± 66.25; $p<0.0001$) and 20 weeks (1318 ± 76.65; $p<0.001$), Figure 41B.

However, there was no significant change neither in the expression of IL-4 or in IL-10 between tumor and non-tumor areas at the intrahepatic tissue level, Figure 42A & B. These results show that during HCC, the expression of pro-inflammatory cytokines is lower in tumor areas compared to non-tumors, while no modification was observed in the case of analyzed anti-inflammatory cytokines.

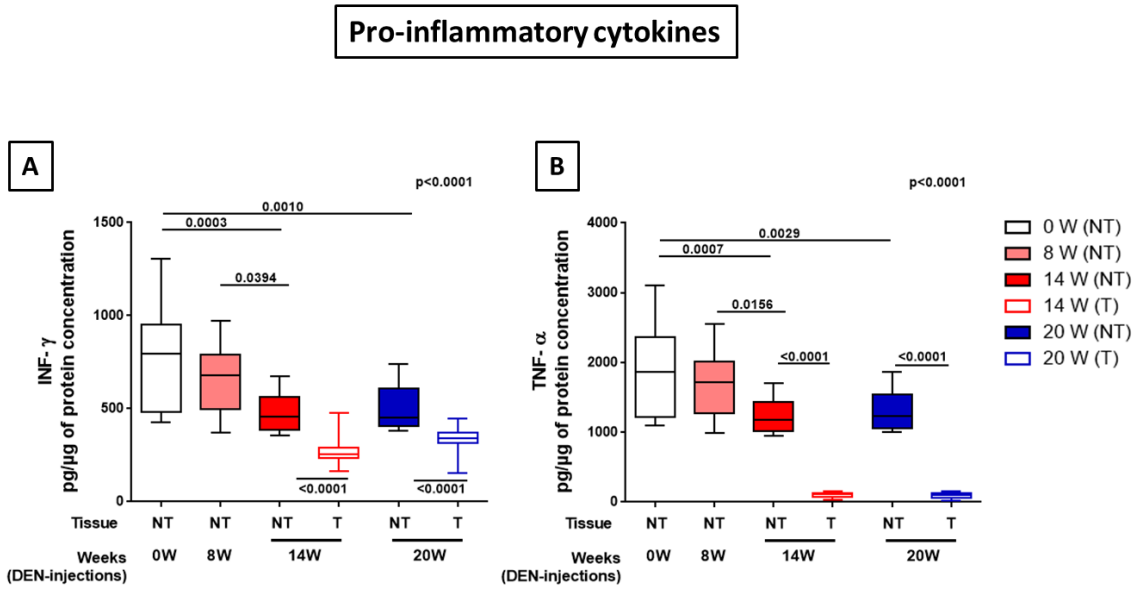

FIGURE 41: ELISA QUANTIFICATION RESULTS OF PROINFLAMMATORY CYTOKINES-INTERFERON GAMME (INF-Γ) AND TUMOR NICROSIS FACTOR ALPHA (TNF-A) EXPRESSION IN BOX&WISKER GRAPH. VALUES ARE MEDIAN ± SE, N=13/GROUP. COMPARISON OF MEAN WAS DONE BY ANOVA TEST WITH TUKEY CORRECTION.

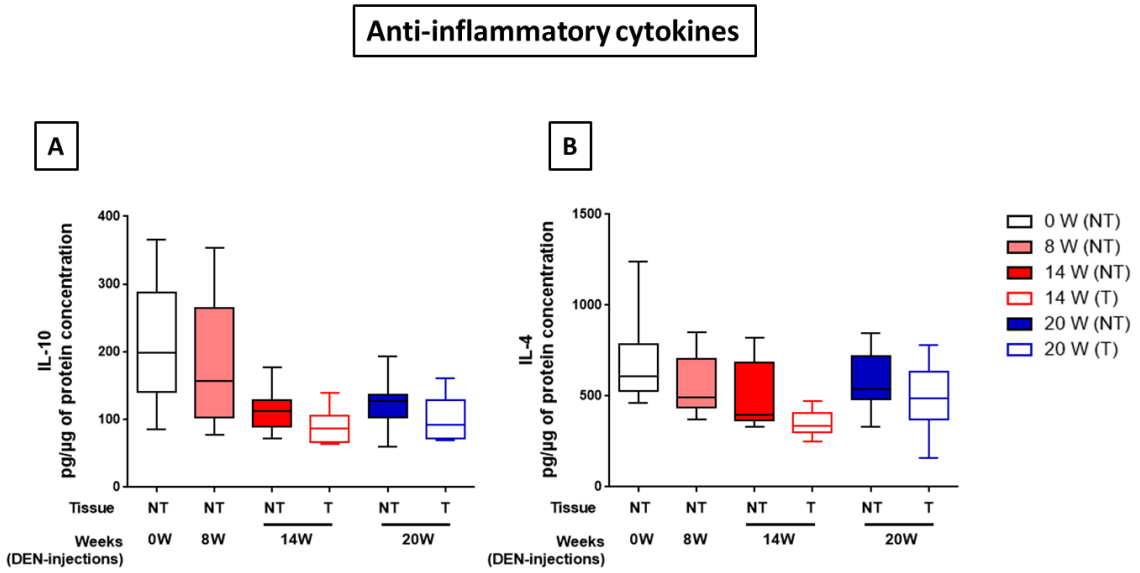

FIGURE 42: ELISA QUANTIFICATION RESULTS OF ANTI-INFLAMMATORY CYTOKINES-INTERLUKIN-10 (IL-10) AND INTERLUKIN-4 (IL-4) EXPRESSION IN BOX&WISKER GRAPH. VALUES ARE MEDIAN ± SE, N=13/GROUP. COMPARISON OF MEAN WAS DONE BY ANOVA TEST WITH TUKEY CORRECTION.

4.1.9.2 Circulating level

The expression levels of majority cytokines tested previously in liver tissue samples did not reach the detection limit of available ELISA kits when measured in serum. Thus, only the results of anti-inflammatory cytokine IL-10 levels were obtained. The result confirmed a significant increase in the expression of circulating IL-10 in 8 (53.84 ± 4.10, p=0.0286), 14 (62.26 ± 5.50, p=0.002) and 20 (65.64 ± 9.99, p=0.0006) weeks compared to 0 week (28.02 ± 1.91), Figure 43. This result confirms that during hepatocarcinogenesis induced by DEN, the circulating levels of immunosuppressive cytokines are increased.

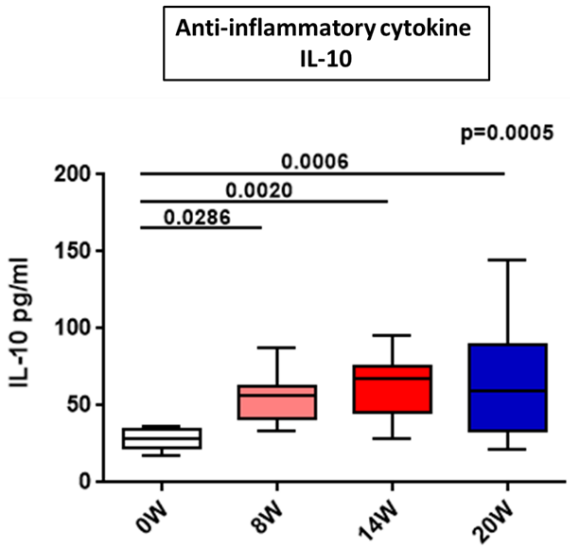

FIGURE 43: ELISA QUANTIFICATION RESULTS OF ANTI-INFLAMMATORY CYTOKINES-INTERLUKIN-10 (IL-10) EXPRESSION IN BOX&WISKER GRAPH. VALUES ARE MEDIAN ± SE, N=13/GROUP.COMPARISON OF MEAN WAS DONE BY ANOVA TEST WITH TUKEY CORRECTION.

Overall cytokine expression profile results by ELISA exemplified the downregulation of pro-inflammatory cytokine expression TNF-α and IFN-γ at the intrahepatic level and upregulation of anti-inflammatory cytokine at circulating level, specify the pro-tumor activity and induction of hepatocarcinogenesis by chronic DEN treatment.

4.2 RESULTS - AKT INHIBITOR (ARQ 751) PROJECT

4.2.1 CLINICAL SAFETY

Primarily, the effect of sorafenib, ARQ 751 and combination (ARQ 751 plus sorafenib) treatment on the body weight of rats was investigated. The results of changes in body weight during 6 weeks of treatment are presented in Figure 44. During the second week of treatment, due to the significant weight loss of cirrhotic rats in ARQ 751 alone and combination (ARQ 751 + Sorafenib) groups, the concentration of the ARQ 751 was reduced to 10mg/kg from 15mg/kg followed till the end of the treatment. Overall, at the end of the treatment, there was no significant body weight loss in the sorafenib, ARQ 751 and combination-treated groups compared to the control group, Table 5.

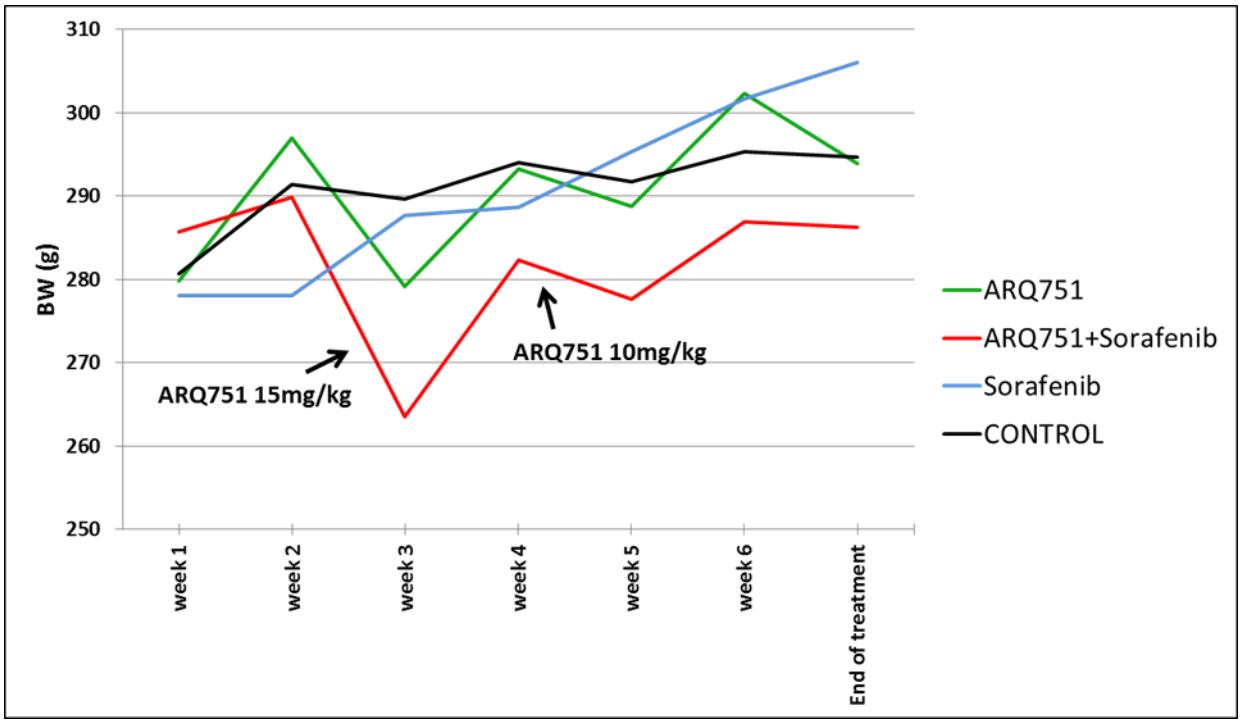

FIGURE 44: EFFECT OF SORAFENIB, ARQ 751 AND COMBINATION TREATMENT ON BODY WEIGHT (BW) OF RATS DURING 6 WEEKS. G=GRAMS. N=7/GROUP

Further clinical safety of the treatment was analyzed and results are summarized in Table 1, which illustrated no significant differences in body weight during treatment. Moreover, there is no difference in the weight of the liver between the treated group and also when compared to the control group. Assessment of triglycerides in the liver did not show any difference between groups (p=0.5783). Blood samples analyses revealed that none of the treatments affect glucose and triglyceride blood concentrations. There was a statistical lower level of aspartate aminotransferase (AST), alanine aminotransferase (ALT), alkaline phosphatase (ALP) and Gamma-glutamyl transpeptidase (GGT) in the combination group compared to control and sorafenib. We also observed significantly lower total bilirubin in ARQ 751 alone and combination group compared to control. No differences were observed between sorafenib and control groups. Thus, our results showed that ARQ 751 and combination treatment improve liver function.

		Control (n=6)	**Sorafenib (n=6)**	**ARQ 751 (n=6)**	**Combination (n=6)**	**ANOVA p-values**
Body Weight (g)		291±5.0	290±4.1	290±3.3	281±3.3	*0.1520*
Liver	Weight (g)	13.0±0.4	13.1±0.3	13.1±0.4	11.6±0.6	*0.0567*
	TG (g/L)	31.5±4.9	26.6±1.9	28.5±2.5	26.3±1.7	*0.5783*
Blood	Albumin (g/dL)	3.5±0.18	3.6±0.06	3.6±0.029	3.3 ±0.05$^{*, \#}$	*0.0033*
	AST (U/L)	97.4±5.9	90.2±4.8	82.9±2.9	75.3±3.6*	*0.0168*
	ALT (U/L)	69.3±3.9	71.2±3.4	61.8±3.4	50.3±3.0$^{**, \#\#}$	*0.0011*

	ALP (U/L)	199.2±9.7	212.0±7.6	184.6±7.1	192.0±5.7	*0.1187*
	GGT (U/L)	14.0±3.0	15.3±2.1	7.7±1.7	2.7±1.1$^{**, \#\#}$	*0.0016*
	PT (s)	18.1±0.5	19.2±1.3	18.0±0.3	18.5±0.5	*0.7327*
	Total Bilirubin (mg/dL)	0.25±0.04	0.18±0.01	0.15±0.006*	0.14±0.009**	*0.0044*
	Creatinine (mg/dL)	0.37±0.02	0.33±0.02	0.4±0.01$^{\#}$	0.31±0.01	*0.0028*
	GLU (mg/dL)	132.3±7.8	141.1±5.7	152.6±7.0	140.0±6.2	*0.2488*
	Cholesterol (mg/dL)	84.4±4.34	86.2±3.0	102.6±2.0$^{**, \#\#}$	84.71±2.2	*0.0015*
	TG (g/L)	78.4±11.1	70.3±10.7	54.01±11.5	60.6±13.13	*0.4764*

TABLE 5: CLINICAL AND BIOLOGICAL ANALYSIS. AST, ASPARTATE AMINOTRANSFERASE; ALT, ALANINE AMINOTRANSFERASE; ALP, ALKALINE PHOSPHATASE; GGT, GAMMA-GLUTAMYL TRANSPEPTIDASE; PT, PROTHROMBIN TIME. VALUES ARE MEANS ± SE. SIGNIFICANT DIFFERENCE COMPARED TO CONTROL; GLU, GLUCOSE; TG, TRIGLYCERIDE *: P<0.05; **: P<0.01; ***: P<0.001; ****: P<0.0001. SIGNIFICANT DIFFERENCE BETWEEN ARQ 751 AND SORAFENIB; ##: P<0.01. N=7/GROUP

4.2.2 MORPHOLOGICAL ANALYSIS

The effect of ARQ 751, sorafenib and the combination of both treatments was studied on tumor progression by liver MRI scan. Figure 45 represents the MRI morphological analysis in the control group.

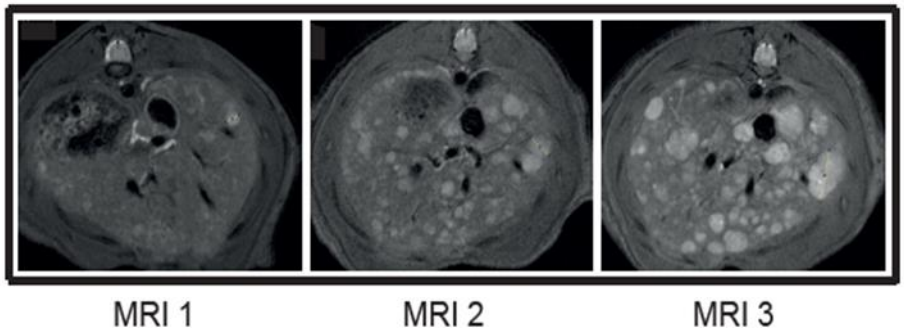

FIGURE 45: REPRESENTATIVE PICTURE OF MRI MORPHOLOGICAL ANALYSIS OF CONTROL GROUP. MRI1 WAS PERFORMED BEFORE RANDOMIZATION OF GROUPS TO DIFFERNET TREATMENTS AND MRI2 & 3 WERE DONE AFTER 3 & 6 WEEKS OF TREATMENT.

MRI data analyses showed that tumor progression was significantly reduced in the sorafenib (105.7± 9.70%; p=0.0050) and ARQ 751 (91.5± 11.9%; p=0.0004) groups compared to control (158.8±11.6), Figure 46. Interestingly, the greatest decrease in tumor progression rate was observed in the combination group (49.4± 5.12%; p<0.0001) when compared with control, indicating an additive effect of sorafenib and ARQ 751 on tumor progression. Similarly, ARQ 751 alone (91.5± 11.9%; p=0.0309) and combination (49.41 ± 5.1%; p=0.0029) treatment significantly reduced tumor progression compared to sorafenib.

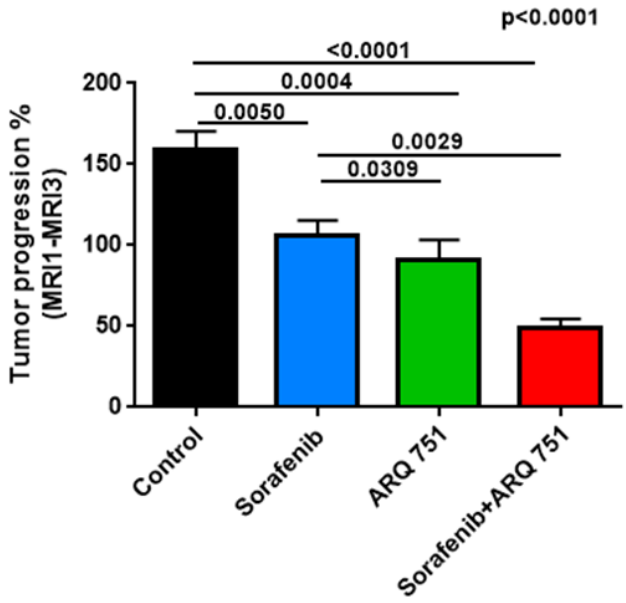

FIGURE 46: TUMOR PROGRESSION ASSESSMENT BY COMPARISON OF TUMOR SIZE ON MRI1, 2 AND 3 IN CONTROL, SORAFENIB, ARQ 751 AND COMBINATION GROUP. QUANTIFICATION OF DATA IS REPRESNTED AS COLUMN BAR GRAPH. VALUES ARE MEANS±SE, N=7/GROUP. COMPARISON OF MEANS DONE BY ANOVA TEST WITH TUKEY CORRECTION

4.2.3 HISTOPATHOLOGICAL ANALYSES

MRI analysis was further confirmed by macroscopic examination of the liver. The macroscopic counting of tumors revealed a significant lower number of tumors in rats treated by sorafenib, ARQ 751 and combination compared to control (ANOVA, $p<0.0001$) (Figure 47A). In fact, numbers of surface liver tumor nodules were decreased by 60% and 80% in rats treated by ARQ 751 (36.6 ± 8.16; $p<0.0001$) and combination (18.2 ± 2.82; $p<0.0001$), compared to control group (100.4 ± 7.302) (Figure 47A). Similarly, ARQ 751 ($p=0.0294$) and combination ($p=0.0003$) group displayed a significantly lower number of tumors compared to sorafenib-treated animals. Likewise, examination of tumor size revealed significantly larger mean tumor size of 9.9 ± 0.9 mm in control group compared to 6.4 ± 0.3 mm in sorafenib ($p=0.0006$), 4.3 ± 0.4 mm in ARQ 751 ($p<0.0001$) and 3.3 ± 0.2 mm in combination group ($p<0.0001$) (Figure 47B). Mean tumor size in ARQ 751

and the combination group was significantly reduced when compared with Sorafenib treatment (p=0.0468 and p=0.0024). Hence, ARQ 751 and combination treatment showed statistically greater efficiency in the control of tumoral initiation and progression.

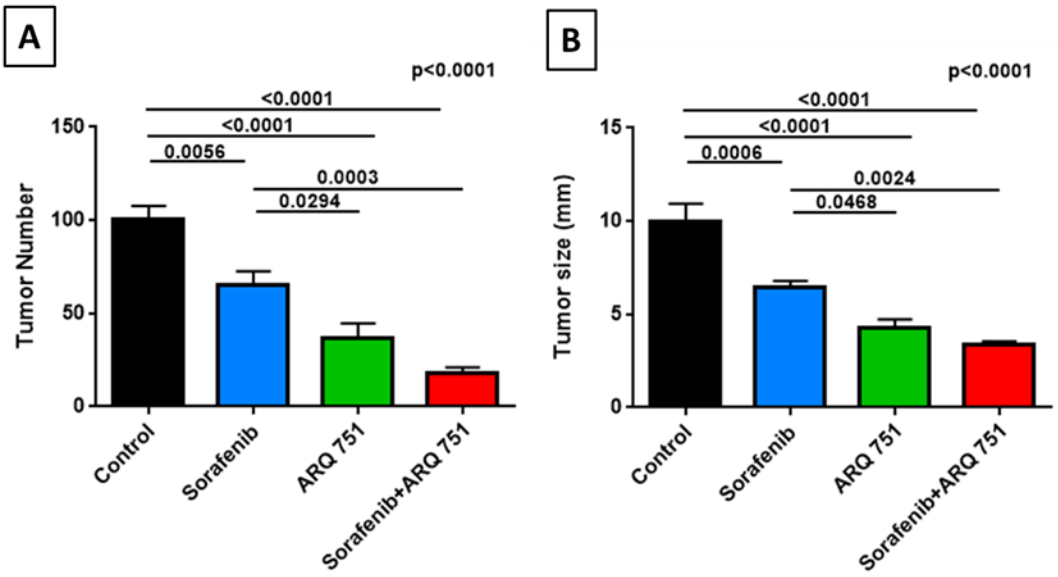

FIGURE 47: EFFECT OF SORAFENIB, ARQ751 AND SORAFENIB+ARQ751 (COMBINATION) TREATMENT ON TUMOR NUMBER AND SIZE. A) MACROSCOPIC EXAMINATION OF LIVERS WITH ASSESSMENT OF TUMOR NUMBER AT THE SURFACE OF LIVERS. B) MACROSCOPIC EXAMINATION OF LIVERS TUMOR SIZE (AVERAGE OF DIAMETER OF THE FIVE LARGEST TUMORS). QUANTIFICATION OF DATA IS REPRESNTED AS COLUMN BAR GRAPH. VALUES ARE MEANS±SE, N=7/GROUP. COMPARISON OF MEANS DONE BY ANOVA TEST WITH TUKEY CORRECTION

4.2.4 EFFECT ON PROLIFERATION

Therefore, immunohistochemistry of Ki67 and Cyclin D1 were performed to analyze the HCC proliferation rate by sorafenib, ARQ 751 and combination treatment compared to the control group (Figure 48A, Figure 49A). Quantification of Ki67 immunohistochemistry staining showed that the frequency of $Ki67^{+}$ nucleus was significantly decreased in ARQ 751 (9.32±1.09, p=0.0011) and combination (5.97±0.76, p=0.0004) groups compared to the control group (43.6±11.3). Moreover, combination (p= 0.0105) and ARQ 751 (p= 0.0312) treated groups had also significantly reduced

frequency of Ki67^{+} nucleus compared to sorafenib-treated group (30.63±3.93& p= 0.0052), (Figure 48B).

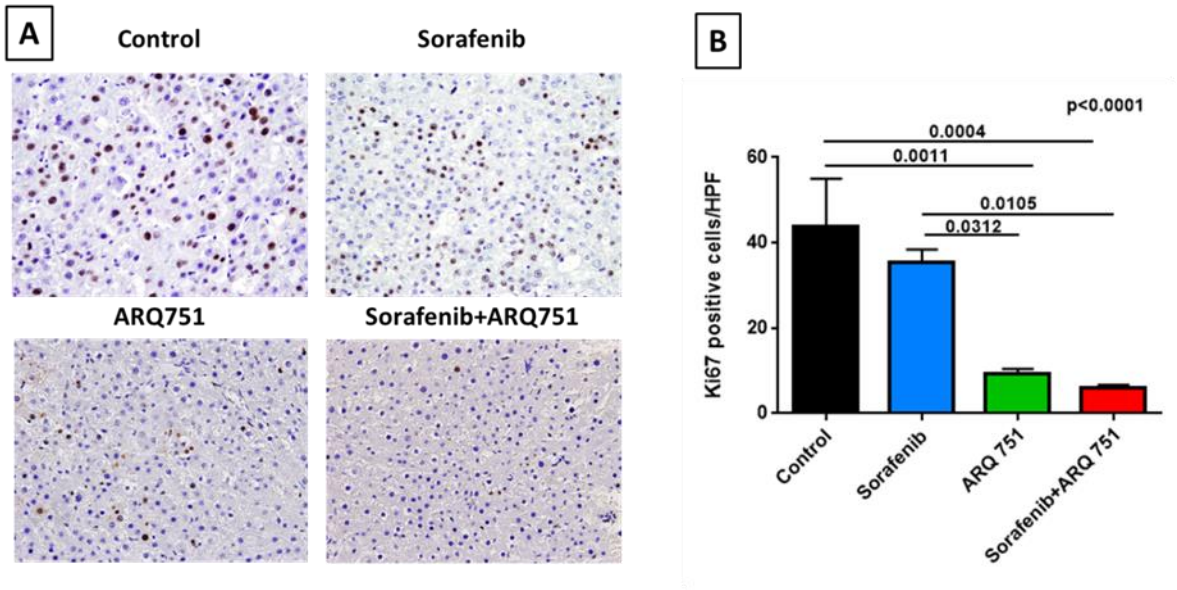

FIGURE 48: EFFECT OF SORAFENIB, ARQ 751 AND SORAFENIB+ARQ 751 (COMBINATION) TREATMENT ON CELL PROLIFERATION A) REPRESENTATIVE IMAGES OF NUCLEAR KI67 STAINING OF CONTROL, SORAFENIB, ARQ751 AND SORAFENIB+ARQ751 (COMBINATION) TREATED GROUP, 20X MAGNIFICATION AND B) QUANTIFICATION OF KI67 STAINING PER HIGH POWER FIELD (HPF). QUANTIFICATION OF DATA IS REPRESNTED AS COLUMN BAR GRAPH. VALUES ARE MEANS±SE, N=7/GROUP. COMPARISON OF MEANS DONE BY ANOVA TEST WITH TUKEY CORRECTION

Similarly, Cyclin D1 immunohistochemistry staining displayed a significant decrease in the frequency of Cyclin D1^{+} nucleus in sorafenib (36.61±6.52, p=0.0467), ARQ 751 (20.07±4.03, p=0.0006) and combination (20.07±4.03, p=0.0006) groups compared to control group (Figure 49B). Thus, results of Ki67 and Cyclin D1 staining demonstrated that ARQ 751 and combination treatment effectively reduced hepatocyte proliferation.

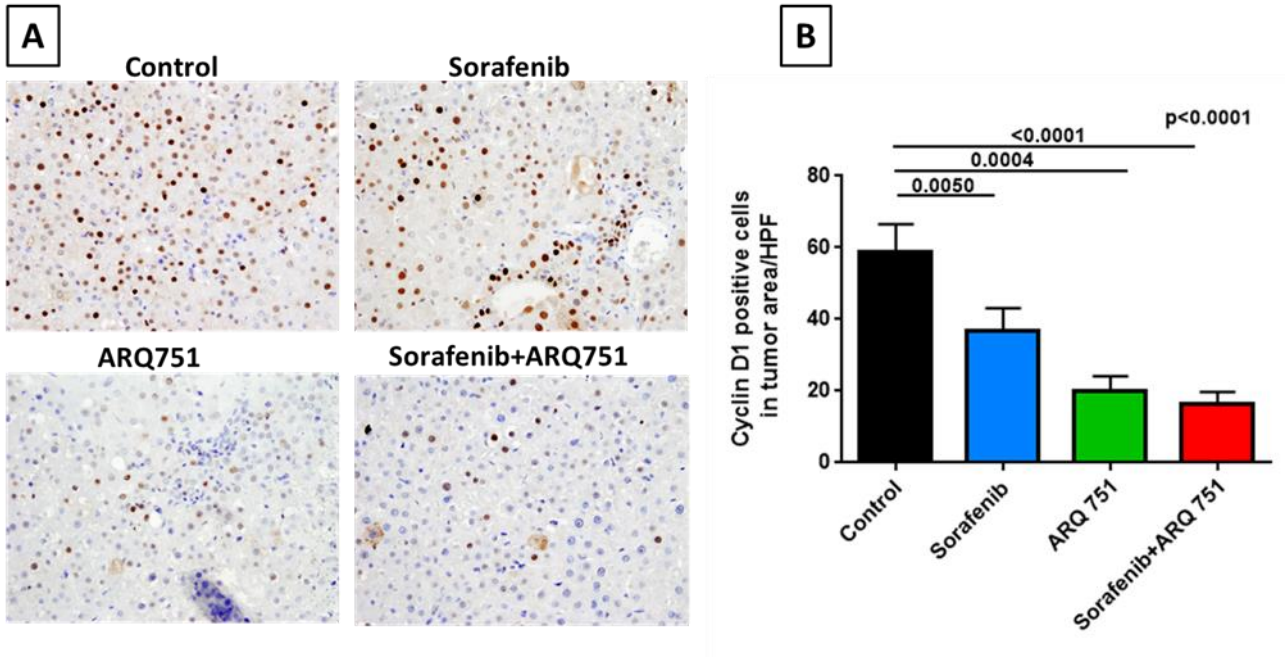

FIGURE 49: EFFECT OF SORAFENIB, ARQ 751 AND SORAFENIB+ARQ 751 (COMBINATION) TREATMENT ON CELL PROLIFERATION A) REPRESENTATIVE IMAGES OF NUCLEAR CYCLIN D1 STAINING OF TREATED GROUP, 20X MAGNIFICATION AND B) QUANTIFICATION OF KI67 STAINING PER HIGH POWER FIELD (HPF). QUANTIFICATION OF DATA IS REPRESNTED AS COLUMN BAR GRAPH. VALUES ARE MEANS±SE, N=7/GROUP. COMPARISON OF MEANS DONE BY ANOVA TEST WITH TUKEY CORRECTION

4.2.5 EFFECT ON ANGIOGENESIS

To prove an anti-angiogenic effect, tumor vascularization was studied by using a rat specific anti-CD34 antibody to perform immunofluorescence staining of liver tissues. While structural abnormalities of the tumor vasculature were numerous in control animals, normalization of vasculature was observed in ARQ 751 and combination groups (Figure 50A). The quantification of vascular density revealed that ARQ 751 decreased vascular density by 62% (38.8±3.34%, $p=0.0204$) and combination treatment, by 68% (32.9±3.79%, $p<0.0001$) compared to control group (100±15.9) (Figure 50B). Therefore, CD34 staining demonstrated that treatment by ARQ 751 and combination leads to vascular normalization and inhibition of tumor angiogenesis.

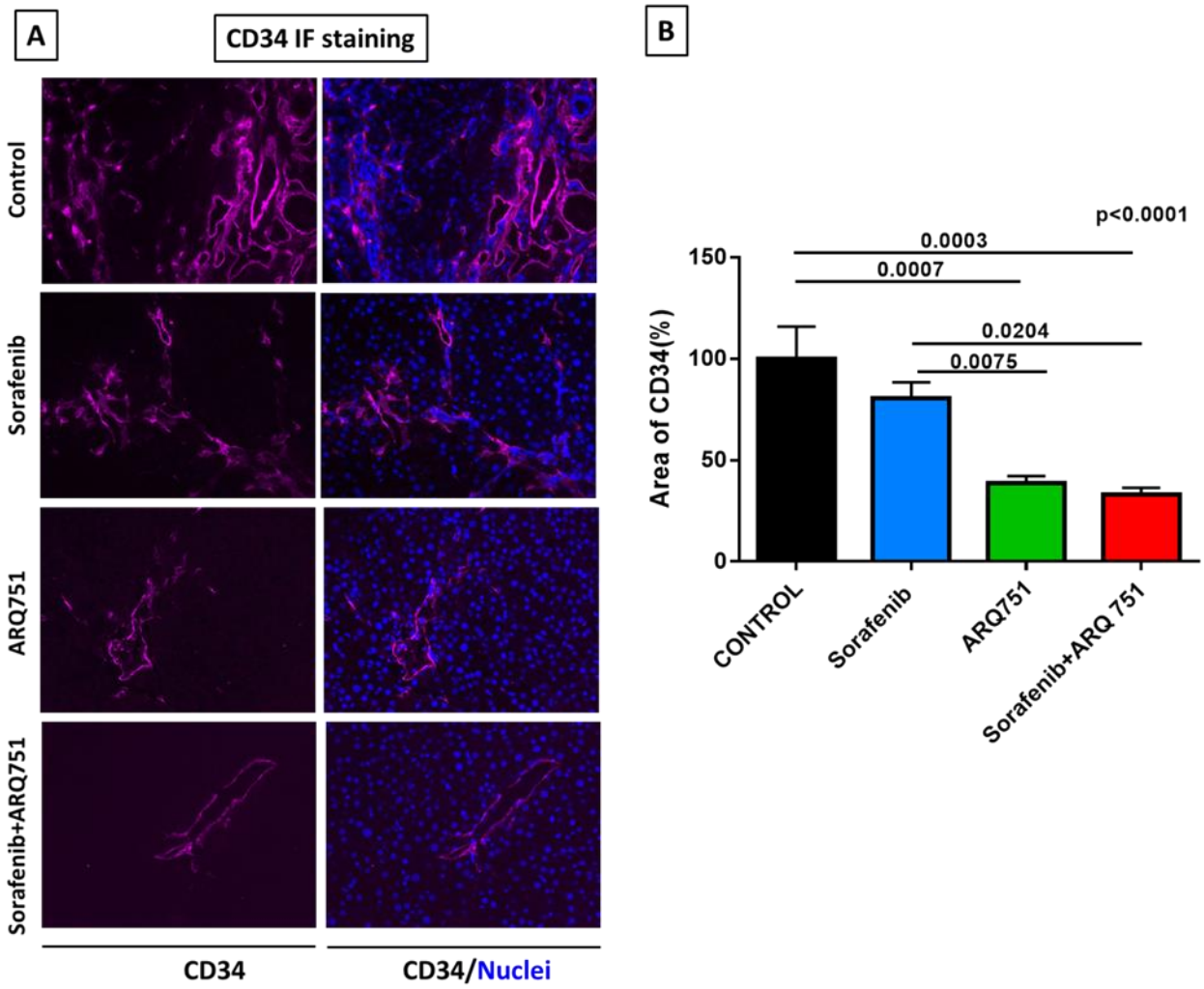

FIGURE 50: EFFECT OF SORAFENIB, ARQ 751 AND SORAFENIB+ARQ 751 (COMBINATION) TREATMENT ON ANGIOGENESIS. A) REPRESENTATIVE IMAGES OF CD34 STAINING OF CONTROL, SORAFENIB, ARQ 751 AND SORAFENIB+ARQ 751 (COMBINATION) TREATED GROUP, 20X MAGNIFICATION AND B) QUANTIFICATION OF CD34+ STAINING SURFACE AREA PER HIGH POWER FIELD (HPF). CONTROL WAS SET AS 100%. QUANTIFICATION OF DATA IS REPRESNTED AS COLUMN BAR GRAPH. VALUES ARE MEANS±SE, N=7/GROUP. COMPARISON OF MEANS DONE BY ANOVA TEST WITH TUKEY CORRECTION

4.2.6 EFFECT ON FIBROSIS

Liver fibrosis was analyzed by Sirius red staining (Figure 51A). As shown in Figure 51B, fibrotic tissue was significantly reduced in ARQ 751 (55.1±6.57%, p=0.0037) and combination (45.1±3.35%, p=0.0004) group compared to the control group (100±10.7%). Besides, the combination group also significantly reduced fibrosis compared to the sorafenib-treated group (p=0.0086).

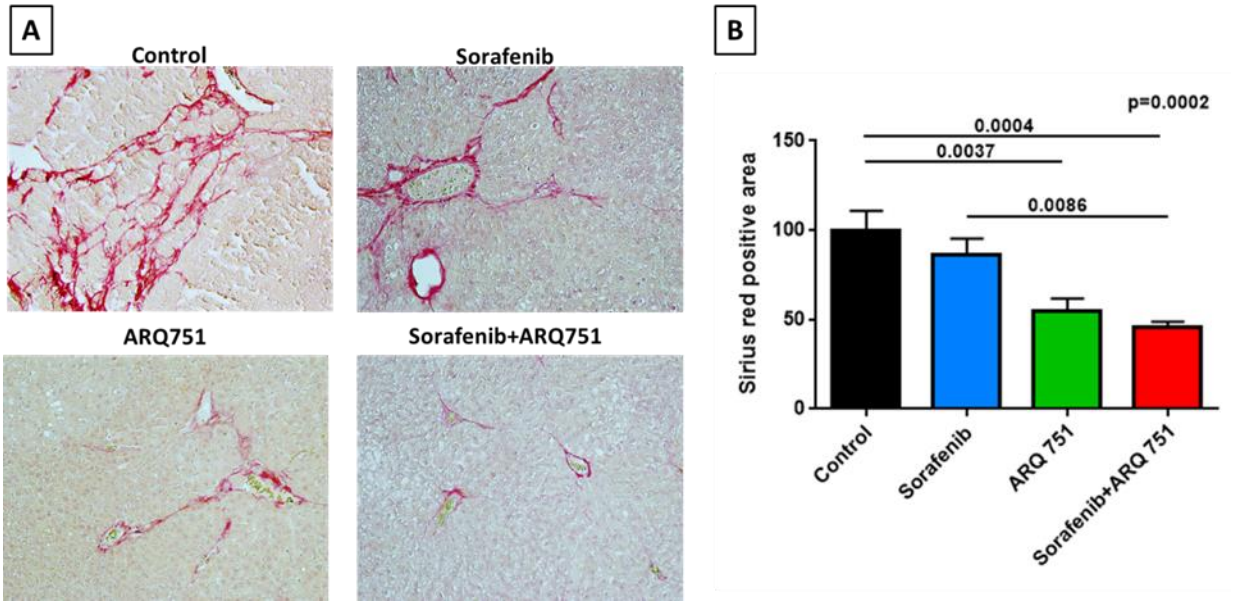

FIGURE 51: EFFECT OF SORAFENIB, ARQ 751 AND SORAFENIB+ARQ 751 (COMBINATION) TREATMENT ON LIVER FIBROSIS. A) REPRESENTATIVE IMAGES OF SIRIUS RED+ STAINING OF CONTROL, SORAFENIB, ARQ 751 AND SORAFENIB+ARQ 751 (COMBINATION) TREATED GROUP, 20X MAGNIFICATION AND B) QUANTIFICATION OF SIRIUS RED+ STAINING SURFACE AREA PER HIGH POWER FIELD (HPF). CONTROL WAS SET AS 100%. QUANTIFICATION OF DATA IS REPRESNTED AS COLUMN BAR GRAPH. VALUES ARE MEANS±SE, N=7/GROUP. COMPARISON OF MEANS DONE BY ANOVA TEST WITH TUKEY CORRECTION

Furthermore, the effect of sorafenib, ARQ 751 and combination treatment on liver fibrosis was examined by qPCR analysis. Liver fibrosis markers such as Collagen 1, α-smooth muscle tissue (α-SMA) and transforming growth factor receptor (TGF-β) were investigated, Figure 52. Results demonstrated that compared to the control group, collagen 1 gene expression was significantly

down regulated in ARQ 751 (p=0.0103) and combination (p=0.0002) group, Figure 52. Also, when compared to sorafenib, combination group had significantly reduced gene expression of collagen1 (p=0.0337), Figure 52. α-SMA gene expression was also significantly down-regulated in sorafenib, ARQ751 and combination group compared to the control group (p<0.0001), Figure 52. Similarly, TGF-β expression was significantly down-regulated in ARQ 751 (p=0.0342) and combination (p=0.0025) group compared to the control group, Figure 52. Overall, ARQ 751 and combination treatment significantly decreased hepatic collagen deposition and fibrosis-associated markers.

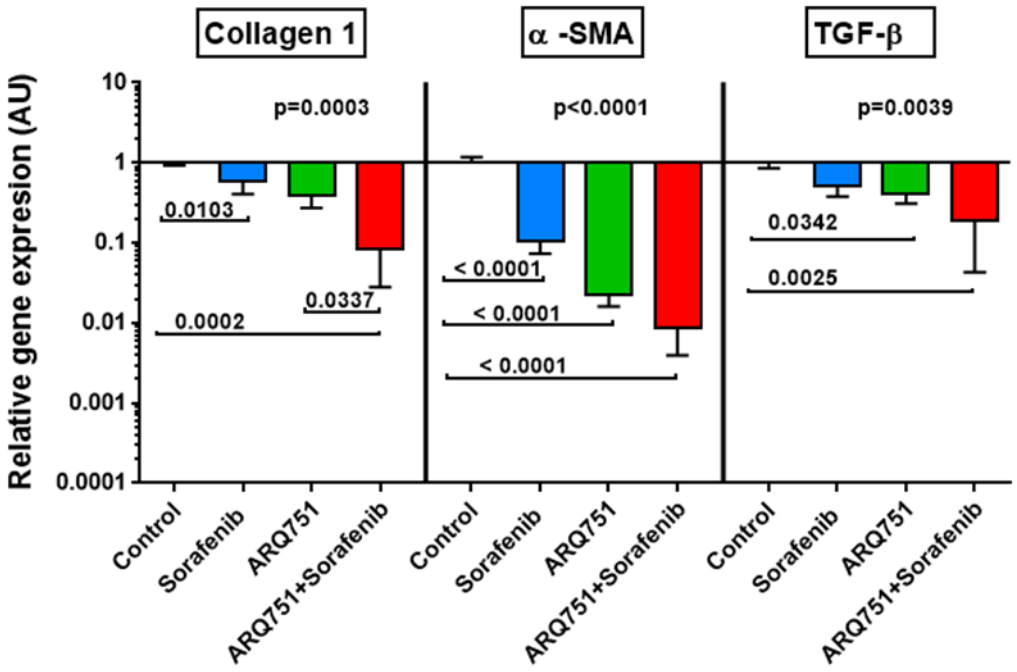

FIGURE 52: RELATIVE GENE EXPRESSION OF COLLAGEN 1, ALPHA-SMOOTH MUSCLE TISSUE (A-SMA) AND TRANSFORMING GROWTH FACTOR (TGF-B) IN NON-TUMOR LIVER TISSUE OF CONTROL, SORAFENIB, ARQ 751 AND ARQ 751+SORAFENIB (COMBINATION) GROUPS (N=7/GROUP). CONTROL WAS SET AS 1. QUANTIFICATION OF DATA IS REPRESNTED AS COLUMN BAR GRAPH. VALUES ARE MEANS±SE, N=7/GROUP. COMPARISON OF MEANS DONE BY ANOVA TEST WITH TUKEY CORRECTION

4.2.7 EFFECT ON MACROPHAGES

Immunohistochemistry of CD68 was performed to characterize the effect of sorafenib, ARQ 751 and combination treatment on macrophages in the tumor microenvironment (Figure 53A). Interestingly, the frequency of $CD68^{+}$ cells was significantly reduced by sorafenib (7.94±0.81, p=0.0325), ARQ 751 (5.43±0.92, p=0.0006) and combination (4.18±0.28, p<0.0001) treatment compared to control group (12.1±1.53), (Figure 53B). Hence, this observation clearly illustrates that macrophages expression is significantly reduced by sorafenib, AKT inhibitor alone or by a combination of ARQ 751 with sorafenib.

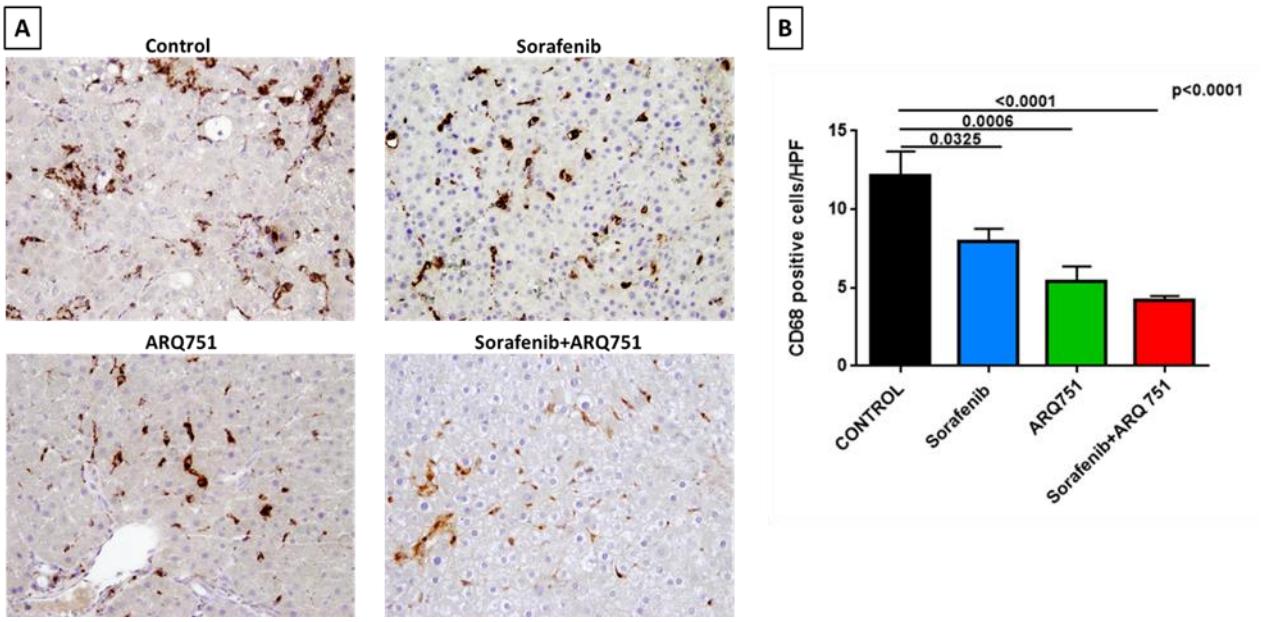

FIGURE 53: EFFECT OF SORAFENIB, ARQ 751 AND SORAFENIB+ARQ 751 (COMBINATION) TREATMENT ON TUMOR MICROENVIRONMENT. A) REPRESENTATIVE IMAGES OF CD68+ STAINING OF CONTROL, SORAFENIB, ARQ 751 AND SORAFENIB+ARQ 751 (COMBINATION) TREATED GROUP, 20X MAGNIFICATION AND B) QUANTIFICATION OF CD68+ STAINING PER HIGH POWER FIELD (HPF). CONTROL WAS SET AS 100%. QUANTIFICATION OF DATA IS REPRESNTED AS COLUMN BAR GRAPH. VALUES ARE MEANS±SE, N=7/GROUP. COMPARISON OF MEANS DONE BY ANOVA TEST WITH TUKEY CORRECTION

5. DISCUSSION

HCC is the most common type of primary liver cancer, ranking as the third most common cause of death from cancer worldwide. It is majorly associated with liver fibrosis or cirrhosis developed from chronic liver injuries related to risk factors as mentioned previously. Although each underlying condition involves different carcinogenic pathways, it occurs predominantly in patients with underlying chronic liver diseases and cirrhosis [234]. Therapeutic options for late-stage liver cancer are very limited and the prognosis is often poor. Hence, a better understanding of the molecular mechanisms involved in the initiation, progression, and metastasis of HCC is critical for developing more rational diagnostic and therapeutic approaches. However, in order to identify specific adverse effects that could be related to the background of cirrhosis, the newly developed drugs should be pre-clinically tested in an appropriate animal model. Therefore, suitable animal models are essential to promote understanding of the molecular, cellular and pathophysiological mechanisms of HCC and for the development of new therapeutic strategies. As fibrosis/cirrhosis modifies liver vascularization, extracellular matrix composition, and drug metabolism, it is essential to use a cirrhotic animal model to test HCC drugs, in order to test efficacy on tumors but also tolerance of the treatment. Indeed, the sequence of pathophysiological alterations in chemically induced models of HCC has a high similarity with that seen in HCC in humans. Thus, one of the models that most faithfully reproduces human cirrhosis is diethyl nitrosamine-injured rats (DEN). Nevertheless, most of HCC models have a background of normal surrounding liver or moderately fibrotic liver and animal that mostly used are mice which are not successful in developing cirrhosis. In this study, we chose a rat model because rats are able to develop extensive fibrosis, compensated cirrhosis, decompensated cirrhosis and HCC after chronic administration of DEN [173]. However, even though the DEN-induced HCC rat model very well mimics the

pathological process of human HCC, limited information existed about inflammation status or immune system features of this model during progression from liver cirrhosis to carcinoma. In order to address these crucial questions, in our study we have characterized the process of fibrosis/cirrhosis and progression to HCC induced by chronic DEN treatment at chosen time points. In this process, primarily the macroscopic and microscopic evaluation of tumors, and histopathological analysis confirmed the induction of HCC (100% tumors) by chronic DEN treatment at 14 weeks. Later the carcinogenesis induced by chronic DEN treatment was analyzed through CD133, GST-P and EPCAM expression. CD133 is regarded as a cancer stem cell biomarker. From the quantification data, the expression of CD133 increased during the development of HCC, which is consistent with the study of Wu K, Ding J, Chen C, et al (2012). They pointed out that the progression of HCC in DEN-injured rats is associated with the accumulation of cancer stem cells in rat liver tissue, similarly as in humans [235]. Similarly, the EPCAM marker of liver cancer stem cell, which is expressed in hepatic progenitor cells and HCC [236], is significantly increased in tumors compared to non-tumors. GST-P is a marker for a pre-neoplastic liver lesion in rat hepatocarcinogenesis, which explains the high expression of GST-P at 8 weeks in our study, while CD133 is still very low at 8 weeks.

High hepatocyte proliferation is a risk factor for the development of HCC. In this study, hepatocarcinogenesis induced by chronic DEN treatment has been accompanied by a significant increase in cell proliferation markers. Similarly, human HCC is known to be a hyper-vascularized tumor. In our study, we have observed a significant increase in the structural abnormalities of the tissue vascularization at 8, 14 and 20 weeks which indicate that chronic DEN treatment enhanced expression of CD34 reflecting phenotypic changes of tissue vascularization, mimicking the human HCC. This is particularly important as the increased and irregular vasculature will allow small

HCC lesions to progress and metastasize, which is a typical situation in the fibrotic liver characterized by constantly increased formation of blood vessels [237]. As a consequence, hepatic fibrosis accumulates extreme connective tissue in the liver representing tissue-damaging in response to chronic and repeated liver cell injury. Further developed fibrosis progresses by disrupting hepatic architecture and eventually function. In this study, Sirius red staining and METAVIR score analysis clearly showed that liver fibrosis significantly increased in 8, 14 and 20 weeks and compare to 0 week. Moreover, the liver fibrotic process by chronic DEN treatment was confirmed by qPCR analysis. The expression of fibrosis markers such as Collagen 1, α-SMA, TGFβ 1 and TIMP1 were upregulated and in contrary MMP2 and MMP9 expression were down-regulated by the effect of chronic DEN treatment. Altogether, our results confirm that chronic DEN treatment effectively induces fibrosis/cirrhosis which is fundamental for the development and progression of HCC. Besides, the occurrence and prognosis of HCC is also closely related to modulations of the immune system [238-240]. The immune system of the liver contributes to the severity of the necrotic-inflammatory tissue damages, to the establishment of the fibrosis and cirrhosis and to the disease progression towards HCC. Moreover, studies on immune cells in livers from patients with HCC have clearly demonstrated changes in inflammatory and immune response as an independent predictor for HCC occurrence/relapse, especially changes in T-cells lymphocyte infiltration and phenotypes and functions of immune cells in general [240]. Therefore, it is crucial to understand the mechanisms of the immune and inflammatory responses of the liver microenvironment in animal models of HCC. In this study, flow cytometry analyses were performed at intrahepatic and circulating level. Most important result demonstrated is a significant decrease in the frequency of $CD8^+$ T cells in tumor areas compared to non-tumor areas. This was also accompanied by a significant increase in Tregs in tumor areas compared to non-tumors. Moreover, we also performed qPCR analysis to study the intrahepatic immune system at the gene level and similar to flow

cytometry data, the expression of CD8 was significantly lower in tumor compared with non-tumor tissue. Altogether, considering the antitumor responses of CD8 cytotoxic T lymphocytes and pro-tumor activity of Treg lymphocytes in liver microenvironment i.e., decreased $CD8^+$ cells and increased $Treg^+$ cells contributes to the promotion of tumorigenesis, as in human HCC [241] [240], which makes the DEN-induced rat model a very useful model mimicking both, tumor microenvironment and immune system of HCC. Furthermore, increased frequency of Treg cells in the tumor at 14 and 20 weeks triggered us to check the CTLA-4 (CD152) expression in liver tissue as the CTLA-4 pathway also involved in the regulation of T-cell mediated immune response. For instance, the presence of CTLA-4 molecule has been demonstrated as a strong inductor of Tregs function [242, 243]. Hence results from flow cytometry analysis depicted that 50% from increased expression of $CTLA\text{-}4^+CD4^+T$ attribute to $CTLA\text{-}4^+Treg^+$ cells at 8 and 14 weeks and 30% at 20 weeks. As a result, the increased expression of $CTLA4^+$Treg cells (by flow cytometry analysis) and CTLA-4+ cells (from immunofluorescence analysis) demonstrated that the immune system has been suppressed which further favors the development and progression of HCC.

Moreover, in this study, we also focused on the phenotype of macrophages during the progression and development of HCC in the DEN rat model. Macrophages play several important roles and are key players in immunity [108]. Besides, having the capability of antigen presentation, they play a role in homeostasis, tissue remodeling and repair as well as phagocytosis. Similar to previous results and observations reported in the literature for DEN-induced liver cancer [189], our results depicted that there is a significant increase in the frequency of macrophages in the livers tissue of DEN injured rats at 14 and 20 weeks. These hepatic macrophages are classified as resident macrophages known as Kuppfer cells and monocyte-derived macrophages that are patrolled from the blood to the liver during liver injury and inflammation. Besides this classification, macrophages

in general are deciphered into two distinct phenotypes: M1 which are pro-inflammatory and anti-tumor macrophages, and M2 macrophages which are anti-inflammatory, immunosuppressive and pro-tumor. Thus, further in this study, TGM2 and galectin-3, which are markers for M2 macrophages in rats, were stained by immunohistochemistry and immune fluorescence. Results from this staining also reveal that the expression of M2 macrophages is increased following DEN injections and HCC progression. Moreover, galectin-3 (a multifunctional member of the galectin family) was shown to have diagnostic and prognostic significances in cancer, including HCC [244, 245]. More precisely, it has been reported that galectin-3 expression is induced in cirrhotic livers and HCC [246] and that galectin-3 overexpression inhibits the immune response by inducing apoptosis in lymphocytes and promoting tumor growth [247, 248]. Therefore, we performed a deep characterization of galectin-3 in rat model of HCC and also studied the possible link between patient survival and galectin3 expression level analysis by GEPIA and UALCAN web portals. Hence, similar to the human scenario, analysis of galectin-3 (a marker of M2 macrophages) expression revealed its involvement in effectively inducing hepatocarcinogenesis in this rat model

Further, to have insights on the ratio of M2/M1 macrophages in tumor and non-tumor areas in the livers of DEN injured rats, the relative protein expression of iNOS, M1 secreted enzyme, and Arg-1 which is a M2 secreted enzyme, was determined by western blotting. The results showed that the expression of Arg-1 in tumor areas is significantly greater than that in non-tumor areas and in controls. On the contrary, the relative protein expression of iNOS in tumor areas was shown to be less than that in non-tumor areas. In addition, the ratio of M2/M1 macrophages in tumor areas was much higher than that in non-tumor areas. Results from western blot reveal that there is an increasing accumulation of M2 macrophages in tumor areas and this sub-population of macrophages plays a role in immunosuppression and tumor development.

Next, we determined the pro-inflammatory and anti-inflammatory cytokine expression by performing ELISA of TNF-α, IFN-γ, IL-4 and IL-10. The results proved that the cytokine milieu is shifted towards a more anti-inflammatory profile rather than pro-inflammatory. These results confirm other studies that showed that during HCC there is an imbalance in the Th1/Th2 ratio characterized by an increase in Th2 profile and a decrease in Th1 cytokine profile [80].

To conclude, by characterizing the DEN-induced HCC rat model, we found that chronic DEN treatment effectively induced hepatocarcinogenesis and fibrosis/cirrhosis required for the development and progression of HCC. We also found that intrahepatic immune cells, especially T lymphocytes and macrophages in this DEN induced cirrhotic rat model, are modified during the development of HCC, mimicking the human HCC. For instance, we showed that during HCC development, Treg, CTLA-4 and the macrophages (which most of them are polarized towards M2 phenotype in tumor areas), contribute to an immunosuppressive environment and probably promoting the progression of HCC. Thus, these findings help to comprehensively understand the DEN-induced HCC rat model which is very well mimicking the pathological process of human HCC, including immune system features and further use this model more correctly to evaluate new treatment efficacy and tolerance in cirrhotic background.

Currently, the approved systemic treatments for HCC, such as sorafenib, regorafenib etc., are multitargeted tyrosine kinase inhibitors showing a modest improvement in overall survival profile [46]. Furthermore, these treatments often cause side effects altering the quality of the patient's life profile [50]. Therefore, there is an urgent need for new, effective and safe therapies. As we demonstrated before, DEN induced rat cirrhotic HCC model closely reproduces human HCC physiopathology. Therefore, we have tested the safety and efficacy of a new allosteric inhibitor

(ARQ 751) and combination of AKT inhibitor (ARQ 751) and sorafenib compared with sorafenib and control. We observed that tumor progression between MRI 1 and MRI 3 was significantly reduced in all groups of treatment compared to control and was the lowest in the combination group. Similarly, according to histological examination, both sorafenib and ARQ 751 significantly reduced the tumor size compared to the control but combination-treated rats displayed the smallest tumor size.

To confirm the anti-tumor activity of AKT inhibition on the liver tissue, we performed Ki67 and Cyclin D1 staining. The inhibition of AKT by ARQ 751 and combination treatments reduced the number of $Ki67^{+}$ and Cyclin $D1^{+}$ cells compared to sorafenib and control. Besides targeting tumor development and progression, ARQ 751 therapy was efficacious in the modulation of liver microenvironment. This is predominantly important, as tumor microenvironment plays a crucial role in tumor progression and influencing tumor response to therapies. For instance, increased and irregular vasculature will allow small HCC lesions to progress and metastasize, which is a typical situation in the fibrotic liver characterized by constantly increased formation of blood vessels [237]. The mechanism of beneficial action of sorafenib on liver vascularisation was described previously [249]. Here, we showed that the ARQ 751 alone and combination with sorafenib improved the vascularization of liver tissue significantly.

The anti-fibrotic effect of sorafenib was demonstrated previously [250], however in our study, sorafenib treatment did not improve the fibrotic status of the liver. On the other hand, liver fibrosis significantly decreased in ARQ 751 and combination groups compared to control and Sorafenib groups. Moreover, sorafenib-ARQ 751 combination therapy greatly shifted the matrix regulatory pathway leading to fibrosis resolution with a strong decrease of collagen accumulation. Another essential determinant of HCC progression and survival is cancer-associated inflammation, with

TGFβ orchestrating a favorable microenvironment for tumor cell growth. Here we showed that expression of α-SMA and TGFβ in non-tumor tissue was downregulated by ARQ 751 treatment and by sorafenib-ARQ 751 combination.

Thus, we identified a novel treatment choice for advanced HCC with a cirrhotic background. Furthermore, our study clearly illustrated the significance of targeting AKT pathways together with sorafenib treatment of HCC. In summary, we have indicated that allosteric inhibitor ARQ 751 alone or in combination with Sorafenib potently inhibit the AKT pathway. Despite difficult conditions with an aggressive model of cancer in cirrhotic rats, single ARQ 751 treatment showed its efficacy in controlling tumor progression, and demonstrated a good safety profile that makes this experimental drug promising in the treatment of HCC in cirrhotic patients. Moreover, the combination with Sorafenib further increased antitumor efficacy of treatment and can be considered as a novel combination strategy of HCC treatment. As a conclusion, the results presented here confirm the importance of targeting AKT in HCC development and progression. The high potency and high selectivity of these compounds warrant further clinical investigation in the patient with HCC.

6. PERSPECTIVES

Our study results from project 1 (characterization of DEN-induced rat model) and project 2 (AKT inhibitor (ARQ751) shown that macrophages are one of the major populations of immune cells recruited during HCC development in the DEN cirrhotic rat model. In this context, we further aim to investigate the phenotype of these macrophages and their role in the development and progression of HCC in DEN cirrhotic rat model. Therefore, for investigation of the phenotype of macrophages, we plan to characterize the activation state of macrophages (using M1/M2 classification) and the potential modification after different treatment with established specific flow cytometry analysis followed by functional tests of liver macrophages isolated from DEN cirrhotic rat model. Simultaneously, to investigate the role of macrophages in the development and progression of HCC in DEN cirrhotic rat model, we plan to deplete macrophages using clodronate liposomes at different time points of our model to interpret their implication in the carcinogenesis of HCC as well as the implication of monocytes derived macrophages compared to resident ones. Hence these investigations further confirm whether DEN induced cirrhotic rat model can be used to perform the pre-clinical study of the drug targeting macrophages.

7. REFERENCES

1. Fitzmaurice, C., et al., *Global, Regional, and National Cancer Incidence, Mortality, Years of Life Lost, Years Lived With Disability, and Disability-Adjusted Life-Years for 29 Cancer Groups, 1990 to 2016: A Systematic Analysis for the Global Burden of Disease Study.* JAMA Oncol, 2018. **4**(11): p. 1553-1568.
2. Park, J.W., et al., *Global patterns of hepatocellular carcinoma management from diagnosis to death: the BRIDGE Study.* Liver Int, 2015. **35**(9): p. 2155-66.
3. *EASL-EORTC clinical practice guidelines: management of hepatocellular carcinoma.* J Hepatol, 2012. **56**(4): p. 908-43.
4. Villanueva, A., *Hepatocellular Carcinoma.* N Engl J Med, 2019. **380**(15): p. 1450-1462.
5. Petruzziello, A., *Epidemiology of Hepatitis B Virus (HBV) and Hepatitis C Virus (HCV) Related Hepatocellular Carcinoma.* Open Virol J, 2018. **12**: p. 26-32.
6. Llovet, J.M., et al., *Hepatocellular carcinoma.* Nat Rev Dis Primers, 2016. **2**: p. 16018.
7. Hernandez-Gea, V., et al., *Role of the microenvironment in the pathogenesis and treatment of hepatocellular carcinoma.* Gastroenterology, 2013. **144**(3): p. 512-27.
8. Liu, Z., et al., *The trends in incidence of primary liver cancer caused by specific etiologies: Results from the Global Burden of Disease Study 2016 and implications for liver cancer prevention.* J Hepatol, 2019. **70**(4): p. 674-683.
9. Alter, M.J., *Epidemiology and prevention of hepatitis B.* Semin Liver Dis, 2003. **23**(1): p. 39-46.
10. Zamor, P.J., A.S. deLemos, and M.W. Russo, *Viral hepatitis and hepatocellular carcinoma: etiology and management.* J Gastrointest Oncol, 2017. **8**(2): p. 229-242.
11. Konopnicki, D., et al., *Hepatitis B and HIV: prevalence, AIDS progression, response to highly active antiretroviral therapy and increased mortality in the EuroSIDA cohort.* Aids, 2005. **19**(6): p. 593-601.
12. Gowans, E.J., et al., *Patterns of single- and double-stranded hepatitis B virus DNA and viral antigen accumulation in infected liver cells.* J Gen Virol, 1983. **64 (Pt 6)**: p. 1229-39.
13. Fattovich, G., et al., *Natural history and prognostic factors for chronic hepatitis type B.* Gut, 1991. **32**(3): p. 294-8.
14. Sumi, H., et al., *Influence of hepatitis B virus genotypes on the progression of chronic type B liver disease.* Hepatology, 2003. **37**(1): p. 19-26.
15. Lee, J.M., C.M. Wong, and I.O. Ng, *Hepatitis B virus-associated multistep hepatocarcinogenesis: a stepwise increase in allelic alterations.* Cancer Res, 2008. **68**(14): p. 5988-96.
16. Toh, S.T., et al., *Deep sequencing of the hepatitis B virus in hepatocellular carcinoma patients reveals enriched integration events, structural alterations and sequence variations.* Carcinogenesis, 2013. **34**(4): p. 787-98.
17. Friedman, S.L., *Mechanisms of hepatic fibrogenesis.* Gastroenterology, 2008. **134**(6): p. 1655-69.
18. Wang, W.H., R.L. Hullinger, and O.M. Andrisani, *Hepatitis B virus X protein via the p38MAPK pathway induces E2F1 release and ATR kinase activation mediating p53 apoptosis.* J Biol Chem, 2008. **283**(37): p. 25455-67.

19. Chung, T.W., Y.C. Lee, and C.H. Kim, *Hepatitis B viral HBx induces matrix metalloproteinase-9 gene expression through activation of ERK and PI-3K/AKT pathways: involvement of invasive potential.* Faseb j, 2004. **18**(10): p. 1123-5.

20. Fattovich, G., et al., *Influence of hepatitis delta virus infection on morbidity and mortality in compensated cirrhosis type B. The European Concerted Action on Viral Hepatitis (Eurohep).* Gut, 2000. **46**(3): p. 420-6.

21. Smith, D.B., et al., *Expanded classification of hepatitis C virus into 7 genotypes and 67 subtypes: updated criteria and genotype assignment web resource.* Hepatology, 2014. **59**(1): p. 318-27.

22. Li, Y., et al., *Hepatitis C virus core protein increases mitochondrial ROS production by stimulation of Ca2+ uniporter activity.* Faseb j, 2007. **21**(10): p. 2474-85.

23. Okuda, M., et al., *Mitochondrial injury, oxidative stress, and antioxidant gene expression are induced by hepatitis C virus core protein.* Gastroenterology, 2002. **122**(2): p. 366-75.

24. Lemon, S.M. and D.R. McGivern, *Is hepatitis C virus carcinogenic?* Gastroenterology, 2012. **142**(6): p. 1274-8.

25. McGivern, D.R. and S.M. Lemon, *Virus-specific mechanisms of carcinogenesis in hepatitis C virus associated liver cancer.* Oncogene, 2011. **30**(17): p. 1969-83.

26. Schulze-Krebs, A., et al., *Hepatitis C virus-replicating hepatocytes induce fibrogenic activation of hepatic stellate cells.* Gastroenterology, 2005. **129**(1): p. 246-58.

27. Kew, M.C., *Aflatoxins as a cause of hepatocellular carcinoma.* J Gastrointestin Liver Dis, 2013. **22**(3): p. 305-10.

28. Liu, Y. and F. Wu, *Global burden of aflatoxin-induced hepatocellular carcinoma: a risk assessment.* Environ Health Perspect, 2010. **118**(6): p. 818-24.

29. Massey, T.E., et al., *Biochemical and molecular aspects of mammalian susceptibility to aflatoxin B1 carcinogenicity.* Proc Soc Exp Biol Med, 1995. **208**(3): p. 213-27.

30. Kumar, P., et al., *Aflatoxins: A Global Concern for Food Safety, Human Health and Their Management.* Front Microbiol, 2016. **7**: p. 2170.

31. Kew, M.C., *Synergistic interaction between aflatoxin B1 and hepatitis B virus in hepatocarcinogenesis.* Liver Int, 2003. **23**(6): p. 405-9.

32. Rushing, B.R. and M.I. Selim, *Aflatoxin B1: A review on metabolism, toxicity, occurrence in food, occupational exposure, and detoxification methods.* Food Chem Toxicol, 2019. **124**: p. 81-100.

33. Stickel, F., *Alcoholic cirrhosis and hepatocellular carcinoma.* Adv Exp Med Biol, 2015. **815**: p. 113-30.

34. Seitz, H.K. and F. Stickel, *Molecular mechanisms of alcohol-mediated carcinogenesis.* Nat Rev Cancer, 2007. **7**(8): p. 599-612.

35. Linhart, K., H. Bartsch, and H.K. Seitz, *The role of reactive oxygen species (ROS) and cytochrome P-450 2E1 in the generation of carcinogenic etheno-DNA adducts.* Redox Biol, 2014. **3**: p. 56-62.

36. Wang, Y., et al., *Ethanol-induced cytochrome P4502E1 causes carcinogenic etheno-DNA lesions in alcoholic liver disease.* Hepatology, 2009. **50**(2): p. 453-61.

37. Mueller, S., et al., *Carcinogenic Etheno DNA Adducts in Alcoholic Liver Disease: Correlation with Cytochrome P-4502E1 and Fibrosis.* 2018. **42**(2): p. 252-259.

38. Yuan, J.M., et al., *Synergism of alcohol, diabetes, and viral hepatitis on the risk of hepatocellular carcinoma in blacks and whites in the U.S.* Cancer, 2004. **101**(5): p. 1009-17.

39. Vandenbulcke, H., et al., *Alcohol intake increases the risk of HCC in hepatitis C virus-related compensated cirrhosis: A prospective study*. J Hepatol, 2016. **65**(3): p. 543-51.

40. Yki-Jarvinen, H., *Non-alcoholic fatty liver disease as a cause and a consequence of metabolic syndrome*. Lancet Diabetes Endocrinol, 2014. **2**(11): p. 901-10.

41. Bjorkstrom, K., et al., *Histologic Scores for Fat and Fibrosis Associate With Development of Type 2 Diabetes in Patients With Nonalcoholic Fatty Liver Disease.* Clin Gastroenterol Hepatol, 2017. **15**(9): p. 1461-1468.

42. Younossi, Z., et al., *Global burden of NAFLD and NASH: trends, predictions, risk factors and prevention.* Nat Rev Gastroenterol Hepatol, 2018. **15**(1): p. 11-20.

43. Nakagawa, H., et al., *Lipid Metabolic Reprogramming in Hepatocellular Carcinoma.* Cancers (Basel), 2018. **10**(11).

44. Heikenwalder, M., Nat Rev Gastroenterol Hepatol.

45. *EASL Clinical Practice Guidelines: Management of hepatocellular carcinoma.* J Hepatol, 2018. **69**(1): p. 182-236.

46. Llovet, J.M., et al., *Molecular therapies and precision medicine for hepatocellular carcinoma.* Nat Rev Clin Oncol, 2018. **15**(10): p. 599-616.

47. Llovet, J.M., et al., *Sorafenib in advanced hepatocellular carcinoma.* N Engl J Med, 2008. **359**(4): p. 378-90.

48. Cheng, A.L., et al., *Efficacy and safety of sorafenib in patients in the Asia-Pacific region with advanced hepatocellular carcinoma: a phase III randomised, double-blind, placebo-controlled trial.* Lancet Oncol, 2009. **10**(1): p. 25-34.

49. Wilhelm, S.M., et al., *Preclinical overview of sorafenib, a multikinase inhibitor that targets both Raf and VEGF and PDGF receptor tyrosine kinase signaling.* Mol Cancer Ther, 2008. **7**(10): p. 3129-40.

50. Zhai, B. and X.Y. Sun, *Mechanisms of resistance to sorafenib and the corresponding strategies in hepatocellular carcinoma.* World J Hepatol, 2013. **5**(7): p. 345-52.

51. Ikeda, K., et al., *Phase 2 study of lenvatinib in patients with advanced hepatocellular carcinoma.* J Gastroenterol, 2017. **52**(4): p. 512-519.

52. Kudo, M., et al., *Lenvatinib versus sorafenib in first-line treatment of patients with unresectable hepatocellular carcinoma: a randomised phase 3 non-inferiority trial.* Lancet, 2018. **391**(10126): p. 1163-1173.

53. Kudo, M., *Extremely High Objective Response Rate of Lenvatinib: Its Clinical Relevance and Changing the Treatment Paradigm in Hepatocellular Carcinoma.* Liver Cancer, 2018. **7**(3): p. 215-224.

54. Johnson, P.J., et al., *Brivanib versus sorafenib as first-line therapy in patients with unresectable, advanced hepatocellular carcinoma: results from the randomized phase III BRISK-FL study.* J Clin Oncol, 2013. **31**(28): p. 3517-24.

55. Cheng, A.L., et al., *Sunitinib versus sorafenib in advanced hepatocellular cancer: results of a randomized phase III trial.* J Clin Oncol, 2013. **31**(32): p. 4067-75.

56. Zhu, A.X., et al., *SEARCH: a phase III, randomized, double-blind, placebo-controlled trial of sorafenib plus erlotinib in patients with advanced hepatocellular carcinoma.* J Clin Oncol, 2015. **33**(6): p. 559-66.

57. Cainap, C., et al., *Linifanib versus Sorafenib in patients with advanced hepatocellular carcinoma: results of a randomized phase III trial.* J Clin Oncol, 2015. **33**(2): p. 172-9.

58. Wilhelm, S.M., et al., *Regorafenib (BAY 73-4506): a new oral multikinase inhibitor of angiogenic, stromal and oncogenic receptor tyrosine kinases with potent preclinical antitumor activity.* Int J Cancer, 2011. **129**(1): p. 245-55.

59. Bruix, J., et al., *Regorafenib for patients with hepatocellular carcinoma who progressed on sorafenib treatment (RESORCE): a randomised, double-blind, placebo-controlled, phase 3 trial.* Lancet, 2017. **389**(10064): p. 56-66.

60. Finn, R.S., et al., *Outcomes of sequential treatment with sorafenib followed by regorafenib for HCC: Additional analyses from the phase III RESORCE trial.* J Hepatol, 2018. **69**(2): p. 353-358.

61. Abou-Alfa, G.K., et al., *Cabozantinib in Patients with Advanced and Progressing Hepatocellular Carcinoma.* N Engl J Med, 2018. **379**(1): p. 54-63.

62. Abou-Alfa, G.K., et al., *Cabozantinib (C) versus placebo (P) in patients (pts) with advanced hepatocellular carcinoma (HCC) who have received prior sorafenib: Results from the randomized phase 3 CELESTIAL trial.* Journal of Clinical Oncology, 2018. **36**(15_suppl): p. 4019-4019.

63. Kudo, M., *Cabozantinib as a Second-Line Agent in Advanced Hepatocellular Carcinoma.* Liver Cancer, 2018. **7**(2): p. 123-133.

64. Zhu, A.X., et al., *Ramucirumab after sorafenib in patients with advanced hepatocellular carcinoma and increased alpha-fetoprotein concentrations (REACH-2): a randomised, double-blind, placebo-controlled, phase 3 trial.* Lancet Oncol, 2019. **20**(2): p. 282-296.

65. Kudo, M., et al., *Ramucirumab as second-line treatment in patients with advanced hepatocellular carcinoma: Japanese subgroup analysis of the REACH trial.* J Gastroenterol, 2017. **52**(4): p. 494-503.

66. Park, J.O., et al., *Second-line ramucirumab therapy for advanced hepatocellular carcinoma (REACH): an East Asian and non-East Asian subgroup analysis.* Oncotarget, 2016. **7**(46): p. 75482-75491.

67. El-Khoueiry, A.B., et al., *Nivolumab in patients with advanced hepatocellular carcinoma (CheckMate 040): an open-label, non-comparative, phase 1/2 dose escalation and expansion trial.* Lancet, 2017. **389**(10088): p. 2492-2502.

68. Hanahan, D. and R.A. Weinberg, *Hallmarks of cancer: the next generation.* Cell, 2011. **144**(5): p. 646-74.

69. Oda, M., H. Yokomori, and J.Y. Han, *Regulatory mechanisms of hepatic microcirculation.* Clin Hemorheol Microcirc, 2003. **29**(3-4): p. 167-82.

70. Berg, R.D., *Bacterial translocation from the gastrointestinal tract.* Trends Microbiol, 1995. **3**(4): p. 149-54.

71. Lumsden, A.B., J.M. Henderson, and M.H. Kutner, *Endotoxin levels measured by a chromogenic assay in portal, hepatic and peripheral venous blood in patients with cirrhosis.* Hepatology, 1988. **8**(2): p. 232-6.

72. Wisse, E., *An electron microscopic study of the fenestrated endothelial lining of rat liver sinusoids.* J Ultrastruct Res, 1970. **31**(1): p. 125-50.

73. Wisse, E., et al., *Structure and function of sinusoidal lining cells in the liver.* Toxicol Pathol, 1996. **24**(1): p. 100-11.

74. Marrone, G., V.H. Shah, and J. Gracia-Sancho, *Sinusoidal communication in liver fibrosis and regeneration.* J Hepatol, 2016. **65**(3): p. 608-17.

75. Knolle, P.A. and D. Wohlleber, *Immunological functions of liver sinusoidal endothelial cells.* Cell Mol Immunol, 2016. **13**(3): p. 347-53.

76. Kubes, P. and C. Jenne, *Immune Responses in the Liver.* Annu Rev Immunol, 2018. **36**: p. 247-277.

77. Takeuchi, O. and S. Akira, *Pattern recognition receptors and inflammation.* Cell, 2010. **140**(6): p. 805-20.

78. Kubes, P. and W.Z. Mehal, *Sterile inflammation in the liver.* Gastroenterology, 2012. **143**(5): p. 1158-1172.

79. Robinson, M.W., C. Harmon, and C. O'Farrelly, *Liver immunology and its role in inflammation and homeostasis.* Cell Mol Immunol, 2016. **13**(3): p. 267-76.

80. Sachdeva, M., Y.K. Chawla, and S.K. Arora, *Immunology of hepatocellular carcinoma.* World J Hepatol, 2015. **7**(17): p. 2080-90.

81. Zhu, J., H. Yamane, and W.E. Paul, *Differentiation of effector CD4 T cell populations (*).* Annu Rev Immunol, 2010. **28**: p. 445-89.

82. Shuai, Z., et al., *Adaptive immunity in the liver.* Cell Mol Immunol, 2016. **13**(3): p. 354-68.

83. Alisa, A., et al., *Analysis of CD4+ T-Cell responses to a novel alpha-fetoprotein-derived epitope in hepatocellular carcinoma patients.* Clin Cancer Res, 2005. **11**(18): p. 6686-94.

84. Witkowski, M., et al., *Lack of ex vivo peripheral and intrahepatic alpha-fetoprotein-specific CD4+ responses in hepatocellular carcinoma.* Int J Cancer, 2011. **129**(9): p. 2171-82.

85. Beyer, M. and J.L. Schultze, *Regulatory T cells in cancer.* Blood, 2006. **108**(3): p. 804-11.

86. Wu, H., et al., *Intratumoral regulatory T cells with higher prevalence and more suppressive activity in hepatocellular carcinoma patients.* J Gastroenterol Hepatol, 2013. **28**(9): p. 1555-64.

87. Kobayashi, N., et al., *FOXP3+ regulatory T cells affect the development and progression of hepatocarcinogenesis.* Clin Cancer Res, 2007. **13**(3): p. 902-11.

88. Unitt, E., et al., *Compromised lymphocytes infiltrate hepatocellular carcinoma: the role of T-regulatory cells.* Hepatology, 2005. **41**(4): p. 722-30.

89. Manigold, T. and V. Racanelli, *T-cell regulation by CD4 regulatory T cells during hepatitis B and C virus infections: facts and controversies.* Lancet Infect Dis, 2007. **7**(12): p. 804-13.

90. Shen, Y., et al., *TGF-beta regulates hepatocellular carcinoma progression by inducing Treg cell polarization.* Cell Physiol Biochem, 2015. **35**(4): p. 1623-32.

91. Hassin, D., et al., *Cytotoxic T lymphocyte perforin and Fas ligand working in concert even when Fas ligand lytic action is still not detectable.* Immunology, 2011. **133**(2): p. 190-6.

92. Guidotti, L.G., et al., *Immunosurveillance of the liver by intravascular effector CD8(+) T cells.* Cell, 2015. **161**(3): p. 486-500.

93. Lucifora, J., et al., *Specific and nonhepatotoxic degradation of nuclear hepatitis B virus cccDNA.* Science, 2014. **343**(6176): p. 1221-8.

94. Thimme, R., et al., *Comprehensive analysis of the alpha-fetoprotein-specific CD8+ T cell responses in patients with hepatocellular carcinoma.* Hepatology, 2008. **48**(6): p. 1821-33.

95. Carulli, L. and C. Anzivino, *Telomere and telomerase in chronic liver disease and hepatocarcinoma.* World J Gastroenterol, 2014. **20**(20): p. 6287-92.

96. Satow, R., et al., *Combined functional genome survey of therapeutic targets for hepatocellular carcinoma.* Clin Cancer Res, 2010. **16**(9): p. 2518-28.

97. Komori, H., et al., *Identification of HLA-A2- or HLA-A24-restricted CTL epitopes possibly useful for glypican-3-specific immunotherapy of hepatocellular carcinoma.* Clin Cancer Res, 2006. **12**(9): p. 2689-97.

98. Bricard, G., et al., *Naturally acquired MAGE-A10- and SSX-2-specific CD8+ T cell responses in patients with hepatocellular carcinoma.* J Immunol, 2005. **174**(3): p. 1709-16.

99. Harding, J.J., I. El Dika, and G.K. Abou-Alfa, *Immunotherapy in hepatocellular carcinoma: Primed to make a difference?* Cancer, 2016. **122**(3): p. 367-77.

100. Wing, K., et al., *CTLA-4 control over Foxp3+ regulatory T cell function.* Science, 2008. **322**(5899): p. 271-5.

101. Rudd, C.E., A. Taylor, and H. Schneider, *CD28 and CTLA-4 coreceptor expression and signal transduction.* Immunol Rev, 2009. **229**(1): p. 12-26.

102. Tai, X., et al., *Basis of CTLA-4 function in regulatory and conventional CD4(+) T cells.* Blood, 2012. **119**(22): p. 5155-63.

103. Naito, M., G. Hasegawa, and K. Takahashi, *Development, differentiation, and maturation of Kupffer cells.* Microsc Res Tech, 1997. **39**(4): p. 350-64.

104. Ju, C. and F. Tacke, *Hepatic macrophages in homeostasis and liver diseases: from pathogenesis to novel therapeutic strategies.* Cell Mol Immunol, 2016. **13**(3): p. 316-27.

105. Bilzer, M., F. Roggel, and A.L. Gerbes, *Role of Kupffer cells in host defense and liver disease.* Liver Int, 2006. **26**(10): p. 1175-86.

106. Beattie, L., et al., *Bone marrow-derived and resident liver macrophages display unique transcriptomic signatures but similar biological functions.* J Hepatol, 2016. **65**(4): p. 758-768.

107. Degroote, H., et al., *Preclinical and Clinical Therapeutic Strategies Affecting Tumor-Associated Macrophages in Hepatocellular Carcinoma.* 2018. **2018**: p. 7819520.

108. Ginhoux, F., et al., *New insights into the multidimensional concept of macrophage ontogeny, activation and function.* Nat Immunol, 2016. **17**(1): p. 34-40.

109. Mosser, D.M. and J.P. Edwards, *Exploring the full spectrum of macrophage activation.* Nat Rev Immunol, 2008. **8**(12): p. 958-69.

110. Sica, A. and A. Mantovani, *Macrophage plasticity and polarization: in vivo veritas.* J Clin Invest, 2012. **122**(3): p. 787-95.

111. Murray, P.J., *Macrophage Polarization.* Annu Rev Physiol, 2017. **79**: p. 541-566.

112. Wijesundera, K.K., et al., *M1- and M2-macrophage polarization in rat liver cirrhosis induced by thioacetamide (TAA), focusing on Iba1 and galectin-3.* Exp Mol Pathol, 2014. **96**(3): p. 382-92.

113. Vogel, D.Y., et al., *Human macrophage polarization in vitro: maturation and activation methods compared.* Immunobiology, 2014. **219**(9): p. 695-703.

114. Vannini, F., K. Kashfi, and N. Nath, *The dual role of iNOS in cancer.* Redox Biol, 2015. **6**: p. 334-343.

115. Martinez, F.O., L. Helming, and S. Gordon, *Alternative activation of macrophages: an immunologic functional perspective.* Annu Rev Immunol, 2009. **27**: p. 451-83.

116. You, J., et al., *The Oncogenic Role of ARG1 in Progression and Metastasis of Hepatocellular Carcinoma.* 2018. **2018**: p. 2109865.

117. Capece, D., et al., *The inflammatory microenvironment in hepatocellular carcinoma: a pivotal role for tumor-associated macrophages.* Biomed Res Int, 2013. **2013**: p. 187204.

118. Shirabe, K., et al., *Role of tumor-associated macrophages in the progression of hepatocellular carcinoma.* Surg Today, 2012. **42**(1): p. 1-7.

119. Pathria, P., T.L. Louis, and J.A. Varner, *Targeting Tumor-Associated Macrophages in Cancer.* Trends Immunol, 2019. **40**(4): p. 310-327.

120. Peranzoni, E., et al., *Macrophages impede CD8 T cells from reaching tumor cells and limit the efficacy of anti-PD-1 treatment.* Proc Natl Acad Sci U S A, 2018. **115**(17): p. E4041-e4050.

121. Qian, B.Z. and J.W. Pollard, *Macrophage diversity enhances tumor progression and metastasis.* Cell, 2010. **141**(1): p. 39-51.

122. Thorgeirsson, S.S. and J.W. Grisham, *Molecular pathogenesis of human hepatocellular carcinoma.* Nat Genet, 2002. **31**(4): p. 339-46.

123. Feitelson, M.A., J. Pan, and Z. Lian, *Early molecular and genetic determinants of primary liver malignancy.* Surg Clin North Am, 2004. **84**(2): p. 339-54.

124. Marotta, F., et al., *The pathogenesis of hepatocellular carcinoma is multifactorial event. Novel immunological treatment in prospect.* Clin Ter, 2004. **155**(5): p. 187-99.

125. Hussain, S.P., et al., *TP53 mutations and hepatocellular carcinoma: insights into the etiology and pathogenesis of liver cancer.* Oncogene, 2007. **26**(15): p. 2166-76.

126. Nault, J.C., et al., *High frequency of telomerase reverse-transcriptase promoter somatic mutations in hepatocellular carcinoma and preneoplastic lesions.* Nat Commun, 2013. **4**: p. 2218.

127. Nault, J.C. and M. Ningarhari, *The role of telomeres and telomerase in cirrhosis and liver cancer.* 2019.

128. Sanz-Cameno, P., et al., *Angiogenesis: from chronic liver inflammation to hepatocellular carcinoma.* J Oncol, 2010. **2010**: p. 272170.

129. Hopfner, M., D. Schuppan, and H. Scherubl, *Growth factor receptors and related signalling pathways as targets for novel treatment strategies of hepatocellular cancer.* World J Gastroenterol, 2008. **14**(1): p. 1-14.

130. Llovet, J.M. and J. Bruix, *Molecular targeted therapies in hepatocellular carcinoma.* Hepatology, 2008. **48**(4): p. 1312-27.

131. Gollob, J.A., et al., *Role of Raf kinase in cancer: therapeutic potential of targeting the Raf/MEK/ERK signal transduction pathway.* Semin Oncol, 2006. **33**(4): p. 392-406.

132. Leicht, D.T., et al., *Raf kinases: function, regulation and role in human cancer.* Biochim Biophys Acta, 2007. **1773**(8): p. 1196-212.

133. Roberts, P.J. and C.J. Der, *Targeting the Raf-MEK-ERK mitogen-activated protein kinase cascade for the treatment of cancer.* Oncogene, 2007. **26**(22): p. 3291-310.

134. Ito, Y., et al., *Activation of mitogen-activated protein kinases/extracellular signal-regulated kinases in human hepatocellular carcinoma.* Hepatology, 1998. **27**(4): p. 951-8.

135. Hoffmann, K., et al., *Correlation of gene expression of ATP-binding cassette protein and tyrosine kinase signaling pathway in patients with hepatocellular carcinoma.* Anticancer Res, 2011. **31**(11): p. 3883-90.

136. Zuo, Q., et al., *Multivariate analysis of several molecular markers and clinicopathological features in postoperative prognosis of hepatocellular carcinoma.* Anat Rec (Hoboken), 2012. **295**(3): p. 423-31.

137. Liu, L., et al., *Sorafenib blocks the RAF/MEK/ERK pathway, inhibits tumor angiogenesis, and induces tumor cell apoptosis in hepatocellular carcinoma model PLC/PRF/5.* Cancer Res, 2006. **66**(24): p. 11851-8.

138. Yang, S. and G. Liu, *Targeting the Ras/Raf/MEK/ERK pathway in hepatocellular carcinoma.* Oncol Lett, 2017. **13**(3): p. 1041-1047.

139. Zhu, Y.J., et al., *New knowledge of the mechanisms of sorafenib resistance in liver cancer.* Acta Pharmacol Sin, 2017. **38**(5): p. 614-622.

140. Yap, T.A., et al., *Targeting the PI3K-AKT-mTOR pathway: progress, pitfalls, and promises.* Curr Opin Pharmacol, 2008. **8**(4): p. 393-412.

141. Dunlop, E.A. and A.R. Tee, *Mammalian target of rapamycin complex 1: signalling inputs, substrates and feedback mechanisms.* Cell Signal, 2009. **21**(6): p. 827-35.

142. Mamane, Y., et al., *mTOR, translation initiation and cancer.* Oncogene, 2006. **25**(48): p. 6416-22.

143. Freeburn, R.W., et al., *Evidence that SHIP-1 contributes to phosphatidylinositol 3,4,5-trisphosphate metabolism in T lymphocytes and can regulate novel phosphoinositide 3-kinase effectors.* J Immunol, 2002. **169**(10): p. 5441-50.

144. Miao, B., et al., *Small molecule inhibition of phosphatidylinositol-3,4,5-triphosphate (PIP3) binding to pleckstrin homology domains.* Proc Natl Acad Sci U S A, 2010. **107**(46): p. 20126-31.

145. Samuels, Y., et al., *High frequency of mutations of the PIK3CA gene in human cancers.* Science, 2004. **304**(5670): p. 554.

146. Brugge, J., M.C. Hung, and G.B. Mills, *A new mutational AKTivation in the PI3K pathway.* Cancer Cell, 2007. **12**(2): p. 104-7.

147. Cully, M., et al., *Beyond PTEN mutations: the PI3K pathway as an integrator of multiple inputs during tumorigenesis.* Nat Rev Cancer, 2006. **6**(3): p. 184-92.

148. Zhou, Q., V.W. Lui, and W. Yeo, *Targeting the PI3K/Akt/mTOR pathway in hepatocellular carcinoma.* Future Oncol, 2011. **7**(10): p. 1149-67.

149. Zhou, L., et al., *The mTOR pathway is associated with the poor prognosis of human hepatocellular carcinoma.* Med Oncol, 2010. **27**(2): p. 255-61.

150. Wallin, J.J., et al., *GDC-0980 is a novel class I PI3K/mTOR kinase inhibitor with robust activity in cancer models driven by the PI3K pathway.* Mol Cancer Ther, 2011. **10**(12): p. 2426-36.

151. Josephs, D.H. and D. Sarker, *Pharmacodynamic Biomarker Development for PI3K Pathway Therapeutics.* Transl Oncogenomics, 2015. **7**(Suppl 1): p. 33-49.

152. Yu, Y., et al., *Targeting AKT1-E17K and the PI3K/AKT Pathway with an Allosteric AKT Inhibitor, ARQ 092.* PLoS One, 2015. **10**(10): p. e0140479.

153. Jilkova, Z.M., et al., *Combination of AKT inhibitor ARQ 092 and sorafenib potentiates inhibition of tumor progression in cirrhotic rat model of hepatocellular carcinoma.* Oncotarget, 2018. **9**(13): p. 11145-11158.

154. Roth, G.S., et al., *Efficacy of AKT Inhibitor ARQ 092 Compared with Sorafenib in a Cirrhotic Rat Model with Hepatocellular Carcinoma.* Mol Cancer Ther, 2017. **16**(10): p. 2157-2165.

155. Brown, J.S. and U. Banerji, *Maximising the potential of AKT inhibitors as anti-cancer treatments.* Pharmacol Ther, 2017. **172**: p. 101-115.

156. Franco, N.H., *Animal Experiments in Biomedical Research: A Historical Perspective.* Animals (Basel), 2013. **3**(1): p. 238-73.

157. Heindryckx, F., I. Colle, and H. Van Vlierberghe, *Experimental mouse models for hepatocellular carcinoma research.* Int J Exp Pathol, 2009. **90**(4): p. 367-86.

158. Santos, N.P., A.A. Colaco, and P.A. Oliveira, *Animal models as a tool in hepatocellular carcinoma research: A Review.* Tumour Biol, 2017. **39**(3): p. 1010428317695923.

159. De Minicis, S., et al., *Liver carcinogenesis: rodent models of hepatocarcinoma and cholangiocarcinoma.* Dig Liver Dis, 2013. **45**(6): p. 450-9.

160. Gopinathan, A. and D.A. Tuveson, *The use of GEM models for experimental cancer therapeutics*. Dis Model Mech, 2008. **1**(2-3): p. 83-6.

161. Richmond, A. and Y. Su, *Mouse xenograft models vs GEM models for human cancer therapeutics.* Dis Model Mech, 2008. **1**(2-3): p. 78-82.

162. Talmadge, J.E., et al., *Murine models to evaluate novel and conventional therapeutic strategies for cancer.* Am J Pathol, 2007. **170**(3): p. 793-804.

163. Kerbel, R.S., *Human tumor xenografts as predictive preclinical models for anticancer drug activity in humans: better than commonly perceived-but they can be improved.* Cancer Biol Ther, 2003. **2**(4 Suppl 1): p. S134-9.

164. Kemp, C.J., *Animal Models of Chemical Carcinogenesis: Driving Breakthroughs in Cancer Research for 100 Years.* Cold Spring Harb Protoc, 2015. **2015**(10): p. 865-74.

165. Hayashi, Y., *Overview of genotoxic carcinogens and non-genotoxic carcinogens.* Exp Toxicol Pathol, 1992. **44**(8): p. 465-71.

166. Lee, S.J., et al., *Distinguishing between genotoxic and non-genotoxic hepatocarcinogens by gene expression profiling and bioinformatic pathway analysis.* Sci Rep, 2013. **3**: p. 2783.

167. Sullivan, B.P., et al., *Acceleration of N-nitrosation reactions by electrophiles.* IARC Sci Publ, 1991(105): p. 370-4.

168. Verna, L., J. Whysner, and G.M. Williams, *N-nitrosodiethylamine mechanistic data and risk assessment: bioactivation, DNA-adduct formation, mutagenicity, and tumor initiation.* Pharmacol Ther, 1996. **71**(1-2): p. 57-81.

169. Valko, M., et al., *Free radicals, metals and antioxidants in oxidative stress-induced cancer.* Chem Biol Interact, 2006. **160**(1): p. 1-40.

170. Yoo, J.S., F.P. Guengerich, and C.S. Yang, *Metabolism of N-nitrosodialkylamines by human liver microsomes.* Cancer Res, 1988. **48**(6): p. 1499-504.

171. Ramakrishna, G., et al., *From cirrhosis to hepatocellular carcinoma: new molecular insights on inflammation and cellular senescence.* Liver Cancer, 2013. **2**(3-4): p. 367-83.

172. Wang, H., et al., *Fibrosis-4 Model Influences Results of Patients with Hepatocellular Carcinoma Undergoing Hepatectomy.* 2018. **2018**: p. 4305408.

173. Schiffer, E., et al., *Gefitinib, an EGFR inhibitor, prevents hepatocellular carcinoma development in the rat liver with cirrhosis.* Hepatology, 2005. **41**(2): p. 307-14.

174. Stohrer, G., *Re: R. Peto et al., Effects on 4080 rats of chronic ingestion of N-nitrosodiethylamine or N-nitrosodimethylamine: a detailed dose-response study. Cancer Res., 51: 6415-6451, 1991, and*

K. S. Crump et al., Fundamental carcinogenic processes and their implications for low dose risk assessment. Cancer Res., 36: 2973-2979, 1976. Cancer Res, 1993. **53**(17): p. 4107-8.

175. Williams, G.M., M.J. Iatropoulos, and A.M. Jeffrey, *Mechanistic basis for nonlinearities and thresholds in rat liver carcinogenesis by the DNA-reactive carcinogens 2-acetylaminofluorene and diethylnitrosamine.* Toxicol Pathol, 2000. **28**(3): p. 388-95.

176. Chen, B., et al., *Dose-dependent ras mutation spectra in N-nitrosodiethylamine induced mouse liver tumors and 4-(methylnitrosamino)-1-(3-pyridyl)-1-butanone induced mouse lung tumors.* Carcinogenesis, 1993. **14**(8): p. 1603-8.

177. Park, T.J., et al., *TIS21 negatively regulates hepatocarcinogenesis by disruption of cyclin B1-Forkhead box M1 regulation loop.* Hepatology, 2008. **47**(5): p. 1533-43.

178. Rao, K.V. and S.D. Vesselinovitch, *Age- and sex-associated diethylnitrosamine dealkylation activity of the mouse liver and hepatocarcinogenesis.* Cancer Res, 1973. **33**(7): p. 1625-7.

179. Teoh, N.C., et al., *Defective DNA strand break repair causes chromosomal instability and accelerates liver carcinogenesis in mice.* Hepatology, 2008. **47**(6): p. 2078-88.

180. Frey, S., et al., *Suppression of apoptosis in C3H mouse liver tumors by activated Ha-ras oncogene.* Carcinogenesis, 2000. **21**(2): p. 161-6.

181. Zimmers, T.A., et al., *Effect of in vivo loss of GDF-15 on hepatocellular carcinogenesis.* J Cancer Res Clin Oncol, 2008. **134**(7): p. 753-9.

182. Nakatani, T., et al., *Sex hormone dependency of diethylnitrosamine-induced liver tumors in mice and chemoprevention by leuprorelin.* Jpn J Cancer Res, 2001. **92**(3): p. 249-56.

183. Sander, L.E., C. Trautwein, and C. Liedtke, *Is interleukin-6 a gender-specific risk factor for liver cancer?* Hepatology, 2007. **46**(4): p. 1304-5.

184. Kakimi, K., et al., *Blocking chemokine responsive to gamma-2/interferon (IFN)-gamma inducible protein and monokine induced by IFN-gamma activity in vivo reduces the pathogenetic but not the antiviral potential of hepatitis B virus-specific cytotoxic T lymphocytes.* J Exp Med, 2001. **194**(12): p. 1755-66.

185. Diwan, B.A., et al., *Inhibition by phenobarbital and lack of effect of amobarbital on the development of liver tumors induced by N-nitrosodiethylamine in juvenile B6C3F1 mice.* Cancer Lett, 1984. **23**(2): p. 223-34.

186. Mao, T.L., et al., *Expression of mutant nuclear beta-catenin correlates with non-invasive hepatocellular carcinoma, absence of portal vein spread, and good prognosis.* J Pathol, 2001. **193**(1): p. 95-101.

187. Butterworth, R.F., et al., *Experimental models of hepatic encephalopathy: ISHEN guidelines.* Liver Int, 2009. **29**(6): p. 783-8.

188. Dapito, D.H., et al., *Promotion of hepatocellular carcinoma by the intestinal microbiota and TLR4.* Cancer Cell, 2012. **21**(4): p. 504-16.

189. Schneider, C., et al., *Adaptive immunity suppresses formation and progression of diethylnitrosamine-induced liver cancer.* Gut, 2012. **61**(12): p. 1733-43.

190. Wei, T., et al., *G protein-coupled estrogen receptor deficiency accelerates liver tumorigenesis by enhancing inflammation and fibrosis.* Cancer Lett, 2016. **382**(2): p. 195-202.

191. Wu, J., et al., *The proinflammatory myeloid cell receptor TREM-1 controls Kupffer cell activation and development of hepatocellular carcinoma.* Cancer Res, 2012. **72**(16): p. 3977-86.

192. Cheng, L., et al., *Hyper-IL-15 suppresses metastatic and autochthonous liver cancer by promoting tumour-specific CD8+ T cell responses.* J Hepatol, 2014. **61**(6): p. 1297-303.

193. Liang, S., et al., *NADPH Oxidase 1 in Liver Macrophages Promotes Inflammation and Tumor Development in Mice.* Gastroenterology, 2019. **156**(4): p. 1156-1172.e6.

194. Mossanen, J.C., et al., *CXCR6 Inhibits Hepatocarcinogenesis by Promoting Natural Killer T- and CD4(+) T-Cell-Dependent Control of Senescence.* Gastroenterology, 2019. **156**(6): p. 1877-1889.e4.

195. Chen, S., et al., *Abberent expression of NOR1 protein in tumor associated macrophages contributes to the development of DEN-induced hepatocellular carcinoma.* 2018. **233**(6): p. 5002-5013.

196. Wilson, C.L., et al., *NFkappaB1 is a suppressor of neutrophil-driven hepatocellular carcinoma.* Nat Commun, 2015. **6**: p. 6818.

197. Li, S., et al., *TLR2 limits development of hepatocellular carcinoma by reducing IL18-mediated immunosuppression.* Cancer Res, 2015. **75**(6): p. 986-95.

198. Bartneck, M., et al., *The CCR2(+) Macrophage Subset Promotes Pathogenic Angiogenesis for Tumor Vascularization in Fibrotic Livers.* Cell Mol Gastroenterol Hepatol, 2019. **7**(2): p. 371-390.

199. Li, W., et al., *STK4 regulates TLR pathways and protects against chronic inflammation-related hepatocellular carcinoma.* J Clin Invest, 2015. **125**(11): p. 4239-54.

200. Song, S., et al., *Dynamic analysis of tumor-associated immune cells in DEN-induced rat hepatocellular carcinoma.* Int Immunopharmacol, 2014. **22**(2): p. 392-9.

201. Wang, Y.C., et al., *Estrogen suppresses metastasis in rat hepatocellular carcinoma through decreasing interleukin-6 and hepatocyte growth factor expression.* Inflammation, 2012. **35**(1): p. 143-9.

202. Yan, H.X., et al., *p53 promotes inflammation-associated hepatocarcinogenesis by inducing HMGB1 release.* J Hepatol, 2013. **59**(4): p. 762-8.

203. Huan, H.B., et al., *Sympathetic nervous system promotes hepatocarcinogenesis by modulating inflammation through activation of alpha1-adrenergic receptors of Kupffer cells.* Brain Behav Immun, 2017. **59**: p. 118-134.

204. Jing, Y., et al., *Tumor necrosis factor-alpha promotes hepatocellular carcinogenesis through the activation of hepatic progenitor cells.* Cancer Lett, 2018. **434**: p. 22-32.

205. Plymoth, A., S. Viviani, and P. Hainaut, *Control of hepatocellular carcinoma through hepatitis B vaccination in areas of high endemicity: perspectives for global liver cancer prevention.* Cancer Lett, 2009. **286**(1): p. 15-21.

206. McLean, M. and M.F. Dutton, *Cellular interactions and metabolism of aflatoxin: an update.* Pharmacol Ther, 1995. **65**(2): p. 163-92.

207. Sharma, R.A. and P.B. Farmer, *Biological relevance of adduct detection to the chemoprevention of cancer.* Clin Cancer Res, 2004. **10**(15): p. 4901-12.

208. Wang, J.S. and J.D. Groopman, *DNA damage by mycotoxins.* Mutat Res, 1999. **424**(1-2): p. 167-81.

209. Sutandyo, N., *Nutritional carcinogenesis.* Acta Med Indones, 2010. **42**(1): p. 36-42.

210. Wild, C.P. and Y.Y. Gong, *Mycotoxins and human disease: a largely ignored global health issue.* Carcinogenesis, 2010. **31**(1): p. 71-82.

211. Wogan, G.N., S. Paglialunga, and P.M. Newberne, *Carcinogenic effects of low dietary levels of aflatoxin B1 in rats.* Food Cosmet Toxicol, 1974. **12**(5-6): p. 681-5.

212. Buetler, T.M. and D.L. Eaton, *Complementary DNA cloning, messenger RNA expression, and induction of alpha-class glutathione S-transferases in mouse tissues.* Cancer Res, 1992. **52**(2): p. 314-8.

213. Cusumano, V., et al., *Functional impairment of rat Kupffer cells induced by aflatoxin B1 and its metabolites.* FEMS Immunol Med Microbiol, 1995. **10**(2): p. 151-5.

214. Dugyala, R.R. and R.P. Sharma, *The effect of aflatoxin B1 on cytokine mRNA and corresponding protein levels in peritoneal macrophages and splenic lymphocytes.* Int J Immunopharmacol, 1996. **18**(10): p. 599-608.

215. Methenitou, G., et al., *Immunomodulative effects of aflatoxins and selenium on human natural killer cells.* Vet Hum Toxicol, 2001. **43**(4): p. 232-4.

216. Weisburger, E.K., *Carcinogenicity studies on halogenated hydrocarbons.* Environ Health Perspect, 1977. **21**: p. 7-16.

217. Sheweita, S.A., M.A. El-Gabar, and M. Bastawy, *Carbon tetrachloride changes the activity of cytochrome P450 system in the liver of male rats: role of antioxidants.* Toxicology, 2001. **169**(2): p. 83-92.

218. Constandinou, C., N. Henderson, and J.P. Iredale, *Modeling liver fibrosis in rodents.* Methods Mol Med, 2005. **117**: p. 237-50.

219. Shi, J., et al., *Evidence of hepatocyte apoptosis in rat liver after the administration of carbon tetrachloride.* Am J Pathol, 1998. **153**(2): p. 515-25.

220. Delire, B., et al., *Chronic liver injury promotes hepatocarcinoma cell seeding and growth, associated with infiltration by macrophages.* Cancer Sci, 2018. **109**(7): p. 2141-2152.

221. Waxman, D.J. and L. Azaroff, *Phenobarbital induction of cytochrome P-450 gene expression.* Biochem J, 1992. **281 (Pt 3)**(Pt 3): p. 577-92.

222. Frueh, F.W., U.M. Zanger, and U.A. Meyer, *Extent and character of phenobarbital-mediated changes in gene expression in the liver.* Mol Pharmacol, 1997. **51**(3): p. 363-9.

223. Kimura, M., et al., *Involvement of multiple cell cycle aberrations in early preneoplastic liver cell lesions by tumor promotion with thioacetamide in a two-stage rat hepatocarcinogenesis model.* Exp Toxicol Pathol, 2013. **65**(7-8): p. 979-88.

224. Dashti, H., et al., *Thioacetamide- and carbon tetrachloride-induced liver cirrhosis.* Eur Surg Res, 1989. **21**(2): p. 83-91.

225. Munoz Torres, E., et al., *Experimental thioacetamide-induced cirrhosis of the liver.* Histol Histopathol, 1991. **6**(1): p. 95-100.

226. Becker, F.F., *Thioacetamide hepatocarcinogenesis.* J Natl Cancer Inst, 1983. **71**(3): p. 553-8.

227. Dasgupta, A., R. Chatterjee, and J.R. Chowdhury, *Thioacetamide-induced hepatocarcinoma in rat.* Oncology, 1981. **38**(4): p. 249-53.

228. Tang, Z., et al., *GEPIA: a web server for cancer and normal gene expression profiling and interactive analyses.* Nucleic Acids Res, 2017. **45**(W1): p. W98-w102.

229. Chandrashekar, D.S., et al., *UALCAN: A Portal for Facilitating Tumor Subgroup Gene Expression and Survival Analyses.* Neoplasia, 2017. **19**(8): p. 649-658.

230. Sato, K., et al., *The placental form of glutathione S-transferase as a new marker protein for preneoplasia in rat chemical hepatocarcinogenesis.* Gan, 1984. **75**(3): p. 199-202.

231. Terris, B., C. Cavard, and C. Perret, *EpCAM, a new marker for cancer stem cells in hepatocellular carcinoma.* J Hepatol, 2010. **52**(2): p. 280-1.

232. Nishida, N., et al., *Amplification and overexpression of the cyclin D1 gene in aggressive human hepatocellular carcinoma.* Cancer Res, 1994. **54**(12): p. 3107-10.

233. Takahashi, T., et al., *Immunologic self-tolerance maintained by CD25(+)CD4(+) regulatory T cells constitutively expressing cytotoxic T lymphocyte-associated antigen 4.* J Exp Med, 2000. **192**(2): p. 303-10.

234. El-Serag, H.B. and K.L. Rudolph, *Hepatocellular carcinoma: epidemiology and molecular carcinogenesis.* Gastroenterology, 2007. **132**(7): p. 2557-76.

235. Wu, K., et al., *Hepatic transforming growth factor beta gives rise to tumor-initiating cells and promotes liver cancer development.* Hepatology, 2012. **56**(6): p. 2255-67.

236. Ogawa, K., et al., *EpCAM-targeted therapy for human hepatocellular carcinoma.* Ann Surg Oncol, 2014. **21**(4): p. 1314-22.

237. Thabut, D. and V. Shah, *Intrahepatic angiogenesis and sinusoidal remodeling in chronic liver disease: new targets for the treatment of portal hypertension?* J Hepatol, 2010. **53**(5): p. 976-80.

238. Ramzan, M., et al., *Liver-infiltrating CD8(+) lymphocytes as prognostic factor for tumour recurrence in hepatitis C virus-related hepatocellular carcinoma.* Liver Int, 2016. **36**(3): p. 434-44.

239. Haybaeck, J., et al., *A lymphotoxin-driven pathway to hepatocellular carcinoma.* Cancer Cell, 2009. **16**(4): p. 295-308.

240. Makarova-Rusher, O.V., et al., *The yin and yang of evasion and immune activation in HCC.* J Hepatol, 2015. **62**(6): p. 1420-9.

241. Gao, Q., et al., *Intratumoral balance of regulatory and cytotoxic T cells is associated with prognosis of hepatocellular carcinoma after resection.* J Clin Oncol, 2007. **25**(18): p. 2586-93.

242. Walker, L.S., *Treg and CTLA-4: two intertwining pathways to immune tolerance.* J Autoimmun, 2013. **45**: p. 49-57.

243. Krummey, S.M. and M.L. Ford, *Braking bad: novel mechanisms of CTLA-4 inhibition of T cell responses.* Am J Transplant, 2014. **14**(12): p. 2685-90.

244. Matsuda, Y., et al., *Expression of galectin-3 involved in prognosis of patients with hepatocellular carcinoma.* Hepatol Res, 2008. **38**(11): p. 1098-111.

245. Chiu, C.G., et al., *Diagnostic utility of galectin-3 in thyroid cancer.* Am J Pathol, 2010. **176**(5): p. 2067-81.

246. Hsu, D.K., et al., *Galectin-3 expression is induced in cirrhotic liver and hepatocellular carcinoma.* Int J Cancer, 1999. **81**(4): p. 519-26.

247. Zubieta, M.R., et al., *Galectin-3 expression correlates with apoptosis of tumor-associated lymphocytes in human melanoma biopsies.* Am J Pathol, 2006. **168**(5): p. 1666-75.

248. Peng, W., et al., *Tumor-associated galectin-3 modulates the function of tumor-reactive T cells.* Cancer Res, 2008. **68**(17): p. 7228-36.

249. Thabut, D., et al., *Complementary vascular and matrix regulatory pathways underlie the beneficial mechanism of action of sorafenib in liver fibrosis.* Hepatology, 2011. **54**(2): p. 573-85.

250. Qu, K., et al., *New Insight into the Anti-liver Fibrosis Effect of Multitargeted Tyrosine Kinase Inhibitors: From Molecular Target to Clinical Trials.* Front Pharmacol, 2015. **6**: p. 300.

Appendix

Conferences

1. Oral presentation at HTE School - Tumor Environment & Immunity in Paris 2019 – “Immune system characterization during hepatocellular carcinogenesis in cirrhotic rat model”
2. Oral presentation at Journée de la Recheche Médicale in Grenoble 2018 – “Immune system characterization during hepatocellular carcinogenesis in cirrhotic rat model”.
3. Poster presentation at VII^{éme} colloque de Génomique Fonctionnelle du Foie in Lyon 2018 March – “Animal model of cirrhosis with hepatocellular carcinoma (HCC): a reliable tool for testing new therapies”.
4. Poster presentation at International Conference Analytical cytometry IX in Prague 2017 October – “Immune changes during development of cirrhotic rat model with hepatocellular carcinoma”.
5. Poster presentation at 3rd International cancer symposium (CRCL) in Lyon 2017 September – “Effect of novel AKT inhibitor ARQ 751 as single agent and its combination with Sorafenib on hepatocellular carcinoma in a cirrhotic rat model”.
6. Poster presentation at Forum de la recherché en cancérologie Auvergne Rhône-Alpes in Lyon 2017 April - “Effect of novel AKT inhibitor ARQ 751 as single agent and its combination with Sorafenib on hepatocellular carcinoma in a cirrhotic rat model”.
7. Poster presentation at EASL; The international liver congress in Amsterdam 2017 April – “Effect of novel AKT inhibitor ARQ 751 as single agent and its combination with Sorafenib on hepatocellular carcinoma in a cirrhotic rat model”.
8. Poster presentation at HCC submit in Genève 2017 February – “Effect of novel AKT inhibitor ARQ 751 as single agent and its combination with Sorafenib on hepatocellular carcinoma in a cirrhotic rat model”.

cancers

MDPI

Review

Animal Models of Hepatocellular Carcinoma: The Role of Immune System and Tumor Microenvironment

Zuzana Macek Jilkova [1,2,3,*], Keerthi Kurma [1,2] and Thomas Decaens [1,2,3,*]

1 Université Grenoble Alpes, CS 10217, 38043 Grenoble, France; Keerthi.Kurma143@gmail.com
2 Institute for Advanced Biosciences, Research Center UGA/Inserm U 1209/CNRS 5309, 38043 Grenoble, France
3 Clinique Universitaire d'Hépato-gastroentérologie, Pôle Digidune, CHU Grenoble Alpes, CS 10217, 38043 Grenoble, France
* Correspondence: zuzana.mjilkova@gmail.com (Z.M.J.); tdecaens@chu-grenoble.fr (T.D.); Tel.: +33-4765-49433 (Z.M.J.); Tel.: +33-4767-65441 (T.D.); Fax.: +33-4767-65179 (T.D.)

Received: 26 August 2019; Accepted: 30 September 2019; Published: 2 October 2019

Abstract: Hepatocellular carcinoma (HCC) is the most common type of liver cancer in adults and has one of the highest mortality rates of solid cancers. Ninety percent of HCCs are associated with liver fibrosis or cirrhosis developed from chronic liver injuries. The immune system of the liver contributes to the severity of the necrotic-inflammatory tissue damage, the establishment of fibrosis and cirrhosis, and the disease progression towards HCC. Immunotherapies have emerged as an exciting strategy for HCC treatment, but their effect is limited, and an extensive translation research is urgently needed to enhance anti-tumor efficacy and clinical success. Establishing HCC animal models that are analogous to human disease settings, i.e., mimicking the tumor microenvironment of HCC, is extremely challenging. Hence, this review discusses different animal models of HCC by summarizing their advantages and their limits with a specific focus on the role of the immune system and tumor microenvironment.

Keywords: animal model; hepatocellular carcinoma; cancer; immune system; tumor microenvironment

1. Introduction

Hepatocellular carcinoma (HCC) is the most common type of liver cancer in adults and has one of the highest mortality rates of solid cancers. The incidence of HCC has been rising over the past 20 years and will soon surpass one million annual cases worldwide [1]. Viral chronic infection with hepatitis B virus (HBV) or hepatitis C virus (HCV), aflatoxin-contaminated foodstuffs, chronic alcohol consumption, and metabolic disorders are the major causes of chronic liver inflammation which leads to fibrosis or cirrhosis, or both, and finally to HCC development (see Figure 1). Even though the distribution of these risk factors is highly variable, depending on the geographic region or ethnic group, 90% of HCC cases are always developed in the background of chronic inflammation and fibrosis/cirrhosis. The immune system of the liver plays a crucial role and inherently contributes to the severity of the necrotic-inflammatory damage, the establishment of liver fibrosis, and disease progression towards HCC [2,3].

Nowadays, less than 30% of patients with HCC are diagnosed at the early stages, when potentially curative treatments (i.e., resection, liver transplantation, and local ablation) are applicable [4]. On the other hand, the majority of patients who are diagnosed at an advanced stage have limited treatment options and, thus, the prognosis of HCC remains very poor. Sorafenib emerged in 2007 as the first effective systemic treatment of HCC for patients with advanced HCC or those progressing from locoregional therapies. However, the objective response rate to sorafenib is exceedingly low (2%).

More recently, several new drugs have shown positive clinical results in first- or second-line setting therapies, as reviewed elsewhere [5]. In addition, immunotherapies, mainly the agents targeting the PD-1/PD-L1 pathway and its combinations with other treatments, have a good chance to significantly improve HCC therapeutic strategies in the future [6]. Despite this progress, new treatments of HCC with a better efficacy remain urgently needed.

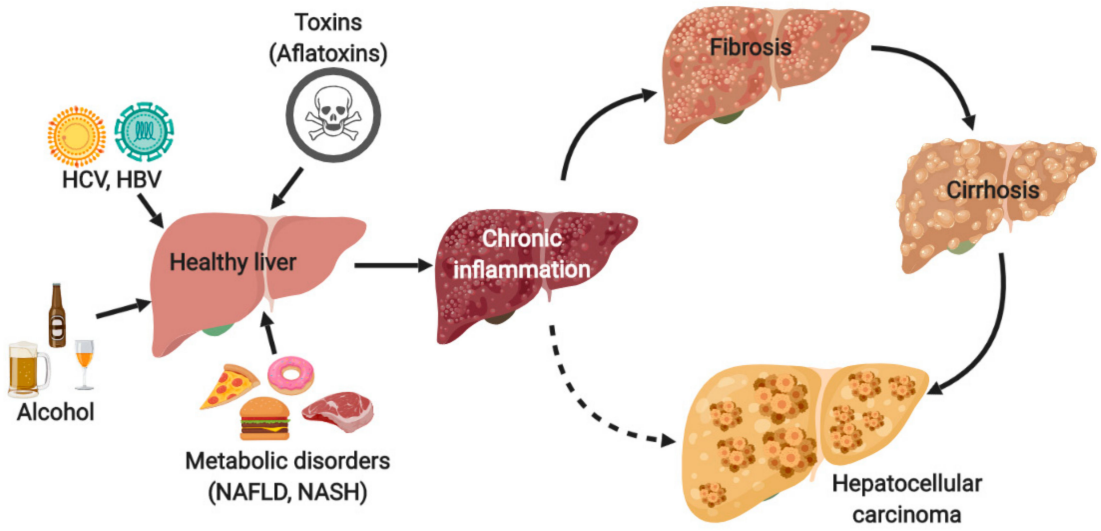

Figure 1. Risk factors and the process leading to the development of hepatocellular carcinoma (HCC). Hepatitis C virus, HCV; hepatitis B virus, HBV; non-alcoholic fatty liver disease, NAFLD; non-alcoholic steatohepatitis, NASH.

Unfortunately, the process of anti-HCC drug discovery and development seems to be very challenging and inefficient as reflected by the high attrition rate of drugs that enter preclinical testing but fail to gain FDA approval [7]. One of the underlying causes is the low predictive value of animal models of HCC that are used before in-human clinical trials are launched. In this review, we have described the different animal models of HCC available, summarizing their advantages and their limits, with a specific focus on their capacity to mirror the human immune system and tumor microenvironment.

2. Animal Models of HCC

Animal experimentation has played a crucial role in cancer research throughout history. As in other areas of cancer research, rodent animal models, especially mice, have become increasingly important in the field of HCC, mainly due to their short lifespan and breeding capacity [8]. However, it is important to mention that every HCC animal model is artificial in some way. Establishing potent animal models that mimic human HCC settings is particularly challenging, due to complex etiology, tumor heterogeneity, and the importance of both chronic inflammation and fibrotic background of human HCC.

HCC animal models can be categorized as follows: (i) chemically induced models, (ii) genetically engineered models, (iii) syngeneic models, (iv) xenograft models including patient-derived xenograft models, and (v) humanized models. The majority of these models can be combined with specific diets to generate NASH-associated HCC as recently reviewed elsewhere [9,10].

The origin of immune cells and tumor cells differ between animal models of HCC, as shown in Figure 2, which can represent the main limitation, depending on the type of research that is planned.

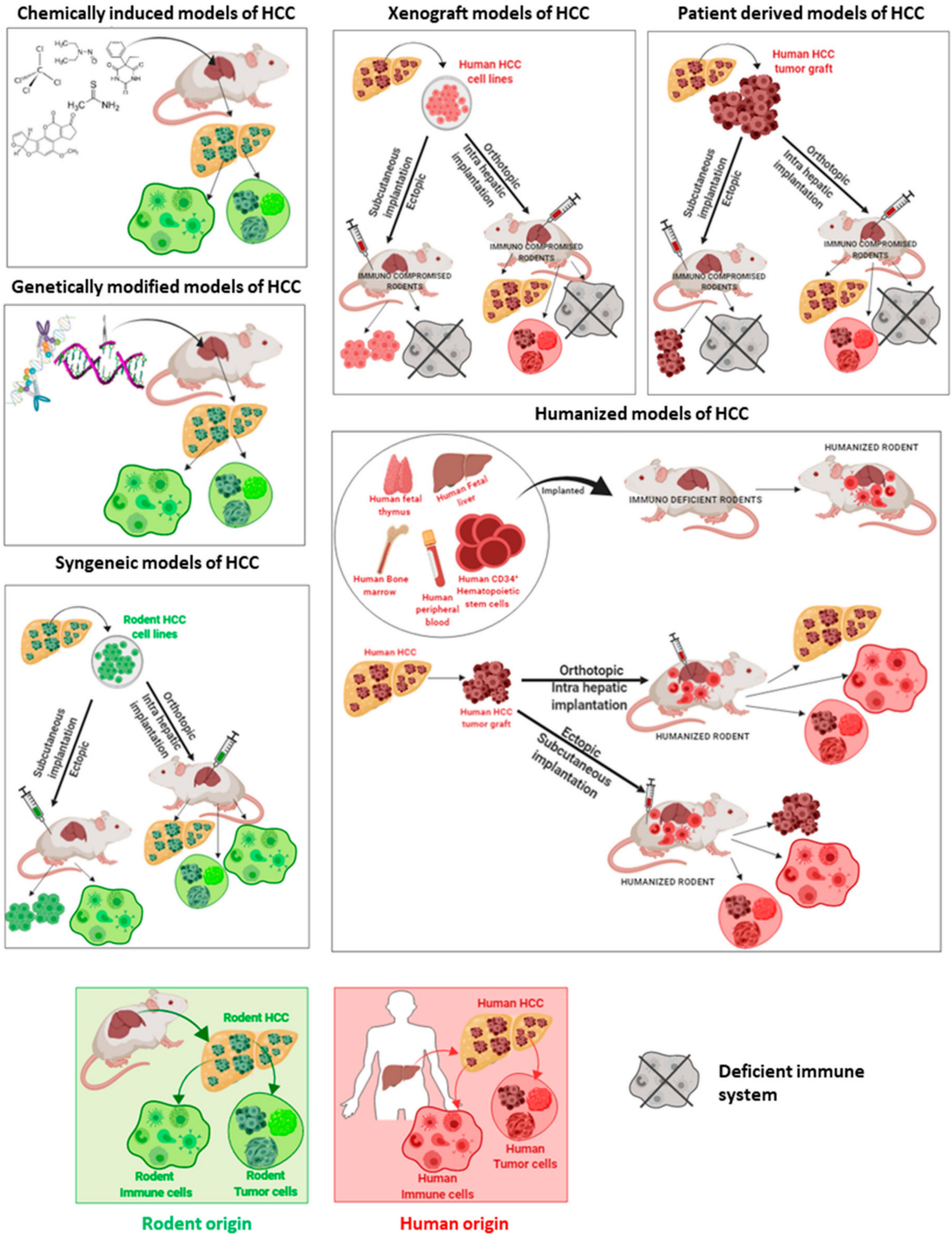

Figure 2. Rodent models of HCC and the origin of immune cells and tumor cells. Rodent HCC, rodent immune cells, and rodent tumor cells (green color); human HCC, human immune cells, and human tumor cells (red color).

Additionally, the knowledge of the pros and the cons of each HCC animal model is essential for obtaining results that are meaningful for the HCC field and for clinical translation, see Table 1.

Table 1. Summary of the pros and the cons of animal models of HCC.

Animal Models of HCC	Pros	Cons	Origin of Immune System
Chemically induced	Functional tumor-immune system interface Chronic inflammation Presence of fibrosis/cirrhosis	Long-time of tumor induction Undefined genetic background of the tumor	Animal immune system
Genetically engineered	Specific gene mutation Functional tumor-immune system interface	Low tumor mutational burden Development of fibrosis/cirrhosis needs to be stimulated	Animal immune system
Syngeneic	Functional tumor-immune system interface Metastasis formation	Limited similarity to human HCC Development of fibrosis/cirrhosis needs to be stimulated	Animal immune system
Xenograft	Low cost and rapid Predictable tumor growth	Unsuitable for studying tumor-immune system interface Absence of fibrosis/cirrhosis	Deficient immune system
Humanized	Recapitulate the tumor-immune system interface of human origin Highly relevant for the testing of immunotherapies	Incomplete reconstitution of the human immune system The high cost and technical difficulties Absence of fibrosis/cirrhosis in the models of today	Human immune system

2.1. Chemically Induced Models

The first chemically induced model of HCC was developed by the Japanese researcher, Riojun Kinosita, who performed a series of experiments (1932–1937) demonstrating that 4-dimethyl-aminoazobenzene strongly induces liver cancer in rats [11]. Since then, chemically induced animal models have been widely used. These models have provided a physiologically relevant tissue microenvironment and immune modifications related to HCC development and progression. Thus, chemically induced animal models are reliable in revealing underlying mechanisms of carcinogenesis, such as genetic, environmental, and immunological factors that influence cancer susceptibility in the human population [12]. The important disadvantage of chemically induced models is the long time taken for tumor induction and the undefined genetic background of the tumor. Furthermore, this is one of the reasons why the use of these models has diminished in the last decades. However, it is precisely the prolonged time that facilitates the development of the chronic inflammatory environmental characteristics of human HCC, including fibrosis, leading to tumor development and progression in the future.

Several chemical compounds are able to induce carcinogenesis after acute, short, or long-term exposure, depending on the chemical structure, concentration, animal susceptibility, etc. Based on their activity and specific pathogenic mechanism, chemical carcinogenic compounds are categorized as either genotoxic carcinogens or non-genotoxic hepatocarcinogens [13].

2.1.1. Genotoxic Carcinogen Induced Models

Genotoxic or direct-acting carcinogens (such as diethylnitrosamine (DEN) or aflatoxins) interact directly with DNA through the formation of covalent bonds, resulting in DNA-carcinogen complexes (DNA adducts). If chronically injected, DEN induces chronic inflammation and then fibrosis. Thus, genotoxic carcinogens are frequently used to induce liver fibrosis and HCC in rodents.

Specifically, after the administration to an animal, DEN is metabolized in the centrilobular hepatocytes, followed by reactions that cause DNA damage [14], which is associated with oxidative stress. These principle metabolizing pathways induced by DEN in rodent models are similar to that of humans [15]. Therefore, the application of DEN has become highly attractive for studies that are aimed at understanding the pathogenetic alterations underlying the formation of liver cancer.

However, HCC development by DEN depends on specific characteristics, such as species, dosage of administration, or the age and sex of the rodents. All these factors impact, among others, the tumor microenvironment and immune status.

A classical mouse model of DEN-induced HCC uses a single injection of a low dose of DEN as an initiator. However, such a model does not develop the features of liver fibrosis, which is crucial to mimic tumor microenvironment of HCC in humans. Therefore, a single injection of DEN is

usually accompanied by repeated dosing of a pro-fibrogenic agent CCl_4 [16]. A classical rat model of DEN-induced HCC is based on chronic exposures to DEN in developing fibrosis to cirrhosis, followed by HCC after 14–20 weeks [17–19]. Furthermore, this accurately recapitulates the scenario of human HCC. Additionally, the functional genomics showed that the gene expression patterns of DEN-induced HCCs were extremely similar to those of the poorer survival group of human HCCs [20]. Recently, the sequencing and analysis of gene copy number changes, similar to morphological findings (abundant inclusion bodies, fatty change), showed that tumors of the DEN model match with human tumor samples of alcohol-induced HCC [21].

In addition, the incidence of DEN-induced HCC development is gender-dependent, with a high prevalence in male rodents, which is similar to humans. In fact, several studies have demonstrated that female mice and rats are largely resistant to DEN-driven hepatocarcinogenesis. This phenomenon is related to estrogen-mediated inhibition of IL-6 production by Kupffer cells in females [22], which clearly sustains the relevance of the immune system in this model.

Indeed, the DEN induced model was used to study the role of immune response and tumor microenvironment in the process of hepatocarcinogenesis. The combination of DEN and CCl_4 was employed in a landmark study in which the contribution of the toll-like receptor 4 (TLR4) signaling on HCC promotion was investigated [23]. Furthermore, the DEN-induced mouse model was used to deeply characterize anti-tumor adaptive immune responses and the role of T and B cells in controlling tumor formation and progression [24]. Recently, the DEN-induced cirrhotic rat model of HCC served as a relevant model for the detailed study of the modulations of tumor microenvironment and immune system by the AKT inhibitor [19]. Additionally, the DEN-induced HCC rat model was used to recapitulate portal hypertension and gut permeability, which are two key players in the pathogenesis of HCC [25].

In contrast with the DEN-induced HCC models, aflatoxin-induced animal models are rarely used. In fact, even though aflatoxin B_1 exposure in food is one of the major risk factors for HCC development in human population [26], aflatoxin-induced genetic alterations of mice models differ from aflatoxin-related human HCC, as susceptibility to HCC development in animals is highly variable, and the development of the tumor takes from several months to a year [27].

2.1.2. Non-Genotoxic Carcinogen Induced Models

Non-genotoxic carcinogens, such as carbon tetrachloride (CCl_4), thioacetamide (TAA), and phenobarbital and peroxisome proliferators have no direct interaction with DNA. These treatments cause hepatic damage by disrupting cellular structures and altering the kinetics of either cell proliferation or of processes that increase the risk of genetic error, which leads to inflammation-associated events, liver fibrosis, and the increased incidence of HCC. Moreover, non-genotoxic carcinogens are usually combined with DEN to develop reproducible mice models of HCC in the context of fibrosis. Furthermore, the CCl_4 model is the best characterized with respect to immunological changes associated with the development of fibrosis [28] and it is wildly used to develop fibrosis in other animal models of HCC.

2.2. Genetically Modified Models

The development of transgenic and gene targeting technologies in the past decades facilitated the generation of genetically modified models (GMMs) to study tumor biology. GMMs have become powerful research animal models as they allow insight into the involvement of specific proteins and signaling pathways in the generation of HCC [29]. In this scenario, the main advantage of GMMs is the knowledge of the initiating mutation, which is particularly important for the testing of molecularly targeted anti-HCC therapies. In addition, HCC spontaneously develops in these models in a coevolving liver microenvironment and the immune system is intact.

However, one important disadvantage of GMMs is the frequent absence of fibrosis/cirrhosis and often the low tumor mutation burden, as the tumors develop from limited genetic alterations.

In contrary, human HCC usually develops in the background of fibrosis and it is known to be heterogeneous with an extensive landscape of altered genes and pathways [30–32]. Thus, although genetically engineered models of HCC have brought a precise step toward recapitulating the human HCC, the resultant spontaneous tumors without chronic inflammation and fibrosis do not recapitulate the stepwise progression of human HCC. Additionally, it is important to mention that the majority of GMMs are time consuming and expensive, as extensive infrastructures are required to achieve sufficient population, especially for preclinical studies. Today, with the advent of clustered regularly interspaced short palindromic repeats (CRISPR)/Cas technology, it is expected that some of these drawbacks could be improved, as editing is relatively fast, which could enhance the value of GMMs. However, CRISPR/Cas technology should be used on the background of liver fibrosis or cirrhosis to correctly mirror the human HCC.

The GMMs of HCC are models that overexpress oncogenes, growth factors, or express viral genes. These approaches need to be quite often combined to obtain shorter latency and increased tumor induction. For instance, β-catenin pathway is thought to be most frequently activated in human HCCs [32] but the second hit from an additional mutation is required to generate HCC in β-catenin transgenic animals. These genetic models of β-catenin–induced hepatocellular transformation were used to characterize the specific inflammatory response and to demonstrate the inflammation as a key player in β-catenin–induced liver tumorigenesis [33]. Additionally, transgenic model targeting only c-Myc proto-oncogene develops cancer in 60–70% of animals [21,34]. The tumors of this model display high heterogeneity and well mimic alcohol-induced HCCs, based on genomic changes [21]. The coexpression of c-Myc with Tgfα in transgenic mouse model leads to a tremendous acceleration of neoplastic development and progressive hepatocyte proliferation [21] on the background of chronic oxidative stress and persistent disruption of immune microenvironment in all animals [34,35]. Furthermore, the gene expression patterns of the c-Myc/Tgfα transgenic mouse model were shown to be extremely similar to those of the poor survival group of human HCCs [20]. This model may help to study the importance of the cross-talk between the tumor microenvironment and immune effector cells in the process of aggressive HCC. Similarly, double transgenic mice (c-Myc OVA tg+) c-Myc-OVA-tTALAP is a model of multifocal and rapidly progressing aggressive HCC. It was used to test combinations of three immunostimulatory monoclonal antibodies targeting OX40, PD-L1, CD137, and adoptive therapy with specific tumor antigen-activated T cells showing a clear synergy between the triple combination of mAbs and adoptive transfer of anti-tumor-specific cells [36]. Recently, a novel Akt1/N-Ras-induced HCC mouse model was generated to elucidate crosstalk between tumor-associated antigen-specific T cells and stromal cells, and the underlying mechanisms governing immunosuppression in the HCC tumor microenvironment [37].

The transgenic model with aberrant expression of the cytokine lymphotoxin (AlbLTαβ model) was crucial to discover a lymphotoxin-driven pathway to HCC and more generally, the inflammation-induced hepatocarcinogenesis [38]. Additionally, tumors from AlbLTαβ transgenic mice revealed a high overlap with NASH-HCC, based on genomic changes [21].

Different types of GMMs were developed to study HBV and HCV infections but these manipulations did not always lead to HCC. In fact, the models of HBV-associated hepatocarcinogenesis usually show long latency and low tumor induction [39]. Still, these models provide the opportunity to study the role of the immune system on spontaneous HCC development in the context of HBV infections. For instance, HBsAg-transgenic (HBs-tg) mice were recently used to demonstrate the importance of HBV-related adaptive immune tolerance, showing the importance of an immune checkpoint, TIGIT, whose blocking or deficiency led to fibrosis and HCC [40]. Concerning HCV-associated hepatocarcinogenesis, the FL-N/35 mouse model, expressing the full HCV genome, is certainly a relevant transgenic mouse model, especially when combined with CCl_4 for investigating fibrosis and HCC development [41,42].

2.3. Syngeneic Models

Syngeneic animal models have been used for interventional studies in HCC since the last decade. In these models, HCC cells from the same species are injected to the immunocompetent animals, usually directly to the liver tissue that can be simultaneously stimulated to develop fibrosis in order to mimic a true HCC microenvironment. Thus, these models are particularly valuable, as they give a possibility to investigate all key players of the immune system and tumor microenvironment, including vasculature, stroma and surrounding lymph system [43]. However, the disadvantage of syngeneic models can be their limited similarity to human HCC as the commonly used cell lines are often driven by mutations that do not mimic those found in human HCC.

It is important to mention that syngeneic orthotopic models of HCC often result in the development of metastases [44], which makes these models particularly interesting for studying the suppression of antitumor immune response during metastasis promotion. Furthermore, due to the functional system of tumor–immune surveillance, syngeneic rat models with a spontaneous tumor regression were used to show the involvement of particular cytokines in an effective anti-tumor immune response [45]. Similarly, the syngeneic mouse orthotopic model of HCC was used to study immunosuppressive properties of hepatic stellate cells and their contribution to the development of HCC [46]. In addition, today, syngeneic models combined with CCl_4 or TAA treatment are well-established models of fibrosis-associated HCC. Recently, these models were used to study the importance of the fibrotic microenvironment and myeloid-derived suppressor cells for the sensitivity of HCC to immune checkpoint therapies [47] or to test new combination therapies targeting tumor microenvironment [48].

2.4. Xenograft Models

In classical xenograft models, HCC is established either by the inoculation of human tumor cell lines or the direct implantation of a fragment of human solid tumors subcutaneously or into the liver of the immunodeficient animal.

Cell-line ectopic xenograft models, where human HCC cells are implanted mostly subcutaneously, have been extensively used in the HCC field for decades. The relative ease and the rapidity by which these models are prepared makes them a compelling preclinical model to screen cytotoxic drugs. However, the results obtained with these models have often inadequately predicted human clinical outcomes, as reviewed elsewhere [49,50]. One of the given reasons is the need to grow tumors in immunodeficient mice, which are not reflective of the dynamic process of tumor–immune surveillance. Thus, the functional immune system is missing in these models. Second, these models do not take the liver microenvironment into account. This leads to the model where the tumor microenvironment is extremely artificial with the complete absence of the surrounding fibrotic tissue. Another common concern is that HCC cells change in culture over time and do not always stably recapitulate the phenotypes or genotypes of human HCC. Nowadays, when targeting tumor microenvironment and immune system becomes a compelling way to tackle HCC, researchers are turning to other models as cell-line ectopic xenograft models have evident limitations for such investigation.

Orthotopic xenograft models reflect the tumor microenvironment, especially the influence of liver vascularization but have many of the same limitations as classical ectopic xenograft models. Mainly, the use of the immunodeficient host does not allow one to study the immunomodulatory effects of drugs in these models.

To better preserve the natural disease state observed in HCC patients, some groups xenograft freshly resected pieces of HCC into immunodeficient animals. This procedure, known as patient-derived xenograft (PDX), preserves histopathologic, transcriptomic, and genomic characteristics of the original HCC and can often well recapitulate the chemotherapeutic drug response. Thus, the PDX models have demonstrated an important utility for the evaluation of personalized precision medicine [51]. The most common is subcutaneous implantation, but, of course, the orthotopic PDX models of HCC better replicate tumor microenvironment and, thus, are more physiologically relevant. However, the PDX models of fibrosis-associated HCC are not yet available. The general limitations of the use of the PDX

models are the long lag period necessary for engraftment and passaging and the high costs of PDX development, maintenance and testing. Nevertheless, the real "Achilles heel" of the PDX models is the lack of a functional immune system, which is common for all xenograft models.

The incorporation of PDX models in HCC research brings substantial improvements and many interesting liver cancer PDX models had been generated and used for preclinical testing of anticancer drugs [51–53]. Recently, Blumer et al. established several PDX models from human HCC biopsies, showing that PDX tumors can retain characteristics of the original HCC biopsies over six generations of retransplantation [54].

2.5. Humanized Animals: Future Models of HCC?

During the last decades, anti-HCC drug development has focused on targets and partially de-emphasized the importance of immune system. Today, the tumor-immune system interface is required to test the majority of treatments. Furthermore, an immune system of the host is required especially for testing of new immunotherapeutic options. In general, the main limitation of animal models is that they do not accurately recapitulate a functional human immune system. Therefore, efforts have been made to create rodents with a human immune system (a "humanized rodent") for immunotherapeutic efficacy testing.

The ultimate goal of humanization is to generate animals expressing human immune cells that mimic realistic tumor-immune system interactions, which are mainly capable of mounting anticancer immune responses for specific immunotherapeutic interventions. The first successful engraftments of human hematopoietic stem cells [55] or human peripheral blood mononuclear cells [56] were established in the late 1980s. Today, due to improvements in the development of immune-deficient rodents, several types of humanized model are routinely employed in cancer research such as: (i) engraftment of human peripheral blood lymphocytes to severe combined (SC) immunodeficient rodents; (ii) engraftment of human $CD34^+$ hematopoietic stem cells acquired from multiple sources, such as bone marrow, fetal liver, or umbilical cord to SC immunodeficient rodents, or (iii) engraftments of 16–22-week gestation fragments of human fetal liver and human fetal thymus to sub renal capsular space of SC immunodeficient rodents. Although the current progress and advances in the humanization of animals are remarkable, the main limitations include the high cost and technical difficulties. Moreover, in the current generation of humanized rodents, certain human immune subpopulations are incompletely reconstructed. For instance, human myeloid cells are usually under-represented or have functional defects [57].

Even though humanized rodents represent one of the most attractive preclinical models for the screening of therapies targeting tumor-immune system interface, they are not yet well established in the HCC field. Thus, more experience with these models in HCC research are urgently needed to improve HCC immunotherapy research.

Recently, Zhao et al. developed a new PDX humanized mouse model to study human-specific tumor microenvironment and immunotherapy. In fact, they xenografted HCC subcutaneously into a mouse model of type I human leucocyte antigen that matched the human immune system in NOD-SC immunodeficient rodents Il2rg−/− (NSG) mice and studied the immune responses as well as the efficacy of immune checkpoint inhibitors [58]. Taking into consideration the advantage of humanized PDX models, the orthotopic humanized PDX models will mainly present in the future an extremely attractive option for studying how a functional human immune system reacts with the tumor in order to reproduce the complexity and specificity in humans HCC of novel immunotherapeutic targets.

3. Conclusions

We come from a period when ectopic xenograft growing in immune-deficient animals were considered sufficient for anti-HCC drug screening. Today, the boom of therapies targeting the immune system and tumor microenvironment highlight the importance of the host, background of chronic

inflammation, and fibrosis. Hopefully, the development and the use of animal models with respect to these principles will improve our capacity to effectively develop and screen novel anti-HCC drugs.

Author Contributions: Writing—original draft preparation, Z.M.J. and K.K.; writing—review and editing, T.D.; visualization, Z.M.J. and K.K.; funding acquisition, T.D.; co-first authorship, Z.M.J and K.K.

Funding: This research was funded by Fond de dotation Agir pour les maladies chroniques and by INCa 2019-033.

Acknowledgments: A special thanks to Patrice N. Marche and Marion Ressejac for their comments and suggestions.

Conflicts of Interest: The authors declare no conflict of interest.

References

1. Bray, F.; Ferlay, J.; Soerjomataram, I.; Siegel, R.L.; Torre, L.A.; Jemal, A. Global cancer statistics 2018: GLOBOCAN estimates of incidence and mortality worldwide for 36 cancers in 185 countries. *CA Cancer J. Clin.* **2018**, *68*, 394–424. [CrossRef] [PubMed]
2. Llovet, J.M.; Zucman-Rossi, J.; Pikarsky, E.; Sangro, B.; Schwartz, M.; Sherman, M.; Gores, G. Hepatocellular carcinoma. *Nat. Rev. Dis. Primers* **2016**, *2*, 16018. [CrossRef] [PubMed]
3. Makarova-Rusher, O.V.; Medina-Echeverz, J.; Duffy, A.G.; Greten, T.F. The yin and yang of evasion and immune activation in HCC. *J. Hepatol.* **2015**, *62*, 1420–1429. [CrossRef] [PubMed]
4. Park, J.W.; Chen, M.; Colombo, M.; Roberts, L.R.; Schwartz, M.; Chen, P.J.; Kudo, M.; Johnson, P.; Wagner, S.; Orsini, L.S.; et al. Global patterns of hepatocellular carcinoma management from diagnosis to death: The BRIDGE Study. *Liver Int.* **2015**, *35*, 2155–2166. [CrossRef] [PubMed]
5. Llovet, J.M.; Montal, R.; Villanueva, A. Randomized trials and endpoints in advanced HCC: Role of PFS as a surrogate of survival. *J. Hepatol.* **2019**. [CrossRef]
6. Gerbes, A.; Zoulim, F.; Tilg, H.; Dufour, J.F.; Bruix, J.; Paradis, V.; Salem, R.; Peck-Radosavljevic, M.; Galle, P.R.; Greten, T.F.; et al. Gut roundtable meeting paper: Selected recent advances in hepatocellular carcinoma. *Gut* **2018**, *67*, 380–388. [CrossRef]
7. Chan, S.L. Drug development for hepatocellular carcinoma: Knowing the past helps to understand the future. *Oncologist* **2014**, *19*, 1115–1117. [CrossRef]
8. Heindryckx, F.; Colle, I.; Van Vlierberghe, H. Experimental mouse models for hepatocellular carcinoma research. *Int. J. Exp. Pathol.* **2009**, *90*, 367–386. [CrossRef]
9. Anstee, Q.M.; Reeves, H.L.; Kotsiliti, E.; Govaere, O.; Heikenwalder, M. From NASH to HCC: Current concepts and future challenges. *Nat. Rev. Gastroenterol. Hepatol.* **2019**, *16*, 411–428. [CrossRef]
10. Santhekadur, P.K.; Kumar, D.P.; Sanyal, A.J. Preclinical models of non-alcoholic fatty liver disease. *J Hepatol.* **2018**, *68*, 230–237. [CrossRef]
11. Ohno, S. Riojun Kinosita: 1893-1977. *Cancer Res.* **1978**, *38*, 870–871. [PubMed]
12. Kemp, C.J. Animal Models of Chemical Carcinogenesis: Driving Breakthroughs in Cancer Research for 100 Years. *Cold Spring Harbor Protoc.* **2015**, *2015*, 865–874. [CrossRef] [PubMed]
13. Lee, S.J.; Yum, Y.N.; Kim, S.C.; Kim, Y.; Lim, J.; Lee, W.J.; Koo, K.H.; Kim, J.H.; Kim, J.E.; Lee, W.S.; et al. Distinguishing between genotoxic and non-genotoxic hepatocarcinogens by gene expression profiling and bioinformatic pathway analysis. *Sci. Rep.* **2013**, *3*, 2783. [CrossRef] [PubMed]
14. Verna, L.; Whysner, J.; Williams, G.M. N-nitrosodiethylamine mechanistic data and risk assessment: Bioactivation, DNA-adduct formation, mutagenicity, and tumor initiation. *Pharmacol. Therapeut.* **1996**, *71*, 57–81. [CrossRef]
15. Yoo, J.S.; Guengerich, F.P.; Yang, C.S. Metabolism of N-nitrosodialkylamines by human liver microsomes. *Cancer Res.* **1988**, *48*, 1499–1504.
16. Uehara, T.; Pogribny, I.P.; Rusyn, I. The DEN and CCl4 -Induced Mouse Model of Fibrosis and Inflammation-Associated Hepatocellular Carcinoma. *Curr. Protoc. Pharmacol.* **2014**, *66*. [CrossRef]
17. Schiffer, E.; Housset, C.; Cacheux, W.; Wendum, D.; Desbois-Mouthon, C.; Rey, C.; Clergue, F.; Poupon, R.; Barbu, V.; Rosmorduc, O. Gefitinib, an EGFR inhibitor, prevents hepatocellular carcinoma development in the rat liver with cirrhosis. *Hepatology* **2005**, *41*, 307–314. [CrossRef]
18. Roth, G.S.; Macek Jilkova, Z.; Zeybek Kuyucu, A.; Kurma, K.; Ahmad Pour, S.T.; Abbadessa, G.; Yu, Y.; Busser, B.; Marche, P.N.; Leroy, V.; et al. Efficacy of AKT Inhibitor ARQ 092 Compared with Sorafenib in a Cirrhotic Rat Model with Hepatocellular Carcinoma. *Mol. Cancer Ther.* **2017**, *16*, 2157–2165. [CrossRef]

19. Jilkova, Z.M.; Kuyucu, A.Z.; Kurma, K.; Ahmad Pour, S.T.; Roth, G.S.; Abbadessa, G.; Yu, Y.; Schwartz, B.; Sturm, N.; Marche, P.N.; et al. Combination of AKT inhibitor ARQ 092 and sorafenib potentiates inhibition of tumor progression in cirrhotic rat model of hepatocellular carcinoma. *Oncotarget* **2018**, *9*, 11145–11158. [CrossRef]
20. Lee, J.S.; Chu, I.S.; Mikaelyan, A.; Calvisi, D.F.; Heo, J.; Reddy, J.K.; Thorgeirsson, S.S. Application of comparative functional genomics to identify best-fit mouse models to study human cancer. *Nat. Genet.* **2004**, *36*, 1306–1311. [CrossRef]
21. Friemel, J.; Frick, L.; Unger, K.; Egger, M.; Parrotta, R.; Boge, Y.T.; Adili, A.; Karin, M.; Luedde, T.; Heikenwalder, M.; et al. Characterization of HCC Mouse Models: Towards an Etiology-Oriented Subtyping Approach. *Mol. Cancer Res. MCR* **2019**, *17*, 1493–1502. [CrossRef] [PubMed]
22. Naugler, W.E.; Sakurai, T.; Kim, S.; Maeda, S.; Kim, K.; Elsharkawy, A.M.; Karin, M. Gender disparity in liver cancer due to sex differences in MyD88-dependent IL-6 production. *Science* **2007**, *317*, 121–124. [CrossRef] [PubMed]
23. Dapito, D.H.; Mencin, A.; Gwak, G.Y.; Pradere, J.P.; Jang, M.K.; Mederacke, I.; Caviglia, J.M.; Khiabanian, H.; Adeyemi, A.; Bataller, R.; et al. Promotion of hepatocellular carcinoma by the intestinal microbiota and TLR4. *Cancer Cell* **2012**, *21*, 504–516. [CrossRef] [PubMed]
24. Schneider, C.; Teufel, A.; Yevsa, T.; Staib, F.; Hohmeyer, A.; Walenda, G.; Zimmermann, H.W.; Vucur, M.; Huss, S.; Gassler, N.; et al. Adaptive immunity suppresses formation and progression of diethylnitrosamine-induced liver cancer. *Gut* **2012**, *61*, 1733–1743. [CrossRef] [PubMed]
25. Zhang, H.L.; Yu, L.X.; Yang, W.; Tang, L.; Lin, Y.; Wu, H.; Zhai, B.; Tan, Y.X.; Shan, L.; Liu, Q.; et al. Profound impact of gut homeostasis on chemically-induced pro-tumorigenic inflammation and hepatocarcinogenesis in rats. *J. Hepatol.* **2012**, *57*, 803–812. [CrossRef]
26. Liu, Y.; Chang, C.C.; Marsh, G.M.; Wu, F. Population attributable risk of aflatoxin-related liver cancer: Systematic review and meta-analysis. *Eur. J. Cancer* **2012**, *48*, 2125–2136. [CrossRef] [PubMed]
27. McGlynn, K.A.; Hunter, K.; LeVoyer, T.; Roush, J.; Wise, P.; Michielli, R.A.; Shen, F.M.; Evans, A.A.; London, W.T.; Buetow, K.H. Susceptibility to aflatoxin B1-related primary hepatocellular carcinoma in mice and humans. *Cancer Res.* **2003**, *63*, 4594–4601.
28. Constandinou, C.; Henderson, N.; Iredale, J.P. Modeling liver fibrosis in rodents. *Meth. Molec. Med.* **2005**, *117*, 237–250. [CrossRef]
29. Li, Y.; Tang, Z.Y.; Hou, J.X. Hepatocellular carcinoma: Insight from animal models. *Nat. Rev. Gastroenterol. Hepatol.* **2011**, *9*, 32–43. [CrossRef]
30. Merle, P.; Trepo, C. Molecular mechanisms underlying hepatocellular carcinoma. *Viruses* **2009**, *1*, 852–872. [CrossRef]
31. Schulze, K.; Imbeaud, S.; Letouze, E.; Alexandrov, L.B.; Calderaro, J.; Rebouissou, S.; Couchy, G.; Meiller, C.; Shinde, J.; Soysouvanh, F.; et al. Exome sequencing of hepatocellular carcinomas identifies new mutational signatures and potential therapeutic targets. *Nat. Genet.* **2015**, *47*, 505–511. [CrossRef] [PubMed]
32. Zucman-Rossi, J.; Villanueva, A.; Nault, J.C.; Llovet, J.M. Genetic Landscape and Biomarkers of Hepatocellular Carcinoma. *Gastroenterology* **2015**, *149*, 1226–1239. [CrossRef] [PubMed]
33. Anson, M.; Crain-Denoyelle, A.M.; Baud, V.; Chereau, F.; Gougelet, A.; Terris, B.; Yamagoe, S.; Colnot, S.; Viguier, M.; Perret, C.; et al. Oncogenic beta-catenin triggers an inflammatory response that determines the aggressiveness of hepatocellular carcinoma in mice. *J. Clin. Invest.* **2012**, *122*, 586–599. [CrossRef] [PubMed]
34. Thorgeirsson, S.S.; Santoni-Rugiu, E. Transgenic mouse models in carcinogenesis: Interaction of c-myc with transforming growth factor alpha and hepatocyte growth factor in hepatocarcinogenesis. *Brit. J. Clin. Pharmacol.* **1996**, *42*, 43–52. [CrossRef]
35. Coulouarn, C.; Factor, V.M.; Conner, E.A.; Thorgeirsson, S.S. Genomic modeling of tumor onset and progression in a mouse model of aggressive human liver cancer. *Carcinogenesis* **2011**, *32*, 1434–1440. [CrossRef] [PubMed]
36. Morales-Kastresana, A.; Sanmamed, M.F.; Rodriguez, I.; Palazon, A.; Martinez-Forero, I.; Labiano, S.; Hervas-Stubbs, S.; Sangro, B.; Ochoa, C.; Rouzaut, A.; et al. Combined immunostimulatory monoclonal antibodies extend survival in an aggressive transgenic hepatocellular carcinoma mouse model. *Cancer Res.* **2013**, *19*, 6151–6162. [CrossRef]

37. Liu, Y.T.; Tseng, T.C.; Soong, R.S.; Peng, C.Y.; Cheng, Y.H.; Huang, S.F.; Chuang, T.H.; Kao, J.H.; Huang, L.R. A novel spontaneous hepatocellular carcinoma mouse model for studying T-cell exhaustion in the tumor microenvironment. *J. Immunother. Cancer* **2018**, *6*, 144. [CrossRef]
38. Haybaeck, J.; Zeller, N.; Wolf, M.J.; Weber, A.; Wagner, U.; Kurrer, M.O.; Bremer, J.; Iezzi, G.; Graf, R.; Clavien, P.A.; et al. A lymphotoxin-driven pathway to hepatocellular carcinoma. *Cancer Cell* **2009**, *16*, 295–308. [CrossRef]
39. Teng, Y.C.; Shen, Z.Q.; Kao, C.H.; Tsai, T.F. Hepatocellular carcinoma mouse models: Hepatitis B virus-associated hepatocarcinogenesis and haploinsufficient tumor suppressor genes. *World J. Gastroenterol. WJG* **2016**, *22*, 300–325. [CrossRef]
40. Zong, L.; Peng, H.; Sun, C.; Li, F.; Zheng, M.; Chen, Y.; Wei, H.; Sun, R.; Tian, Z. Breakdown of adaptive immunotolerance induces hepatocellular carcinoma in HBsAg-tg mice. *Nat. Commun.* **2019**, *10*, 221. [CrossRef]
41. Lerat, H.; Honda, M.; Beard, M.R.; Loesch, K.; Sun, J.; Yang, Y.; Okuda, M.; Gosert, R.; Xiao, S.Y.; Weinman, S.A.; et al. Steatosis and liver cancer in transgenic mice expressing the structural and nonstructural proteins of hepatitis C virus. *Gastroenterology* **2002**, *122*, 352–365. [CrossRef] [PubMed]
42. Chouteau, P.; Defer, N.; Florimond, A.; Calderaro, J.; Higgs, M.; Gaudin, A.; Merour, E.; Dhumeaux, D.; Lerat, H.; Pawlotsky, J.M. Hepatitis C virus (HCV) protein expression enhances hepatic fibrosis in HCV transgenic mice exposed to a fibrogenic agent. *J. Hepatol.* **2012**, *57*, 499–507. [CrossRef] [PubMed]
43. Brown, Z.J.; Heinrich, B.; Greten, T.F. Mouse models of hepatocellular carcinoma: An overview and highlights for immunotherapy research. *Nat. Rev. Gastroenterol. Hepatol.* **2018**, *15*, 536–554. [CrossRef] [PubMed]
44. Reiberger, T.; Chen, Y.; Ramjiawan, R.R.; Hato, T.; Fan, C.; Samuel, R.; Roberge, S.; Huang, P.; Lauwers, G.Y.; Zhu, A.X.; et al. An orthotopic mouse model of hepatocellular carcinoma with underlying liver cirrhosis. *Nat. Protoc.* **2015**, *10*, 1264–1274. [CrossRef] [PubMed]
45. Buijs, M.; Geschwind, J.F.; Syed, L.H.; Ganapathy-Kanniappan, S.; Kunjithapatham, R.; Wijlemans, J.W.; Kook Kwak, B.; Ota, S.; Vali, M. Spontaneous tumor regression in a syngeneic rat model of liver cancer: Implications for survival studies. *J. Vasc. Interven. Radiol. JVIR* **2012**, *23*, 1685–1691. [CrossRef] [PubMed]
46. Zhao, W.; Zhang, L.; Xu, Y.; Zhang, Z.; Ren, G.; Tang, K.; Kuang, P.; Zhao, B.; Yin, Z.; Wang, X. Hepatic stellate cells promote tumor progression by enhancement of immunosuppressive cells in an orthotopic liver tumor mouse model. *Lab. Invest.* **2014**, *94*, 182–191. [CrossRef] [PubMed]
47. Liu, M.; Zhou, J.; Liu, X.; Feng, Y.; Yang, W.; Wu, F.; Cheung, O.K.; Sun, H.; Zeng, X.; Tang, W.; et al. Targeting monocyte-intrinsic enhancer reprogramming improves immunotherapy efficacy in hepatocellular carcinoma. *Gut* **2019**. [CrossRef]
48. Rodriguez, M.M.; Fiore, E.; Bayo, J.; Atorrasagasti, C.; Garcia, M.; Onorato, A.; Dominguez, L.; Malvicini, M.; Mazzolini, G. 4Mu Decreases CD47 Expression on Hepatic Cancer Stem Cells and Primes a Potent Antitumor T Cell Response Induced by Interleukin-12. *Mol. Ther.* **2018**, *26*, 2738–2750. [CrossRef]
49. Kung, A.L. Practices and pitfalls of mouse cancer models in drug discovery. *Advan. Cancer Res.* **2007**, *96*, 191–212. [CrossRef]
50. Sanmamed, M.F.; Chester, C.; Melero, I.; Kohrt, H. Defining the optimal murine models to investigate immune checkpoint blockers and their combination with other immunotherapies. *Ann. Oncol.* **2016**, *27*, 1190–1198. [CrossRef]
51. Gao, H.; Korn, J.M.; Ferretti, S.; Monahan, J.E.; Wang, Y.; Singh, M.; Zhang, C.; Schnell, C.; Yang, G.; Zhang, Y.; et al. High-throughput screening using patient-derived tumor xenografts to predict clinical trial drug response. *Nature Med.* **2015**, *21*, 1318–1325. [CrossRef] [PubMed]
52. Zhao, Q.; Zhou, H.; Liu, Q.; Cao, Y.; Wang, G.; Hu, A.; Ruan, L.; Wang, S.; Bo, Q.; Chen, W.; et al. Prognostic value of the expression of cancer stem cell-related markers CD133 and CD44 in hepatocellular carcinoma: From patients to patient-derived tumor xenograft models. *Oncotarget* **2016**, *7*, 47431–47443. [CrossRef] [PubMed]
53. Kissel, M.; Berndt, S.; Fiebig, L.; Kling, S.; Ji, Q.; Gu, Q.; Lang, T.; Hafner, F.T.; Teufel, M.; Zopf, D. Antitumor effects of regorafenib and sorafenib in preclinical models of hepatocellular carcinoma. *Oncotarget* **2017**, *8*, 107096–107108. [CrossRef] [PubMed]
54. Blumer, T.; Fofana, I.; Matter, M.S.; Wang, X.; Montazeri, H.; Calabrese, D.; Coto-Llerena, M.; Boldanova, T.; Nuciforo, S.; Kancherla, V.; et al. Hepatocellular Carcinoma Xenografts Established from Needle Biopsies Preserve the Characteristics of the Originating Tumors. *Hepatol. Commun.* **2019**, *3*, 971–986. [CrossRef]

55. Kamel-Reid, S.; Dick, J.E. Engraftment of immune-deficient mice with human hematopoietic stem cells. *Science* **1988**, *242*, 1706–1709. [CrossRef] [PubMed]
56. Mosier, D.E.; Gulizia, R.J.; Baird, S.M.; Spector, S.; Spector, D.; Kipps, T.J.; Fox, R.I.; Carson, D.A.; Cooper, N.; Richman, D.D.; et al. Studies of HIV infection and the development of Epstein-Barr virus-related B cell lymphomas following transfer of human lymphocytes to mice with severe combined immunodeficiency. *Curr. Topics Microbiol. Immunol.* **1989**, *152*, 195–199.
57. De La Rochere, P.; Guil-Luna, S.; Decaudin, D.; Azar, G.; Sidhu, S.S.; Piaggio, E. Humanized Mice for the Study of Immuno-Oncology. *Trends Immunol.* **2018**, *39*, 748–763. [CrossRef]
58. Zhao, Y.; Shuen, T.W.H.; Toh, T.B.; Chan, X.Y.; Liu, M.; Tan, S.Y.; Fan, Y.; Yang, H.; Lyer, S.G.; Bonney, G.K.; et al. Development of a new patient-derived xenograft humanised mouse model to study human-specific tumour microenvironment and immunotherapy. *Gut* **2018**, *67*, 1845–1854. [CrossRef]

Immunologic Features of Patients With Advanced Hepatocellular Carcinoma Before and During Sorafenib or Anti-programmed Death-1/Programmed Death-L1 Treatment

Zuzana Macek Jilkova, PhD[1,2,3], Caroline Aspord, PhD[1,2,4], Keerthi Kurma[1,2], Anouck Granon, MD[1,2], Christian Sengel, MD[5], Nathalie Sturm, MD, PhD[1,2,6], Patrice N. Marche, PhD[1,2] and Thomas Decaens, MD, PhD[1,2,3]

INTRODUCTION: **Hepatocellular carcinoma (HCC) is one of the leading causes of cancer-related death worldwide. Today, a promising treatment strategy is focused on the enhancement of antitumor immune responses by immune checkpoint modification. However, as only 20% of patients with HCC are responders, identification of predictive factors is urgently required. Therefore, for the first time, the features of the intrahepatic and circulating immune system in patients with advanced-stage HCC, before and during the treatment, were analyzed.**

METHODS: **We collected fresh HCC biopsies, along with adjacent tumor-free liver tissues and peripheral blood samples, from 21 patients with advanced HCC. Furthermore, we performed an extensive immunomonitoring of patients with HCC treated with sorafenib or programmed death (PD)-1/PD-L1 pathway blockade using multiparametric flow cytometry.**

RESULTS: **We observed that regardless of the treatment, low baseline intratumoral $CD4^+/CD8^+$ T-cell ratio was associated with better overall survival ($P = 0.0002$). The baseline frequency of intratumoral PD-1^{high} $CD8^+$ T cells was significantly lower in patients responding to sorafenib treatment than in the nonresponders ($P = 0.0117$), and the frequency of circulating PD-1^{high} T cells increased with tumor progression ($P = 0.0329$). By contrast, responders to PD-1/PD-L1 pathway blockade showed a trend of high baseline frequency of intratumoral PD-1^{high} $CD8^+$ T cells. Moreover, we observed a trend of LAG3 and TIM3 upregulation on circulating T cells in nonresponding patients to PD-1/PD-L1 pathway blockade.**

DISCUSSION: **Immunosuppressive state, characterized by an enhanced intratumoral $CD4^+/CD8^+$ T-cell ratio, was associated with poor prognosis. Additionally, our results suggest that the frequency of intratumoral PD-1^{high} $CD8^+$ T cells may serve as a biomarker to identify which individuals will benefit from which treatment and support the use of combination strategies.**

SUPPLEMENTARY MATERIAL accompanies this paper at http://links.lww.com/CTG/A58

Clinical and Translational Gastroenterology 2019;00:e-00058. https://doi.org/10.14309/ctg.0000000000000058

INTRODUCTION

In the last few decades, hepatocellular carcinoma (HCC)-related mortality has increased at a rate faster than mortality related to any other cancer type (1). Primarily for patients with advanced HCC, the available treatment options are extremely limited and the prognosis is very poor. A multi-tyrosine kinase inhibitor, sorafenib, is considered as a gold standard treatment of patient with HCC. However, its efficacy is limited, improved survival time is modest (2), and predictive factors of response are lacking. Therefore, there is an urgent need to determine an effective

[1]Institute for Advanced Biosciences, Université Grenoble-Alpes, Saint-Martin-d'Hères, France; [2]Research Center Inserm U1209-CNRS 5309/UGA, Grenoble, France; [3]Service d'Hépato-gastroentérologie, Pôle Digidune, CHU Grenoble Alpes, France; [4]Etablissement Français du Sang, Rhône-Alpes Auvergne, France; [5]Service de radiologie, CHU Grenoble Alpes, France; [6]Service d'anatomopathologie, Pôle biologie, CHU Grenoble Alpes, France. **Correspondence:** Thomas Decaens, MD, PhD. E-mail: tdecaens@chu-grenoble.fr.

Received January 9, 2019; accepted May 14, 2019; published online XXXX

therapy for the treatment of patients with HCC. At present, an enhancement of antitumor immune responses via immunotherapies serves as a promising treatment strategy in the field of oncology. HCC is an important target for immunotherapy as chronic liver inflammation, which is associated with HCC risk factors (including chronic hepatitis B and C and metabolic disorders), and it promotes an immunosuppressive environment and T-cell exhaustion (3–6). Several inhibitory checkpoint molecules have been associated with this process, including the programmed death (PD)-1/PD-L1 immune checkpoint pathway. In patients suffering from HCC, the expression of PD-1 is constantly increased on $CD8^+$ T cells (7), and the high frequency of circulating and tumor-infiltrating $PD\text{-}1^+$ $CD8^+$ T cells was associated with disease progression after curative hepatic resection (8). High PD-L1 expression was also determined as a predictor of tumor recurrence for patients with HCC (9) and was associated with tumor aggressiveness (10).

In September 2017, the Food and Drug Administration granted an accelerated approval to anti-PD-1 antibody nivolumab for the treatment of patients with HCC after a previous sorafenib, regardless of the PD-L1 status, based on the objective response rate observed in the phase I/II CheckMate 040 trial (15% in a dose-escalation cohort and 20% in a dose-expansion cohort (11)). Moreover, pembrolizumab (Keytruda; Merck, Kenilworth, NJ) was also tested in a phase 2 study concerning second-line treatment for advanced HCC after sorafenib failure, and the study confirmed an objective response rate of 17% (12). Based on this finding, in November 2018, the FDA approved pembrolizumab for the treatment of patients with HCC who have been previously treated with sorafenib. Nevertheless, more than 80% of such patients do not respond to this therapy. Therefore, there is an urgent need to better understand the subversion of the immune system during HCC and its modulations during treatment. Although important research has been already conducted in the field of melanoma and other types of cancer, wherein immunotherapies have been used for some time now, almost no data exist for the field of HCC. In fact, limited information is available at present regarding the effect of HCC therapies on the immune system of patients with advanced HCC, including the coexpression and potential compensatory changes of inhibitory and stimulatory checkpoint molecules. A deeper understanding of the mechanisms, functional relevance, and the pattern of coexpression of immune checkpoint molecules in HCC, surrounding liver and in circulation, is mandatory to develop more effective immunotherapeutic strategies and determine a better response for its treatment.

Recently, Zhou et al. (13) analyzed inhibitory immune checkpoint molecules in patients with early-stage HCC and pointed out the importance of PD-1, TIM3, and LAG3 pertaining to the inhibition of tumor-infiltrating lymphocytes' function. Considering the complexity of the receptor network that may have either similar or distinct pathways to the modulate immune system, extensive studies need to be conducted to clarify the expression of both inhibitory and stimulatory checkpoint molecules on several cell subsets. Moreover, extremely limited information is available at present concerning potential treatment-associated modulations of various immune checkpoint molecules during HCC therapy. Additionally, immune checkpoint blockade strategies are currently being tested in cases of advanced HCC. Hence, systematic analysis of immune checkpoint molecules at an advanced stage is required.

In this study, we provide a characterization of immune checkpoint expression in advanced HCC, at the circulating and liver tissue levels, based on fresh blood and liver biopsies. In addition, we provide detailed immunomonitoring of patients with HCC treated by means of the classical treatment (sorafenib) or by immunotherapies and present the link with the clinical evolution of patients.

METHODS

Patients and sample processing

Twenty-one patients (17 men and 4 women) suffering from advanced HCC were included in this study and were selected before the treatment (Department of Gastroenterology and Hepatology, CHU Grenoble-Alpes). The mean age of the patients was 71.6 ± 0.4 years, among which 81% were male individuals, and 52% of the patients had fibrosis (stage F4). Detailed patient characteristics are provided in Supplementary Table 1 (see Supplementary Digital Content 1, http://links.lww.com/CTG/A58). Subsequently, blood samples obtained from 7 healthy donors were used for comparison. Liver biopsies (tumor and nontumor tissues) were divided into 2 parts. One part was used for histologic examination assessed by experienced liver pathologists to define whether biopsy was performed within HCC, whereas the other part was processed within 1 hour after the clinical biopsy to conduct extensive phenotypic and functional immunologic analyses.

Furthermore, the patients were treated with sorafenib (n = 7), anti-PD-L1/transforming growth factor-β TRAP (n = 4), anti-PD-1 antibodies (nivolumab, n = 1; pembrolizumab, n = 3), c-Met inhibitor Tepotinib (n = 2), or were untreated (n = 4). In addition, anti-PD-L1/TGF-β TRAP and pembrolizumab were the second-line treatments provided after sorafenib, whereas nivolumab was the first-line treatment. For immunomonitoring, blood samples were collected during the time of treatment; the sampling plan is detailed in Figure 1.

Based on their radiologic response to therapy, the treated patients were later categorized into the following groups: (i) responders (complete or partial response), (ii) stable disease (SD), and (iii) nonresponders (progression) according to the Response Evaluation Criteria in Solid Tumors (RECIST) 1.1. Additionally, the immunomonitoring parameters were analyzed with regard to the progression-free status of patients at 16 weeks as well as their overall survival. This study was performed in accordance with the Declaration of Helsinki and the French legislation based on local sample collection (DC-2014-2295), and all of its participants provided written informed consent.

Flow cytometry analyses

Immediately after the liver biopsy, tumor and nontumor samples were transferred in the RPMI medium and cells were recovered through mechanical disruption. Moreover, fresh peripheral blood and intrahepatic cell suspensions were immunostained without any stimulation, using the antihuman antibodies of surface markers, as described in SI.

Stimulation of immune cells

Peripheral blood mononuclear cells (PBMCs) were isolated using the Ficoll-Paque method, and cryopreserved PBMCs were stored in liquid nitrogen. Cells were resuspended (1×10^6/mL), and stimulation was performed by phorbol 12-myristate 13acetate

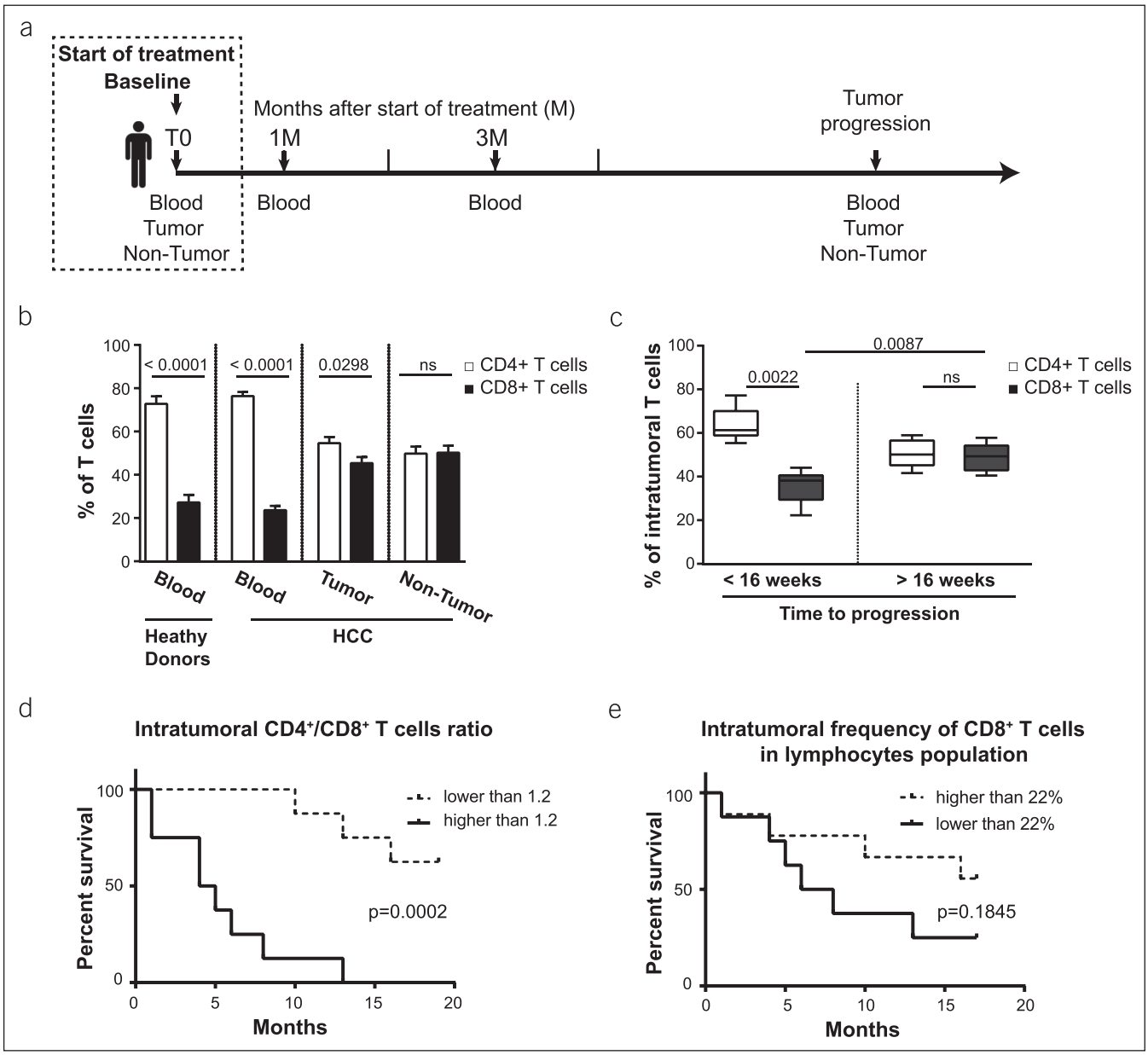

Figure 1. $CD4^+/CD8^+$ T-cell ratio at the baseline is related to clinical evolution in advanced HCC. (**a**) Sampling plan of patients with HCC. Samples were collected only when the condition of the patient allowed it. (**b**) Baseline frequency of $CD4^+$ vs $CD8^+$ T cells in the blood of healthy donors (n = 7), blood of patients with HCC (n = 21), tumor tissue (n = 16), and nontumoral tissue (n = 13); 2-tailed *P* value. (**c**) Frequency of T cells in the tumor tissues before the treatment. Patients were followed up to determine the time to tumor progression, and they were divided into groups with short time to tumor progression (<16 weeks, n = 6) and with progression-free status at 16 weeks (>16 weeks, n = 5); 2-tailed *P* value. (**d**) Log-rank (Mantel-Cox) overall survival curves segregating the cohort of patients according to the ratio of $CD4^+/CD8^+$ T cells in the tumor tissue at the baseline. (**e**) Log-rank (Mantel-Cox) overall survival curves segregating the cohort of patients according to the median of the frequency of intratumoral $CD8^+$ T cells per lymphocyte population (per $CD45^+$ cell) at the baseline. HCC, hepatocellular carcinoma.

(50 ng/mL; Sigma Aldrich [L'isle-d'Abeau Chesnes, France]) and ionomycin (1 μg/mL, Iono; Sigma) for 16 h at 37 °C in a CO_2 incubator.

Cytometric bead array

The supernatant derived from stimulated and nonstimulated PBMC cultures was collected, after which the amount of cytokines produced by immune cells was evaluated using cytometric bead array (BD Bioscience, San Diego, CA), and the data were analyzed by the FCAP Array Software. Subsequently, the following cytokines were determined: interferon gamma, tumor necrosis factor α, granzyme B, IL-4, IL-6, IL-10, IL-13, and IL-17.

Assessment of soluble immune checkpoint molecules by multiplex immunoassays

Serum samples were analyzed via multiprofiling of immune checkpoint molecules using the Luminex MAGPIX system (Research Platform, Département de Biochimie, Toxicologie et

Pharmacologie, Institut de Biologie et Pathologie, CHU Grenoble-Alpes) with the following panels: PD-1, PD-L1, PD-L2, CTLA-4, TIM-3, GITR, GITRL, LAG-3, and CD137 (4-1BB).

Statistical analysis

Analyses were performed using the statistical software GraphPad Prism 6 (GraphPad Software, CA). Normal distribution was tested using the D'Agostino-Pearson omnibus normality test. When data derived from both cohorts were normally distributed, the unpaired *t* test was used to determine significant differences observed between the groups. Contrarily, when data from either cohort were not normally distributed, the Mann-Whitney test was performed. The nonparametric Kruskal-Wallis one-way analysis of variance was used for multiple comparisons. Furthermore, the Spearman correlation nonparametric test was conducted to determine the degree of correlation between 2 variables, and *P* value of <0.05 was considered significant.

RESULTS

$CD4^+/CD8^+$ T-cell ratio is strongly linked to the clinical outcomes

Our cohort was based on 21 patients suffering from advanced HCC. Only liver biopsy samples that were histologically approved by pathologists for sampling within HCC area (tumor samples) and nontumor area (nontumor samples) were included in this study.

For the flow cytometry analysis, fresh samples were stained using 2 panels for the identification of the major lymphocyte populations and the expression of immune checkpoint molecules (refer to Methods). Moreover, we investigated T cells, natural killer (NK) cells, and NKT cells in the blood, in conjunction with nontumor and tumor liver tissue obtained from patients with advanced HCC, by the strategy concerning the principle of gating as previously described (14–16) (Supplementary Figure 1a, see Supplementary Digital Content 1, http://links.lww.com/CTG/A58), whereas isotype controls were used to define the positivity of each marker (Supplementary Figure 1b, see Supplementary Digital Content 1, http://links.lww.com/CTG/A58).

In our cohort of patients with advanced HCC, $CD3^+CD56^-$ T cells found in the blood accounted for more than 60% of all $CD45^{high}$ lymphocytes, whereas in the liver, their frequency reduced to 50%. Contrarily, $CD3^+CD56^+$ cells (NKT and $CD3^{bright}CD56^+$ T cells) and $CD3^-CD56^+$ NK cells represented a significantly smaller population in the blood (7 and 11%), whereas their frequency increased up to 21 and 21% in nontumor liver tissues and 19 and 17% in tumor liver tissues, respectively (Supplementary Figures 1b and 2a, see Supplementary Digital Content 1, http://links.lww.com/CTG/A58).

As expected, 24% of the circulating T cells were $CD8^+$; the absolute number of T cells is listed in Supplementary Table 2 (see Supplementary Digital Content 1, http://links.lww.com/CTG/A58). In the liver, $CD8^+$ T cells represented approximately 45% of the T-cell population in the tumor tissue and 50% in the nontumoral part of the tissue (Figure 1b). Notably, in our cohort of patients, the frequency of intratumoral $CD8^+$ T cells before the treatment was associated with clinical outcomes. Moreover, the patients were divided into 2 groups according to their progression-free status at 16 weeks. We observed that irrespective of the following treatment, the frequency of intratumoral $CD8^+$ T cells at the baseline was higher in patients who were free of progression at 16 weeks ($P = 0.0087$), as depicted in Figure 1c. In fact, in patients with time to tumor progression higher than 16 weeks, the intratumoral T-cell population is composed of 50.7% $\pm$ 2.9% of $CD4^+$ cells and 49.3% $\pm$ 2.9% of $CD8^+$ cells (not significant), whereas in patients with time to tumor progression shorter than 16 weeks, the intratumoral $CD4^+$ T-cell population was significantly higher (63.8% $\pm$ 3.1%) compared with $CD8^+$ T cells (36.2% $\pm$ 3.1%; $P = 0.0022$).

The median intratumoral $CD4^+/CD8^+$ T-cell ratio was 1.2. Based on this median, a high intratumoral $CD4^+/CD8^+$ T-cell ratio was a negative predictive factor of the patients' overall survival ($P = 0.0002$) (Figure 1d). The median overall survival of patients with a ratio lower than 1.2 was 16.2 $\pm$ 1.6 months in comparison with 4.6 $\pm$ 1.4 months for patients with a ratio higher than 1.2 ($P = 0.0002$) (Figure 1d). Subsequently, we separated the cohort of patients according to the median of the frequency of the intratumoral $CD8^+$ T cells per lymphocyte population (per $CD45^+$ cell) at the baseline. We observed the tendency of association regarding the high frequency of intratumoral $CD8^+$ T cells per lymphocyte population at the baseline with improved survival ($P = 0.1845$) (Figure 1e).

In addition, cytokine secretion on stimulation of PBMCs, with phorbol 12-myristate 13acetate/Iono analyzed by cytometric bead array, showed that from all cytokines, only secreted IL-10 levels of both unstimulated and stimulated PBMCs were positively correlated to $CD4^+$ T cells and negatively correlated to $CD8^+$ T cells. In fact, we found a significant positive correlation between the IL-10 levels secreted by PBMCs in circulation and $CD4^+/CD8^+$ T-cell ratio in both tumoral and nontumoral tissues (Supplementary Table 3, see Supplementary Digital Content 1, http://links.lww.com/CTG/A58). However, there was no direct association with the clinical outcomes. Collectively, our results show that the immunosuppressive state, characterized by enhanced IL-10 levels and high intrahepatic $CD4^+/CD8^+$ T-cell ratio, was associated with poor prognosis.

Immune checkpoint distribution on lymphocyte subsets in advanced HCC before therapy

We investigated the frequency of NK cells, $CD3^+CD56^+$ cells (NKT and $CD3^{bright}CD56^+$ T cells), and T cells expressing immune checkpoint molecules on the cell surface (PD-1, TIM3, LAG3, CTLA4, 4-1BB, and OX40) in fresh samples of peripheral blood and analyzed tumoral and nontumoral biopsies of patients with advanced HCC. As the expression of PD-1 increases constantly in patients with HCC (7), we focused directly on the PD-1^{high} population (Supplementary Figure 1b, see Supplementary Digital Content 1, http://links.lww.com/CTG/A58), as observed in the recent publications (17,18).

In our cohort, the frequency of PD-1^{high} or $LAG3^+$ NK cells was negligible compared with that of $CD3^+CD56^+$ cells or the T-cell population in the blood, tumor tissues, and/or nontumor tissues (Figure 2a). However, in terms of their frequency, NK cells expressing TIM3, CTLA-4, 4-1BB, and OX40 were similar to T cells and $CD3^+CD56^+$ cells (Figure 2a).

Subsequently, we analyzed the distribution of immune checkpoint molecules in the population of $CD4^+$ and $CD8^+$ T cells (Figure 2b, Supplementary Figure 2b, see Supplementary Digital Content 1, http://links.lww.com/CTG/A58). Furthermore, the inhibitory checkpoint molecules PD-1, LAG3, and TIM3 were expressed primarily by $CD8^+$ T cells, whereas a stimulatory checkpoint molecule, OX40, was expressed

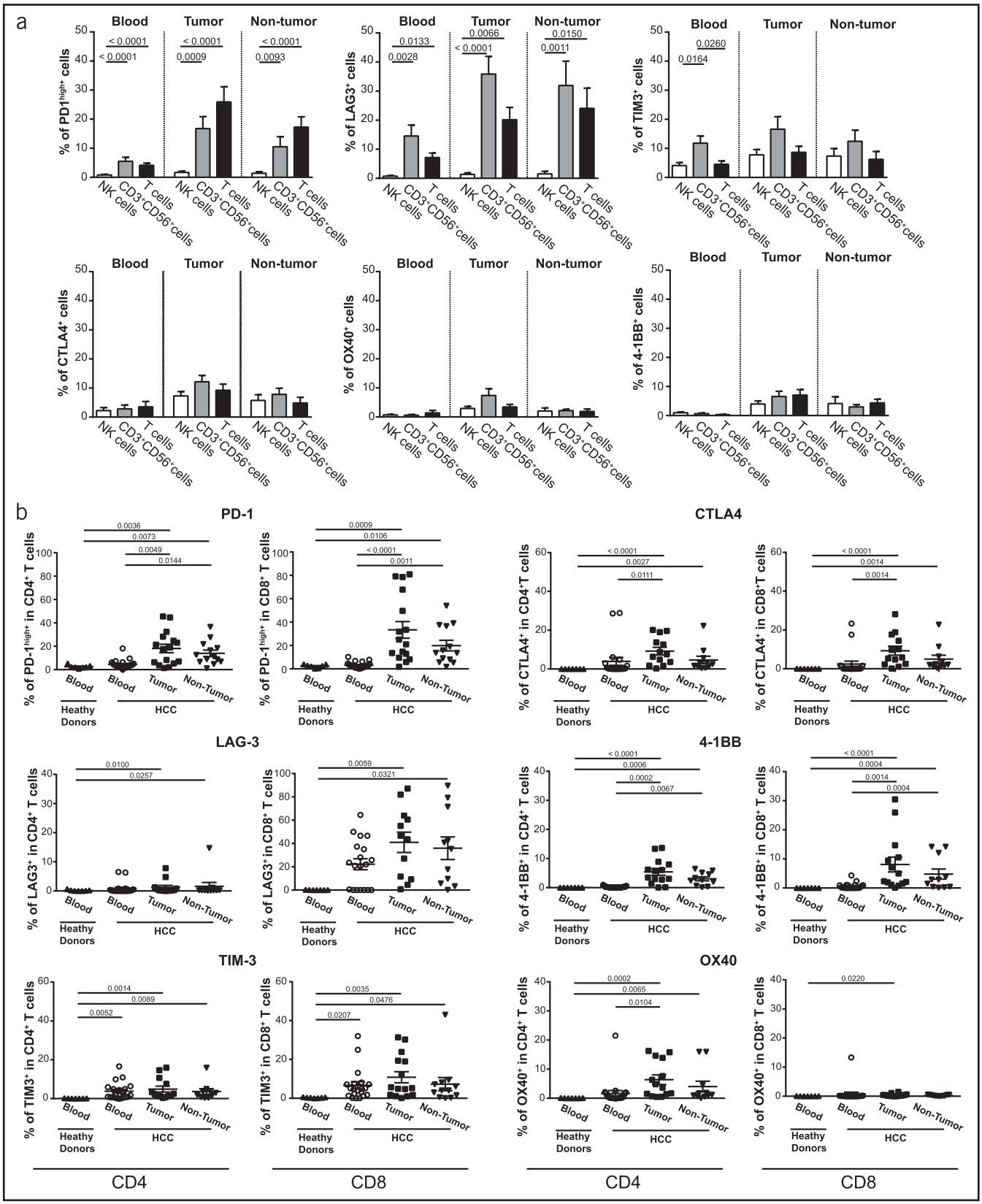

Figure 2. Immune checkpoint distribution on lymphocyte subsets in advanced HCC at the baseline. (**a**) The percentage of immune checkpoint-positive cells among NK, $CD3^+CD56^+$ cells (NKT and $CD3^{bright}CD56^+$ T cells), and T cells in the blood (n = 21), tumor tissue (n = 16), and nontumoral tissue (n = 13). (**b**) The percentage of immune checkpoint-positive cells among $CD4^+$ or $CD8^+$ T cells in the blood (n = 21), tumor tissue (n = 16), and nontumoral tissue (n = 13). Each dot represents a patient. The nonparametric Kruskal-Wallis one-way analysis of variance was used for multiple comparisons. HCC, hepatocellular carcinoma.

preferentially by CD4$^+$ T lymphocytes (Figure 2b, Supplementary Figure 2b, see Supplementary Digital Content 1, http://links.lww.com/CTG/A58). CTLA4 and 4-1BB were equally expressed in CD8$^+$ and CD4$^+$ T cells. Moreover, the expression of immune checkpoint molecules was not statistically different between the tumor and nontumor tissues (Figure 2b).

Because we analyzed the markers of immune checkpoint receptors in 2 separated tubes, we cannot provide data pertaining to their coexpression per individual cell for the entire cohort. However, the positive correlation between the percentage of PD-1^{high} CD8$^+$ T cells and TIM3$^+$ CD8$^+$ T cells in circulation suggested frequent coexpression of those receptors (r = 0.7276, P = 0.0003), as shown in Figure 3a. Contrarily, a negative correlation was observed between the cells expressing the inhibitory receptor LAG3 and the stimulatory receptor 4-1BB (r = −0.6863, P = 0.0008) (Figure 3b). Similarly, the frequency of LAG3$^+$ and 4-1BB$^+$ T cells in the blood was associated with PD-1^{high} T cells in nontumoral tissues (Figure 3c).

As expected, we found positive correlations between the circulating and liver tissue expression of the immune checkpoint receptors (Supplementary Table 4, see Supplementary Digital Content 1, http://links.lww.com/CTG/A58), notably between the circulating and intratumoral frequency of 4-1BB$^+$ T cells (r = 0.6143, P = 0.0255) and PD-1^{high} cells (r = 0.4857, P = 0.0505), indicating that the expression of immune checkpoint molecules in the tumor tissue is partially reflected on the circulating levels.

Interestingly, the frequency of intratumoral PD-1^{high} T cells, LAG3$^+$ T cells, OX40$^+$ T cells, and CD69$^+$ CD4$^+$ T cells was positively correlated to the most widely used biomarker of HCC, circulating alpha-fetoprotein, as shown in Supplementary Table 5 (see Supplementary Digital Content 1, http://links.lww.com/CTG/A58), indicating the possible link between one's immune status and tumor growth.

In a small cohort of patients with HCC, we directly determined the coexpression of PD-1, TIM3, and LAG3. Representative flow cytometry plots of patients with advanced HCC with a high frequency of intratumoral PD-1^{high} T cells (Figure 4a) show that TIM3 and LAG3 expressions were predominantly observed in PD1^{high} intratumoral CD8$^+$ T cells. Evidently, most intratumoral PD-1^{high} CD8$^+$ T cells coexpressed TIM3, but only a part of PD-1^{high} CD8$^+$ T cells expressed LAG3 (Figure 4b).

Immunologic features of sorafenib-treated patients

In our cohort, 7 patients were treated with sorafenib, and we collected the results from their blood samples (n = 7) and liver biopsies (n = 6). First, we sought to identify the cell population that best described the differences between the responders and nonresponders with respect to sorafenib at the baseline of treatment. Sorafenib-treated patients were categorized into the following groups based on the radiologic response to therapy: (i) responders (partial response; n = 3) and (ii) nonresponders (tumor progression; n = 4). From all immune checkpoint molecules, only PD-1 expression was found to be different at the baseline when comparing the responders with the nonresponders. In fact, in the tumor tissues, the baseline frequency of PD-1^{high} CD8$^+$ T cells was drastically and significantly lower in responders to sorafenib treatment (15.9% ± 7.2%, n = 3) in comparison with the nonresponders (69.1% ± 9.7%, n = 3; P = 0.0117), as shown in Figure 5a. In the blood, the same tendency was observed, but the difference did not reach the significance

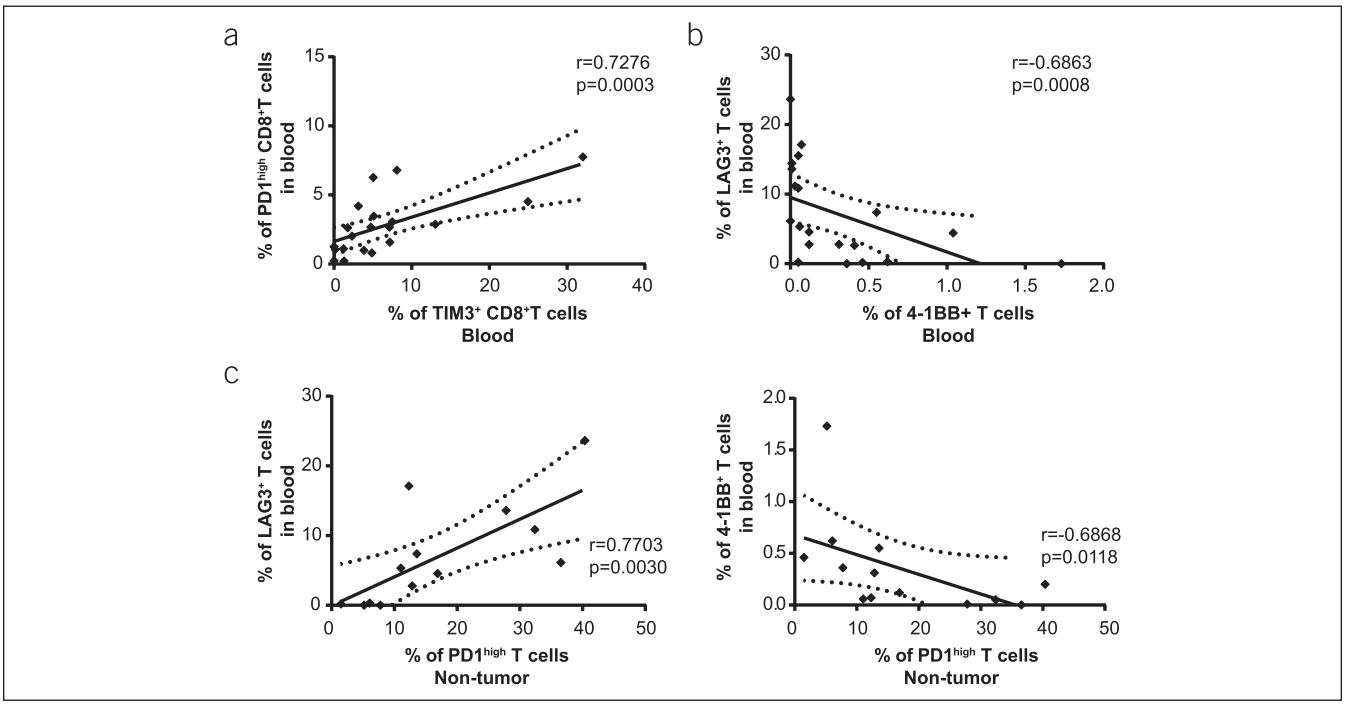

Figure 3. Correlations between immune checkpoint-positive cells. (**a**) Correlation between PD-1^{high} CD8$^+$ T cells and TIM3$^+$ CD8$^+$ T cells in the blood of patients with HCC. (**b**) Correlation between the frequency of circulating LAG3$^+$ and 4-1BB$^+$ T cells. (**c**) Correlation between the frequency of circulating LAG3$^+$ T cells (left) or 4-1BB$^+$ T cells (right), with PD-1^{high} T cells in the liver tissue. Each dot represents a patient. HCC, hepatocellular carcinoma; PD, programmed death; r, Spearman correlation coefficient.

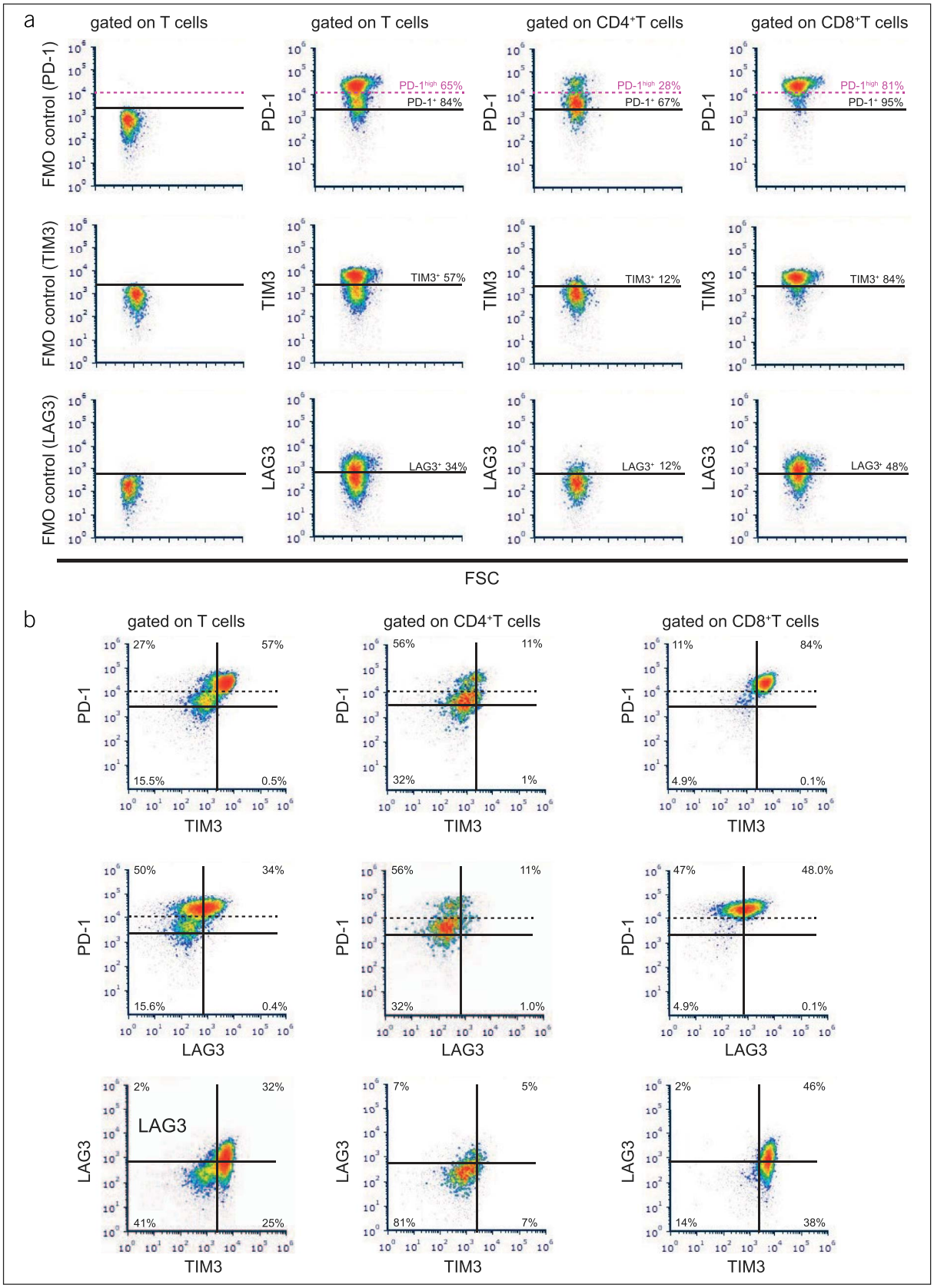

Figure 4. TIM3 and LAG3 expressions are predominantly observed in PD1^{high} intratumoral CD8^{+} T cells in advanced HCC. (**a**) Representative flow cytometry plots of immune checkpoint molecules, including FMO controls. (**b**) Coexpression patterns of PD-1, TIM3, and LAG3 in the intratumoral T cells of patients with advanced HCC. FSC, forward scatter; FMO, fluorescence minus one; HCC, hepatocellular carcinoma; PD, programmed death.

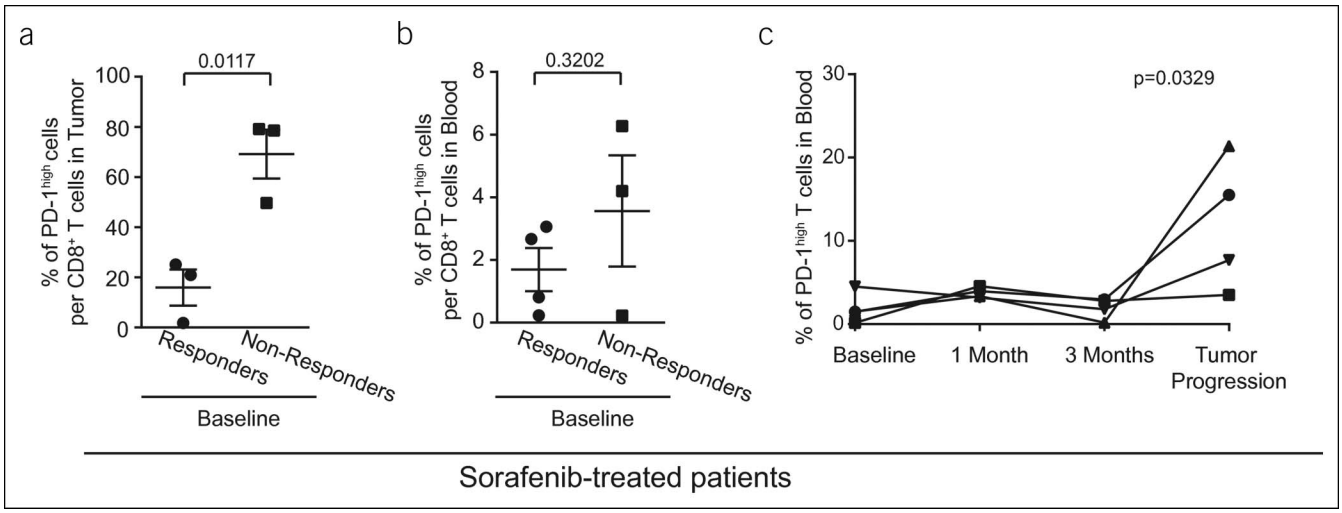

Figure 5. PD-1^{high} CD8^{+} T-cell status in sorafenib-treated patients. (**a**) Intratumoral frequency of PD-1^{high} CD8^{+} T cells at the baseline of patients who later responded to sorafenib (n = 3) or those who do not do so (n = 3). (**b**) Frequency of PD-1^{high} CD8^{+} T cells in the blood at the baseline of patients who later responded to sorafenib (n = 4) or those who do not do so (n = 3). Mann-Whitney *U* test was used to compare responders and nonresponders. (**c**) Immunomonitoring of patients treated with sorafenib (n = 4). Circulating PD-1^{high} T cells at 4 different time points: (i) before treatment, (ii) 1 month after the commencement of sorafenib treatment, (iii) 3 months after the beginning of treatment, and (iv) in case of tumor progression (based on radiologic evaluation); nonparametric Friedman test. Each dot represents a patient; mean ± SE, 2-tailed *P* value. PD, programmed death.

(responders: 1.7% ± 0.7%, n = 3; nonresponders: 3.6% ± 1.8%, n = 4; $P = 0.3202$) (Figure 5b).

In addition, in 4 sorafenib-treated patients, we got the opportunity to perform detailed immunomonitoring. To follow the immunologic changes induced during the treatment, we performed flow cytometry analyses of the blood at 4 different time points: (i) before treatment, (ii) 1 month after the start of sorafenib treatment, (iii) 3 months after the start of the treatment, and (iv) in case of tumor progression (based on radiologic evaluation). We determined that out of all immune checkpoint molecules, only the frequencies of PD-1^{high} cells were modified during the immunomonitoring period. In fact, the mean frequency of the circulating PD-1^{high} T cells was 1.92% ± 0.92% at the baseline and increased to 12.04% ± 3.99% during tumor progression (Figure 5c). This indicates that the expression of PD-1 on circulating levels may reflect the progression of HCC during sorafenib treatment and can serve as a biomarker of response and PD-1 expression on intratumoral T cells. Moreover, it could be used as a predictive factor of response.

Immunomonitoring of PD-1/PD-L1 pathway blockade-treated patients

In our cohort, 8 patients were treated via PD-1/PD-L1 pathway blockade therapies by either anti-PD-L1/TGF-β TRAP (n = 4) or PD-1 antibodies (nivolumab, n = 1; pembrolizumab, n = 3). In 6 of these patients, we had access to their liver biopsies.

To describe the differences between the responders and nonresponders to PD-1/PD-L1 pathway blockade at the baseline of treatment, the patients were divided into the following categories based on their radiologic evaluation: (i) responders (complete or partial response, n = 2), (ii) SD (n = 3), and (iii) nonresponders (tumor progression, n = 3).

As expected from their response to checkpoint blockade, we found that patients who were classified as responders had lower CD4^{+}/CD8^{+} ratio and therefore higher frequency of CD8^{+} T cells per T-cell population in both blood and tumor tissue in comparison with the nonresponders (Figure 6a), but due to the low sample number, this difference is not significant. In contrast to the results obtained from sorafenib-treated patients, responders to PD-1/PD-L1 pathway blockade had 8 times higher baseline frequency of intratumoral PD-1^{high} cells within the CD8^{+} T-cell population compared with the nonresponders (80.0% ± 0.9%, n = 2 vs 9.4% ± 3.5%, n = 2; $P = 0.3333$) (Figure 6b). Similarly, slightly higher frequency of intratumoral TIM3^{+} cells within the CD8^{+} T-cell population was observed in responders to PD-1/PDL-1 treatment when compared with the nonresponders (23.9% ± 2.5%, n = 2 vs 12.3% ± 4.5%, n = 2; $P = 0.4586$).

To follow the immunologic changes induced during PD-1/PD-L1 pathway blockade, we performed immunomonitoring on the circulating level. Additionally, we analyzed fresh blood samples taken during different time points from 3 patients treated with anti-PD-1 antibody (Figure 7a) and from 4 patients treated with anti-PD-L1/TGF-β TRAP (Figure 7b). The results of the same are expressed as a heat map-based frequency of the positive cells compared with the mean frequency of a corresponding subpopulation of the entire cohort of patients with advanced HCC before treatment (T0), i.e., low (<mean frequency, −20%), medium (mean frequency, ±20%), and high (>mean frequency, +20%).

Furthermore, we noticed that after anti-PD-1 antibody administration, the expression of PD-1 was hardly detectable in the fresh blood samples (Figure 7a), probably owing to receptor occupancy by the therapeutic antibody. However, the antibodies that specifically detect therapeutic anti-PD-1 antibodies were not used in this study to directly investigate the PD-1 receptor occupancy after anti-PD-1 treatment. As expected, this effect on PD-1 detection was not observed in patients treated with anti-PD-L1/TGF-β TRAP (Figure 7b), as the said treatment directly targets PD-L1.

Interestingly, in patients who did not respond to PD-1/PD-L1 pathway blockade, we observed the compensatory upregulation

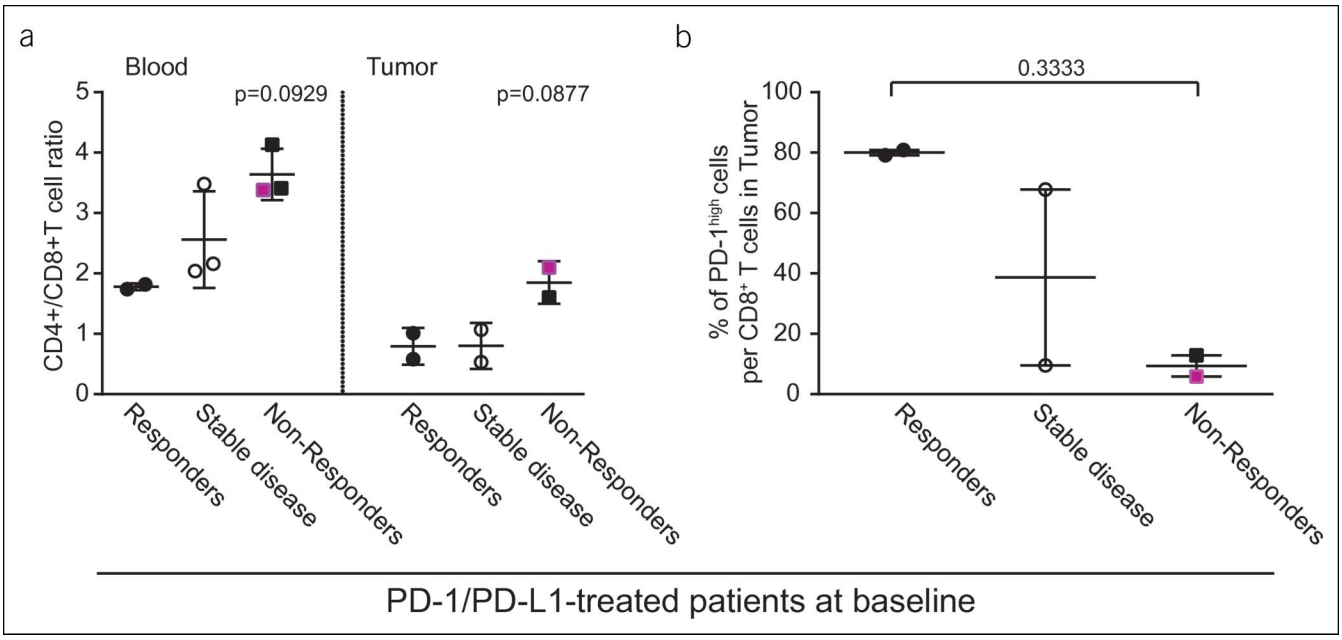

Figure 6. T-cell status in PD-1/PD-L1 pathway blockade-treated patients at the baseline. (**a**) $CD4^+/CD8^+$ T-cell ratio in the blood and tumor tissues at the baseline and (**b**) intratumoral frequency of PD-1^{high} $CD8^+$ T cells at the baseline of the patients who later responded to PD-1/PD-L1 therapy (n = 2), display stable disease (n = 3/2), or those who were nonresponders (n = 2). Fuchsia denotes a patient with anti-PD-1 antibody as the first-line treatment, whereas black denotes a patient with anti-PD-1/PD-L1 treatment as the second-line treatment after sorafenib. Each dot represents a patient; mean ± SE. PD, programmed death.

of LAG3 and TIM3 inhibitory immune checkpoints on circulating T cells. Contrarily, the frequency of inhibitory immune checkpoint-positive T cells decreased in patients who achieved long-term SD or complete response (Figure 7a,b). It is noteworthy that we found no significant correlation between the immune checkpoints on circulating immune cells and the concentration of corresponding soluble immune checkpoints measured by multiplex immunoassays.

Collectively, we provided an evidence of feasibility along with the potential significance of detailed immunomonitoring performed by multiparameter flow cytometry during the treatment of patients suffering from advanced HCC. Importantly, compensatory changes in TIM3 and LAG3 after PD-1/PD-L1 pathway blockade therapy may support the use of immunotherapy combination strategies targeting multiple immune checkpoints in advanced HCC.

DISCUSSION

In this study, we focused on a cohort of patients with advanced-stage HCC. To the best of our knowledge, this is the first study to analyze immunologic intrahepatic and circulating parameters before treatment, which followed the immunologic changes induced during HCC treatment. By performing extensive phenotypic and functional analyses of the immune cells, we highlighted unique clinical correlates. To elaborate, we achieved the following in this study: (i) defined the immune checkpoint expression on both circulating and tumor-infiltrating lymphocytes in advanced HCC, (ii) highlighted prognostic factors of clinical evolution and (iii) pointed out specific immune features, allowing one to distinguish responders and nonresponders to targeted therapy with tyrosine kinase inhibitor and immunotherapy treatments. This study is limited due to the low number of patients receiving each treatment, but it demonstrates the importance of detailed immunomonitoring during HCC therapies and the importance of analyzing fresh biopsies of patients to define predictive factors of response. Moreover, our results suggest that the $CD4^+/CD8^+$ T-cell ratio and the frequency of intratumoral PD-1^{high} $CD8^+$ T cells may serve as markers to identify which patients will benefit from which treatment. In our study, the baseline frequency of $CD8^+$ T cells per T-cell population in the tumor tissue was significantly associated with a positive clinical outcome, which is in accordance with the findings of research works conducted on most other cancers (19,20) including HCC (21,22), wherein an increased number of tumor-infiltrating $CD8^+$ T cells predicts a favorable prognosis. Furthermore, $CD8^+$ T cells are the key effector cells for antitumor immunity, mainly tumor-associated, antigen-specific $CD8^+$ T cells, which are known to represent an important component of the host's immune response against a tumor.

By contrast, Tregs, the dominant subset of $CD4^+$ T cells in the late stages of cancer (23), are known to be unfavorable prognostic markers in patients with HCC (24–26). In more advanced stages of HCC, the entire CD4/CD8 T-cell ratio is modified as the $CD8^+$ T-cell population reduces, which is associated with an increase in the frequency of $CD4^+$ T cells (22,27). In this research, we show that intratumoral CD4/CD8 T-cell ratio is clearly associated with tumor progression and overall survival in patients with advanced HCC, independent of the following treatment. This is not surprising as Tregs are preferentially enriched in the $CD4^+$ T-cell population in patients with HCC and repress $CD8^+$ T-cell functions, as demonstrated previously (25,27–29). However, we could not analyze the proportion of Tregs in the $CD4^+$ T-cell population in this study, which limits the interpretation of its results.

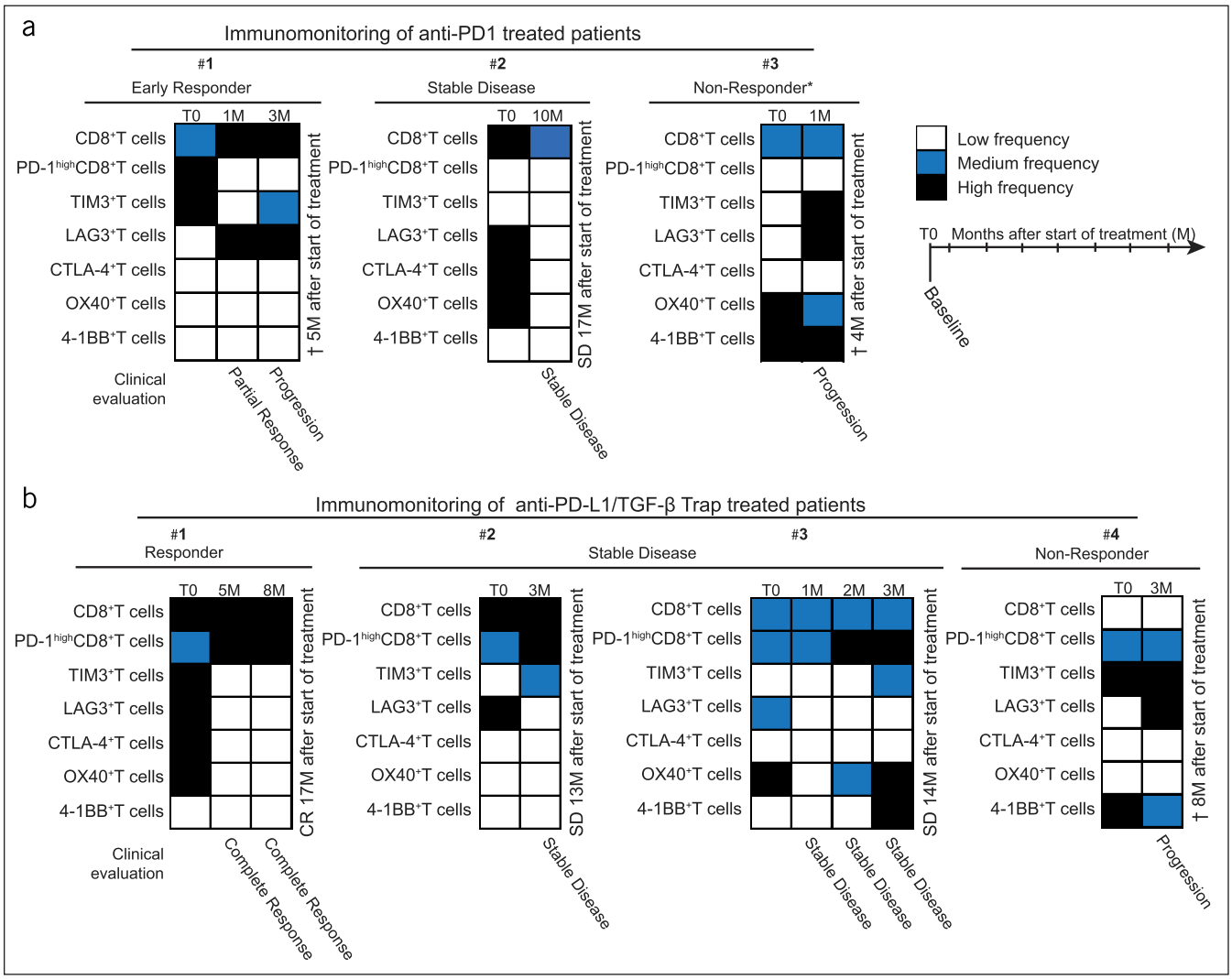

Figure 7. Immunomonitoring of PD-1/PD-L1 pathway blockade-treated patients in the blood. (**a**) Immunomonitoring of patients treated with anti-PD-1 antibody (n = 3). (**b**) Immunomonitoring of patients treated with anti-PD-L1/TGF-β Trap (n = 4); T0, baseline; M, month after the start of treatment. Results are expressed as a heat map-based frequency of positive cells compared with the mean frequency of a corresponding subpopulation of the entire cohort at the baseline (T0): low (white; <mean, −20%), medium (blue; mean, ±20%), and high (black; >mean, +20%). *Anti-PD-1 antibody as the first-line treatment; the rest were second-line treatments after sorafenib. PD, programmed death.

We highlighted that PD-1 expression on T cells is another important marker associated with treatment's response. Our results suggest that reduced intratumoral frequency of PD-1^{high} cells within the CD8$^+$ T-cell population at the baseline predicts the patient's response to sorafenib treatment. This is in line with a recent report proposing low intratumoral frequency of PD-1$^+$ CD8$^+$ T cells as a biomarker of response to sorafenib treatment in patients with HCC (30). In addition, reduction in circulating PD-1$^+$ T cells correlates to the survival of patients with HCC after sorafenib therapy (31). Similarly, our results demonstrate that circulating PD-1$^+$ T cells increase during tumor progression, suggesting that the expression of PD-1 on the circulating level reflects the progression of HCC during sorafenib treatment.

The opposite situation occurs in the patients receiving immunotherapy, blocking the PD-1/PD-L1 inhibitory pathway. The principle of PD-1/PD-L1 pathway blockade therapy is to reinvigorate preexisting intratumoral T cells by removing the inhibition induced by the activation of the PD-1/PD-L1 axis and finally induce tumor rejection. Thus, the accumulation of PD-1$^+$ CD8$^+$ T cells in a tumor at the baseline often defines a subgroup of patients who are able to respond to PD-1/PD-L1 pathway blockade therapy (as reviewed by Simon and Labarriere (20)). Especially, the PD-1^{high} CD8$^+$ T cells seem to be crucial as this subset shows the following: (i) higher capacity for tumor recognition and (ii) markedly different transcriptional and metabolic profiles compared with PD-1^{neg} and PD-1^{int} lymphocytes (18). Significantly, the frequency of intratumoral PD-1^{high} cells was strongly predictive for both the response and survival of patients with non–small cell lung cancer treated with PD-1 blockade (18). Similarly, patients with advanced malignant melanoma, who received anti-PD-1 antibodies and had more than 20% of tumor-infiltrating CTLA-4^{high} PD-1^{high} cells within their CD8$^+$ T-cell population, showed

a favorable response to treatment compared with patients with 20% and less CTLA-4^{high} PD-1^{high} cells per CD8$^+$ T-cell population (17). Accordingly, we observed a very high baseline frequency of intratumoral PD-1^{high} cells per CD8$^+$ T cell in patients experiencing tumor response to PD-1/PD-L1 pathway blockade, whereas a low frequency was observed in nonresponders. Importantly, a recent study investigating CD8$^+$ T cells isolated from HCC specimens also demonstrated that tumors with high proportions of PD-1^{high} CD8$^+$ T cells are susceptible to immune checkpoint blockade-based therapies, as this subset expresses multiple immune checkpoint receptors and could be further reinvigorated by immune checkpoint blockade (32). Similarly, Chew et al. recently demonstrated that HCC tissues' resident memory PD-1$^+$ CD8$^+$ T cells constitute the predominant T-cell subset responsive to anti-PD-1 treatment *in vitro* (29).

Unfortunately, PD-1 expression on CD8$^+$ T cells was not assessed as a part of the CheckMate 040 clinical trial; only the PD-L1 expression on tumor cells was noted. Moreover, objective responses were observed in 26% of the patients with PD-L1 expression on at least 1% of tumor cells and in 19% of patients with PD-L1 on less than 1% of tumor cells, showing no significant difference in this regard (11). However, data pertaining to PD-1 and PD-L1 expression on tumor-infiltrating immune cells are not available for a CheckMate 040 clinical trial.

Today, anti-PD-1 antibody nivolumab is approved in the United States for the treatment of patients with HCC after the first-line treatment of sorafenib. From this perspective, the frequency of intratumoral PD-1^{high} CD8$^+$ T cells may serve as an immune marker to divide patients with HCC to a subgroup with a low frequency of intratumoral PD-1^{high} CD8$^+$ T cells, which may benefit from sorafenib treatment, and a subgroup with a high frequency of intratumoral PD-1^{high} CD8$^+$ T cells that should instead be treated directly via PD-1/PD-L1 pathway blockade.

There is growing evidence that the efficacy of single immunotherapies is often limited by compensatory induction of other immune checkpoint molecules, which contributes to a feedback loop that acts to mediate immune suppression. Compensatory upregulation of inhibitory checkpoint molecules after PD-1 blockade was recently described in mouse models of lung adenocarcinoma (33) and in ovarian tumor (34). Herein, we analyzed the immune changes that take place in peripheral blood during treatment and observed the compensatory upregulation of LAG3 and TIM3 inhibitory immune checkpoints on T cells in nonresponding patients to PD-1/PD-L1 pathway blockade. However, further analyses are needed to validate these findings, preferentially as translational protocols in clinical trial cohorts. Such information will be crucial for the rational design of combinatorial immune checkpoint blockade in advanced HCC, to increase the number of responders and the efficacy of treatment. For instance, simultaneous blockade of the PD-L1 and TGF-β pathways by anti-PD-L1/TGF-β bifunctional immunotherapy fusion protein showed superior antitumor activity in relation to monotherapies (35). Similarly, in our study, we observed that 3 of the 4 patients treated with anti-PD-L1/TGF-β clearly benefited from this therapy. Thus, combination therapies constitute a logical step in this regard, and adequate information to select proper immunotherapy combination partners and the biomarkers of response is required currently. However, the possibility that additional TGF-beta treatment affected the immunomonitoring results also needs to be taken into account.

In this study, we thoroughly characterized immune checkpoint distribution on lymphocyte subsets. Recently, Zhou et al. published the characterization of inhibitory immune checkpoint molecules in the early stages of HCC13 based on samples obtained from surgical resection. The authors reported that the expression of PD-1, TIM3, LAG3, and CTLA4 is significantly higher on T cells isolated from tumor tissue than from nontumoral tissue. In our cohort of patients with advanced HCC, we observed only a slightly higher frequency of immune checkpoint molecules in the tumor tissue compared with nontumoral tissues. This is an important observation reflecting the difference between early-stage and advanced-stage HCC4. Similarly, we observed a very high frequency of LAG3-positive cells, which is probably also related to the advanced stage of HCC. Previously, it has been shown that in lung cancer, LAG3 increases with disease stage (36). Contrarily, the CTLA-4 surface expression was low in our study. The intracellular staining would be needed to characterize CTLA-4 completely as most of the CTLA-4 protein resides intracellularly (37).

In addition, in this study we provided information about the expression of stimulatory immune checkpoint molecules OX40 and 4-1BB. The former is known to be expressed mainly by Treg, promoting immune tolerance (38). High OX40 expression was associated with high serum alpha-fetoprotein levels and shorter survival of patients with HCC (39). Accordingly, we observed that OX40 is expressed primarily by CD4$^+$ T cells and that intratumoral frequency of OX40$^+$ T cells and OX40$^+$ CD4$^+$ T cells strongly correlates to the alpha-fetoprotein levels. The stimulatory immune checkpoint 4-1BB was expressed by both CD4$^+$ and CD8$^+$ T cells, and the expression correlated negatively to the expression of inhibitory immune checkpoints. Interestingly, 4-1BB agonist utomilumab was recently used in a phase I study of patients with advanced cancer (40), and it is currently tested in combination with anti-PD-1 antibodies in solid cancers.

The analysis of immune checkpoint expression highlighted that CD3$^+$CD56$^+$ cells express a high level of immune checkpoint molecules, indicating that NKT and CD3^{bright}CD56$^+$ T cells may also be targeted by immune checkpoint blockers and could be a part of the mechanism of action.

The main limitation of our study is the sample size, which especially hampers subgroup analyses that might be of interest. Further study with larger number of patients, also including patients with different stages of HCC, will be necessary. To conclude, apart from the characterization of immune checkpoint molecules on crucial antitumor effectors in advanced HCC, we also demonstrated the feasibility and potential importance of detailed immunomonitoring during therapies, to define predictive factors of response and the mechanism of immunotherapy resistance.

CONFLICTS OF INTEREST

Guarantor of the article: Thomas Decaens, MD, PhD.
Specific author contributions: Z.M.J., C.A., P.N.M., T.D.: conception and design of the study. C.S., T.D.: sample collection. Z.M.J., C.A., K.K., A.G., N.S., T.D.: acquisition of data. Z.M.J., C.A., K.K., A.G., N.S., T.D.: analysis and interpretation of the data. Z.M.J.: drafting of the article. Z.M.J., C.A., P.N.M., T.D.: critical revision of

the article for important intellectual content. Z.M.J., C.A., K.K., A.G., C.S., N.S., P.N.M., T.D.: approval of the final version.

Financial support: This work is funded by la Ligue Nationale Contre le Cancer under Grant 2016-R16145CC—Le comité de Haute-Savoie de La Ligue Contre le Cancer (CD74).

Potential competing interests: None.

Study Highlights

WHAT ISKNOWN

- ✓ Immunity is a major player in HCC.
- ✓ Immune checkpoint therapy is a promising treatment of HCC, but less than 20% of patients respond to this treatment.
- ✓ Predictors of tumor response to HCC treatment are missing.

WHAT IS NEWHERE

- ✓ Intratumoral $CD4^+/CD8^+$ T-cell ratio at the baseline negatively correlates with the overall survival.
- ✓ A high baseline frequency of intratumoral PD-1^{high} $CD8^+$ T cells is negatively associated with tumor response to sorafenib but positively associated with tumor response to PD-L1/PD-1 pathway blockade.

TRANSLATIONAL IMPACT

- ✓ Immunomonitoring helps identify the best combination strategies for HCC treatment.
- ✓ The frequency of intratumoral PD-1^{high} $CD8^+$ T cells may serve as a biomarker to identify which individuals will benefit from which treatment.

REFERENCES

1. Sawyers CL, Abate-Shen C, Anderson KC, et al. AACR cancer progress report 2013. Clin Cancer Res 2013;19:S4–98.
2. Sangiovanni A, Colombo M. Treatment of hepatocellular carcinoma: Beyond international guidelines. Liver Int 2016;36(Suppl 1):124–9.
3. Ringelhan M, Pfister D, O'Connor T, et al. The immunology of hepatocellular carcinoma. Nat Immunol 2018;19:222–32.
4. Elsegood CL, Tirnitz-Parker JE, Olynyk JK, et al. Immune checkpoint inhibition: Prospects for prevention and therapy of hepatocellular carcinoma. Clin Transl Immunol 2017;6:e161.
5. Roth GS, Decaens T. Liver immunotolerance and hepatocellular carcinoma: Patho-physiological mechanisms and therapeutic perspectives. Eur J Cancer 2017;87:101–12.
6. Ramzan M, Sturm N, Decaens T, et al. Liver-infiltrating CD8(+) lymphocytes as prognostic factor for tumour recurrence in hepatitis C virus-related hepatocellular carcinoma. Liver Int 2016;36: 434–44.
7. Wang BJ, Bao JJ, Wang JZ, et al. Immunostaining of PD-1/PD-Ls in liver tissues of patients with hepatitis and hepatocellular carcinoma. World J Gastroenterol 2011;17:3322–9.
8. Shi F, Shi M, Zeng Z, et al. PD-1 and PD-L1 upregulation promotes CD8(+) T-cell apoptosis and postoperative recurrence in hepatocellular carcinoma patients. Int J Cancer 2011;128:887–96.
9. Gao Q, Wang XY, Qiu SJ, et al. Overexpression of PD-L1 significantly associates with tumor aggressiveness and postoperative recurrence in human hepatocellular carcinoma. Clin Cancer Res 2009;15:971–9.
10. Calderaro J, Rousseau B, Amaddeo G, et al. Programmed death ligand 1 expression in hepatocellular carcinoma: Relationship with clinical and pathological features. Hepatology 2016;64:2038–46.
11. El-Khoueiry AB, Sangro B, Yau T, et al. Nivolumab in patients with advanced hepatocellular carcinoma (CheckMate 040): An open-label, non-comparative, phase 1/2 dose escalation and expansion trial. Lancet 2017;389:2492–502.
12. Zhu AX, Finn RS, Edeline J, et al. Pembrolizumab in patients with advanced hepatocellular carcinoma previously treated with sorafenib (KEYNOTE-224): A non-randomised, open-label phase 2 trial. Lancet Oncol 2018;19:940–52.
13. Zhou G, Sprengers D, Boor PPC, et al. Antibodies against immune checkpoint molecules restore functions of tumor-infiltrating T cells in hepatocellular carcinomas. Gastroenterology 2017;153:1107–19.e10.
14. Jouvin-Marche E, Macek Jilkova Z, Thelu MA, et al. Lymphocytes degranulation in liver in hepatitis C virus carriers is associated with IFNL4 polymorphisms and ALT levels. J Infect Dis 2014;209:1907–15.
15. Macek Jilkova Z, Decaens T, Marlu A, et al. Sex differences in spontaneous degranulation activity of intrahepatic natural killer cells during chronic hepatitis B: Association with estradiol levels. Mediators Inflamm 2017; 2017:3214917.
16. Macek Jilkova Z, Afzal S, Marche H, et al. Progression of fibrosis in patients with chronic viral hepatitis is associated with IL-17(+) neutrophils. Liver Int 2016;36:1116–24.
17. Daud AI, Loo K, Pauli ML, et al. Tumor immune profiling predicts response to anti-PD-1 therapy in human melanoma. J Clin Invest 2016; 126:3447–52.
18. Thommen DS, Koelzer VH, Herzig P, et al. A transcriptionally and functionally distinct PD-1(+) CD8(+) T cell pool with predictive potential in non-small-cell lung cancer treated with PD-1 blockade. Nat Med 2018;24:994–1004.
19. Han S, Zhang C, Li Q, et al. Tumour-infiltrating CD4(+) and CD8(+) lymphocytes as predictors of clinical outcome in glioma. Br J Cancer 2014;110:2560–8.
20. Simon S, Labarriere N. PD-1 expression on tumor-specific T cells: Friend or foe for immunotherapy? Oncoimmunology 2017;7:e1364828.
21. Gabrielson A, Wu Y, Wang H, et al. Intratumoral CD3 and CD8 T-cell densities associated with relapse-free survival in HCC. Cancer Immunol Res 2016;4:419–30.
22. Foerster F, Hess M, Gerhold-Ay A, et al. The immune contexture of hepatocellular carcinoma predicts clinical outcome. Sci Rep 2018;8:5351.
23. Huang Y, Ma C, Zhang Q, et al. CD4+ and CD8+ T cells have opposing roles in breast cancer progression and outcome. Oncotarget 2015;6: 17462–78.
24. Gao Q, Qiu SJ, Fan J, et al. Intratumoral balance of regulatory and cytotoxic T cells is associated with prognosis of hepatocellular carcinoma after resection. J Clin Oncol 2007;25:2586–93.
25. Flecken T, Schmidt N, Hild S, et al. Immunodominance and functional alterations of tumor-associated antigen-specific CD8+ T-cell responses in hepatocellular carcinoma. Hepatology 2014;59:1415–26.
26. Yao W, He JC, Yang Y, et al. The prognostic value of tumor-infiltrating lymphocytes in hepatocellular carcinoma: A systematic review and meta-analysis. Sci Rep 2017;7:7525.
27. Chen KJ, Lin SZ, Zhou L, et al. Selective recruitment of regulatory T cell through CCR6-CCL20 in hepatocellular carcinoma fosters tumor progression and predicts poor prognosis. PLoS One 2011;6:e24671.
28. Zheng C, Zheng L, Yoo JK, et al. Landscape of infiltrating T cells in liver cancer revealed by single-cell sequencing. Cell 2017;169:1342–56.e16.
29. Chew V, Lai L, Pan L, et al. Delineation of an immunosuppressive gradient in hepatocellular carcinoma using high-dimensional proteomic and transcriptomic analyses. Proc Natl Acad Sci USA 2017;114:E5900-9.
30. Chen J, Ji T, Zhao J, et al. Sorafenib-resistant hepatocellular carcinoma stratified by phosphorylated ERK activates PD-1 immune checkpoint. Oncotarget 2016;7:41274–84.
31. Kalathil SG, Lugade AA, Miller A, et al. PD-1+ and Foxp3+ T cell reduction correlates with survival of HCC patients after sorafenib therapy. JCI Insight 2016;1:e86182.
32. Kim HD, Song GW, Park S, et al. Association between expression level of PD1 by tumor-infiltrating CD8(+) T cells and features of hepatocellular carcinoma. Gastroenterology 2018;155:1936–50.e17.
33. Koyama S, Akbay EA, Li YY, et al. Adaptive resistance to therapeutic PD-1 blockade is associated with upregulation of alternative immune checkpoints. Nat Commun 2016;7:10501.
34. Huang RY, Francois A, McGray AR, et al. Compensatory upregulation of PD-1, LAG-3, and CTLA-4 limits the efficacy of single-agent checkpoint blockade in metastatic ovarian cancer. Oncoimmunology 2017;6:e1249561.
35. Lan Y, Zhang D, Xu C, et al. Enhanced preclinical antitumor activity of M7824, a bifunctional fusion protein simultaneously targeting PD-L1 and TGF-beta. Sci Transl Med 2018;10:eaan5488.

36. Thommen DS, Schreiner J, Muller P, et al. Progression of lung cancer is associated with increased dysfunction of T cells defined by coexpression of multiple inhibitory receptors. Cancer Immunol Res 2015;3:1344–55.
37. Walker LS, Sansom DM. Confusing signals: Recent progress in CTLA-4 biology. Trends Immunol 2015;36:63–70.
38. Xiao X, Gong W, Demirci G, et al. New insights on OX40 in the control of T cell immunity and immune tolerance in vivo. J Immunol 2012;188: 892–901.
39. Xie K, Xu L, Wu H, et al. OX40 expression in hepatocellular carcinoma is associated with a distinct immune microenvironment, specific mutation signature, and poor prognosis. Oncoimmunology 2018;7:e1404214.
40. Segal NH, He AR, Doi T, et al. Phase I study of single-agent utomilumab (PF-05082566), a 4-1BB/CD137 agonist, in patients with advanced cancer. Clin Cancer Res 2018;24:1816–23.

www.impactjournals.com/oncotarget/ Oncotarget, 2018, Vol. 9, (No. 13), pp: 11145-11158

Research Paper

Combination of AKT inhibitor ARQ 092 and sorafenib potentiates inhibition of tumor progression in cirrhotic rat model of hepatocellular carcinoma

Zuzana Macek Jilkova[1,2], Ayca Zeybek Kuyucu[1,2,3], Keerthi Kurma[1,2], Séyédéh Tayébéh Ahmad Pour[1,2], Gaël S. Roth[1,2,6], Giovanni Abbadessa[4], Yi Yu[4], Brian Schwartz[4], Nathalie Sturm[1,2,5], Patrice N. Marche[1,2], Pierre Hainaut[1,2] and Thomas Decaens[1,2,6]

[1]Université Grenoble-Alpes, Saint-Martin-d'Hères, France

[2]Institute for Advanced Biosciences, Research Center Inserm U1209/CNRS 5309/UGA, Grenoble, France

[3]Izmir Institute of Technology, Department of Bioengineering, Izmir, Turkey

[4]ArQule Inc., Woburn, MA, USA

[5]CHU-Grenoble Département d'Anatomie et de Cytologie Pathologiques, La Tronche, France

[6]CHU-Grenoble Clinique Universitaire d'Hépato-Gastroentérologie, Pôle Digidune, France

Correspondence to: *Thomas Decaens,* ***email:*** *tdecaens@chu-grenoble.fr*
Zuzana Macek Jilkova, ***email:*** *zuzana.mjilkova@gmail.com*

Keywords: *liver cancer; combination treatment; fibrosis; DEN-induced model; AKT inhibitor*

Received: *August 11, 2017* ***Accepted:*** *January 13, 2018* ***Published:*** *January 23, 2018*

ABSTRACT

The prognosis of patients with advanced hepatocellular carcinoma (HCC) is very poor. The AKT pathway is activated in almost half of HCC cases and in addition, long term exposure to conventional drug treatment of HCC, sorafenib, often results in over-activation of AKT, leading to HCC resistance. Therefore, it is important to assess the safety and the efficacy of selective allosteric AKT inhibitor ARQ 092 (Miransertib) in combination with sorafenib.

Here, we demonstrated *in vitro* that the combination of ARQ 092 with sorafenib synergistically suppressed proliferation, promoted apoptosis, and reduced migration. To test the effect of the combination *in vivo*, rats with diethylnitrosamine-induced cirrhosis and fully developed HCC were randomized and treated with vehicle, sorafenib, ARQ 092 or the combination of ARQ 092 with sorafenib; (n=7/group) for 6 weeks. Tumor progression, size of tumors and the mean tumor number were significantly reduced by the combination treatment compared to the control or single treatments. This effect was associated with a significant increase in apoptotic response and reduction in proliferation and angiogenesis. Sirius red staining showed a decrease in liver fibrosis. Moreover, treatments improved immune response in blood and in tumor microenvironment.

Thus, the combination of ARQ 092 with sorafenib potentiates inhibition of tumor progression and gives the possibility of therapeutic improvement for patients with advanced HCC.

INTRODUCTION

Liver cancer (mainly hepatocellular carcinoma (HCC)) is reported to be the fifth most common cancer with second highest mortality among all cancers in adult men [1]. Viral hepatitis, chronic alcohol consumption and non-alcoholic steatohepatitis are the major causes of chronic liver inflammation which finally leads to HCC development. HCC that is diagnosed at an advanced stage has a very poor prognosis, and sorafenib is the

only approved drug available. The multikinase inhibitor sorafenib, originally developed as a Raf kinase inhibitor, targets the MAPK/ERK pathway but also the vascular endothelial growth factor receptors (VEGF-R) and the platelet-derived growth factor receptor (PDGF-R). Even though sorafenib is the first drug that significantly increases clinical outcome of advanced HCC, its efficacy is modest with a median overall survival of 10.7 months versus 7.9 months with placebo in the pivotal phase III trial [2]. Moreover, long-term exposure to sorafenib often results in reduced sensitivity of the tumor cells, leading to acquired resistance. Therefore, new therapeutic treatments of HCC with better efficacy are urgently needed.

Growing evidence indicates that the phosphatidylinositol-3 kinase (PI3K)/AKT/mTOR-pathway is activated in approximately 50% of patients with cirrhosis and HCC [3, 4]. Moreover, sorafenib has been demonstrated to activate the AKT pathway in HCC cells [5] and this overactivation is considered to be one of the mechanisms of resistance to sorafenib treatment [6].

The serine/threonine kinase AKT, also known as protein kinase B or PKB, has become a major focus of attention mainly because of its critical role in regulating diverse cellular functions including metabolism, growth, proliferation, survival, transcription and protein synthesis. Activated AKT is known to inhibit apoptosis through its ability to phosphorylate several targets, including BAD, FoxO transcription factors, Raf-1 and caspase-9, that are critical for cell survival [7]. Therefore, the combination of sorafenib with an AKT-inhibitor could represent a new therapeutic strategy which could improve anti-tumor efficacy and overcome sorafenib resistance in HCC.

Recently, the combination strategy of sorafenib with mTOR inhibitors in HCC has been shown to be toxic and ineffective. Specifically, mTOR1 inhibitor everolimus in combination with sorafenib failed to show significant survival benefits compared to sorafenib alone [8]. Moreover, the same drug failed to demonstrate survival benefit in second line after failure of sorafenib, compared to placebo in a randomized phase 3 trial without patient's selection [9]. It is necessary to emphasize that everolimus, similarly as other mTOR inhibitors, affects the mTORC1 protein complex, and not the mTORC2. This leads to increased AKT phosphorylation via inhibition on the mTORC1 negative feedback loop, while maintaining the mTORC2 positive feedback to AKT [10].

In contrast with mTOR inhibitors, direct inhibition of AKT seems to be an effective and nontoxic strategy. In recent work, we have demonstrated anti-tumor efficacy of ARQ 092, a highly selective allosteric inhibitor [11] that suppresses pan-AKT activity by blocking its phosphorylation and by preventing the inactive form from localizing into plasma membrane which together leads to strong and specific downregulation of downstream targets of AKT. Such high specificity was missing in catalytic AKT inhibitors that have been previously developed [12]. In addition, it was recently demonstrated that AKT inhibitors may reverse the acquired resistance to sorafenib *in vitro* [13]. However, to our knowledge the effect of the combination therapy of sorafenib + highly specific AKT inhibitor was never tested on HCC *in vivo*.

Therefore, in this study we combined ARQ 092 with sorafenib to investigate whether this therapeutic strategy could provide an improvement in treatment of advanced HCC, without increased toxicity.

In order to identify specific adverse events that could be related to the background of cirrhosis, newly developed therapeutic strategies should be pre-clinically tested in a relevant animal model of HCC developed on a cirrhotic liver. One of the well-established models that at present best reproduces human cirrhosis is diethylnitrosamine (DEN)-injured rats [14]. Therefore, we used the DEN-induced cirrhotic rat model with HCC to test safety and anti-tumor efficacy of the combination of sorafenib with AKT-inhibitor ARQ 092 (Supplementary Figure 1).

RESULTS

Combination of sorafenib and ARQ 092 suppresses cell proliferation, promotes cell apoptosis, and reduces migration

We previously determined the half maximal inhibitory concentration (IC_{50}) of single treatment on each cell lines ([11], Supplementary Table 1). To determine the effect of the combination treatment on cell growth, we used a mixture of IC_{50} of single treatments (i.e. $IC_{50}^{Sorafenib}$+$IC_{50}^{ARQ\ 092}$). MTT assays showed a drastic decrease in proliferation rate for Hep3B (Figure 1A), HepG2, Huh-7 and PLC/PRF cell-lines (Supplementary Figure 2A). The calculated combination index (CI) values (for details see supporting information), revealed strong synergistic effect of the combination treatment of sorafenib and ARQ 092 on cell growth as summarised in the Supplementary Table 2. Combination IC_{50}/200 ($IC_{50}^{Sorafenib}$+$IC_{50}^{ARQ\ 092}$/200) and Combination IC_{50}/10 ($IC_{50}^{Sorafenib}$+$IC_{50}^{ARQ\ 092}$/10) were used for further experiments.

We observed a significant decrease in cell-viability in the combination and single treated groups in all tested cell lines in comparison to the control ($p<0.0001$), (Figure 1B and Supplementary Figure 3). Combination IC_{50}/10 significantly increased early apoptotic cells in Hep3B compared to sorafenib IC_{50} ($p=0.003$) or ARQ 092 IC_{50} ($p=0.023$), (Figure 1B).

A wound-healing assay revealed that after 24h, the combination IC_{50}/10 reduced migration of Hep3B significantly more than the sorafenib IC_{50} (Figure 1C, Supplementary Figure 4B). Moreover, in other cell lines, the migration of cells was decreased significantly in the combination IC_{50}/10 treatment compared to both of the IC_{50} single treatments (Supplementary Figure 4A, 4B).

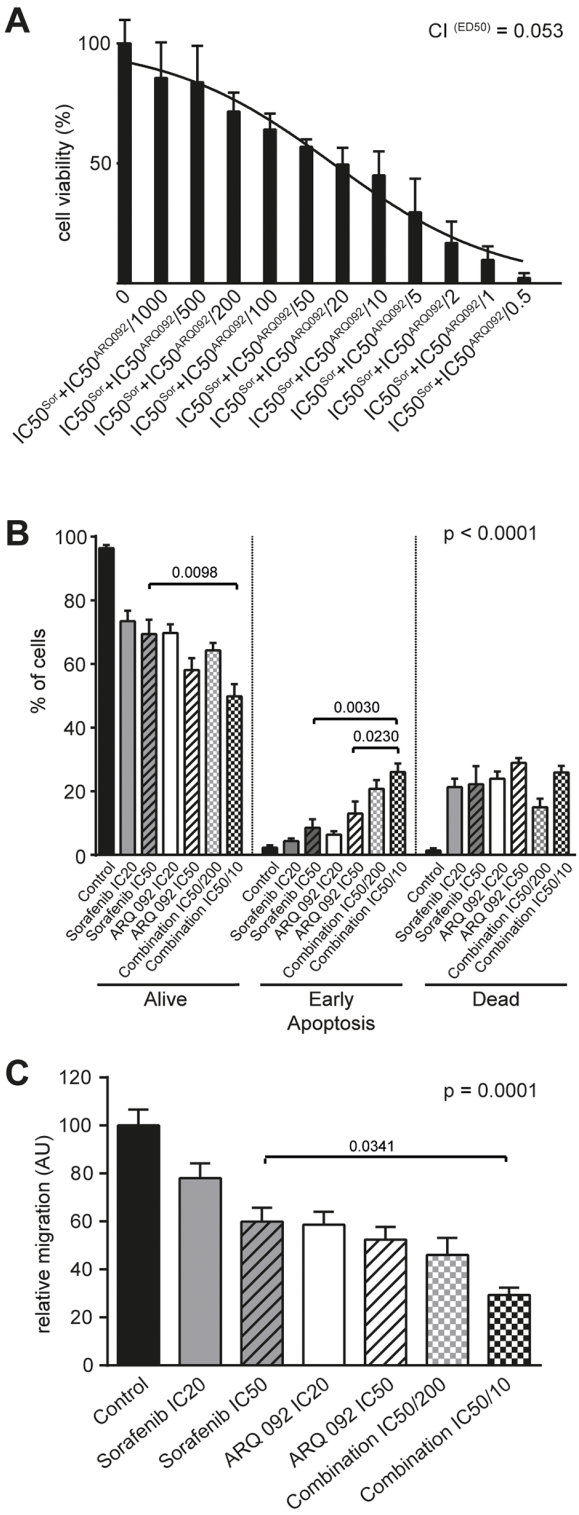

Figure 1: Effect of Combination treatment on Hep3B cell viability, apoptosis and cell migration. **(A)** MTT assay on Hep3B cell line after 48h of treatments showing significant decrease in cell viability with increasing concentrations of combination treatment of ARQ 092 and sorafenib (constant ratio IC_{50}: IC_{50}). Combination index (CI = 0.053) at effective dose 50 (ED_{50}) revealed strong synergy. **(B)** Additive effects of combination treatment of ARQ 092 and sorafenib on apoptosis in Hep3B after 48h of exposure. P values in graph represent ANOVA comparison of ARQ 092 IC_{50}, sorafenib IC_{50} and Combination IC_{50}/10. P value of ANOVA test of all groups is indicated in the corner of the graph ($p < 0.0001$). **(C)** The quantification of migration (decrease of width of the wound after 24h) in Hep3B. Additive effects of combination treatment of ARQ 092 and sorafenib. P values in graph represent ANOVA comparison of ARQ 092 IC_{50}, sorafenib IC_{50} and Combination I IC_{50}/10. P value of ANOVA test of all groups is indicated in the corner of the graph ($p = 0.0001$). Control was set as 100%, values are means ± SE from three independent experiments performed in triplicates (A) and in duplicates (B, C).

Table 1: Clinical and biological analyses

		Control (n=7)	Sorafenib (n=7)	ARQ 092 (n=7)	Combination (n=7)	ANOVA p-values
Body Weight (g)		290±7.4	291±2.0	270±6.0	274±5.6	*ns*
Liver	Weight (g)	14.8±1.3	13.4±0.7	11.0±0.5*	10.9±0.5$^{**,\#}$	*0.0026*
	TG (g/L)	28.9±4.4	30.5±3.4	29.1±3.0	30.1±2.1	*ns*
Blood	Albumin (g/dL)	3.69±0.03	3.71±0.01	4.07±0.11$^{*,\#\#}$	3.76±0.05	*0.0046*
	AFP (ng/mL)	0.82±0.17	0.44±0.12	0.33±0.09*	0.27±0.04*	*0.0151*
	AST (U/L)	101.3±3.3	95.2±3.9	92.3±3.6	91.1±2.5	*ns*
	ALT (U/L)	73.1±5.2	73.0±3.9	67.6±6.3	68.4±2.2	*ns*
	ALP (U/L)	224±7.1	219±7.7	255±24.8	264±14.2	*ns*
	GGT (U/L)	21.5±3.8	15.9±2.8	13.3±1.9	7.4±1.4**	*0.0073*
	PT (s)	16.3±0.4	18.7±1.8	16.7±0.2	16.5±0.4	*ns*
	Total Bilirubin (mg/dL)	0.21±0.01	0.18±0.01	0.16±0.01*	0.17±0.01	*0.0211*
	Creatinine (mg/dL)	0.35±0.03	0.36±0.02	0.38±0.02	0.36±0.02	*ns*
	GLU (mg/dL)	128±3.4	142±4.3	153±4.7	142±4.8	*ns*
	Cholesterol (mg/dL)	86.6±6.5	84.9±4.0	102±7.3	88.7±5.1	*ns*
	TG (g/L)	62.2±11.5	75.1±11.2	60.2±7.7	67.7±10.1	*ns*

Abbreviations: AFP, alphafetoprotein; AST, aspartate aminotransferase; ALT, alanine aminotransferase; ALP, alkaline phosphatase; GGT, Gamma-glutamyl transpeptidase; PT, Prothrombin time. Values are means ± SE. Significant difference compared to control; *: $p<0.05$; **: $p<0.01$; ***: $p<0.001$; ****: $p<0.0001$. Significant difference between ARQ 092 and Sorafenib; $^{\#\#}$: $p<0.01$.

Similar results were obtained when cell velocity was assessed by cell tracking with time-lapse microscopy showing that wound-healing slow was related to cell migration inhibition and not decrease of cell proliferation (Supplementary Figure 4C).

All together, these results demonstrate that the combination of sorafenib and ARQ 092 synergistically suppresses cell proliferation, promotes cell apoptosis, and in an additive manner reduces migration in all tested human cell-lines.

Combination treatment in DEN-induced cirrhotic rat with HCC

To characterise the safety in a cirrhotic model and the anti-tumor efficacy of the combination of sorafenib and ARQ 092 in HCC, DEN-induced cirrhotic rats with HCC were treated during six weeks by sorafenib, ARQ 092, the combination of both drugs or the untreated control group, as specified in Supplementary Figure 1. In a previous study, the treatment schedule of ARQ 092 was 7 days on and 7 days off [11] but in this study, the schedule was changed to 5 days on and 9 days off in the ARQ 092 single treatment group and in the combination group to prevent possible side effects when combining with sorafenib treatment.

Safety data are summurized in Table 1. No significant differences in body weight were observed at the end of the treatment. The weight of the liver was lower in the ARQ 092 group compared to the control group, and in the combination group compared to the control and sorafenib group. Assessment of triglycerides in liver did not show any difference between groups (p=0.9743). Blood sample analysis revealed that none of treatments affect glucose, cholesterol or triglyceride blood concentrations. Similarly, kidney functions were not affected by treatments as plasmatic creatinine levels did not differ between groups. There was no statistical difference in transaminases, alkaline phosphatase (ALP) and prothrombin time among all groups. However, serum levels of AFP were significantly decreased by ARQ 092 and the combination treatment compared to the control group. We observed a significant decrease in total bilirubin and an increase in albumin level in ARQ 092 group compared to the control, and a decrease in GGT level in the combination group compared to the control.

No difference was observed between the sorafenib and control groups.

Thus, our results showed that ARQ 092 and the combination treatment improve liver function but do not interfere with lipid or glucose metabolism (two major side effects of mTOR inhibitors).

The effect of ARQ 092, sorafenib and the combination of both agents on tumor progression was assessed by a liver MRI scan, Figure 2A. As illustrated in Figure 2B, tumor progression was significantly reduced by sorafenib (by 33.0±10.3%; p=0.005) and ARQ 092 (by 33.8±10.6%; p=0.005) compared to the control. The greatest decrease in tumor progression rate was observed in the combination group when compared with the control (66.6±10.6%; p<0.0001), indicating an additive effect of sorafenib and ARQ 092 on the control of tumor progression. Similarly, the combination treatment significantly reduced tumor progression compared to sorafenib (50.1±13.3%; p=0.006) and ARQ 092 (49.6±14.1%; p=0.010).

MRI analyses were further confirmed by macroscopic examination of the liver (Figure 2C), which revealed significantly smaller mean tumor size in the sorafenib (6.3 ± 0.8 mm), ARQ 092 (6.2 ± 0.8 mm) and combination group (3.0 ± 1.1 mm) compared to the control rats (9.9 ± 1.1 mm) with statistical significance p=0.0092, p=0.0101 and p<0.0001, respectively. Mean tumor size in the combination group was significantly reduced compared to single agents, sorafenib (p=0.0187) or ARQ 092 (p=0.0308), confirming that the combination treatment is superior to the single agents.

The macroscopic counting of tumors revealed a significantly lower number in rats treated by ARQ 092 and the combination group compared to the control and sorafenib groups. In fact, while the mean number of tumors on the liver surface of the control rats was 109.5±14.5, significant reduction was observed in the ARQ 092 treated rats (31.5±14.8; p<0.0001) and in the combination (21.21±14.5; p<0.0001). Similarly, the ARQ 092 and combination groups displayed a significantly lower number of tumors compared to tumor numbers (69.21±11.5) in the sorafenib-treated animals (p=0.0188 and p=0.0016 respectively), Figure 2C. Accordingly, the frequency of Ki67-positive nuclei was significantly reduced in ARQ 092 (p=0.0421) and in the combination group (p=0.0206) compared to the control group. The combination treatment also significantly reduced the Ki67 proliferation marker compared to sorafenib group (p=0.0487), Figure 2D. TUNEL immunostaining showed that only the combination group significantly induced apoptosis (p=0.0272), Figure 2E. The sorafenib treatment showed no statistical significance for Ki67 (89.8 ± 12.1 % of control, p=0.9563) or TUNEL (124.9 ± 9.6 % of control, p=0.4566), Figure 2D and 2E.

Real time qPCR analyses of alpha fetoprotein (AFP), HCC tumor marker, showed a reduced expression in all treated groups compared to the control (Figure 2F), with a much stronger effect in the combination group (p=0.0138).

Overall, we observed an additive effect of the combination of sorafenib and ARQ 092 on tumor progression and tumor size. Moreover, the combination significantly reduced tumor proliferation in DEN-induced HCC rat model, and was clearly more effective than sorafenib and/or ARQ 092 monotherapies.

Effect of combination treatment on tumor vascularization and liver fibrosis

Anti-angiogenic effect of treatment was determined by immunostaining of liver tissue, using a rat-specific anti-CD34 antibody. Major structural abnormalities of the vasculature were observed in control livers, and tissues from all treated groups demonstrated normalization of vasculature, Figure 3A. Similarly, the quantification of vascular density revealed that both sorafenib and ARQ 092 significantly decreased angiogenesis, but to smaller extent than the combination treatment. In fact, sorafenib decreased vascular density by 30% (p=0.0012), ARQ 092 by 58% (p<0.0001) and the combination by 75% (p<0.0001) compared to non-treated rats (Figure 3B). The gene expression of hypoxia-inducible factor (HIF-1), considered a marker of tumor hypoxia, tended to be decreased by all treatments but only the combination treatment significantly reduced HIF-1 expression in tumor tissue compared to the control (p=0.0194), Figure 3C.

Liver fibrosis was analyzed by Sirius red staining. As shown in Figure 3D and 3E, fibrotic tissues were significantly reduced in the ARQ 092 and combination groups compared to the control and sorafenib groups.

Improvement of liver fibrosis by ARQ 092 and the combination treatment was confirmed by qPCR analysis of non-tumoral tissue (Figure 3F). The expression of markers of liver fibrosis (alpha smooth muscle actin (α-SMA), collagen 1 and transforming growth factor β1 (TGFβ 1)) was significantly downregulated in non-tumor liver samples in ARQ 092 and the combination groups compared to the control group. Accordingly, the tissue inhibitor of metalloproteinases-1 (TIMP-1) was decreased by all treatments compared to the control whereas matrix metalloproteinases MMP2 and MMP9 were significantly upregulated in the combination group compared to the control and sorafenib groups. This effect on the matrix pathway was specific for non-tumor tissue. Thus, ARQ 092 and the combination treatment significantly decreased hepatic collagen deposition and improved liver fibrosis in DEN-induced cirrhotic rats, while sorafenib only had a mild effect.

Effect of combination treatment on AKT and ERK pathway

Western blot analyses showed that ARQ 092 and the combination of ARQ 092 with sorafenib treatment blocked phosphorylation of $AKT^{(Ser473)}$ in all human HCC cell

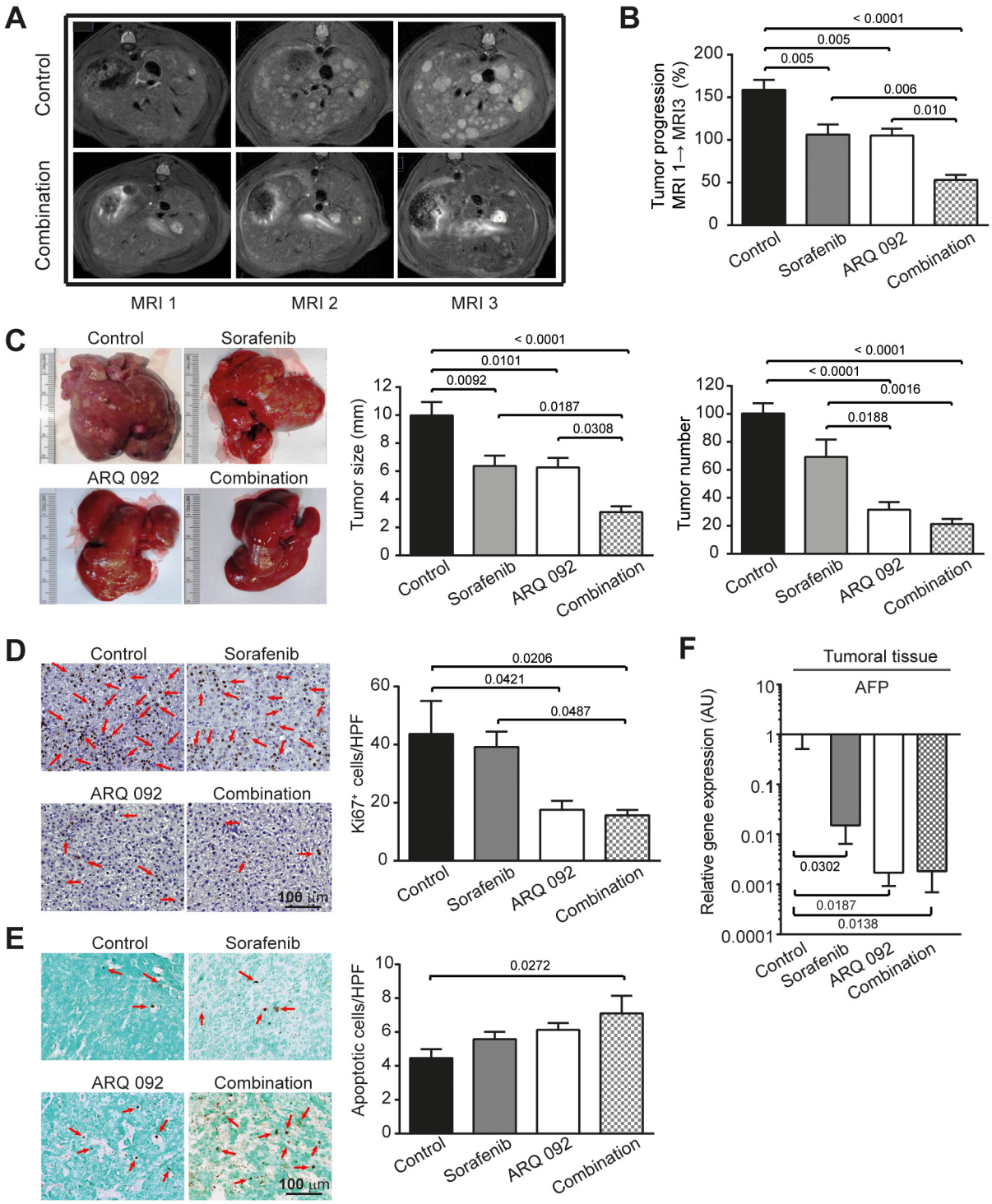

Figure 2: Anti-tumor effect of combination treatment. **(A)** Representative pictures of abdominal MRI 1, 2 and 3 scan of non-treated rat and rat treated by combination treatment. **(B)** Tumor progression assessment by comparison of tumor size on MRI 1, 2 and 3 in Control, sorafenib, ARQ 092 and Combination group. **(C)** Macroscopic examination of livers with assessment of tumor size (middle panel) and tumor number at the surface of livers (right panel). **(D)** Representative images of nuclear Ki67 staining (arrow), 20x magnification with quantification of Ki67 staining per high power field (HPF). **(E)** Representative images of apoptosis induction (right panel) determined by TUNEL immunostaining (arrow), 20x magnification with quantification of apoptotic cells per HPF. **(F)** qPCR analysis of alpha fetoprotein (AFP) gene expression in tumor liver samples. The scale of the Y axes are Log 10, control was set as 1, values are means ± SE, n=7/group. Comparison of means was done by ANOVA test with Tukey correction.

lines at both IC_{20} and IC_{50} concentrations (Supplementary Figure 5).

In the *in vivo* model, ARQ 092 and the combination treatment strongly inhibited phosphorylation of $AKT^{(Ser473)}$ in both tumor and non-tumor liver tissues (Figure 4A and 4B). qPCR analyses demonstrated a significant decrease in AKT gene expression in tumor tissue of the ARQ 092 and combination treated groups compared to the control group. This effect was expected as ARQ 092 inhibitor blocks AKT phosphorylation and prevents the inactive form from localizing into plasma membrane, protein levels of AKT are stable but AKT gene expression is decreased. Moreover, ARQ 092 and the combination treatment strongly downregulated the AKT-pathway downstream effector mTORC1 specifically in tumoral tissue while there is no significant difference in non-tumoral tissue. Ribosomal protein S6 kinase beta-1 (S6K1), another downstream effector of AKT and mTORC1, was significantly decreased by ARQ 092 and the combination in both tumoral and non-tumoral liver tissue.

Next, we studied whether sorafenib still inhibits the MAPK/ERK pathway or whether cells are already resistant to sorafenib. There was no difference in pERK/ERK ratio among all groups (Figure 4A and 4B) and MAPK1 mRNA levels were not altered among all groups (Figure 4C).

Effect of treatment on immune system and tumor microenvironment

To characterize the effect of treatment on the immune system, whole fresh blood was analyzed by flow cytometry. Immune cells were identified based on CD45 expression and different populations of lymphocytes were then identified accordingly to their respective rat-specific markers: NK ($CD161^{high+}CD3^{-}$), NKT ($CD161^{low+}CD3^{+}$) and T ($CD161^{-}CD3^{+}$), Figure 5A. No difference in frequency of circulating NK or NKT cells was observed between groups (Supplementary Table 3). Interestingly, the frequency of T-cells in population of $CD45^{+}$ was increased

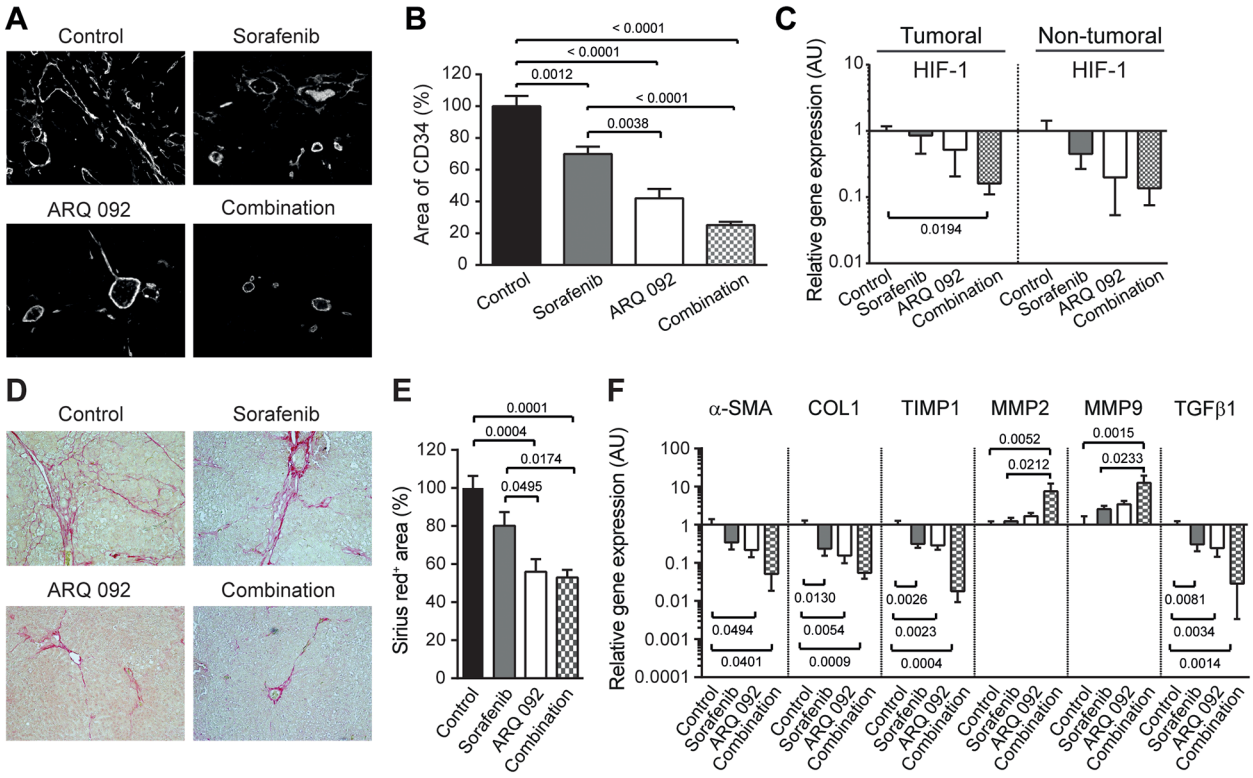

Figure 3: Effect of Combination treatment on tumor vascularization and liver fibrosis. (A) Representative pictures of CD34 immunofluorescence staining of liver tissue. **(B)** Quantification of CD34 staining, control was set as 100, values are means ± SE. **(C)** qPCR analysis of Hypoxia-inducible factor (HIF)-1 gene expression in tumoral and non-tumoral liver samples. Control was set as 1. Values are means ± SE. N=7/group. Comparison of means was done by ANOVA test with Tukey correction. **(D)** Representative histological images of livers stained with Sirius red. **(E)** Quantification of Sirius red staining area per total area; control was set as 100 %. **(F)** qPCR analysis of alpha smooth muscle actin (α-SMA), Collagen (COL)1, TIMP Metallopeptidase Inhibitor 1 (TIMP1), Matrix metalloproteinase-2 (MMP2), Matrix metalloproteinase-9 (MMP9) and transforming growth factor (TGF)β gene expression in non-tumoral liver tissue. The scale of the Y axes are Log 10, control was set as 1. Values are means ± SE. N=7/group. Comparison of means was done by ANOVA test with Tukey correction.

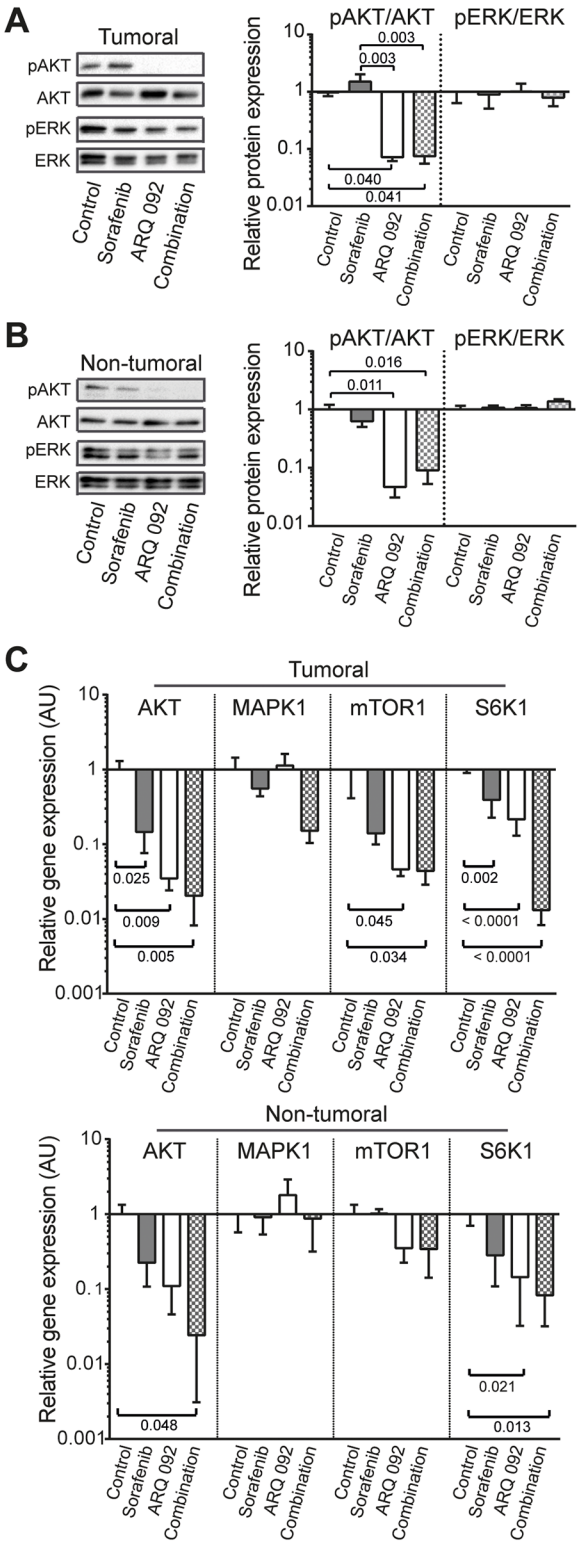

Figure 4: Effect of Combination treatment on AKT and ERK pathways. Western blot analysis of pAKT/AKT and pERK/ERK in **(A)** tumoral and **(B)** non-tumoral liver tissue. pAKT and pERK were stained first and after development, the membranes were stripped followed by staining of AKT and ERK. **(C)** qPCR analysis of the expression of AKT, MAPK, mTOR, S6K1 in tumoral (upper panel) and non-tumoral (lower panel) liver tissue. The scale of the Y axes are Log 10, control was set as 1, values are means ± SE. N=7/group. Comparison of means was done by ANOVA test with Tukey correction.

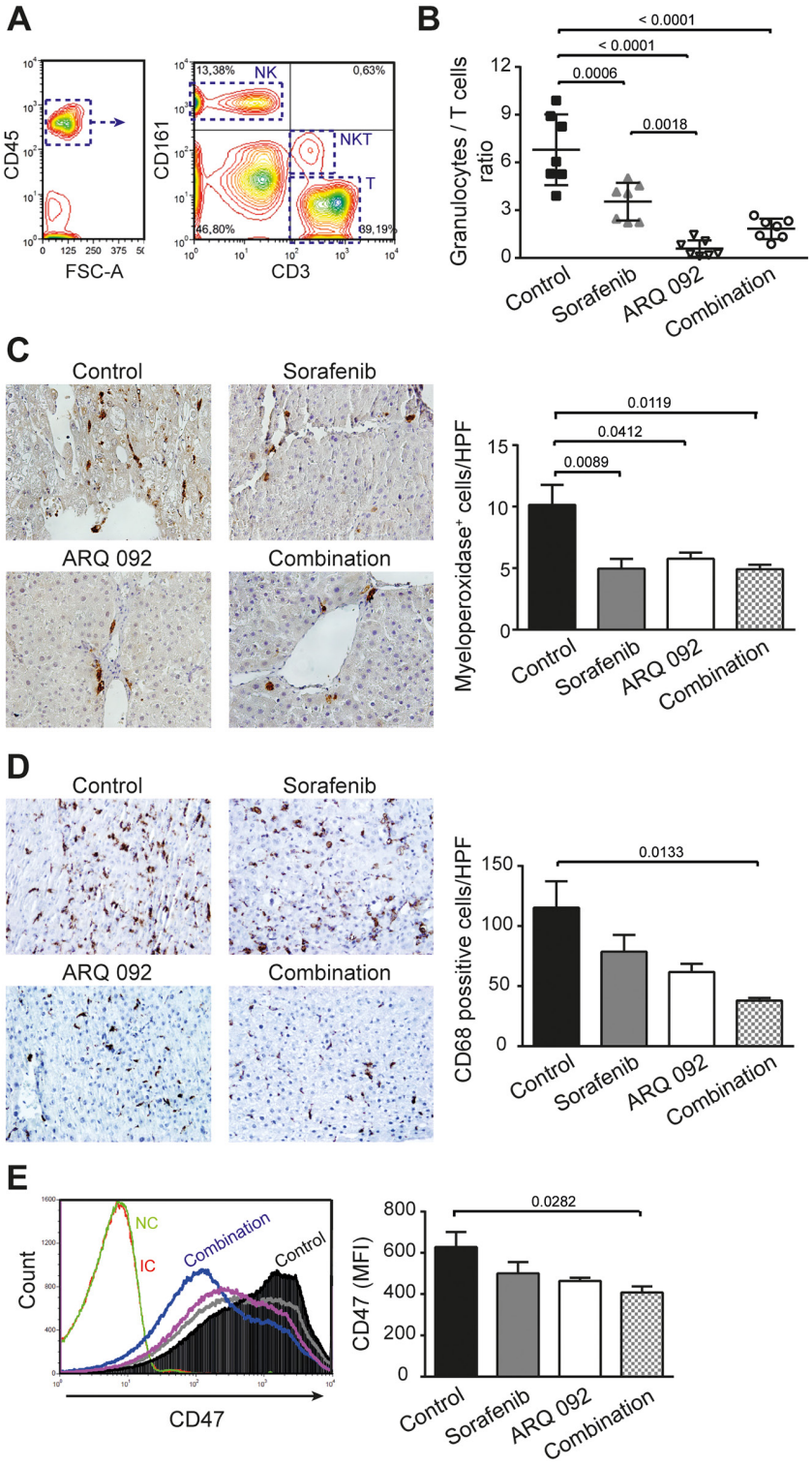

Figure 5: Effect of combination treatment on immune system and tumor microenvironment. (A) Gating flow cytometry strategy to investigate immune cells. Lymphocytes were first identified according their FSC and SSC parameters and further gated based on their CD45^{+} expression. Among the CD45^{+} population, NK (CD161^{high+}CD3^{-}), NKT (CD161^{low+}CD3^{+}) and T (CD161^{-}CD3^{+}) cells were selected. **(B)** Granulocytes to lymphocytes ratio. Values are means ± SE. N=7/group. Comparison of means was done by ANOVA test with Tukey correction. **(C)** Representative histological images of livers stained with myeloperoxidase and the quantification of positive cells (neutrophils) per high power field (HPF). **(D)** Representative histological images of livers stained with CD68 and the quantification of positive cells (macrophages) per HPF. **(E)** Expression of CD47 in tumor liver tissue and quantification of mean fluorescence intensity (MFI) of CD47, sorafenib (grey line), ARQ 092 (purple line). Values are means ± SE. N=7/group. Comparison of means was done by ANOVA test with Tukey correction.

by ARQ 092 and the combination treatment compared to control and sorafenib. This effect was accompanied by a strong reduction in the number of circulating granulocytes (Supplementary Table 3), which together led to significant reduction of Granulocyte/T cell ratio, Figure 5B.

In liver tissue, flow cytometry analyses showed no differences in the population of T-cells, NK cells or NKT cells between experimental groups. Similarly, by immunohistochemistry, we observed no significant differences between groups in the frequency of intrahepatic CD3- and CD8-positive cells (data not shown).

In accordance with the decrease in granulocytes frequency in blood, we observed a significant decrease in accumulated neutrophils in the liver tissue of all treated groups compared to control, as determined by myeloperoxidase staining, Figure 5C. Another population of immune cells, which was significantly reduced in the tumor microenvironment of the treated animals compared to control, were macrophages. We observed significant reduction of $CD68^+$ cells in rats treated by the combination treatment compared to control group, Figure 5D.

Tumor-initiating cells are characterized by high expression of CD47 [15]. Moreover, over-expression of CD47 is involved in sorafenib resistance [16]. Flow cytometry analyses revealed that highly expressing CD47 population in liver tissue was decreased by all treatments, with a significant effect in the combination group (Figure 5E).

All together, our data demonstrated that the combination treatment improves anti-tumor immune balance in the tumor itself and in blood, potentially explaining in part the anti-tumor effect of this combination. Moreover, the combination treatment significantly decreased a population of tumor-initiating cells.

DISCUSSION

The heterogeneity of HCC is both genetic [17] and phenotypical/morphological [18], with the hallmarks of cancer exhibited in a complex manner such as localizations and times. This complex and multivariate tumor network that constantly responds to and influences liver environment is the main reason of the limited success of different targeted monotherapies tested in HCC [19]. Thus, combining multiple anti-cancer drugs seems to be a rational approach in the prevention of tumor resistance. Nonetheless, as this strategy usually induces a huge increase of toxicity, there is an urgent need to find well-tolerated and effective combinations of targeted therapy to treat HCC patients.

HCC is a hypervascularized tumor with an anarchic neoangiogenesis and is usually surrounded by a cirrhotic liver. These characteristics obviously influence drug metabolism, by making systemic drug delivery less effective and by leading to severe adverse events. Therefore, before testing the safety and efficacy of multitarget therapies in clinical trials, pre-clinical studies are essential and the most optimal animal model need to be chosen. Thus, to test the combination of sorafenib and the AKT inhibitor ARQ 092, we used a cirrhotic rat model with HCC that closely reproduce human HCC physiopathology. We observed that the combination of ARQ 092 with sorafenib additively reduced tumor progression and tumor size with a significant higher efficacy than sorafenib and ARQ 092 monotherapies. The anti-tumor effect was associated with a significant reduction of tumor cell proliferation and an increased apoptosis *in vivo*. Treatment of ARQ 092 showed marked reduction of tumor number similar to the combination treatment, whereas sorafenib only had a modest effect on tumor initiation. Similarly, the cell proliferation, determined by Ki67 staining, was strongly reduced exclusively by ARQ 092, suggesting that AKT inhibition may even block tumor initiation. To confirm this hypothesis in our animal model, further experiments with an earlier introduction of ARQ 092 (during the DEN-induction phase) are needed.

Sorafenib-ARQ 092 combination therapy was very successful not only in targeting the tumor, but also in amelioration of liver microenvironment. This is particularly important, because after HCC initiation, the tumor progression is finely regulated by tumor microenvironment which even later influences the tumor response to therapies. For instance, increased and irregular vasculature will allow small HCC lesions to progress and metastasize, which is a typical situation in the fibrotic liver characterised by constantly increased formation of blood vessels [20]. The mechanism of beneficial action of sorafenib on liver vascularisation was described previously [21]. Here, we showed that the combination of ARQ 092 and sorafenib improved the vascularization of liver tissue in an additive manner and additionally decreases expression of HIF-1 in tumor tissue. Similarly, the anti-fibrotic effect of sorafenib was clearly demonstrated by numerous experimental studies (reviewed in [22]). In our study, the anti-fibrotic effect of sorafenib was relatively modest. On the contrary, the sorafenib-ARQ 092 combination greatly shifted matrix regulatory pathway, leading to fibrosis resolution with a strong decrease of collagen accumulation. Another essential determinant of HCC progression and survival is cancer-associated inflammation, with TGFβ orchestrating a favorable microenvironment for tumor cell growth. Here we showed that expression of TGFβ in non-tumor tissue was downregulated in an additive way by sorafenib-ARQ 092 combination.

Recently, a meta-analysis showed that a high neutrophil-to-lymphocyte ratio indicates a poor prognosis in patients with HCC, representing a shift towards an increased pro-tumor inflammation and decreased anti-tumor immune functions [23, 24]. In our model, all treatments significantly decreased granulocyte-to-

lymphocyte ratio compared to the control. The strong reduction of circulating neutrophils in rats treated by ARQ 092 monotherapy should to be taken into account. In fact, ARQ 092 was recently used to block neutrophils and decrease inflammation in sickle cell disease [25]. However, because neutrophils are the first responders to sites of acute injury and infection, the effect of ARQ 092 on circulating neutrophils needs to be mentioned.

The frequency of liver infiltrating neutrophils was similarly reduced by all treatments, while accumulation of macrophages was additively decreased by the sorafenib-ARQ 092 combination. This is particularly important as there is growing evidence of the key-role of neutrophils and macrophages in liver fibrosis and HCC progression [26–28]. On the other hand, we did not find significant changes in intrahepatic T-cells. However, we may not be able to study particular T-cell subpopulations due to specificity of antibodies against rat.

Despite difficulties induced by the presence of a cirrhosis in our DEN-rat model of HCC, the sorafenib-ARQ 092 combination showed enhanced efficacy with a good safety profile. The dose strategy 5 days on - 9 days off for ARQ 092 was based on a toxicity study (unpublished data) with very good tolerance. Similarly, to decrease sorafenib toxicity, the concentration of 10 mg/kg was used. In fact, our pilot experiments showed that in cirrhotic rats treated with sorafenib, a dose of 20 mg/kg causes severe adverse events including an important weight loss, demonstrating the complexity of HCC treatment and the importance of using an appropriate animal model to test HCC treatment efficacy and safety.

We identified a novel treatment choice for advanced HCC with cirrhotic background. The resutls from *in vitro* and *in vivo* studies clearly illustrated the significance of targeting AKT pathways that potentiates sorafenib treatment of HCC. The safety and efficacy of this combination strategy provides the possibility of improvement of therapeutic outcomes for advanced HCC patients.

MATERIALS AND METHODS

Cell lines and *in vitro* studies

In this study, we used three different human HCC cell lines (Hep3B, HuH7, and PLC/PRF/5) and one hepatoblastoma cell line (HepG2). While Hep3B is p53-depleted, HuH-7 and PLC/PRF/5 present p53 mutations and HepG2 is a wild-type p53-expressing cell line. No mutations in AKT were detected in mentioned cell lines (COSMIC database). Expression of p-AKT was reported to be normal in Hep3B and low in HepG2, HuH-7 and PLC/PRF/5 cell lines [4]. Culture conditions are described in supporting information.

A cell viability assay was performed by MTT (3-(4, 5-Dimethylthiazol-2-yl)-2, 5-diphenyltetrazolium bromide), apoptosis was assessed by flow cytometry analysis and cell migration was studied using a wound healing assay and by cell tracking with time-lapse microscopy as described in supporting information.

Preparation of treatments

Preparation of ARQ 092 (ArQule Inc, USA), sorafenib (*in vitro* study: Bay 43-9006, Sigma-Aldrich, Germany; *in vivo* study: Nexavar®, Bayer HealthCare, Germany) and the combination treatment for *in vitro* and *in vivo* experiments is described in detail in the supporting information.

Rat model and groups of treatment

Twenty-eight 6-week-old Fischer 344 male rats (Charles River Laboratories, France) were housed in the animal facility of Plateforme de Haute Technologie Animale (Jean Roget, University of Grenoble-Alpes, France). Rats were treated weekly with intra-peritoneal injections of 50 mg/kg of diethylnitrosamine (DEN) (Sigma-Aldrich, Germany), diluted in olive oil in order to obtain a fully developed HCC on a cirrhotic liver after 14 weeks [14]. Rats were randomized in 4 different groups (n=7/group) and treated during six weeks by i) sorafenib, ii) ARQ 092, iii) combination of ARQ 092 and sorafenib or iv) rested untreated (control), as specified in Supplementary Figure 1. ARQ 092 alone, sorafenib alone and combination (Sorafenib plus ARQ 092) treatments were dispensed by oral gavage for a period of six weeks. ARQ 092 treatment was administered 5 days on 9 days off, at the dose of 15 mg/kg/day for single treatment group same as for combination group, as recommended by the ArQule Inc. Sorafenib was administered continuously at the dose of 10 mg/kg/day for single treatment group as well as for the combination group. We used 10 mg/kg/day because igher concentrations of sorafenib were demonstrated to be toxic for cirrhotic rats ([11], pilot experiments and personal communication with Bayer AG).

Nutritional state was monitored by daily weighing of rats and protein-rich nutrition was added to the standard food in every cage where a loss of weight was observed. Food was withheld for 3-4 hours before animals were sacrificed.

All animals received humane care in accordance with Guidelines on the Humane Treatment of Laboratory Animals, and experiments were approved by the animal Ethic Committee: GIN Ethics Committee n°004.

MRI studies

The imaging study was conducted on a 4.7 Tesla MR Imaging system (BioSpec 47/40 USR, Bruker Corporation, Germany). As illustrated in Supplementary Figure 1, all rats were subjected to 3 MRI scans: MRI1 was performed before randomization, MRI2 was performed after 3 weeks

of treatment and MRI3 after 6 weeks of treatment. The protocol for image acquisition and analysis is detailed in supporting information. MRI analysis was done by an investigator who was blinded of treatment allocation.

Histopathological, immunohistochemical and immunofluorescence analyses

After the third MRI scan, all rats were euthanized with vena cava blood sampling for haematologic and biochemical analyses. Each liver was weighed, the diameter of the five largest tumors was measured and the number of tumors larger than 1 mm on the surface of the liver was counted, all in a blinded manner. Tumor proliferation and apoptosis were studied by using anti-Ki67 antibody and TUNEL marker. Tissue vascularization was determined by CD34 immunostaining. Histological analysis of fibrosis was performed by sirius red-staining of collagen. Analyses were performed in collaboration with experienced pathologist (CHU-Grenoble Département d'Anatomie et de Cytologie Pathologiques). Protocols are described in supporting information.

Serum and plasma were tested for liver and kidney safety markers (albumin, ALP, ALT, AST, prothrombin time, total bilirubin, cholesterol, GGT, glucose, creatinine, Table 1) by Charles River Clinical pathology Services using Olympus and Stago instruments. Liver triglycerides were measured as described previously [11].

Pathways analysis

Western blot analysis of pAKT$^{(Ser473)}$/AKT and pERK/ERK, and real-time polymerase chain reaction (qPCR) analyses were performed on tumor and non-tumor tissues. Protocols are described in the supporting information.

Flow cytometric analysis

Cells were recovered from liver tissue by mechanical disruption as described previously [29] and whole blood samples were used in case of blood analyses. Cells without any stimulation were immune-stained for flow cytometric analysis. The protocol is described in the supporting information.

Statistical analysis

All comparisons of means were calculated by using ANOVA tests with Tukey HSD correction for multiple means comparisons, and independent T-tests only when two means were compared. Data are presented as mean values ± standard error mean (SEM). Statistical analyses were performed using Prism 6 (GraphPad Software Inc., CA, USA).

Abbreviations

HCC: Hepatocellular carcinoma; VEGF-R: vascular endothelial growth factor receptor; PDGF-R: platelet-derived growth factor receptor; PI3K: phosphatidylinositol-3 kinases; AKT: Protein kinase B, PKB; mTOR: mechanistic target of rapamycin; mTORC1: mTOR complex 1; MTT: 3-(4, 5-dimethylthiazolyl-2)-2, 5-diphenyltetrazolium bromide; DEN: diethylnitrosamine; MRI: Magnetic Resonance Imaging; pAKT: phosphorylated AKT; ERK: extracellular-signal-regulated kinase; pERK: phosphorylated ERK; qPCR: real-time polymerase chain reaction; SEM: standard error mean; IC50: inhibitory concentration 50; CI: combination index; ALP: Alkaline Phosphatase; GGT: Gamma glutamyl transpeptidase; AFP: Alpha fetoprotein; HIF-1: hypoxia-inducible factor; α-SMA: alpha smooth muscle actin; TGFβ1: Transforming growth factor β1; TIMP-1: tissue inhibitor of metalloproteinases-1; MMP: matrix metalloproteinase; S6K1: Ribosomal protein S6 kinase.

Author contributions

Conception and design of the study: ZMJ, AZK, GSR, GA, YY, BS, PH, PM, NS, PH, TD;

Acquisition of data: ZMJ, AZK, KK, STAP;

Analysis and interpretation of data: ZMJ, AZK, KK, GSR, NS, TD;

Drafting the article: ZMJ, TD;

Critical revising the article for important intellectual content: ZMJ, GSR, YY, TD;

Approval of the final version: ZMJ, AZK, KK, STAP, GSR, GA, YY, BS, PM, NS, PH, TD.

ACKNOWLEDGMENTS

We are grateful to CHU-Grenoble Département d'Anatomie et de Cytologie Pathologiques for help with histology. We thank Animal platform, Grenoble Institute of Neurosciences, Grenoble, France for the quality of their animal care. We thank Vasile Stupar (MRI platform, Grenoble Institute of Neurosciences, Grenoble, France) for his help in the realization of MRI acquisitions.

CONFLICTS OF INTEREST

GA, YY, BS are employees of ArQule Inc, USA.

FUNDING

Work was funded by la Ligue contre le Cancer CD63 (2016-R16145CC), AZK was supported by The Scientific and Technological Research Council of Turkey (TUBITAK 2214B).

REFERENCES

1. Torre LA, Bray F, Siegel RL, Ferlay J, Lortet-Tieulent J, Jemal A. Global cancer statistics, 2012. CA Cancer J Clin. 2015; 65:87-108. https://doi.org/10.3322/caac.21262.
2. Llovet JM, Ricci S, Mazzaferro V, Hilgard P, Gane E, Blanc JF, de Oliveira AC, Santoro A, Raoul JL, Forner A, Schwartz M, Porta C, Zeuzem S, et al, and SHARP Investigators Study Group. Sorafenib in advanced hepatocellular carcinoma. N Engl J Med. 2008; 359:378-90. https://doi.org/10.1056/NEJMoa0708857.
3. Matter MS, Decaens T, Andersen JB, Thorgeirsson SS. Targeting the mTOR pathway in hepatocellular carcinoma: current state and future trends. J Hepatol. 2014; 60:855-65. https://doi.org/10.1016/j.jhep.2013.11.031.
4. Kunter I, Erdal E, Nart D, Yilmaz F, Karademir S, Sagol O, Atabey N. Active form of AKT controls cell proliferation and response to apoptosis in hepatocellular carcinoma. Oncol Rep. 2014; 31:573-80. https://doi.org/10.3892/or.2013.2932.
5. Chen KF, Chen HL, Tai WT, Feng WC, Hsu CH, Chen PJ, Cheng AL. Activation of phosphatidylinositol 3-kinase/Akt signaling pathway mediates acquired resistance to sorafenib in hepatocellular carcinoma cells. J Pharmacol Exp Ther. 2011; 337:155-61. https://doi.org/10.1124/jpet.110.175786.
6. Zhai B, Hu F, Yan H, Zhao D, Jin X, Fang T, Pan S, Sun X, Xu L. Bufalin Reverses Resistance to Sorafenib by Inhibiting Akt Activation in Hepatocellular Carcinoma: The Role of Endoplasmic Reticulum Stress. PLoS One. 2015; 10:e0138485. https://doi.org/10.1371/journal.pone.0138485.
7. Hanada M, Feng J, Hemmings BA. Structure, regulation and function of PKB/AKT—a major therapeutic target. Biochim Biophys Acta. 2004; 1697:3-16. https://doi.org/10.1016/j.bbapap.2003.11.009.
8. Koeberle D, Dufour JF, Demeter G, Li Q, Ribi K, Samaras P, Saletti P, Roth AD, Horber D, Buehlmann M, Wagner AD, Montemurro M, Lakatos G, et al, and Swiss Group for Clinical Cancer Research (SAKK). Sorafenib with or without everolimus in patients with advanced hepatocellular carcinoma (HCC): a randomized multicenter, multinational phase II trial (SAKK 77/08 and SASL 29). Ann Oncol. 2016; 27:856-61. https://doi.org/10.1093/annonc/mdw054.
9. Zhu AX, Kudo M, Assenat E, Cattan S, Kang YK, Lim HY, Poon RT, Blanc JF, Vogel A, Chen CL, Dorval E, Peck-Radosavljevic M, Santoro A, et al. Effect of everolimus on survival in advanced hepatocellular carcinoma after failure of sorafenib: the EVOLVE-1 randomized clinical trial. JAMA. 2014; 312:57–67. https://doi.org/10.1001/jama.2014.7189.
10. Breuleux M, Klopfenstein M, Stephan C, Doughty CA, Barys L, Maira SM, Kwiatkowski D, Lane HA. Increased AKT S473 phosphorylation after mTORC1 inhibition is rictor dependent and does not predict tumor cell response to PI3K/mTOR inhibition. Mol Cancer Ther. 2009; 8:742-53. https://doi.org/10.1158/1535-7163.mct-08-0668.
11. Roth GS, Macek Jilkova Z, Zeybek Kuyucu A, Kurma K, Ahmad Pour ST, Abbadessa G, Yu Y, Busser B, Marche PN, Leroy V, Decaens T. Efficacy of AKT inhibitor ARQ 092 compared with sorafenib in a cirrhotic rat model with hepatocellular carcinoma. Mol Cancer Ther. 2017; 16:2157–65. https://doi.org/10.1158/1535-7163.MCT-16-0602-T.
12. Rodon J, Dienstmann R, Serra V, Tabernero J. Development of PI3K inhibitors: lessons learned from early clinical trials. Nat Rev Clin Oncol. 2013; 10:143-53. https://doi.org/10.1038/nrclinonc.2013.10.
13. Zhai B, Hu F, Jiang X, Xu J, Zhao D, Liu B, Pan S, Dong X, Tan G, Wei Z, Qiao H, Jiang H, Sun X. Inhibition of Akt reverses the acquired resistance to sorafenib by switching protective autophagy to autophagic cell death in hepatocellular carcinoma. Mol Cancer Ther. 2014; 13:1589-98. https://doi.org/10.1158/1535-7163.mct-13-1043.
14. Schiffer E, Housset C, Cacheux W, Wendum D, Desbois-Mouthon C, Rey C, Clergue F, Poupon R, Barbu V, Rosmorduc O. Gefitinib, an EGFR inhibitor, prevents hepatocellular carcinoma development in the rat liver with cirrhosis. Hepatology. 2005; 41:307-14. https://doi.org/10.1002/hep.20538.
15. Lee TK, Cheung VC, Lu P, Lau EY, Ma S, Tang KH, Tong M, Lo J, Ng IO. Blockade of CD47-mediated cathepsin S/protease-activated receptor 2 signaling provides a therapeutic target for hepatocellular carcinoma. Hepatology. 2014; 60:179-91. https://doi.org/10.1002/hep.27070.
16. Lo J, Lau EY, Ching RH, Cheng BY, Ma MK, Ng IO, Lee TK. Nuclear factor kappa B-mediated CD47 up-regulation promotes sorafenib resistance and its blockade synergizes the effect of sorafenib in hepatocellular carcinoma in mice. Hepatology. 2015; 62:534-45. https://doi.org/10.1002/hep.27859.
17. Schulze K, Imbeaud S, Letouze E, Alexandrov LB, Calderaro J, Rebouissou S, Couchy G, Meiller C, Shinde J, Soysouvanh F, Calatayud AL, Pinyol R, Pelletier L, et al. Exome sequencing of hepatocellular carcinomas identifies new mutational signatures and potential therapeutic targets. Nat Genet. 2015; 47:505-11. https://doi.org/10.1038/ng.3252.
18. Friemel J, Rechsteiner M, Frick L, Bohm F, Struckmann K, Egger M, Moch H, Heikenwalder M, Weber A. Intratumor heterogeneity in hepatocellular carcinoma. Clin Cancer Res. 2015; 21:1951-61. https://doi.org/10.1158/1078-0432.ccr-14-0122.
19. Ding XX, Zhu QG, Zhang SM, Guan L, Li T, Zhang L, Wang SY, Ren WL, Chen XM, Zhao J, Lin S, Liu ZZ, Bai YX, et al. Precision medicine for hepatocellular carcinoma: driver mutations and targeted therapy. Oncotarget. 2017; 8:55715-30. https://doi.org/10.18632/oncotarget.18382.
20. Thabut D, Shah V. Intrahepatic angiogenesis and sinusoidal remodeling in chronic liver disease: new targets for the

treatment of portal hypertension? J Hepatol. 2010; 53:976-80. https://doi.org/10.1016/j.jhep.2010.07.004.

21. Thabut D, Routray C, Lomberk G, Shergill U, Glaser K, Huebert R, Patel L, Masyuk T, Blechacz B, Vercnocke A, Ritman E, Ehman R, Urrutia R, et al. Complementary vascular and matrix regulatory pathways underlie the beneficial mechanism of action of sorafenib in liver fibrosis. Hepatology. 2011; 54:573-85. https://doi.org/10.1002/hep.24427.

22. Qu K, Huang Z, Lin T, Liu S, Chang H, Yan Z, Zhang H, Liu C. New Insight into the Anti-liver Fibrosis Effect of Multitargeted Tyrosine Kinase Inhibitors: From Molecular Target to Clinical Trials. Front Pharmacol. 2016; 6:300. https://doi.org/10.3389/fphar.2015.00300.

23. Xiao WK, Chen D, Li SQ, Fu SJ, Peng BG, Liang LJ. Prognostic significance of neutrophil-lymphocyte ratio in hepatocellular carcinoma: a meta-analysis. BMC Cancer. 2014; 14:117. https://doi.org/10.1186/1471-2407-14-117.

24. Xue TC, Zhang L, Xie XY, Ge NL, Li LX, Zhang BH, Ye SL, Ren ZG. Prognostic significance of the neutrophil-to-lymphocyte ratio in primary liver cancer: a meta-analysis. PLoS One. 2014; 9:e96072. https://doi.org/10.1371/journal.pone.0096072.

25. Kim K, Li J, Barazia A, Tseng A, Youn SW, Abbadessa G, Yu Y, Schwartz B, Andrews RK, Gordeuk VR, Cho J. ARQ 092, an orally-available, selective AKT inhibitor, attenuates neutrophil-platelet interactions in sickle cell disease. Haematologica. 2017; 102:246-59. https://doi.org/10.3324/haematol.2016.151159.

26. Zhou SL, Zhou ZJ, Hu ZQ, Huang XW, Wang Z, Chen EB, Fan J, Cao Y, Dai Z, Zhou J. Tumor-Associated Neutrophils Recruit Macrophages and T-Regulatory Cells to Promote Progression of Hepatocellular Carcinoma and Resistance to Sorafenib. Gastroenterology. 2016; 150:1646–1658.e17. https://doi.org/10.1053/j.gastro.2016.02.040.

27. Wilson CL, Jurk D, Fullard N, Banks P, Page A, Luli S, Elsharkawy AM, Gieling RG, Chakraborty JB, Fox C, Richardson C, Callaghan K, Blair GE, et al. NFkappaB1 is a suppressor of neutrophil-driven hepatocellular carcinoma. Nat Commun. 2015; 6:6818. https://doi.org/10.1038/ncomms7818.

28. Macek Jilkova Z, Afzal S, Marche H, Decaens T, Sturm N, Jouvin-Marche E, Huard B, Marche PN. Progression of fibrosis in patients with chronic viral hepatitis is associated with IL-17(+) neutrophils. Liver Int. 2016; 36:1116-24. https://doi.org/10.1111/liv.13060.

29. Macek Jilkova Z, Decaens T, Marlu A, Marche H, Jouvin-Marche E, Marche PN. Sex Differences in Spontaneous Degranulation Activity of Intrahepatic Natural Killer Cells during Chronic Hepatitis B: Association with Estradiol Levels. Mediators Inflamm. 2017; 2017:3214917. https://doi.org/10.1155/2017/3214917.

Published OnlineFirst May 31, 2017; DOI: 10.1158/1535-7163.MCT-16-0602-T

Small Molecule Therapeutics

Molecular Cancer Therapeutics

Efficacy of AKT Inhibitor ARQ 092 Compared with Sorafenib in a Cirrhotic Rat Model with Hepatocellular Carcinoma

Gaël S. Roth[1,2,3], Zuzana Macek Jilkova[1,2], Ayca Zeybek Kuyucu[1,2], Keerthi Kurma[1,2], Séyédéh Tayébéh Ahmad Pour[1,2], Giovanni Abbadessa[4], Yi Yu[4], Benoit Busser[1,2,5], Patrice N. Marche[1,2], Vincent Leroy[1,2,3], and Thomas Decaens[1,2,3]

Abstract

Hepatocellular carcinoma (HCC) is the second most common cause of cancer-related mortality worldwide. The AKT pathway has been found activated in 50% of HCC cases, making it a promising target. Therefore, we assess efficacy of the allosteric AKT inhibitor ARQ 092 compared with untreated control and standard treatment, sorafenib, *in vitro* and *in vivo*. ARQ 092 blocked phosphorylation of AKT *in vitro* and strongly inhibited cell growth with significantly higher potency than sorafenib. Similarly, apoptosis and cell migration were strongly reduced by ARQ 092 *in vitro*. To mimic human advanced HCC, we used a diethylnitrosamine-induced cirrhotic rat model with fully developed HCC. MRI analyses showed that ARQ 092 significantly reduced overall tumor size. Furthermore, number of tumors was decreased by ARQ 092, which was associated with increased apoptosis and decreased proliferation. Tumor contrast enhancement was significantly decreased in the ARQ 092 group. Moreover, on tumor tissue sections, we observed a vascular normalization and a significant decrease in fibrosis in the surrounding liver of animals treated with ARQ 092. Finally, pAKT/AKT levels in ARQ 092–treated tumors were reduced, followed by downregulation of actors of AKT downstream signaling pathway: pmTOR, pPRAS40, pPLCγ1, and pS6K1. In conclusion, we demonstrated that ARQ 092 blocks AKT phosphorylation *in vitro* and *in vivo*. In the HCC-rat model, ARQ 092 was well tolerated, showed antifibrotic effect, and had stronger antitumor effect than sorafenib. Our results confirm the importance of targeting AKT in HCC. *Mol Cancer Ther; 16(10); 2157–65. ©2017 AACR.*

Introduction

Hepatocellular carcinoma (HCC) is the fifth most common cancer and the second cause of cancer-related death worldwide with 600,000 deaths per year (1). Liver cirrhosis, the latest stage of liver fibrosis, underlies HCC in approximately 90% of cases. The most frequent causes of liver cirrhosis are hepatitis B and C, chronic alcohol consumption, and nonalcoholic steato-hepatitis. Only 30% of the cases are accessible for curative treatment. In advanced stage, the only approved drug for HCC is sorafenib, a multikinase inhibitor targeting the vascular endothelial growth factor receptor, the platelet-derived growth factor receptor, and Raf. However, its efficacy is modest with a median overall survival of 10.7 versus 7.9 months with placebo in the pivotal phase III trial (2). Therefore, new treatment options with improved therapeutic efficacy are urgently needed.

Immunohistochemical and genomic studies indicate that the PI3K/AKT/mTOR signaling pathway is activated in approximately 50% of patients with HCC and cirrhosis of any cause (3–5). This pathway is divided into two unique complexes with distinct regulations and activities: mTOR complex 1 (mTORC1) and mTOR complex 2 (mTORC2). The serine/threonine kinase AKT is an important upregulator of mTORC1, which is involved in diverse cellular functions such as lipogenesis, energy metabolism, and lysosome biogenesis, and is a key actor in the control of protein synthesis (3, 4, 6).

This underlines that AKT is an essential player in liver tumorigenesis and progression, therefore making it a potential target in the management of HCC. Thus, we postulate that therapy with an AKT inhibitor capable of inhibiting the PI(3)K/AKT/mTOR pathway will be effective in treating fully developed HCC.

However, in order to identify specific adverse effects that could be related to the background of cirrhosis, inhibition of AKT should be preclinically tested in an appropriate animal model. Indeed, sorafenib antitumor efficacy is tested in xenograft mice models in more than 90% of cases which are immunocompromised animal with a normal liver function (7). As HCC develops on a cirrhotic liver with a modified vascularization, a severe fibrosis, and a liver deficiency which can influence drug metabolism, xenograft mice model does not reproduce the most frequent human HCC scenario. One of the models that most faithfully reproduces human HCC physiopathology is the

[1]Université Grenoble Alpes, Grenoble, France. [2]Institute for Advanced Biosciences - Inserm U1209/CNRS UMR 5309/Université de Grenoble-Alpes, Grenoble, France. [3]Clinique Universitaire d'Hépato-gastroentérologie, Pôle Digidune, CHU Grenoble Alpes, Grenoble, France. [4]ArQule Inc., Woburn, MA. [5]Département de biochimie, toxicologie et pharmacologie, Pôle de biologie, CHU Grenoble Alpes, Grenoble, France.

Note: Supplementary data for this article are available at Molecular Cancer Therapeutics Online (http://mct.aacrjournals.org/).

G.S. Roth and Z.M. Jilkova equally contributed to this article.

Corresponding Author: Thomas Decaens, CHU Grenoble Alpes, CS 10217, 38000 Grenoble, France. Phone: 33476766739; Fax: 33476765179; E-mail: tdecaens@chu-grenoble.fr

doi: 10.1158/1535-7163.MCT-16-0602-T

Published OnlineFirst May 31, 2017; DOI: 10.1158/1535-7163.MCT-16-0602-T

diethylnitrosamine (DEN)-injured–induced rats model which develops an extensive fibrosis, leading to a compensated cirrhosis with a multifocal HCC after 14 weeks of induction (8).

Therefore, in this study, we tested safety and efficacy of a new allosteric AKT inhibitor, ARQ 092 (9), in a DEN-induced cirrhotic rat model with HCC and compared it with sorafenib-treated rats and untreated rats. In addition, we tested the effect of ARQ 092 on four different human cell lines.

Materials and Methods

Cell lines

Three different human HCC cell lines [Hep3B, Huh7, and phospholipase C (PLC)/PRF/5], one human hepatoblastoma cell line [HepG2; provided by Snorri S. Thorgeirsson (NCI, NHI, Bethesda, MDA) without authentication by the authors], and one rat HCC cell line (HR4) were used in this study [provided by Istvan Blazsek (INSERM U1193, Villejuif, France) without authentication by the authors]. HepG2 is expressing normal p53, while Hep3B is p53-depleted and PLC/PRF/5 and HuH-7 present p53 mutations. Based on COSMIC database, no mutations in AKT were detected in mentioned cell lines. Expression of p-AKT was reported to be normal in Hep3B, whereas it was decreased in HepG2, PLC/PRF/5, and HuH-7 cell lines (5). Rat HR4 cell line was obtained from DEN-induced rat model of HCC (10). All cell lines were tested for mycoplasma infection every 2 weeks by using the MycoAlert Mycoplasma Detection Kit (Lonza). Culture conditions are described in the Supplementary Information.

Preparation of treatments

Preparation of ARQ 092 (ArQule Inc.) and sorafenib (*in vitro* study: Bay 43-9006, Sigma-Aldrich; *in vivo* study: Nexavar, Bayer HealthCare) solutions for *in vitro* and *in vivo* experiments is described in the Supplementary Information.

In vitro studies

Cell viability assay was performed by (3-(4,5-Dimethylthiazol-2-yl)-2,5-diphenyltetrazolium bromide) (MTT), apoptosis analysis was assessed by flow cytometry analysis, and cell migration was studied by wound-healing assay. All *in vitro* experiments were realized in 4 different human liver cancer cell lines and in one rat cell line, and protocols are detailed in the Supplementary Information.

Rat model and groups of treatment

Twenty-six 8-week-old Fischer 344 male rats (Charles River Laboratories) were housed in the animal facility of the Grenoble Institute of Neuroscience (INSERM, University of Grenoble-Alpes, France). They were treated weekly with intraperitoneal injections of 50 mg/kg DEN (Sigma-Aldrich, Germany), diluted in pure olive oil in order to obtain a fully developed HCC on a cirrhotic liver after 14 weeks as previously described (8, 11).

After 14 weeks, rats were randomized in 3 different groups as follows: 10 in the ARQ 092 group, 10 in the sorafenib group, and 6 in the control group. Both treatments were dispensed by daily oral gavage during 6 weeks. ARQ 092 was administered for 7 days every other week (for a total of 3 weeks of treatment), at a dose of 15 mg/kg/day as recommended by ArQule Inc., whereas sorafenib was administered every day at a dose of 10 mg/kg/day.

Nutritional state was monitored by daily weighing of rats, and treatment doses were adapted accordingly. Protein-rich nutrition was added to the standard food in every cage where a loss of weight was observed.

All animals received humane care in accordance with Guidelines on the Humane Treatment of Laboratory Animals, and experiments were approved by the animal Ethic Committee.

MRI studies

Imaging study was conducted on a 4.7 Tesla MR Imaging system (BioSpec 47/40 USR, Bruker Corporation) in the Grenoble MRI facility IRMaGE.

All rats were subjected to 3 MRI scans: MRI1 was performed before randomization, MRI2 and MRI3 were respectively done after 3 and 6 weeks of treatment. Morphological analyses were performed on all MRIs, and perfusion study was done on MRI1 and MRI3 scans, both with blinded outcome assessment. Protocols for image acquisition and analysis are detailed in the Supplementary Information.

Histopathologic, immunohistochemical, and immunofluorescence analyses

After the third MRI scan, all rats were euthanized with intracardiac blood sampling for hematologic and biochemical analyses. Each liver was weighed, the number of tumors larger than 1 mm on the surface of the liver was counted, and the diameter of the five largest tumors was measured in a blinded manner. The sum of these five diameters was calculated in order to obtain a histopathologic estimation of the tumor volume.

Histologic analysis of fibrosis and steatosis was performed with collagen staining by sirius red, and lipid staining with Oil Red O staining, respectively.

Tumor proliferation, apoptosis, and tissue vascularization were studied by using anti-Ki67 antibody, TUNEL marker, and anti-CD34 antibody. Protocols are described in the Supplementary Information.

Serum and plasma were taken in order to test biological safety and efficacy parameters as detailed in the Supplementary Information.

Measurement of liver triglycerides

Frozen liver fragments (~50 mg) were digested in 0.15 mL of 3 mol/L alcoholic potassium hydroxide (70°C, 2 hours), diluted 7 times in distilled water. Amount of liver triglycerides was measured by a Triglycerides kit (Erba Mannheim, Czech Republic), and samples' absorbance was measured by spectroscopy at 505 nm.

Pathways analysis

Western blot analysis of $pAKT^{(Ser473)}$/AKT and pERK/ERK, and the real-time qPCR analysis of Ras and AKT pathways downstream actors were performed on tumor and nontumor tissues of each group. The Phospho-Kinase Array Kit (Proteome Profiler Antibody Array; R&D Systems) was used according to the manufacturer's instructions. Experimental protocols are described in the Supplementary Information.

Statistical analysis

All comparisons of means were calculated by using ANOVA tests with Tukey HSD correction for multiple means comparisons, and independent *t* tests only when two means were compared. A P value of <0.05 was regarded as statistically significant, and data are presented as mean values ± SEM.

Published OnlineFirst May 31, 2017; DOI: 10.1158/1535-7163.MCT-16-0602-T

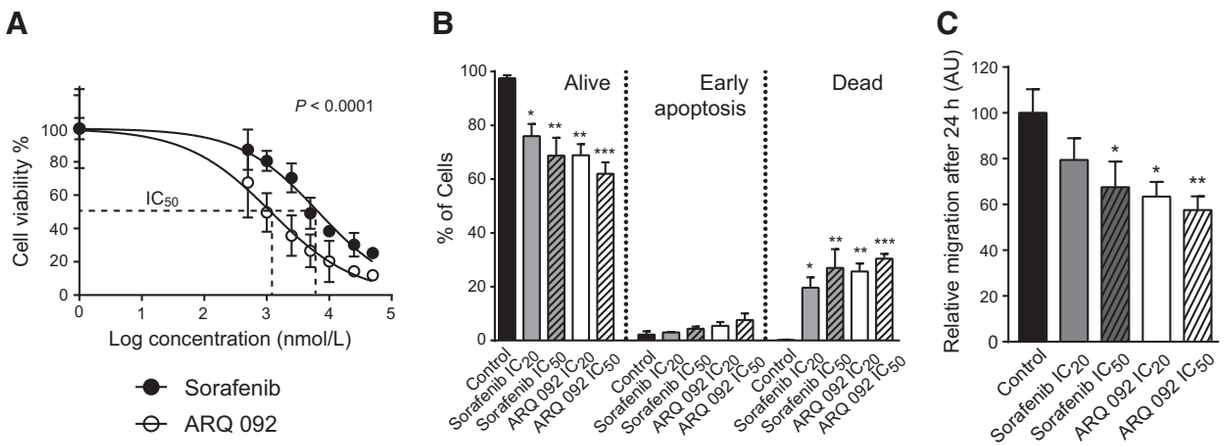

Figure 1.

Effect of ARQ 092 and sorafenib on Hep3B cell viability, apoptosis, and migration. **A,** MTT assay on Hep3B cell line after 48 hours of treatment showing significant difference in IC_{50} of ARQ 092 and sorafenib ($P < 0.0001$). **B,** Dose-dependent effects of ARQ 092 and sorafenib on apoptosis in Hep3B after 48 hours of exposure. **C,** The quantification of migration (decrease of width of the wound after first 24 hours) in Hep3B. Control was set as 100%; values are mean ± SEM from three independent experiments performed in triplicates (**A**) and in duplicates (**B**, **C**). *, $P \leq 0.05$; **, $P \leq 0.01$; and ***, $P \leq 0.001$ vs. control.

Statistical analyses were performed using IBM SPSS Statistics software, version 20.0 (IBM Corp.), and Prism 6 (GraphPad Software Inc.).

Results

In vitro

MTT assays showed a drastic decrease in proliferation rate for Hep3B (Fig. 1A), HepG2, Huh-7, PLC/PRF, and HR4 cell lines after ARQ 092 treatment. IC_{50} were 2 to 6 times lower when compared with sorafenib, suggesting that ARQ 092 is more potent than sorafenib. The calculated IC_{20} and IC_{50} values are summarized in Supplementary Table S1.

Next, we examined whether growth arrest due to ARQ 092 treatment was associated with enhanced apoptosis. Compared with control cells, we observed significant dose-dependent decrease of cell viability in all tested HCC cell lines treated with ARQ 092 or sorafenib (Fig. 1B and Supplementary Fig. S1).

We next investigated whether ARQ 092 affected migratory behavior of human HCC cell lines by wound-healing assay. After 24 hours, both IC_{20} and IC_{50} of ARQ 092 strongly reduced migration of Hep3B, while sorafenib had significant effect at IC_{50} only (Fig. 1C). In other cell lines, ARQ 092 decreased migration similarly to sorafenib (Supplementary Fig. S2A). Although control Hep3B cells almost recovered the wound by 72 hours, ARQ 092–treated cells had their wound area unhealed (Supplementary Fig. S2B). Similarly, ARQ 092 treatment decreased cell velocity (Supplementary Fig. S3A) and strongly reduced cell invasion (Supplementary Fig. S3B).

These results demonstrate that ARQ 092 suppresses proliferation and migration and promotes apoptosis in all tested cell lines.

In vivo

At the end of the study, the mean weight loss was 5.8% ± 5.5% in the sorafenib group and 0.8% ± 0.6% in the ARQ 092

Table 1. Clinical and biological analyses

		Control ($n = 6$)	Sorafenib ($n = 10$)	ARQ 092 ($n = 10$)	ANOVA *P* values (Tukey HSD)
Mean Δ body weight (% of initial weight)		+5.9 ± 3.1	−5.8 ± 5.5	−0.8 ± 0.6	*0.164*
Liver tissue	Intrahepatic TG (g/L)	34.8 ± 6.9	28.0 ± 3.0	30.2 ± 1.9	*0.467*
	Oil Red O (%)	10.9 ± 4.4	6.5 ± 1.9	11.2 ± 1.8	*0.355*
Blood samples	Albumin (g/dL)	3.7 ± 0.2	3.7 ± 0.1	4.1 ± 0.3$^{*, \#\#}$	*0.006*
	AST (IU/L)	320 ± 29	325 ± 46	357 ± 104	*0.250*
	ALT (IU/L)	303 ± 28	206 ± 28	269 ± 81	*0.171*
	ALP (IU/L)	306 ± 6	212 ± 3*	230 ± 11	*0.023*
	GGT (IU/L)	147 ± 15	47 ± 8	82 ± 26	*0.087*
	Glucose (mg/dL)	131 ± 3	142 ± 7	153 ± 4	*0.086*
	Cholesterol (g/L)	1.19 ± 0.01	0.99 ± 0.06	1.20 ± 0.07	*0.071*
	TG (g/L)	1.19 ± 0.04	1.31 ± 0.15	1.30 ± 0.21	*0.927*
	Total bilirubin (mg/L)	4.09 ± 0.58	1.46 ± 0.19**	1.75 ± 0.18**	*0.0003*
	Direct bilirubin (mg/L)	2.05 ± 0.29	0.58 ± 0.00***	0.58 ± 0.00***	*<0.0001*
	Prothrombin time (s)	16.3 ± 0.9	18.7 ± 4.4	16.7 ± 0.5	*0.301*
	AFP (ng/mL)	0.85 ± 0.15	0.44 ± 0.12	0.33 ± 0.09*	*0.041*

NOTE: Values are mean ± SEM, significant difference compared with control. *, $P < 0.05$; **, $P < 0.001$; ***, $P < 0.0001$.
Significant difference between ARQ 092 and sorafenib; $^{\#\#}$, $P < 0.01$.
Abbreviations: ALP, alkaline phosphatase; ALT, alanine aminotransferase; AST, aspartate aminotransferase; GGT, gamma-glutamyl transpeptidase.

Published OnlineFirst May 31, 2017; DOI: 10.1158/1535-7163.MCT-16-0602-T

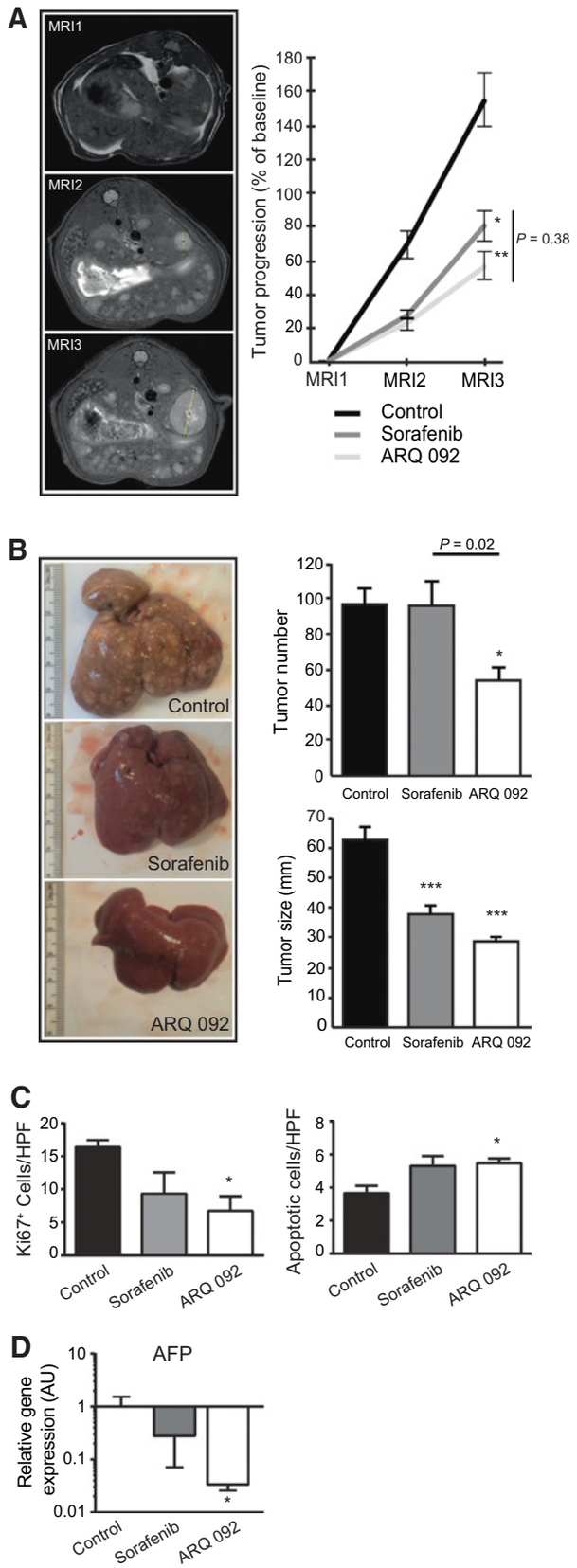

group compared with a gain of 5.9% ± 3.1% in the control group ($P = 0.164$; Table 1). Blood sample analyses (Table 1) revealed better liver function in the ARQ 092 and sorafenib groups compared with control, with a significantly lower total bilirubin level (ARQ 092: $P = 0.0007$, sorafenib: $P = 0.0002$). Albumin level was significantly higher in ARQ 092 compared with nontreated rats ($P = 0.0170$) and sorafenib group ($P = 0.0098$). There was no statistical difference in transaminases, alkaline phosphatase and gamma-glutamyl transpeptidase levels, but serum levels of AFP were significantly decreased by ARQ 092 treatment compared with control ($P = 0.0328$). Glucose, cholesterol, and triglyceride blood concentrations were similar to the control group. Assessment of triglycerides in liver and Oil Red O staining did not show any significant difference between groups ($P = 0.467$ and 0.355; Table 1; Supplementary Fig. S4A). Therefore, our results showed that ARQ 092 treatment does not interfere with lipid metabolism and improves liver function.

Antitumor effect

On MRI1 ($n = 26$), tumor sizes were comparable between groups with 21.3 ± 1.7 mm, 18.0 ± 1.2 mm, and 20.6 ± 2.0 mm in the control, sorafenib, and ARQ 092 groups ($P = 0.424$), respectively. As illustrated by Fig. 2A, on MRI2 ($n = 24$), tumor progression was significantly reduced in the sorafenib (+28.5% ± 3.0%; $P < 0.0001$) and ARQ 092 (+20.9% ± 3.8%; $P < 0.00001$) groups compared with control (+69.6% ± 9.0%). No statistical difference was found between sorafenib and ARQ 092 groups ($P = 0.45$). On MRI3 ($n = 22$), tumor progression rate was +57.0% ± 8.1% in the ARQ 092 group compared with +80.2% ± 9.3% in sorafenib group ($P = 0.273$) and +155.3% ± 16.0% in the control group ($P < 0.0001$; Fig. 2A).

These observations were further confirmed by macroscopic examination of the liver (Fig. 2B), which revealed a tumor size of 28.8 ± 1.8 mm in the ARQ 092 group compared with 37.9 ± 3.1 mm in the sorafenib group ($P = 0.092$) and 62.7 ± 4.4 mm in the control group ($P < 0.0001$).

Rats from the group treated with ARQ 092 also displayed a significantly lower number of tumors (53.9 ± 7.0 tumors) when compared with sorafenib-treated animals (96.3 ± 13.5 tumors, $P = 0.021$) and controls (96.8 ± 9.4 tumors, $P = 0.031$).

Expert pathologic analysis with hematoxylin and eosin staining of liver section confirmed that tumors were HCC with several degree of tumor differentiation (Supplementary Fig. S3B).

Figure 2.
Effect of ARQ 092 and sorafenib on tumor progression and proliferation. **A,** MRI morphologic analysis with representative T2 turboRARE images and tumor progression assessment by comparison of tumor size on MRI1, 2, and 3 in the control, sorafenib, and ARQ 092 groups (MRI1 was considered as the baseline in each group, and MRI2 and 3 were expressed as a percentage of MRI1). **B,** Macroscopic examination of livers with assessment of tumor number (top bar chart) and tumor size (sum of diameter of the five largest tumors, bottom bar chart) at the surface of livers. **C,** Immunohistochemistry analysis of tumor proliferation (left bar chart) and apoptosis induction (right bar chart) with Ki67 and TUNEL immunostainings, respectively. **D,** qPCR analysis of AFP gene expression in tumor liver samples. Control was set as 1; values are mean ± SEM. Comparison of mean was done by ANOVA test, with Tukey correction P value of groups compared with control is represented as follows: *, $P < 0.05$; **, $P < 0.01$; ***, $P < 0.001$; and ****, $P < 0.0001$.

Published OnlineFirst May 31, 2017; DOI: 10.1158/1535-7163.MCT-16-0602-T

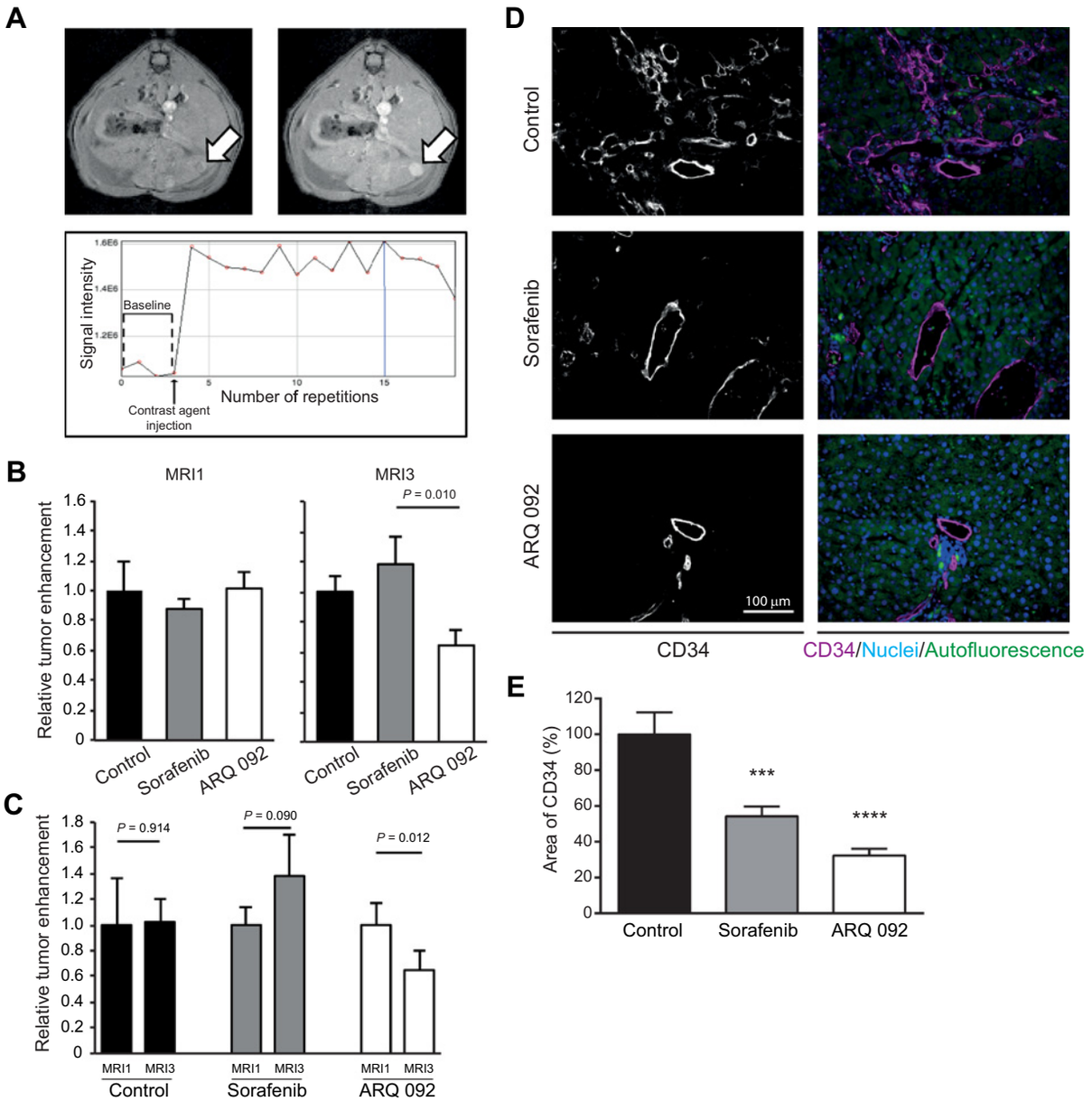

Figure 3.

Effect of ARQ 092 and sorafenib on tumor vascularization. **A,** DCE MRI pictures of a control rat before (left picture) and after (right picture) injection of contrast agent with a typical enhancement curve obtained by analysis of signal intensity on the tumor area illustrated by previous pictures. **B,** Comparison of MRI1 (left) and MRI3 (right) tumor enhancement of ARQ 092, sorafenib, and control groups. Control group was set as 1, and ARQ 092 and sorafenib groups are expressed as a percentage of control. **C,** Comparison of MRI1 and 3 was realized in each group to study the effect of sorafenib and ARQ 092 on tumor enhancement. MRI1 was set as 1, and MRI3 is expressed as a percentage of MRI1. **D,** Representative pictures of CD34 immunofluorescence staining of liver tissue. **E,** Quantification of CD34 immunostaining. Control was set as 100, and values are mean ± SEM. ***, $P < 0.001$ and ****, $P < 0.0001$ vs. control.

Ki67 and TUNEL immunostaining (Fig. 2C; Supplementary Fig. S4C) showed that only ARQ 092 significantly decreased proliferation (41.1% ± 13.3% of control, $P = 0.042$) and induced apoptosis (148.6% ± 7.7% of control, $P = 0.045$), whereas sorafenib showed no statistical significance concerning these parameters (Ki67: 56.9% ± 19.6% of control, $P = 0.160$; TUNEL: 144.2% ± 16.5% of control, $P = 0.072$).

qPCR analyses of alpha fetoprotein (AFP) expression (Fig. 2D) revealed that only ARQ 092 significantly reduced expression by 96.6% ± 0.8% compared with control ($P = 0.038$), whereas sorafenib reduced AFP expression by 72.4% ± 20.5% without statistical difference ($P = 0.163$). Similarly, in ARQ 092–treated rats, serum levels of AFP were significantly decreased by 61% of control ($P = 0.041$; Table 1).

Published OnlineFirst May 31, 2017; DOI: 10.1158/1535-7163.MCT-16-0602-T

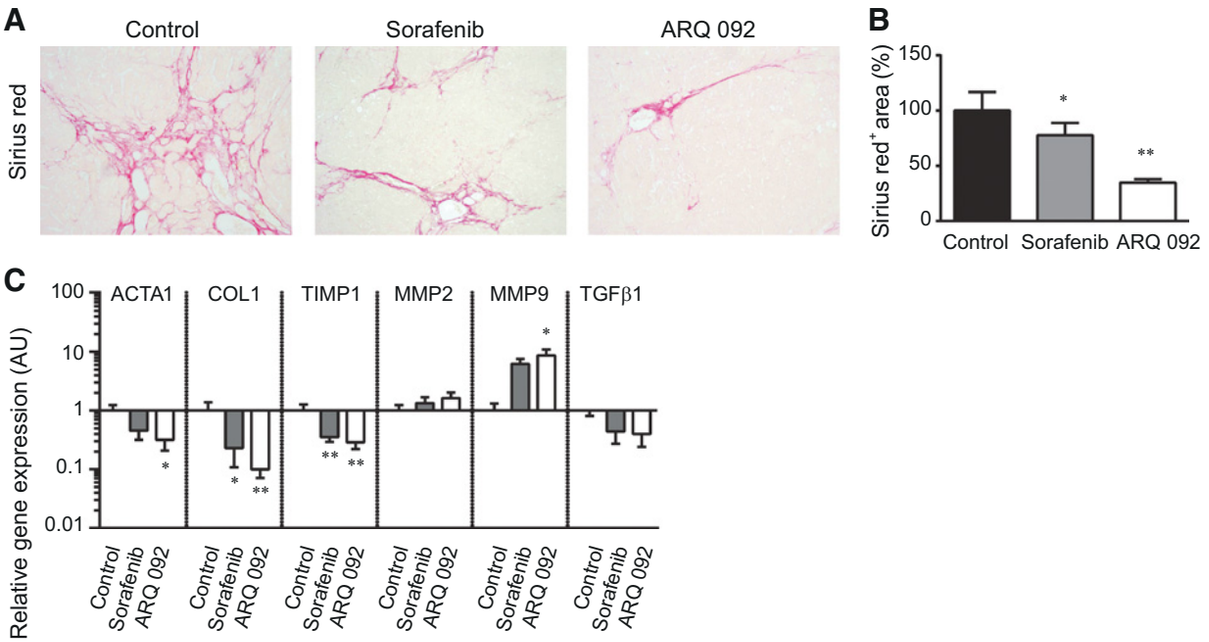

Figure 4.

Effect of ARQ 092 and sorafenib on liver fibrosis. **A,** Representative histologic images of livers stained with Sirius red from control, sorafenib, or ARQ 092 rats; magnification, ×10. **B,** Quantification of fibrosis on 10 random fields/slide, 1 slide per animal (Sirius red staining area per total area; control was set as 100%). **C,** Relative mRNA expression of ACTA1, Collagen 1 (COL1), TIMP-1, matrix metalloproteinases MMP2 and MMP9, and TGFβ1 in nontumor liver tissues ($n = 5$). Control was set as 1, and values are mean ± SEM. *, $P < 0.05$ and **, $P < 0.01$ vs. control.

Therefore, ARQ 092 significantly reduces tumor progression and proliferation in DEN-induced HCC, and has a higher antitumor effect than sorafenib.

Antiangiogenic effect

Antiangiogenic effect of treatments was assessed with dynamic contrast-enhanced (DCE) MRI as described in the Supplementary Information and illustrated in Fig. 3A. At baseline (MRI1), tumor enhancement was comparable between the groups ($P = 0.732$; Fig. 2B).

On MRI3, tumor enhancement was significantly different between groups ($P = 0.013$). ARQ 092 induced a lower tumor enhancement with 64.2% ± 8.5% of control ($P = 0.114$) and 54.4% ± 7.1% of sorafenib ($P = 0.010$; Fig. 3B). In each group of treatment, comparison between baseline and the end of the treatment (MRI1 and MRI3) revealed that only ARQ 092 treatment was associated with a significant decrease of tumor enhancement ($P = 0.012$; Fig. 3C).

Tumor vascularization was also studied by using a rat-specific anti-CD34 antibody to perform immunofluorescence staining of liver tissues. Although structural abnormalities of the tumor vasculature were numerous in control animals, normalization of vasculature was observed in both treated groups (Fig. 3D). Quantification of vascular density revealed that sorafenib decreased vascular density by 46% ($P = 0.0008$) and ARQ 092 by 68% ($P < 0.0001$) compared with nontreated rats (Fig. 3E). Thus, MRI results and CD34 staining proved that treatment by ARQ 092 leads to vascular normalization and inhibition of tumor angiogenesis.

Liver fibrosis assessment

As shown in Fig. 4A and B, collagen accumulation assessed by sirius red staining was significantly reduced in the ARQ 092 group compared with the control group ($P = 0.001$) and with the sorafenib group ($P = 0.021$). Difference between the control and the sorafenib groups was not significant ($P = 0.348$). No effects of treatment were observed concerning fibronectin levels (Supplementary Fig. S4D).

Improvement of liver fibrosis by ARQ 092 treatment was confirmed by qPCR analysis (Fig. 4C). The expression of fibrosis markers was downregulated in nontumor liver samples of the ARQ 092 group compared with the control group with significant differences for actin alpha (ACTA)1 (31.7% ± 10.9% of control, $P = 0.029$) and collagen 1 (9.9% ± 2.9% of control, $P = 0.007$). Accordingly, tissue inhibitor of metalloproteinases-1 (TIMP-1) was significantly decreased by ARQ 092 treatment compared with control, and matrix metalloproteinase MMP9 was upregulated.

No significant difference was observed for TGFβ1 (40.1% ± 15.9% of control, $P = 0.115$). For sorafenib group, collagen 1 and TIMP-1 were the only significantly downregulated fibrosis markers.

Overall, ARQ 092 significantly decreased hepatic collagen deposition and improved liver fibrosis in DEN-induced cirrhotic rat model of HCC.

Pathway analysis

Western blot analyses showed that ARQ 092 treatment completely blocks phosphorylation of $AKT^{(Ser473)}$ in all human HCC cell lines at both IC_{20} and IC_{50} concentrations

Published OnlineFirst May 31, 2017; DOI: 10.1158/1535-7163.MCT-16-0602-T

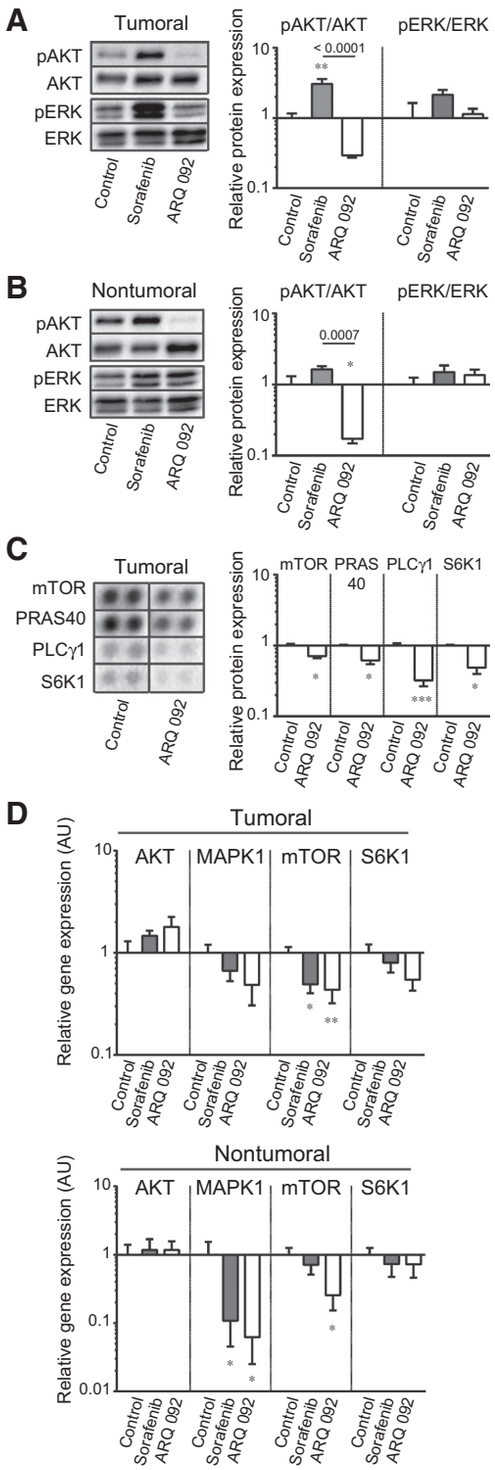

Figure 5.

Effect of ARQ 092 and sorafenib on AKT and ERK pathways. Western blot analysis of pAKT/AKT and pERK/ERK in (**A**) tumor and (**B**) nontumor liver tissue and the quantification of Western blots. **C,** Phosphoprotein analyses of downstream kinases of the AKT pathway in tumor tissue. **D,** qPCR analysis of gene expression in tumor and nontumor liver samples. Control was set as 1, and values are mean ± SEM. *, $P \leq 0.05$; **, $P \leq 0.01$; and ***, $P \leq 0.001$ vs. control.

(Supplementary Fig. S5). Immunofluorescence staining of p-AKT on liver tissues confirmed these results (Supplementary Fig. S6).

Accordingly, ARQ 092 inhibited phosphorylation of AKT$^{(Ser473)}$ in both tumor and nontumor liver tissues (Fig. 5A and B), with a pAKT/AKT ratio of 29.5% ± 2.27% of control ($P = 0.002$) in tumor samples and 17.2% ± 2.33% of control ($P = 0.034$) in surrounding liver samples. Interestingly, sorafenib treatment significantly increased the pAKT/AKT ratio in tumor samples ($P < 0.0001$) compared with the control group. By profiling kinase phosphorylation (Supplementary Table S2), we found that the levels of phosphorylated mTOR, proline-rich Akt/PKB substrate 40 kDa (PRAS 40), PLCγ1, and Ribosomal protein S6 kinase (S6K1) were significantly decreased in tumor tissues after the ARQ 092 treatment compared with the control (Fig. 5C). As expected, qPCR analyses did not show a significant difference in AKT gene expression, but confirmed that ARQ 092 downregulates AKT pathway downstream actors such as mTORC1 (44.2% ± 11.4% of control, $P = 0.005$) or S6K1 (54.6% ± 11.9% of control, $P = 0.142$), as shown in Fig. 5D.

Regarding the ERK pathway, Western blot analyses did not show significant differences in the pERK/ERK ratio between the groups. Accordingly, we observed no differences between the groups in gene expression of ERK in tumor samples. Interestingly, the gene expression of ERK was downregulated in nontumor tissues of both ARQ 092 and sorafenib-treated groups compared with the nontreated group ($P = 0.029$ and 0.039).

Discussion

In this study, ARQ 092 showed antitumor, antiangiogenic, and antifibrotic effects with significantly better efficacy than sorafenib in terms of tumor number, as well as tumor contrast enhancement, and the level of liver fibrosis. *In vitro*, ARQ 092 was also highly efficient in HCC cell lines with a 2 to 6 times more potent effect on cell viability than sorafenib.

ARQ 092 was easily managed in rats with a mean weight loss of only 0.8% at the end of the study. The most frequent side effects of mTOR inhibitors are diabetes and hyperlipidemia. In our hands, with ARQ 092, there was no increase in glucose, cholesterol, and triglyceride blood levels as well as liver cholesterol and triglyceride levels compared with control- and sorafenib-treated rats. The dose strategy for ARQ 092 for *in vivo* study was based on a previous toxicity study (data provided by ArQule Inc.). The "one week on/one week off" schedule probably contributed to the good tolerability of the tested regimen.

Previous publications have demonstrated the effect of sorafenib on HCC in noncirrhotic rats with a good tolerability at doses between 10 mg/kg in association with another drug (12) and 30 mg/kg when given alone (13–15). In a previous pilot study, we tested a 20 mg/kg sorafenib dose in our cirrhotic rat model with HCC, but due to an important weight loss and other symptoms, after first days of sorafenib administration, we had to stop the study. Therefore, in this study, we have chosen 10 mg/kg for sorafenib. This underlines that HCC new drugs have to be tested in cirrhotic animal models to better assess their side effects that can be very different between noncirrhotic and cirrhotic patients.

Published OnlineFirst May 31, 2017; DOI: 10.1158/1535-7163.MCT-16-0602-T

Another particularity of this study is the demonstration of the kinetic of tumor progression through three sequential MRI scans per rat. The dramatic increase of tumor size after 6 weeks in control rats (+155.3% ± 16.0%) confirmed the high level of aggressiveness of the DEN model. Tumor progression between MRI1 and 3 was significantly reduced in both groups of treatment compared with the control. There was no statistical difference between ARQ 092 and sorafenib groups possibly because of a type 2 error.

Similarly, according to histologic examination, both sorafenib and ARQ 092 significantly reduced the tumor size compared with the control, but only ARQ 092–treated rats displayed a significantly lower number of tumors. This suggests that ARQ 092 inhibits tumor initiation. To be confirmed, this hypothesis needs further experiments with an earlier introduction of ARQ 092 during the DEN-induction phase like it was done for erlotinib (11).

Our *in vivo* and *in vitro* analyses confirmed that the ARQ 092 treatment strongly and selectively affects the AKT pathway. In fact, ARQ 092 is a highly selective allosteric inhibitor that suppresses pan-AKT activity by blocking its phosphorylation and by preventing the inactive form from localizing into plasma membrane which together leads to strong and specific downregulation of downstream targets of AKT (9). Such high specificity was missing in action of catalytic AKT inhibitors that have been previously developed (16). Besides, as sorafenib, ARQ 092 plasma protein binding is very high, around 99% in both rat and human (data provided by ArQule Inc.). Despite this fact, *in vitro* study showed that ARQ 092 IC_{50} and IC_{20} were lower than sorafenib's ones, suggesting a higher efficacy of this new drug.

In sorafenib-treated rats, the absence of downregulation of the ERK pathway on qPCR and Western blot analyses can be surprising, as it has been previously shown that sorafenib downregulates pERK in rat HCC (12). Nonetheless, as DEN induces a strongly aggressive type of HCC, multiple resistance mechanisms have probably already been developed in this model. The overexpression of pAKT in this group is a surrogate marker of such resistance.

Thus, despite difficult conditions with an aggressive model of cancer in cirrhotic rats, ARQ 092 showed its efficacy in controlling tumor progression and demonstrated a good safety profile that makes this experimental drug promising in the treatment of HCC in cirrhotic patients. The results presented here also confirm the importance of targeting AKT in HCC development and progression.

Disclosure of Potential Conflicts of Interest

G. Abbadessa has ownership interest (including patents) in ArQule. No potential conflicts of interest were disclosed by the other authors.

Authors' Contributions

Conception and design: G.S. Roth, Z.M. Jilkova, G. Abbadessa, Y. Yu, T. Decaens

Development of methodology: G.S. Roth, Z.M. Jilkova, T. Decaens

Acquisition of data (provided animals, acquired and managed patients, provided facilities, etc.): G.S. Roth, Z.M. Jilkova, A.Z. Kuyucu, K. Kurma, S.T. Ahmad Pour, B. Busser, T. Decaens

Analysis and interpretation of data (e.g., statistical analysis, biostatistics, computational analysis): G.S. Roth, Z.M. Jilkova, A.Z. Kuyucu, K. Kurma, S.T. Ahmad Pour, G. Abbadessa, Y. Yu, B. Busser, V. Leroy, T. Decaens

Writing, review, and/or revision of the manuscript: G.S. Roth, Z.M. Jilkova, A.Z. Kuyucu, G. Abbadessa, Y. Yu, B. Busser, P.N. Marche, V. Leroy, T. Decaens

Administrative, technical, or material support (i.e., reporting or organizing data, constructing databases): G.S. Roth, G. Abbadessa, P.N. Marche, T. Decaens

Study supervision: T. Decaens

Acknowledgments

We thank Sylvain Andrieu, Pauline Durrenbach, Manon Leportier, and Fabien Mehr (Animal platform, Grenoble Institute of Neurosciences, Grenoble, France) for the quality of their animal care and their crucial help in oral gavage, and Vasile Stupar (MRI platform, Grenoble Institute of Neurosciences, Grenoble, France) for his help in the realization of MRI acquisitions.

Grenoble MRI facility IRMaGe was partly funded by the French program "Investissement d'Avenir" run by the `Agence Nationale pour la Recherche' and the grant `Infrastructure d'avenir en Biologie Santé' - ANR-11-INBS-0006.

Professor Nathalie Sturm, Head of the Pathology Department of Grenoble-Alpes University Hospital.

Dr. Istvan Blazsek for DEN rat cell lines.

Grant Support

T. Decaens was awarded an AFEF (Association Française pour l'Etude du Foie) research bursary in 2013.

The costs of publication of this article were defrayed in part by the payment of page charges. This article must therefore be hereby marked *advertisement* in accordance with 18 U.S.C. Section 1734 solely to indicate this fact.

Received September 9, 2016; revised May 2, 2017; accepted May 22, 2017; published OnlineFirst May 31, 2017.

References

1. Jemal A, Bray F, Center MM, Ferlay J, Ward E, Forman D. Global cancer statistics. CA Cancer J Clin 2011;61:69–90.
2. Llovet JM, Ricci S, Mazzaferro V, Hilgard P, Gane E, Blanc JF, et al. Sorafenib in advanced hepatocellular carcinoma. N Engl J Med 2008; 359:378–90.
3. Villanueva A, Chiang DY, Newell P, Peix J, Thung S, Alsinet C, et al. Pivotal role of mTOR signaling in hepatocellular carcinoma. Gastroenterology 2008;135:1972–83, 83 e1–11.
4. Matter MS, Decaens T, Andersen JB, Thorgeirsson SS. Targeting the mTOR pathway in hepatocellular carcinoma: current state and future trends. J Hepatol 2014;60:855–65.
5. Kunter I, Erdal E, Nart D, Yilmaz F, Karademir S, Sagol O, et al. Active form of AKT controls cell proliferation and response to apoptosis in hepatocellular carcinoma. Oncol Rep 2014;31:573–80.
6. Laplante M, Sabatini DM. mTOR signaling in growth control and disease. Cell 2012;149:274–93.
7. Mattina J, MacKinnon N, Henderson VC, Fergusson D, Kimmelman J. Design and reporting of targeted anti-cancer preclinical studies: a meta-analysis of animal studies investigating sorafenib antitumor efficacy. Cancer Res 2016;76:4627–36.
8. Schiffer E, Housset C, Cacheux W, Wendum D, Desbois-Mouthon C, Rey C, et al. Gefitinib, an EGFR inhibitor, prevents hepatocellular carcinoma development in the rat liver with cirrhosis. Hepatology 2005;41:307–14.
9. Lapierre JM, Eathiraj S, Vensel D, Liu Y, Bull CO, Cornell-Kennon S, et al. Discovery of 3-(3-(4-(1-aminocyclobutyl)phenyl)-5-phenyl-3H-imidazo[4,5-b]pyridin-2-yl)pyridin -2-amine (ARQ 092): an orally bioavailable, selective, and potent allosteric AKT inhibitor. J Med Chem 2016;59:6455–69.
10. Thièry JP, Blazsek I, Legras S, Marion S, Reynes M, Anjo A, et al. Hepatocellular carcinoma cell lines from diethylnitrosamine phenobarbital-treated rats. Characterization and sensitivity to endothall, a

Published OnlineFirst May 31, 2017; DOI: 10.1158/1535-7163.MCT-16-0602-T

protein serine/threonine phosphatase-2A inhibitor. Hepatology 1999; 29:1406–17.
11. Fuchs BC, Hoshida Y, Fujii T, Wei L, Yamada S, Lauwers GY, et al. Epidermal growth factor receptor inhibition attenuates liver fibrosis and development of hepatocellular carcinoma. Hepatology 2014;59:1577–90.
12. Sieghart W, Pinter M, Dauser B, Rohr-Udilova N, Piguet AC, Prager G, et al. Erlotinib and sorafenib in an orthotopic rat model of hepatocellular carcinoma. J Hepatol 2012;57:592–9.
13. Gu FM, Li QL, Gao Q, Jiang JH, Huang XY, Pan JF, et al. Sorafenib inhibits growth and metastasis of hepatocellular carcinoma by blocking STAT3. World J Gastroenterol 2011;17:3922–32.
14. Wang Q, Shi G, Wang L, Liu X, Wu R. Early prediction of response of sorafenib on hepatocellular carcinoma by CT perfusion imaging: an animal study. Br J Radiol 2014;87:20130695.
15. Yan J, Tan C, Gu F, Jiang J, Xu M, Huang X, et al. Sorafenib delays recurrence and metastasis after liver transplantation in a rat model of hepatocellular carcinoma with high expression of phosphorylated extracellular signal-regulated kinase. Liver Transpl 2013;19: 507–20.
16. Rodon J, Dienstmann R, Serra V, Tabernero J. Development of PI3K inhibitors: lessons learned from early clinical trials. Nat Rev Clin Oncol 2013;10:143–53.

Published OnlineFirst May 31, 2017; DOI: 10.1158/1535-7163.MCT-16-0602-T

Molecular Cancer Therapeutics

Efficacy of AKT Inhibitor ARQ 092 Compared with Sorafenib in a Cirrhotic Rat Model with Hepatocellular Carcinoma

Gaël S. Roth, Zuzana Macek Jilkova, Ayca Zeybek Kuyucu, et al.

Mol Cancer Ther 2017;16:2157-2165. Published OnlineFirst May 31, 2017.